

Electronic Thesis and Dissertation Repository

11-19-2010 12:00 AM

Motion Coordination of Aerial Vehicles

Abdelkader Abdessameud, *The University of Western Ontario*

Supervisor: Dr. Abdelhamid Tayebi, *The University of Western Ontario*

A thesis submitted in partial fulfillment of the requirements for the Doctor of Philosophy degree
in Electrical and Computer Engineering

© Abdelkader Abdessameud 2010

Follow this and additional works at: <https://ir.lib.uwo.ca/etd>



Part of the [Controls and Control Theory Commons](#)

Recommended Citation

Abdessameud, Abdelkader, "Motion Coordination of Aerial Vehicles" (2010). *Electronic Thesis and Dissertation Repository*. 40.

<https://ir.lib.uwo.ca/etd/40>

This Dissertation/Thesis is brought to you for free and open access by Scholarship@Western. It has been accepted for inclusion in Electronic Thesis and Dissertation Repository by an authorized administrator of Scholarship@Western. For more information, please contact wlsadmin@uwo.ca.

Motion Coordination of Aerial Vehicles

(Spine title: Motion Coordination of Aerial Vehicles)

(Thesis format: Monograph)

by

ABDELKADER ABDESSAMEUD

Graduate Program
in
Engineering Science
Electrical and Computer Engineering

A thesis submitted in partial fulfillment
of the requirements for the degree of
Ph.D of Engineering Science

School of Graduate and Postdoctoral Studies
The University of Western Ontario
London, Ontario, Canada

© Abdelkader ABDESSAMEUD 2010

Certificate of Examination

THE UNIVERSITY OF WESTERN ONTARIO
SCHOOL OF GRADUATE AND POSTDOCTORAL STUDIES
CERTIFICATE OF EXAMINATION

Chief Advisor:

Examining Board:

Dr. Abdelhamid Tayebi

Dr. Polushin, Ilia

Advisory Committee:

Dr. McIsaac, Ken

Dr. Naish, Michael D.

Dr. Schwartz, Howard

The thesis by
ABDELKADER ABDESSAMEUD
entitled:
Motion Coordination of Aerial Vehicles
is accepted in partial fulfillment of the
requirements for the degree of
Ph.D of Engineering Science

Date: _____

Chair of Examining Board

Abstract

The coordinated motion control of multiple vehicles has emerged as a field of major interest in the control community. This thesis addresses two topics related to the control of a group of aerial vehicles: the output feedback attitude synchronization of rigid bodies and the formation control of Unmanned Aerial Vehicles (UAVs) capable of Vertical Take-Off and Landing (VTOL). The information flow between members of the team is assumed fixed and undirected.

The first part of this thesis is devoted to the attitude synchronization of a group of spacecraft. In this context, we propose control schemes for the synchronization of a group of spacecraft to a predefined attitude trajectory without angular velocity measurements. We also propose some velocity-free consensus-seeking schemes allowing a group of spacecraft to align their attitudes, without reference trajectory specification.

The second part of this thesis is devoted to the control of a group of VTOL-UAVs in the Special Euclidian group $SE(3)$, *i.e.*, position and orientation. In this context, we propose a few position coordination schemes without linear-velocity measurements. We also propose some solutions to the same problem in the presence of communication time-delays between aircraft.

To solve the above mentioned problems, several new technical tools have been introduced in this thesis to overcome the deficiencies of the existing techniques in this field.

Acknowledgements

I am forever indebted to my supervisor Professor Abdelhamid Tayebi for his motivation and support during the period I spent at the UWO. His patience, encouragement and constructive feedback have not only enabled the completion of this work, but also endured my maturing in the field of control. I am also grateful to Dr. Abdallah Shami who served as my alternate supervisor at Western during the PhD program.

I would like to thank the members of my doctoral examination committee; Professor Howard Schwartz, Dr. Ilia Polushin, Dr. Ken McIsaac and Dr. Michael D. Naish for their constructive comments and feedback.

My PhD colleague and friend Andrew Roberts deserves big thanks for the several discussions we shared, which have initiated some of the work achieved in this thesis. Also, I would like to thank the staff of the department of Electrical and Computer Engineering, in particular Sandra Vilovski, for helping me with every administrative issue.

I wish also to thank the members of my family, in particular my mother and father for their endless support and encouragements, with the Atlantic ocean separating us, and I am truly grateful to my wife and two children for their love and entire support and for allowing me accomplish my dreams without questions.

Table of Contents

Certificate of Examination	ii
Abstract	iii
Acknowledgements	iv
List of figures	viii
List of symbols	x
1 Introduction	1
1.1 General introduction	1
1.2 Coordination approaches	2
1.3 Scope of thesis	5
1.3.1 Attitude synchronization of rigid bodies	5
1.3.2 Formation control of VTOL UAVs	8
1.4 Statement of contributions	11
1.4.1 List of publications	13
1.5 Thesis outline	15
2 Background and preliminaries	17
2.1 Notation	17
2.2 System modeling	17
2.2.1 Coordinate frames	18
2.2.2 Attitude representation - Unit quaternion	18
2.2.3 Rotational dynamics	19
2.2.4 Translational dynamics of VTOL UAVs	20
2.3 Attitude error	20
2.3.1 Attitude tracking error	21
2.3.2 Relative attitude	22
2.4 Stability definitions	23
2.5 Information flow modeling	24
2.6 Preliminary results	25

3	Output feedback attitude synchronization of spacecraft formation	28
3.1	Introduction	28
3.2	Problem formulation	30
3.3	State feedback design	30
3.4	Auxiliary systems-based output feedback - First approach	33
3.4.1	Attitude synchronization with time-varying reference trajectory	34
3.4.2	Attitude synchronization without reference assignment	37
3.5	Auxiliary systems-based output feedback - Second approach	40
3.5.1	Attitude synchronization with time-varying reference	40
3.5.2	Attitude synchronization without reference assignment	42
3.6	Combined design	44
3.7	Simulation results	45
3.8	Concluding Remarks	47
4	Global trajectory tracking of VTOL UAVs	56
4.1	Introduction	56
4.2	Problem formulation	57
4.3	Controlling VTOL UAVs	58
4.3.1	Thrust and desired attitude extraction	58
4.3.2	Control design procedure	59
4.3.3	Intermediary control input constraints	60
4.4	Trajectory tracking control of a single aircraft	60
4.4.1	Intermediary position control design	61
4.4.2	Attitude control design	62
4.4.3	Stability of the overall System	62
4.5	Design without linear-velocity measurements	64
4.5.1	Intermediary position control design	64
4.5.2	Attitude control design	66
4.5.3	Stability of the overall System	67
4.6	Simulation results	69
4.7	Concluding remarks	70
5	Formation control of VTOL UAVs	74
5.1	Introduction	74
5.2	Problem formulation	75
5.3	Formation control in the full state information case	76
5.4	Formation control without linear-velocity measurements	81
5.5	Design with reduced communication requirements	84
5.6	Simulation results	88
5.7	Concluding remarks	89

6	Formation control with communication delays	94
6.1	Introduction	94
6.2	Problem formulation	95
6.3	Delay-dependent formation control scheme	96
6.3.1	Extension to time-varying communication delays	99
6.4	Delay-independent formation control design	101
6.5	Virtual vehicle approach to the formation control problem	103
6.6	Simulation result	106
6.7	Concluding remarks	107
7	Conclusion	113
	Bibliography	116
	Appendices	
A	Detailed proofs	127
A.1	Preliminaries	127
A.1.1	Proof of Lemma 2.4	127
A.1.2	Proof of Lemma 2.5	128
A.1.3	Proof of Lemma 2.6	130
A.2	Attitude synchronization	131
A.2.1	Proof of Theorem 3.1	131
A.2.2	Proof of Theorem 3.2	135
A.2.3	Proof of Theorem 3.3	137
A.2.4	Proof of Theorem 3.4	139
A.2.5	Proof of Theorem 3.5	140
A.3	Trajectory tracking of VTOL aircraft	141
A.3.1	Proof of Lemma 4.1	141
A.3.2	Proof of Theorem 4.1	142
A.3.3	Proof of Theorem 4.2	143
A.4	Formation control of VTOL UAVs	146
A.4.1	proof of Theorem 5.1	146
A.4.2	Proof of Theorem 5.2	148
A.4.3	Proof of Theorem 5.3	152
A.5	Formation control with delayed communication	153
A.5.1	Proof of Theorem 6.1	153
A.5.2	Proof of Theorem 6.2	157
A.5.3	Proof of Theorem 6.3	159
A.5.4	Proof of Lemma 6.1	161
A.5.5	Proof of Theorem 6.4	162
	Curriculum Vitae	164

List of Figures

2.1	VTOL aircraft (Courtesy of A. Roberts)	20
2.2	Example of an undirected/directed graph	25
3.1	Implementation of the control law in Theorem 3.1.	37
3.2	Implementation of the control law in Theorem 3.3.	43
3.3	Information flow graph	46
3.4	Spacecraft angular velocities: (a) Theorem 3.1, (b) Theorem 3.3.	49
3.5	Spacecraft attitudes: (a) Theorem 3.1, (b) Theorem 3.3.	50
3.6	Norm of input torques: (a) Theorem 3.1, (b) Theorem 3.3.	51
3.7	Spacecraft angular velocities: (a) Theorem 3.2, (b) Theorem 3.4.	52
3.8	Spacecraft attitudes: (a) Theorem 3.2, (b) Theorem 3.4.	53
3.9	Norm of input torques: (a) Theorem 3.2, (b) Theorem 3.4.	54
3.10	Simulation results in case of Theorem 3.5: (a) Spacecraft angular velocities (b) Spacecraft attitudes	55
4.1	The control structure for a single VTOL aircraft	60
4.2	Intermediary control block diagram.	65
4.3	Implementation of the control scheme in Theorem 4.2.	69
4.4	Simulation results in case of Theorem 4.1.	72
4.5	Simulation results in case of Theorem 4.2.	73
5.1	Implementation of the control scheme in Theorem 5.1.	80
5.2	Intermediary control block diagram.	85
5.3	Simulation results in case of Theorem 5.1: (a) Systems trajectories (b) Linear-velocity error $\tilde{\mathbf{v}}_i$	91
5.4	Simulation results in case of Theorem 5.2: (a) Systems trajectories (b) Linear-velocity error $\tilde{\mathbf{v}}_i$	92
5.5	Simulation results in case of Theorem 5.3: (a) Systems trajectories (b) Linear-velocity error $\tilde{\mathbf{v}}_i$	93
6.1	Simulation results in case of Theorem 6.1: (a) Systems trajectories (b) Aircraft linear velocities	109
6.2	Simulation results in case of Theorem 6.2: (a) Systems trajectories (b) Aircraft linear velocities	110
6.3	Simulation results in case of Theorem 6.3: (a) Systems trajectories (b) Aircraft linear velocities	111

List of Figures

6.4	Simulation results in case of Theorem 6.4: (a) Systems trajectories (b) Aircraft linear velocities	112
-----	--	-----

List of symbols

\mathbf{p}	<i>position vector</i>
$\tilde{\mathbf{p}}$	<i>position tracking error vector</i>
\mathbf{v}	<i>linear velocity vector</i>
$\tilde{\mathbf{v}}$	<i>linear velocity tracking error vector</i>
\mathbf{Q}	<i>unit quaternion representing the absolute attitude</i>
$\tilde{\mathbf{Q}}$	<i>unit quaternion representing the attitude tracking error</i>
\mathbf{q}	<i>vector part of a unit quaternion</i>
η	<i>scalar part of a unit quaternion</i>
$\bar{\mathbf{Q}}$	<i>auxiliary unit quaternion</i>
\mathbf{Q}^e	<i>error unit quaternion</i>
$\tilde{\mathbf{Q}}^e$	<i>error unit quaternion</i>
$\mathbf{R}(\mathbf{Q})$	<i>rotation matrix associated to \mathbf{Q}</i>
$\boldsymbol{\omega}$	<i>angular velocity vector</i>
$\tilde{\boldsymbol{\omega}}$	<i>angular velocity tracking error</i>
$\boldsymbol{\Omega}$	<i>angular velocity error vector</i>
$\tilde{\boldsymbol{\Omega}}$	<i>angular velocity error vector</i>
$\boldsymbol{\beta}$	<i>angular velocity vector (design variable)</i>
$\boldsymbol{\Gamma}$	<i>torque input</i>
T	<i>thrust input</i>
T^b	<i>upper bound of the thrust input</i>
$\boldsymbol{\xi}$	<i>position error vector</i>
$\hat{\boldsymbol{\xi}}$	<i>estimate of the position vector</i>
\mathbf{z}	<i>linear velocity error vector</i>
$\hat{\mathbf{z}}$	<i>estimate of the linear velocity vector</i>
\mathbf{F}	<i>intermediary control</i>
$\boldsymbol{\theta}$	<i>auxiliary variable</i>
$\boldsymbol{\alpha}$	<i>auxiliary variable</i>
\mathbf{u}	<i>auxiliary input (design variable)</i>

List of symbols

ϕ	<i>auxiliary input (design variable)</i>
ψ	<i>output of a first order filter</i>
σ	<i>scalar saturation function</i>
\mathbf{J}_f	<i>inertia matrix</i>
m	<i>mass</i>
g	<i>acceleration due to gravity</i>
\mathcal{G}	<i>communication graph</i>
\mathcal{N}	<i>set of nodes of the graph \mathcal{G}</i>
\mathcal{E}	<i>set of edges of the graph \mathcal{G}</i>
\mathcal{K}	<i>adjacency matrix of the graph \mathcal{G}</i>

Most of the above variables will be used with indices. Subscript ‘ d ’ indicates a desired vector, ‘ i ’ attributes the variable to the i^{th} vehicle, and subscript ‘ ij ’ indicates a relative vector between the i^{th} and j^{th} vehicles.

Chapter 1

Introduction

1.1 General introduction

Coordinated motion of groups of autonomous vehicles such as aircraft, spacecraft, mobile robots and underwater vehicles is emerging as a new and exciting field of research. With recent advances in sensors, energy storage devices, networking infrastructure, information technology and the development of powerful control techniques, it is perceived that large groups of low-cost automated vehicles can now be coordinated in an effective manner for a variety of tasks including enhanced surveillance systems, hazardous material handling systems, search and rescue missions, and deep space observation. In many of these tasks, it is desirable to put the group members in a formation, and by doing so, precondition the motion of the group to show certain desirable features as observed in many practical situations and biological systems.

In Ethology, it is shown that formation behaviors benefit the animals in various ways. For instance, each animal in a herd benefits by minimizing its encounters with predators. By grouping, animals also combine their sensors to more efficiently forage for food. These behaviors are beneficiary not only pertaining to the survival of the group individuals, but also to the performance of the group. For flocks of birds, it is suggested that the energy savings for a group of individuals flying in their V-shaped formation will allow them to increase their flight range by 70 per cent over that of a lone bird (Lissaman and Shollenberger, 1970; May, 1979). In addition, the endurance for fish traveling in schools could be considerably increased due to the effect of increased hydrodynamic swimming efficiency (Wiehs, 1973). Studies of flocking and schooling show that these behaviors emerge as a combination of a desire to stay in the group and to keep a separation distance from other members of the group (Cullen *et al.*, 1965).

Naturally occurring formations has inspired several directions of research within the control community. All with the goal of designing coordination control schemes which enable mechanical systems to accomplish a predefined task in a formation. Formation is important in many military applications where sensor assets are limited. Formations allow individual team members to concentrate their sensors across a portion of the environment, while their partners cover other area of the environment. For example, fighter pilots direct their visual and radar search responsibilities depending on their positions in a formation. Robotic scouts also benefit by directing

their sensors in different areas to ensure full coverage. The approach is potentially applicable in many other domains, such as search and rescue, agricultural coverage tasks, and security patrols.

The ability to maintain the position of a group of autonomous vehicles relative to each other or relative to a reference is known as formation control. The study of formation control is motivated by the advantages achieved by using formations of multiple vehicles, instead of a single vehicle, in a specified mission. These include cost and energy efficiency and increased feasibility, accuracy, robustness and flexibility (Ren, 2004). For example, cost and energy efficiency may be maximized if multiple vehicles can coordinate their motion in a certain way. This can be seen in multiple aircraft mimicking the V-shape flight formation of birds to maximize fuel efficiency. In addition, in deep spacecraft interferometry applications, it has been shown that using formations of multiple micro satellites instead of a single spacecraft can reduce the mission cost and improve system robustness and accuracy (Hadaegh *et al.*, 1998). Furthermore, the probability of success will be improved if multiple vehicles are used to carry out a mission in a coordinated fashion, e.g., multiple Unmanned Air Vehicles (UAV) are assigned to a certain target (Beard *et al.*, 2002) or multiple Autonomous Underwater Vehicles (AUV) are used to search for an underwater object (Stilwell and Bishop, 2000).

In many of these applications, and because of the highly distributed nature of the vehicles sensing and actuation modules, shared information plays a central role and facilitates the coordination of the group - information which may be subject to transmission delays. For this reason, there has been over the past few years widespread interest in the study of the nature of interconnections in linear multi-agent networks. The use of graph theory produced many interesting results (see for example Olfati-Saber *et al.*, 2007; Ren *et al.*, 2007, and references therein). Also, the effects of communication delays in networks of multi-agent systems with simple dynamics have also been studied in several works such as Olfati-Saber and Murray (2004) and Sun and Wang (2009).

This thesis focuses on the motion coordination of aerial vehicles, which nowadays are widely used in several applications ranging from simple surveillance missions to space exploration. In the next section we give a general overview on approaches used in formation control, then we define the problems discussed in this thesis as well as the thesis contributions.

1.2 Coordination approaches

The control of relative motion of mechanical systems fits nicely into the general motion coordination perspectives, and has resulted in a large interest in several fields over the last few decades. Coordinated control of multiple agents (vehicles) involve the design of controllers, and sometimes observers, where the ultimate goal is to coordinate the

motion of two or more agents to accomplish an objective or a task. The controller design for motion coordination can be centralized, decentralized or a combination of both, depending on the definition of the decision making agent. In centralized control, a single agent with a global control algorithm specifies where the other agents should move based on measurements of the states of all agents. This increases the possibility of achieving the formation task, but introduces a single point of failure and a large amount of multidirectional information flow between agents is generally required. Decentralized control requires the implementation of local controllers assigning hence the control decisions to the local control agents. The local control actions are designed based on information exchange between local agents so that they perform their local control tasks, and coordinate with one another to control the global system. The result is that the requirements for the information flow are decreased and relatively simple control laws are implemented. In addition, failure of a single local control agent in a decentralized controlled system does not lead to the destabilization of the entire system. The main difficulty of decentralized controllers is that they are difficult to analyze analytically.

Existing approaches to vehicle formation control generally fall into three categories: leader-follower, behavior-based, or virtual structure approaches. Each approach has its advantages and disadvantages, and the right approach for a specific problem is dependent on the nature of the problem and the purpose of control.

Leader-follower approach: In the leader-follower approach, some vehicles are designated as leaders, whereas the others as followers. Follower vehicles are designated to track the position and orientation of the leader, possibly with some prescribed offset. In mobile robotics, this approach has been used for different purposes such as to capture a target by mobile robots (Yamaguchi, 1999), to control a group of robots to move a box (Sugar and Kumar, 1998), and to control multiple robots navigating in environments with obstacles (Desai, 2002). The leader-follower approach has also been used in coordinated control of robot manipulators (Bondhus *et al.*, 2005; Rodriguez-Angeles and Nijmeijer, 2004), mobile manipulators (Lizarralde *et al.*, 1995; Freund and Rossmann, 2003), spacecraft formation (Wang and Hadaegh, 1996; Wang *et al.*, 1999), marine vehicles (Ihle *et al.*, 2004, 2005) and unmanned aerial vehicles (Giulietti *et al.*, 2000; Seiler *et al.*, 2004; Gu *et al.*, 2006).

The positive point of the leader-follower approach is that specifying the leaders motion directs the group behavior. The weakness, however, is that the leader is a single point of failure for the formation. Also, there is no explicit feedback to the formation. Therefore, the leader cannot be informed if it is moving too fast for the follower vehicles to track or if one of the followers is late due to disturbances for example.

Behavioral approach: The basic idea in the behavioral architecture is to prescribe several desired behaviors for each agent in the group, and construct control inputs for an individual agent based on a weighted average of the control inputs for each

behavior. Possible behaviors include trajectory and neighbor tracking, collision and obstacle avoidance, and formation-keeping (Balch and Arkin, 1998). This approach lends itself to a decentralized implementation and deals with multiple objectives very well. Another important feature of the behavioral approach is that explicit formation feedback is included through the communication between neighbors. However, because of the lack of an explicit definition of the group behavior, it is difficult to guarantee some characteristics of the formation. In some applications in which the behaviors are defined based on potential functions that are motivated by natural physics laws, behavioral constraints can be proved (Spears *et al.*, 2004).

A behavior-based approach to formation control for mobile robots is derived based on averaging competing behaviors in Khatib (1986). Creating line and circle formations by mobile robots is investigated in Yun *et al.* (1997). This approach has been also applied for mobile robot vehicles with flocking motions (Lawton *et al.*, 2000, 2003; Tanner *et al.*, 2003; Moshtagh and Jadbabaie, 2007), for search and exploration missions driven by a sensed environment (Ögren *et al.*, 2004), including collision avoidance schemes (Krishna and Hexmoor, 2004; Antonelli and Chiaverini, 2006). It has also been used with success in spacecraft formations (Lawton and Beard, 2000), formation control of under-actuated marine vessels (Arrichiello *et al.*, 2006), cooperative control of unmanned underwater vehicles (Stilwell and Bishop, 2000), and robot manipulators grasping the same object (Caccavale *et al.*, 1998).

Virtual structure approach: In the virtual structure approach, the entire formation is treated as a single virtual body (Scharf *et al.*, 2004). The specified dynamics of the virtual body are used to generate reference trajectories for agents to track using individual agent controllers. Accordingly, the formation can be treated conceptually as a virtual structure with placeholders describing the desired motion of the individual agents (Young *et al.*, 2001). The application of this approach to formations of mobile robots is described in Lewis and Tan (1997) and to formations of spacecraft in Beard and Hadaegh (1998); Beard *et al.* (2001). In Young *et al.* (2001), formation control of a virtual structure of a group of mobile robots has been considered, and group feedback is introduced from the robots to the virtual structure to improve group stability and robustness.

A variant of this approach is to use virtual vehicles to define the reference trajectories of individual agents in the team. In a leader-follower framework, the virtual vehicle approach consists of using a virtual copy of the leader to act as an observer for the leader's states through a virtual control law. The virtual vehicle approach has been proposed for coordinated control of robots (Egerstedt *et al.*, 2001; Hu *et al.*, 2003) and ship replenishment (Kyrkjebø *et al.*, 2006).

1.3 Scope of thesis

The above applications and ideas have stimulated great interest and have led to the definition of many challenging problems in several application fields. This thesis explores two topics related to aerial vehicles formation control: The attitude synchronization problem of multiple rigid bodies and the formation control of Unmanned Aerial Vehicles (UAVs) capable of Vertical Take Off and Landing (VTOL). In the following sections, we motivate these two topics, highlight the particular control problems we discuss in this thesis, and review the relevant literature.

1.3.1 Attitude synchronization of rigid bodies

The attitude synchronization of multiple aerial vehicles involves the design of attitude control schemes so that a group of rigid bodies (or spacecraft) align their orientation (attitude) to a common final attitude. While all vehicles are assumed within a pre-defined geometric formation pattern, members of the team need to share their states information to generate appropriate control actions so that the group objective is achieved. This problem has been considered in deep space applications where replacing traditionally large and complex spacecraft with clusters of simpler micro-satellites was shown to present several advantages regarding mission performance and cost.

An interesting application of spacecraft formations is long baseline interferometry. Interferometry is a method to detect extra-solar planets for the Terrestrial Planet Finder (TPF). One of the concepts being considered for the TPF uses a formation of free-flying spacecraft, separated by hundreds of meters, equipped with optical sensors acting as an interferometer. The recent study in Lindensmith (2003) has revealed that free-flying spacecraft interferometer provides better performance than a structurally connected interferometer by allowing greater baselines, *i.e.*, distances between spacecraft, leading to greater resolutions. Spacecraft formations are also useful in synthetic aperture radar (SAR), where several satellites with SAR capabilities cooperate in formation to improve the amount and quality of data retrieved, and enables continuous measurements of different physical quantities of the Earth. This allows for measurements of atmospheric variations, terrain elevations, moving objects on the ground and water current fields, applicable to activities such as environmental monitoring, surveillance, oceanography and disaster detection. By using a team of satellites for science instrumentation, there is an enhanced fault-tolerance. If one small satellite should fail, it is easier to replace this by a new satellite, than to repair or change the instruments on the large single satellite. Attitude synchronization in the above applications is not only necessary to achieve the required task of the spacecraft formation, but it also allows spacecraft in Low Earth Orbit (LEO) to maintain tighter formations. As a matter of fact, spacecraft formations in LEO are subject to an atmospheric drag force, which can be effectively reduced by maintaining a small relative attitude error between spacecraft (Vandyke and Hall, 2006).

In Wang and Hadaegh (1996), a coordinated attitude control scheme for multiple micro-spacecraft with multiple leaders in the team has been proposed. The authors use the concept of *nearest neighbor* controller and show global asymptotic stability of the spacecraft formation. The same formulation was used in Wang *et al.* (1999) to develop one-leader based coordinated control laws for position and attitude control of a group of spacecraft. In Kang and Yeh (2002) the case where the leader satellite is not able to follow its reference attitude trajectory due to environmental disturbances is considered. A reference projection is proposed, so that the follower satellite is commanded to follow a combination of its reference attitude and the measured/communicated leader satellite attitude. Following the idea in Young *et al.* (2001), the authors in Ren and Beard (2002) presented a centralized implementation of a virtual structure coordination strategy, where formation feedback from spacecraft to the virtual structure has been introduced. In Ren and Beard (2004), the virtual structure approach has been applied in a decentralized scheme.

In Lawton and Beard (2000), the authors introduced the so-called *coupled dynamics* controller for the spacecraft attitude control problem, where behavior-based formation control strategies have been derived. The controller consists of an attitude alignment part and a formation keeping part. The authors in Lawton and Beard (2002) proposed an attitude alignment control scheme for a group of spacecraft, using a ring communication topology. The results in Lawton and Beard (2002) were extended to a more general communication graph in Ren (2007a). Similar problems have been considered in the work of Vandyke and Hall (2006), where globally significant kinematic error variables have been defined and used in the development of a class of decentralized attitude alignment laws. Based on the passivity approach, Arcaç (2007) developed synchronization algorithms, which have been extended to the attitude synchronization problem of rigid bodies in Bai *et al.* (2008). A different approach has been used in Ren (2007b) and Dimarogonas *et al.* (2009) to extend the leader-follower architecture by allowing communication between the followers and the leaders.

While measurements of spacecraft attitudes and angular velocities are required in the above approaches, a few works have been done when only absolute attitudes are available for feedback. This problem is attractive in the case where spacecraft angular velocities are either imprecisely measured or not measured to relieve the necessity of onboard velocity sensors, leading to reduced cost and weight of participating spacecraft. In addition, the implementation of redundant velocity-free control laws will enhance the reliability of the system to possible sensors failure. As a matter of fact, in a study on on-orbit failures, the author in Tafazoli (2009) has reported that the mechanical gyroscopes, used to provide angular velocity measurements, have high failure rates in the Attitude and Orbital Control Subsystem in a spacecraft. Therefore, a challenging control problem emphasized in this thesis is to design attitude synchronization schemes without the need of angular rate measurements.

The attitude synchronization problem is more challenging when the angular

velocity information is not available for feedback. In fact, the design of nonlinear observers that provide estimates of the missing angular velocity and relative angular velocities between neighboring spacecraft is a difficult task due to the nonlinear attitude dynamics. The main complication comes from the fact that the angular velocity cannot be integrated to an equivalent orientation variable. In the case of a single rigid body, or spacecraft, some attempts to solve this problem have been reported in the literature, such as the work of Salcudean (1991) and Caccavale and Villani (1999). In the former reference, an angular velocity observer was proposed without any proof for the stability of the overall closed-loop system (observer-controller). The latter paper gives a local attitude trajectory tracking control scheme based on the combined controller-observer design proposed in Berghuis and Nijmeijer (1993a). The authors in Lizarralde and Wen (1996) proposed a velocity-free control scheme for rigid-body attitude stabilization using a lead filter to preserve the passivity of the closed loop system. A similar approach was used in Tsotras (1998) where the Modified Rodriguez Parameters (MRP) representation of the attitude is considered. The extension of the above mentioned controllers to the attitude tracking problem is not an obvious task especially when seeking a global result (Caccavale and Villani, 1999; Costic *et al.*, 2001; Akella, 2001; Singla *et al.*, 2006). It is important to point out that the lead filter-based control scheme has been proposed in the work of Berghuis and Nijmeijer (1993b) to solve the regulation problem of robot manipulators without velocity measurements.

The lead filter method has been applied in Lawton and Beard (2002) to the multi-spacecraft attitude alignment problem without velocity measurements. Using the unit-quaternion representation for spacecraft rotations, the authors provide a local velocity-free scheme when a ring communication topology is assumed. In Ren (2009), the MRP representation have been used to extend the work of Lawton and Beard (2002) to the case of a general undirected communication topology. Besides the fact that the MRP representation presents a singularity, the authors consider the case where the final angular velocity is zero, and the extension of the obtained results to the trajectory tracking case is not obvious. The two velocity-free control laws proposed in Caccavale and Villani (1999) have been extended to the attitude control of two spacecraft in a leader-follower architecture in Kristiansen *et al.* (2009), using lead filters, and in Grötli and Gravdahl (2008), using the combined observer-controller design, and uniform practical stability is shown in both works.

More recently, a unit-quaternion-based velocity-free attitude tracking control scheme for a single spacecraft has been proposed in Tayebi (2008). The requirement of the angular velocity is obviated by the introduction of an auxiliary system. The main difference between the lead filter in Lizarralde and Wen (1996) and the auxiliary system proposed in Tayebi (2008) resides on the construction of the latter system based on the nonlinear quaternion dynamics, which is more natural when dealing with orientation as compared to linear filters. As a result, almost global stability results are achieved. Note that besides the fact that the quaternion representation

of the attitude is globally nonsingular, almost global stability is the best one can achieve using continuous control schemes for the attitude control problem (Bhat and Bernstein, 2000).

1.3.2 Formation control of VTOL UAVs

Advances in avionics and flight control techniques have brought unmanned aerial vehicle (UAV) technology to a point where it is routinely used in applications where human interaction is difficult or dangerous. These applications range from military to civilian and include reconnaissance operations, border patrol missions, forest fire detection, surveillance and search and rescue missions. In simple applications, a single autonomous vehicle can be managed by a crew using a ground station provided by the vehicle manufacturer. The execution of more challenging missions, however, requires the use of multiple vehicles working in cooperation to achieve a common objective. When deployed in a formation, UAVs engaged in surveillance or exploration activity are typically able to synthesize an antenna of dimension far larger than an individual vehicle (Anderson *et al.*, 2008).

For this type of applications, the research in the area of autonomous aerial vehicles has recently moved beyond considering a single vehicle. Researchers have considered aerial pursuit/evasion games in three dimensions on a fixed-wing aircraft by implementing and testing a nonlinear model-predictive tracking controller (Eklund *et al.*, 2005). In Gu *et al.* (2006), formation control using YF-22 research UAVs has been demonstrated, where a follower aircraft is driven to maintain a formation with a radio controlled leader.

While reasonable amount of work has been achieved with fixed wing UAV's, less work exists in the literature dealing with formations of the class of VTOL UAVs, which includes several types of thrust propelled aircraft such as helicopters, quad-rotor and ducted fan vehicles. This type of aircraft constitutes an important class of UAVs with their ability to hover and maneuver in confined or restricted areas making them suitable for a broad range of applications requiring stationary flights like surveillance and monuments/bridge inspection. In Fahimi (2008), a geometrical formation scheme for a group of helicopters is presented. The authors propose a sliding mode controller to deal with external disturbances, where the boundedness of the systems states is an essential assumption to achieve the stability of the system. A conceptually similar approach to formation control of the same systems has been discussed in Saffarian and Fahimi (2009) using nonlinear model predictive control. However, the formation control of the general class of VTOL UAVs still poses several problems.

Without any doubt, the formation control of multiple vehicles relies on strong individual vehicle control methods and the non-negligible results in the motion coordination of multi-agent systems. Networks of multi-agent systems with simple dynamics have been extensively considered in the recent literature leading to several interesting

control algorithms (see for instance Fax and Murray, 2004; Jadbabaie *et al.*, 2003; Lee and Spong, 2007; Mesbahi and Hadaegh, 2001; Olfati-Saber, 2006; Tanner *et al.*, 2007, and references therein). However, the main difficulty in the control of formations of VTOL aircraft resides on the under-actuated nature of these systems and the lack of simple control design methods for a single aircraft in this class. In fact, the position control of a single VTOL UAV in SE(3) is a very challenging problem especially when it is desirable to achieve global or semi-global results. This can be noticed from the several attempts to solve this problem in the literature, such as the feedback linearization method in Koo and Sastry (1998), the backstepping approach in Frazzoli *et al.* (2000), Hamel *et al.* (2002), Pflimlin *et al.* (2007) and Aguiar and Hespanha (2007), the sliding mode technique in Madani and Benallegue (2007), and other control strategies based on gain scheduling (Kaminer *et al.*, 1998) or on a nested saturation technique (Kendoul *et al.*, 2006).

The above control schemes rely on perfect knowledge of the aircraft linear-velocity. For flying vehicles, velocity estimations can be obtained via approximate derivation of the successive measurements from GPS sensors. For fast moving vehicles, the standard procedure consists of integrating the acceleration, and coupling this result with the derivative of the GPS measurements (Benzemrane *et al.*, 2007). This estimation method suffers from several problems, namely the fact that the errors induced by a GPS system may reach many meters, and in practice, numerical integration along with measurement noise introduces a very fast growing velocity measurement error. There are several technical solutions to overcome these problems such as using high-precision sensors like D-GPS. However, the GPS signal is not available in indoor and urban applications (structure/bridge inspection for example) due to signal blockage and attenuation, which may deteriorate the positioning accuracy. To solve the linear-velocity estimation problem without the use of a GPS, several authors have considered the combination of artificial vision and the inertial sensors as done in Cheviron *et al.* (2007) and Rondon *et al.* (2009). Another solution is to use observers to estimate the missing states, as done in Do *et al.* (2003), where the trajectory tracking problem of a *planar*-VTOL is treated. It is worth mentioning that in the case where a GPS is not available, there are several techniques that allow to obtain the UAV position, such as the combination of an inertial measurement unit (IMU) with a vision system; or the use of a network of Ultra-wideband (UWB) receivers which track a large number of small (inexpensive) UWB transmitters.

The main objective in this part of the thesis is to propose solutions to the formation control problem of the class of under-actuated VTOL aircraft when the full state vector is available for feedback and in the case where aircraft linear-velocities are not measured. The latter problem is not only motivated by the practical applications discussed above, it is also important from a theoretical viewpoint since no real solution to this problem in the case of a single VTOL aircraft can be found in the literature. The first step towards achieving these objectives is to develop a simple and effective control design methodology for a single VTOL aircraft. In fact,

we propose a singularity-free control design procedure allowing to effectively separate the translational and rotational input design leading to global results. However, this control design method requires as a first step the design of an intermediary input subject to some constraints. These constraints make the application of formation control laws developed for linear multi-agents difficult and in some cases not trivial especially when linear-velocities are not available for feedback.

In addition, we consider the problem of communication delays that are often present in data transmission systems. The effects of communication delays in multi-agent systems with first and second order dynamics has been studied respectively in Olfati-Saber and Murray (2004), Wang and Slotine (2006), Lee and Spong (2006), Sun and Wang (2009) and Münz *et al.* (2008), Seuret *et al.* (2009) to cite a few, and sufficient conditions have been derived to achieve the stability of the system. In Münz *et al.* (2008) and Seuret *et al.* (2009) for example, the authors consider the Rendezvous problem of multi agents and provide different delay dependent conditions using Lyapunov-Krasovskii functionals. The authors in Hong-Yong *et al.* (2010) use the Nyquist stability criterion in the analysis of leader-following consensus algorithms in the presence of input and communication delays, assuming that the velocity of the leader is constant. A particular case of this last problem (zero leader's velocity) has been discussed in Meng *et al.* (2010), where the authors show that Lyapunov-Krasovskii functionals can provide sufficient conditions based on the solution of a linear matrix inequality. The output consensus problem of higher order linear single-input single output systems has been discussed in Münz *et al.* (2010) using the generalized Nyquist criterion. It is important to mention that the above analysis tools are generally used when the coupling between agents is linear, such as using linear differences to define the relative states of agents.

The communication delays in nonlinear systems have also been considered to solve the spacecraft formation control problem, (Chung *et al.*, 2009), and the synchronization of bilateral teleoperators (Polushin *et al.*, 2006; Chopra *et al.*, 2008; Nuño *et al.*, 2010). However, only a few work has been done for nonlinear systems with nonlinear coupling that may arise when control saturations are considered for example. In this context, the work of Chopra and Spong (2006) presents an output synchronization scheme for passive nonlinear systems with nonlinear coupling. The authors use the scattering variables formulation and show that output synchronization is achieved for arbitrary time delays between communicating members of the team. An important assumption in the above papers, however is that the full state vector is available for feedback.

In spite of the interesting results cited above, much work remains to be done to develop control algorithms for a group of vehicles with complex dynamics in the presence of communication delays and take into consideration the systems input constraints in the full and partial state information cases. These difficulties are specially challenging for the class of under-actuated VTOL UAVs since, as will become clear

throughout the thesis, the aircraft input is subject to several constraints and some of the aircraft states are not generally available or precisely measured.

1.4 Statement of contributions

In this thesis, several contributions to coordinated motion control of multiple aerial vehicles are presented. Different output feedback attitude synchronization schemes are proposed for spacecraft formations. The principle of auxiliary systems, acting as indirect observers for spacecraft angular velocities and relative angular velocities, constitutes the heart of the proposed approaches to solve this problem. As for the control of VTOL aircraft, we proposed a control design procedure that is shown to be effective in separating the translational and rotational input design, and applicable to the trajectory tracking control of a single aircraft as well as to formations of aircraft governed by a similar model. Using this design method, state feedback and output feedback formation control schemes are presented. Also, solutions to these problems when the communication between aircraft is delayed are provided.

The contributions of the work presented in this thesis can thus be summarized as follows:

- Several solutions to the output feedback attitude synchronization for spacecraft formations are presented. The proposed design approach is inspired by the concept of the first-order auxiliary system introduced in the attitude tracking of a single spacecraft in Tayebi (2008). Two output feedback design methods are proposed based on auxiliary systems with different order. Using either methods depends on the problem requirements as each method presents some advantages and limitations discussed in details in Chapter 3. These methods are applied to solve two attitude synchronization problems already discussed in the full state information case, namely the simultaneous attitude tracking and synchronization and the attitude synchronization without reference trajectory. The proposed output feedback schemes achieve similar results as in the full state information case and, in some situations, reduce the information exchange requirement between spacecraft in the team. It is worth pointing out that by removing the velocity measurements for a formation with a large number of spacecraft, we reduce the cost related to the sensors and the communication flow between spacecraft, and guarantee a certain level of immunity against angular velocity sensors failure.

Contrary to the velocity-free synchronization schemes available in the literature, the proposed output feedback design methods allow to handle time-varying reference trajectories, and achieve almost global stability results with *a priori* bounded inputs. The obtained results in this part have been published in Abdessameud and Tayebi (2008*a,b*, 2009*a,b*).

- For VTOL UAVs, a simple control design procedure for this class of systems is presented in Chapter 4. We exploit the cascade nature of the aerial system to derive an extraction algorithm for the system thrust and orientation. The thrust input is applied to the translational dynamics and the input torque is designed to track the extracted aircraft orientation. In this way, the translational dynamics are reduced to the dynamics of a perturbed linear system with a constrained intermediary input. The main difference between the proposed extraction algorithm and existent extraction methods is that it provides non-singular solutions in terms of the unit-quaternion representation of the attitude of a rigid body. The proposed design procedure constitutes the main step in all the control schemes discussed in the remaining parts of this thesis. The author would like to acknowledge the contribution of his Ph.D. colleague Andrew Roberts who participated in developing the extraction algorithm and defining the necessary conditions under which it is applicable.
- In the framework of trajectory tracking of a single VTOL aircraft, state and output feedback control schemes are proposed. The state feedback controller complements the literature by providing a global result in terms of the position. In the case where the linear-velocity information is not available for feedback, the proposed output feedback control action can be considered as a first solution to this problem for the class of under-actuated systems under study. The requirement of the linear-velocity is obviated by using a partial state feedback in the translational control and a nonlinear observer in the rotational input design. Instrumental in this scheme are second-order auxiliary systems used to reduce the design complexity and achieve global results. The contributions of the thesis in this part appeared in Abdessameud and Tayebi (2010a).
- Solutions to the formation control of VTOL aircraft in the full state information case and in the case where aircraft linear-velocities are not measured are presented. The extraction algorithm and the auxiliary systems are essential elements in the design of these schemes to achieve global results. The proposed state feedback formation control scheme has several advantages over classical methods when following the developed design procedure: First, the extraction algorithm condition can be satisfied without any considerations on the communication topology between aircraft; Second, the designer can set limits of the applied thrust to each aircraft independently from the number of its neighbors; Third, the torque input is simplified; and finally, the communication requirement between members of the team is considerably reduced.

For the output feedback case, the tracking control law for a single aircraft is extended to the formation control problem and sufficient conditions on the gains are derived to achieve the control objectives. Similarly to the single vehicle case, a partial state feedback and a nonlinear observer are used to obviate the need for the linear-velocity information. This scheme is then modified to reduce the

communication requirements between vehicles. The main modification consists on the introduction of a second auxiliary system that completely separates the translational and rotational dynamics in the stability analysis of the overall system. The above results are reported in Abdessameud and Tayebi (2009c, 2010b,c).

- In the case of delayed communication between VTOL aircraft, three control schemes are presented in the full state information case. The effect of constant communication delays on the performance of the state feedback formation control law described above is studied first, and sufficient delay-dependent conditions are established. This control law is modified next to the cases of bounded time-varying and arbitrary constant delays. When the linear-velocity is not measured, a virtual vehicle approach is proposed to design an output feedback formation control scheme with constant communication delays. With the lack of analysis methods when part of the state is not available and the communication is delayed, the virtual vehicle approach reduces the problem to the formation control of virtual vehicles with available states. Similarly to the delay-free case, the obtained results are global in terms of the position. The contribution of the thesis in this part are reported in Abdessameud and Tayebi (2010g,f).
- The auxiliary systems used in the design of the control schemes for VTOL UAVs, with the results of Lemma 2.6, can be considered as a new control technique for systems with input saturations. In fact, this technique is suitable in the design of control laws for networks of multi-vehicles modeled as double integrators with input saturations in the cases where the velocity is not available for feedback and/or the presence of communication delays. This constitutes a new contribution in this area since these three problems cannot be considered simultaneously using available control methods. In fact, this control approach have been successfully applied to multi-agent systems modeled by second order dynamics in Abdessameud and Tayebi (2010h,d,e).

1.4.1 List of publications

The following list contains the publications produced during the course of the work presented in this thesis, including also recently submitted papers:

Journal publications:

- Abdessameud, A. and Tayebi, A. (2009). Attitude synchronization of a group of spacecraft without velocity measurements. *IEEE Transactions on Automatic Control*, 54(11), 2642-2648.

- Abdessameud, A. and Tayebi, A. (2010). Global trajectory tracking control of VTOL-UAVs without linear velocity measurements. *Automatica*, 46(6), 1053-1059.
- Abdessameud, A. and Tayebi, A. (2010). Motion Coordination of a group of VTOL UAVs. (Submitted).
- Abdessameud, A. and Tayebi, A. (2010). Formation Stabilization of VTOL Unmanned Aerial Vehicles with Communication Delays. (Submitted).

Refereed conference publications:

- Abdessameud, A. and Tayebi, A. (2008). Decentralized Attitude Alignment control of Spacecraft within a Formation Without Velocity Measurements. *In Proceedings of the 17th IFAC World Congress*, 1766-1771.
- Abdessameud, A. and Tayebi, A. (2008). Attitude Synchronization of a Spacecraft Formation Without Velocity Measurement. *In Proceedings of the 47th IEEE Conference on Decision and Control*, 3719-3724.
- Abdessameud, A. and Tayebi, A. (2009). On the coordinated attitude alignment of a group of spacecraft without velocity measurements. *In Proceedings of the 48th IEEE Conference on Decision and Control*, 1476-1481.
- Abdessameud, A. and Tayebi, A. (2009). Formation control of VTOL-UAVs. *In Proceedings of the 48th IEEE Conference on Decision and Control*, 3454-3459.
- Abdessameud, A. and Tayebi, A. (2010). Formation Control of VTOL UAVs Without Linear-Velocity Measurements. *In Proceedings of the American Control Conference*, 2107-2112.
- Abdessameud, A. and Tayebi, A. (2010). Formation stabilization of VTOL UAVs subject to communication delays. *IEEE Conference on Decision and Control*, To appear.

In addition, the following publications were also produced during the same period of time, including the application of some of the proposed solutions to multi-agent networks.

Journal publications:

- Abdessameud, A. and Tayebi, A. (2010). On consensus algorithms for double-integrator dynamics without velocity measurements and with input constraints. *Systems and Control Letters*, 59, 812-821.

Refereed conference publications:

- Abdessameud, A., and Tayebi, A. (2010). Velocity-free consensus algorithms for double-integrator dynamics with input saturations constraints. *The 49th IEEE Conference on Decision and Control*, To appear.
- Abdessameud, A., and Tayebi, A. (2010). Consensus of Double-integrator Multi-agents under Communication Delays – The Partial State Feedback Case. (Submitted).

1.5 Thesis outline

This thesis is organized as follows:

Chapter 2 presents the notation, background and preliminaries used throughout the thesis. Also, the dynamic model of the aerial vehicles considered in this work and some definitions from graph theory are given to model the information flow between members of the team.

Chapter 3 is devoted to the output feedback attitude synchronization problem of multiple rigid bodies. It presents the principle of auxiliary systems used to obviate the requirement of angular velocity measurements, and proposes several output feedback control schemes to synchronize the attitudes of a group of spacecraft with and without reference trajectory assignment. Stability results are presented, and the results are verified through simulation examples.

Chapter 4 presents a new control design methodology for a class of under-actuated VTOL aircraft. Global trajectory tracking control schemes for a single VTOL aircraft are proposed in the full state information case and in the case where the aircraft linear-velocity is not available for feedback. Stability results are presented, and simulation results are given to illustrate the effectiveness of the obtained results.

Chapter 5 is devoted to the formation control problem of VTOL aircraft. Following the control design method developed in Chapter 4, solutions to the problem of steering a group of VTOL aircraft to a desired formation with a reference linear-velocity are provided in the full and partial state information cases. Stability results are presented, and the effectiveness of the obtained results is shown through simulations.

Chapter 6 presents formation control schemes for VTOL UAVs in the presence of communication delays, which provide delay-dependent and delay-independent results in the full state information case. Also, it introduces the virtual vehicle approach used

to design a linear-velocity-free formation control scheme with constant communication delays. Stability results are presented using Lyapunov-Krasovskii functionals, and the results are validated through simulations.

Chapter 7 presents some concluding remarks on the motion coordination schemes proposed in this thesis.

Appendix A presents the detailed proofs of lemmas and theorems stated throughout this thesis.

Chapter 2

Background and preliminaries

This chapter presents the notation, background and some preliminary results that are employed throughout the thesis. The mathematical model of the aerial vehicles considered in this work is given and the information flow between members of the group is modeled using some definitions from graph theory.

2.1 Notation

In the following, \mathbb{R} denotes the set of all real numbers, the Euclidean n -dimensional space is denoted by \mathbb{R}^n , $\text{SO}(3)$ is the Special Orthogonal group of order three, and $\text{SE}(3)$ denotes the Special Euclidian group. The notation $\|\cdot\|$ is used for the Euclidean norm of a vector and the induced \mathcal{L}_2 norm of a matrix, and $\|\cdot\|_\infty$ is used for the ∞ -norm of a vector. The identity matrix of dimension n is denoted by \mathbf{I}_n . The time derivative of a vector \mathbf{x} is denoted by $\dot{\mathbf{x}}$, *i.e.*, $\dot{\mathbf{x}} = d\mathbf{x}/dt$, and moreover, $\ddot{\mathbf{x}} = d^2\mathbf{x}/dt^2$ and $\dddot{\mathbf{x}} = \mathbf{x}^{(3)} = d^3\mathbf{x}/dt^3$, For sake of clarity of presentation, the argument of all time-dependent signals (vectors) will be omitted [*e.g.* $\mathbf{x} \leftrightarrow \mathbf{x}(t)$], except for those which are time delayed [*e.g.* $\mathbf{x}(t - \tau)$ for a constant delay and $\mathbf{x}(t - \tau(t))$ for time-varying delay]. Accordingly, the argument of the signals inside an integral is omitted, which is assumed to be equal to the variable on the differential, unless otherwise stated [*e.g.* $\int_0^t \mathbf{x} ds \leftrightarrow \int_0^t \mathbf{x}(s) ds$]. Also, the limit of a signal at infinity is replaced by an arrow [*e.g.* $\mathbf{x} \rightarrow 0 \leftrightarrow \lim_{t \rightarrow \infty} \mathbf{x}(t) = 0$, and $\mathbf{x} \rightarrow \mathbf{y} \leftrightarrow \lim_{t \rightarrow \infty} \mathbf{x}(t) = \lim_{t \rightarrow \infty} \mathbf{y}(t)$].

2.2 System modeling

In this section, we derive the dynamic equations of the systems considered in this thesis. Aerial vehicles are governed by their translational and rotational dynamics. For the orientation, the attitude representation adopted in this work is defined and the attitude dynamics of a rigid body are derived. Next, the translational dynamics of a VTOL aircraft are given.

2.2.1 Coordinate frames

To represent the position and orientation of a vehicle, we use coordinate frames given by a set of three orthonormal vectors that obey the right hand rule. The inertial frame, denoted by \mathcal{F}_o , is attached to a point in the surface of the Earth. We associate to \mathcal{F}_o the set of axes $\{\hat{e}_1, \hat{e}_2, \hat{e}_3\}$, where \hat{e}_1 points North, \hat{e}_2 points East and \hat{e}_3 points towards the center of the Earth assumed to be flat. The frame attached to the center of gravity of a vehicle is referred to as the body frame and is denoted by \mathcal{F}_i , where $i = b$ in the case of a single vehicle and $i \in \mathcal{N} := \{1, \dots, n\}$ in the case of n -vehicles. We associate to \mathcal{F}_i the set of axes $\{\hat{e}_{1i}, \hat{e}_{2i}, \hat{e}_{3i}\}$, where \hat{e}_{1i} is directed towards the front of the vehicle, \hat{e}_{2i} points to the right and \hat{e}_{3i} is directed downwards.

2.2.2 Attitude representation - Unit quaternion

The orientation of a vehicle is represented in this thesis in terms of the four-parameters representation known as unit-quaternion (Shuster, 1993). The quaternion

$$\mathbf{Q} = (\mathbf{q}^T, \eta)^T, \quad (2.1)$$

is composed of a vector $\mathbf{q} \in \mathbb{R}^3$ and a scalar component $\eta \in \mathbb{R}$, satisfying the unity constraints

$$\eta^2 + \mathbf{q}^T \mathbf{q} = 1, \quad (2.2)$$

and a rotation by an angle ϑ about an arbitrary axis denoted by the unit vector $\kappa \in \mathbb{R}^3$ can be described by a unit-quaternion \mathbf{Q} such that

$$\mathbf{q} = \kappa \sin\left(\frac{\vartheta}{2}\right) \quad \eta = \cos\left(\frac{\vartheta}{2}\right). \quad (2.3)$$

The rotation matrix that brings the inertial frame into the body frame is related to the corresponding unit-quaternion \mathbf{Q} through the Rodriguez formula

$$\mathbf{R}(\mathbf{Q}) = (\eta^2 - \mathbf{q}^T \mathbf{q})\mathbf{I}_3 + 2\mathbf{q}\mathbf{q}^T - 2\eta\mathbf{S}(\mathbf{q}), \quad (2.4)$$

where the matrix $\mathbf{S}(\cdot)$ is the cross product operator given by

$$\mathbf{S}(\mathbf{x}) = \begin{pmatrix} 0 & -x_3 & x_2 \\ x_3 & 0 & -x_1 \\ -x_2 & x_1 & 0 \end{pmatrix}, \quad (2.5)$$

with $\mathbf{x} = (x_1, x_2, x_3)^T$. In addition, the inverse rotation is given by the inverse unit-quaternion \mathbf{Q}^{-1} as

$$\mathbf{Q}^{-1} = (-\mathbf{q}^T, \eta)^T. \quad (2.6)$$

The set of quaternion is a vector space over \mathbb{R}^4 , which provides a globally nonsingular parametrization of the $SO(3)$ group of rotation matrices. The set forms a group with quaternion multiplication, which is distributive and associative, but not commutative, and the quaternion multiplication of two quaternion $\mathbf{Q}_1 = (\mathbf{q}_1^T, \eta_1)^T$ and $\mathbf{Q}_2 = (\mathbf{q}_2^T, \eta_2)^T$ is defined as

$$\mathbf{Q}_1 \odot \mathbf{Q}_2 = \begin{pmatrix} \eta_1 \mathbf{q}_2 + \eta_2 \mathbf{q}_1 + \mathbf{S}(\mathbf{q}_1) \mathbf{q}_2 \\ \eta_1 \eta_2 - \mathbf{q}_1^T \mathbf{q}_2 \end{pmatrix}, \quad (2.7)$$

with the identity element $(\mathbf{0}^T, 1)^T \in \mathbb{R}^4$. It should be noted that the quaternion representation is an inherent redundant representation. Due to this redundancy, \mathbf{Q} and $-\mathbf{Q}$ represent the same physical orientation, however one is rotated 2π relative to the other about an arbitrary axis.

2.2.3 Rotational dynamics

Let the orientation of a rigid body be represented by the unit-quaternion \mathbf{Q} . The time-derivative of the rotation matrix $\mathbf{R}(\mathbf{Q})$ given in (2.4) can be obtained as

$$\dot{\mathbf{R}}(\mathbf{Q}) = -\mathbf{S}(\boldsymbol{\omega})\mathbf{R}(\mathbf{Q}), \quad (2.8)$$

with $\boldsymbol{\omega}$ is the angular velocity of the body expressed in the body-fixed frame, \mathcal{F}_b , and $\mathbf{S}(\cdot)$ is described in (2.5). The kinematic differential equation of the attitude of the rigid body can be obtained as (Shuster, 1993)

$$\dot{\mathbf{Q}} = \mathbf{T}(\mathbf{Q})\boldsymbol{\omega}, \quad (2.9)$$

with $\mathbf{T}(\mathbf{Q})$ is given by

$$\mathbf{T}(\mathbf{Q}) = \frac{1}{2} \begin{pmatrix} \eta \mathbf{I}_3 + \mathbf{S}(\mathbf{q}) \\ -\mathbf{q}^T \end{pmatrix}, \quad (2.10)$$

and satisfies $\mathbf{T}(\mathbf{Q})^T \mathbf{T}(\mathbf{Q}) = \mathbf{I}_3$. The rotational dynamics of the rigid body can be derived using the Euler's moment equation as (Shuster, 1993)

$$\mathbf{J}_f \dot{\boldsymbol{\omega}} = \boldsymbol{\Gamma} - \mathbf{S}(\boldsymbol{\omega})\mathbf{J}_f \boldsymbol{\omega}, \quad (2.11)$$

with $\mathbf{J}_f \in \mathbb{R}^{3 \times 3}$ is the symmetric positive definite constant inertia matrix of the body with respect to \mathcal{F}_b and $\boldsymbol{\Gamma} \in \mathbb{R}^3$ is the external torque applied to the system expressed in \mathcal{F}_b .

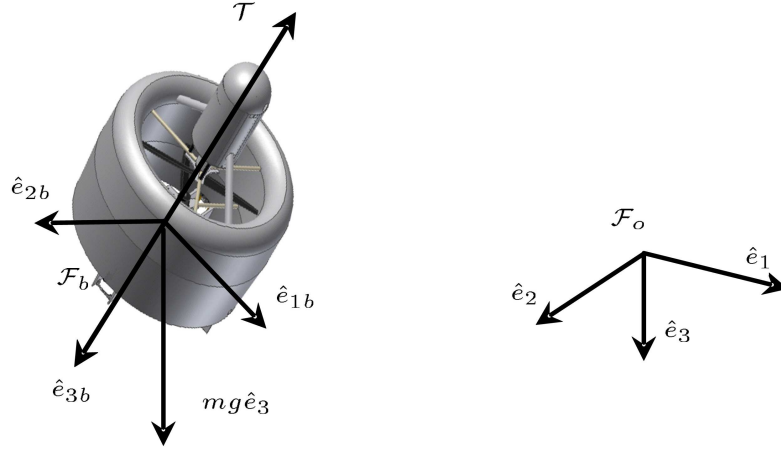


Figure 2.1: VTOL aircraft (Courtesy of A. Roberts)

2.2.4 Translational dynamics of VTOL UAVs

An example of a thrust propelled VTOL aerial vehicle is depicted in Fig. 2.1. The translational motion of the vehicle is generated using a positive thrust input directed in the \hat{e}_{3b} direction, whereas the rotational motion is controlled by a three component torque input. Therefore, the rotational dynamics of the VTOL aircraft are described by the dynamics given in (2.9)-(2.11). Let the position and linear-velocity of the aerial vehicle in \mathcal{F}_o be denoted respectively by $\mathbf{p} \in \mathbb{R}^3$ and $\mathbf{v} \in \mathbb{R}^3$ with $\mathbf{v} = \dot{\mathbf{p}}$. The translational dynamics can be derived using Newton's equation of motion as

$$\dot{\mathbf{v}} = g\hat{e}_3 - \frac{\mathcal{T}}{m}\mathbf{R}(\mathbf{Q})^T\hat{e}_3, \quad (2.12)$$

where m and g denote respectively the mass of the aircraft and the gravitational acceleration and the positive scalar \mathcal{T} represents the magnitude of the thrust applied to the vehicle in the direction of \hat{e}_{3b} .

It should be noticed that the VTOL UAV is an under-actuated system since the force responsible for the translational motion is generated in a single direction, and the two other components of the position vector cannot be “directly” controlled.

2.3 Attitude error

In this thesis, we will need two types of attitude errors; the attitude tracking error and the relative attitude. The attitude tracking error describes the orientation mismatch between the body fixed frame and an assigned desired frame, whereas the relative attitude is the discrepancy between the orientations of two different bodies.

2.3.1 Attitude tracking error

Consider a group of n -vehicles governed by the orientation dynamics described in the previous section. Let the orientation of the i^{th} aerial vehicle be represented by the unit-quaternion $\mathbf{Q}_i = (\mathbf{q}_i^T, \eta_i)^T$ and let the orientation of the desired frame assigned to the i^{th} aerial vehicle be represented by $\mathbf{Q}_{d_i} = (\mathbf{q}_{d_i}^T, \eta_{d_i})^T$. The attitude tracking error describing the discrepancy between the vehicle's attitude and its assigned desired attitude is represented by the unit-quaternion $\tilde{\mathbf{Q}}_i = (\tilde{\mathbf{q}}_i^T, \tilde{\eta}_i)^T$, and is defined as

$$\tilde{\mathbf{Q}}_i = \mathbf{Q}_{d_i}^{-1} \odot \mathbf{Q}_i. \quad (2.13)$$

The attitude error dynamics can be described similar to (2.9) as

$$\dot{\tilde{\mathbf{Q}}}_i = \mathbf{T}(\tilde{\mathbf{Q}}_i) \tilde{\boldsymbol{\omega}}_i, \quad \mathbf{T}(\tilde{\mathbf{Q}}_i) = \frac{1}{2} \begin{pmatrix} \tilde{\eta}_i \mathbf{I}_3 + \mathbf{S}(\tilde{\mathbf{q}}_i) \\ -\tilde{\mathbf{q}}_i^T \end{pmatrix}, \quad (2.14)$$

where

$$\tilde{\boldsymbol{\omega}}_i = \boldsymbol{\omega}_i - \mathbf{R}(\tilde{\mathbf{Q}}_i) \boldsymbol{\omega}_{d_i}, \quad (2.15)$$

is the angular velocity tracking error vector, $\boldsymbol{\omega}_{d_i}$ is the desired angular velocity of the i^{th} aircraft, which is related to \mathbf{Q}_{d_i} as

$$\dot{\boldsymbol{\omega}}_{d_i} = 4\mathbf{T}(\mathbf{Q}_{d_i})^T \dot{\mathbf{Q}}_{d_i}, \quad (2.16)$$

and the matrix $\mathbf{R}(\tilde{\mathbf{Q}}_i)$ is the rotation matrix related to $\tilde{\mathbf{Q}}_i$, and is given by

$$\mathbf{R}(\tilde{\mathbf{Q}}_i) = \mathbf{R}(\mathbf{Q}_i) \mathbf{R}(\mathbf{Q}_{d_i})^T. \quad (2.17)$$

We can see that attitude tracking is achieved when \mathbf{Q}_i coincides with \mathbf{Q}_{d_i} , or $\tilde{\mathbf{Q}}_i = (0, 0, 0, \pm 1)^T$, which corresponds to the same orientation due to the inherent redundancy of the quaternion representation.

An important property necessary in the control schemes presented in this work is given as follows.

Property 2.1. *The following relation holds:*

$$\left(\mathbf{R}(\mathbf{Q}_i)^T - \mathbf{R}(\mathbf{Q}_{d_i})^T \right) \hat{e}_3 = 2\mathbf{R}(\mathbf{Q}_i)^T \mathbf{S}(\bar{\mathbf{q}}_i) \tilde{\mathbf{q}}_i, \quad (2.18)$$

with \hat{e}_3 is the third axis associated to \mathcal{F}_o , $\tilde{\mathbf{q}}_i = (\tilde{q}_{1i}, \tilde{q}_{2i}, \tilde{q}_{3i})^T$, $\bar{\mathbf{q}}_i = (\tilde{q}_{2i}, -\tilde{q}_{1i}, -\tilde{\eta}_i)^T$ and $\mathbf{S}(\cdot)$ is defined in (2.5).

This property can be verified using the definition of the rotation matrix and the attitude tracking error. In fact, using (2.17), we can show that

$$\left(\mathbf{R}(\mathbf{Q}_i)^T - \mathbf{R}(\mathbf{Q}_{d_i})^T\right) \hat{e}_3 = \mathbf{R}(\mathbf{Q}_i)^T \left(\mathbf{I}_3 - \mathbf{R}(\tilde{\mathbf{Q}}_i)\right) \hat{e}_3. \quad (2.19)$$

Then, using (2.4), we can write

$$\begin{aligned} \left(\mathbf{I}_3 - \mathbf{R}(\tilde{\mathbf{Q}}_i)\right) \hat{e}_3 &= 2 \begin{pmatrix} \tilde{\eta}_i \tilde{q}_{2i} - \tilde{q}_{1i} \tilde{q}_{3i} \\ -\tilde{\eta}_i \tilde{q}_{1i} - \tilde{q}_{2i} \tilde{q}_{3i} \\ (\tilde{q}_{1i}^2 + \tilde{q}_{2i}^2) \end{pmatrix} \\ &= 2 \begin{pmatrix} 0 & \tilde{\eta}_i & -\tilde{q}_{1i} \\ -\tilde{\eta}_i & 0 & -\tilde{q}_{2i} \\ \tilde{q}_{1i} & \tilde{q}_{2i} & 0 \end{pmatrix} \begin{pmatrix} \tilde{q}_i \\ \tilde{q}_{2i} \\ \tilde{q}_{3i} \end{pmatrix}. \end{aligned}$$

2.3.2 Relative attitude

The relative attitude between the i^{th} and j^{th} vehicles is represented by the unit-quaternion $\mathbf{Q}_{ij} = (\mathbf{q}_{ij}^T, \eta_{ij})^T$, and is defined as

$$\mathbf{Q}_{ij} = \mathbf{Q}_j^{-1} \odot \mathbf{Q}_i, \quad (2.20)$$

and analogous to (2.14), the relative attitude kinematics can be represented as

$$\dot{\mathbf{Q}}_{ij} = \mathbf{T}(\mathbf{Q}_{ij}) \boldsymbol{\omega}_{ij}, \quad (2.21)$$

$$\boldsymbol{\omega}_{ij} = \boldsymbol{\omega}_i - \mathbf{R}(\mathbf{Q}_{ij}) \boldsymbol{\omega}_j, \quad (2.22)$$

where the vector $\boldsymbol{\omega}_{ij}$ is the relative angular velocity of \mathcal{F}_i with respect to \mathcal{F}_j expressed in \mathcal{F}_i and $\mathbf{R}(\mathbf{Q}_{ij})$ is the rotation matrix related to \mathbf{Q}_{ij} , which represents the rotation from \mathcal{F}_j to \mathcal{F}_i , and is given by

$$\mathbf{R}(\mathbf{Q}_{ij}) = \mathbf{R}(\mathbf{Q}_i) \mathbf{R}(\mathbf{Q}_j)^T \quad (2.23)$$

Therefore, using (2.20) and (2.23), we can verify the following relations

$$\mathbf{R}(\mathbf{Q}_{ji})^T = \mathbf{R}(\mathbf{Q}_{ij}), \quad (2.24)$$

$$\mathbf{q}_{ji} = -\mathbf{q}_{ij} = -\mathbf{R}(\mathbf{Q}_{ji}) \mathbf{q}_{ij}. \quad (2.25)$$

Note that the relative attitude between the i^{th} and j^{th} vehicles can be either computed in each vehicle using the above relations if their absolute attitudes are communicated to each other, or measured if each spacecraft is equipped with relative attitude sensors.

2.4 Stability definitions

This thesis considers stability in the sense of Lyapunov, which can be deduced by analysis of energy-like functions whose time-derivatives satisfy certain conditions. The stability definitions in the general Lyapunov sense are usually stated as stability properties of the equilibrium points (or sets) of systems. An equilibrium is said to be stable if any solution of the system starting sufficiently close remains arbitrary close for all future time. In contrast, an equilibrium which is not stable is said to be unstable. Furthermore, if the solutions of the system converge to the stable equilibrium from any initial conditions within a domain of attraction as time goes to infinity, the system is denoted asymptotically stable. The latter property is said to be global if the domain of attraction contains all initial conditions, and semi-global if the domain of attraction can be arbitrarily increased by increasing system parameters. Moreover, if the solutions converge, and in addition their norms are upper bounded by an appropriate exponentially decaying function, the system is said to be exponentially stable. These stability definitions are relevant for autonomous systems, whose behavior is a result of evolution over time from any initial time t_0 . Similar uniform stability definitions exist for non-autonomous systems, whose solutions may depend both on t and t_0 , and as such, their behavior may vary for varying t_0 . More formal definitions of the above stability properties can be found in Khalil (2002).

In this thesis, the notion of *almost* global asymptotic stability is used. The terminology of almost global asymptotic stability for the attitude control problem means asymptotic stability over an open and dense set in the set of the special group of rotation matrices $SO(3)$. This means that all the solutions apart from those starting in a nowhere dense set of measure zero converge asymptotically to the desired equilibrium point. As has been shown in Bhat and Bernstein (2000), it is impossible to achieve global asymptotic stability of a desired attitude using continuous control laws. For this reason, all the obtained results in this work are almost global since attitude control is involved and we do not consider discontinuous control schemes as done in Fragopoulos and Innocenti (2004) and Kristiansen *et al.* (2009).

To study the systems stability in this thesis, we focus on showing the global boundedness and asymptotic convergence of the error signals to zero. To this end, the following Lemmas are frequently used in the analysis of the presented results.

Lemma 2.1. (*Barbălat Lemma (Khalil, 2002)*) *Let $y : \mathbb{R} \rightarrow \mathbb{R}$ be a uniformly continuous function on $[0, \infty)$. Suppose that $\lim_{t \rightarrow \infty} \int_0^t y(s) ds$ exists and is finite. Then,*

$$y(t) \rightarrow 0 \quad \text{as } t \rightarrow \infty. \quad (2.26)$$

One of the applications of Barbălat Lemma is described in the following result (Slotine and Li, 1991)

Lemma 2.2. *If a scalar function $V(x, t)$ satisfies the following conditions*

- $V(x, t)$ is lower bounded
- $\dot{V}(x, t)$ is negative semi-definite
- $\dot{V}(x, t)$ is uniformly continuous in time

then, $\dot{V}(x, t) \rightarrow 0$ as $t \rightarrow \infty$.

An extended version of Barbălat Lemma that provides less restrictive conditions is formulated in the following lemma found in Hua *et al.* (2009).

Lemma 2.3. (*Extended Barbălat Lemma*) Let $x(t)$ denote a solution to the differential equation; $\dot{x} = a(t) + b(t)$, with $a(t)$ a uniformly continuous function. Suppose that $x(t) \rightarrow c$ and $b(t) \rightarrow 0$ as $t \rightarrow \infty$, with c a constant value. Then,

$$\dot{x}(t) \rightarrow 0 \quad \text{as } t \rightarrow \infty. \quad (2.27)$$

2.5 Information flow modeling

To achieve formation among a group of VTOL aircraft or guarantee attitude synchronization in a spacecraft formation, it is necessary to design control schemes using local information exchange. Therefore, aerial vehicles need to transmit some of their states information between each other. Throughout the thesis, we assume that the information flow between members of the team is fixed and bi-directional. This information exchange is described using weighted undirected graphs. Some important definitions and properties used in this work are given in this section, and the reader is referred to Jungnickel (2005) for more details.

A weighted undirected graph \mathcal{G} consists of the triplet $(\mathcal{N}, \mathcal{E}, \mathcal{K})$, with $\mathcal{N} = \{1, \dots, n\}$ being the set of nodes or vertices, describing the set of vehicles in the group, \mathcal{E} the set of unordered pairs of nodes, called edges, and $\mathcal{K} = [k_{ij}] \in \mathbb{R}^{n \times n}$ is a weighted adjacency matrix. An edge (i, j) in a weighted undirected graph indicates that nodes i and j are adjacent, or neighbors, and an undirected link exists between them. A link between two adjacent vehicles indicates that they can obtain information from one another. The weighted adjacency matrix of a weighted undirected graph is defined such that $k_{ii} = 0$ and

$$\begin{cases} k_{ij} = k_{ji} > 0, & \text{if } (i, j) \in \mathcal{E}, \\ k_{ij} = k_{ij} = 0, & \text{otherwise.} \end{cases} \quad (2.28)$$

Note that the magnitude of a nonzero k_{ij} determines the strength of the connection between two vehicles. Therefore, various coordination architectures can be used by different choices of these gains.

If there is a path between any two distinct nodes of a weighted undirected graph \mathcal{G} , then \mathcal{G} is said to be **connected**. A cycle is a connected graph with each node

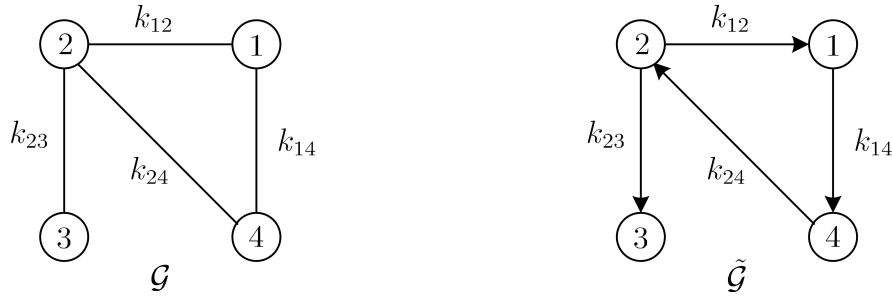


Figure 2.2: Example of an undirected/directed graph

having exactly two neighbors. “ \mathcal{G} contains a cycle” refers to a subgraph in \mathcal{G} that is a cycle. An acyclic graph is a graph with no cycles. A weighted undirected graph which is connected and acyclic is called a **tree**. If an orientation is assigned to the edges of the graph \mathcal{G} , we will obtain the weighted directed graph, $\tilde{\mathcal{G}} = (\mathcal{N}, \tilde{\mathcal{E}}, \tilde{\mathcal{K}})$, with $\tilde{\mathcal{E}}$ the set of ordered edges of the graph. If a path between any two distinct nodes exists in this case, then the graph is weakly connected. Figure 2.2 shows an example of an undirected graph \mathcal{G} and the resulted directed graph when a direction is assigned to the edges (randomly for illustration) to obtain $\tilde{\mathcal{G}}$.

Having a weighted directed graph $\tilde{\mathcal{G}}$, we define the weighted incidence matrix of the graph to be the matrix $\mathbf{D} = [d_{ij}]$ with rows indexed by vertices and columns indexed by edges with the (u, f) entry equals to $+k_f$ if vertex u is the source of the directed edge f , $-k_f$ if u is the sink of f , and 0 if u is not in the edge f . For example, the incidence matrix of the directed graph $\tilde{\mathcal{G}}$ in Fig. 2.2 is given as

$$\mathbf{D} = \begin{pmatrix} -k_{12} & 0 & k_{14} & 0 \\ k_{12} & k_{23} & 0 & -k_{24} \\ 0 & -k_{23} & 0 & 0 \\ 0 & 0 & -k_{14} & k_{24} \end{pmatrix} \quad (2.29)$$

The incidence matrix \mathbf{D} has a dimension of n -by- m , where m is the total number of edges in the graph, and satisfies the following property (Jungnickel, 2005).

Property 2.2. *The rank of the incidence matrix \mathbf{D} is $(n - 1)$ if the directed graph $\tilde{\mathcal{G}}$ is weakly connected, and it is full column rank if this graph is weakly connected and acyclic.*

2.6 Preliminary results

Some preliminary results needed in the analysis of some parts of the thesis are given here. Using properties of graphs discussed briefly in section 2.5, and the definition of the attitude error vectors given in section 2.3, we can show the following two results.

Lemma 2.4. Consider a group of n -rigid bodies and the set of equations

$$k_i^p \tilde{\mathbf{q}}_i + \sum_{j=1}^n k_{ij}^p \mathbf{q}_{ij} = 0, \quad \text{for } i \in \mathcal{N}, \quad (2.30)$$

with $\tilde{\mathbf{q}}_i$ and \mathbf{q}_{ij} are the vector parts of the unit quaternion representing respectively the attitude tracking error, defined in (2.13) with $\mathbf{Q}_{d_i} = \mathbf{Q}_d$ for all $i \in \mathcal{N}$, and the relative attitude between the i^{th} and j^{th} rigid bodies, defined in (2.20). The scalar k_i^p is a positive gain and k_{ij}^p is the $(i, j)^{\text{th}}$ entry of the adjacency matrix of weighted undirected graph \mathcal{G} describing the communication flow between the rigid-bodies. If the control gains satisfy

$$k_i^p > 2 \sum_{j=1}^n k_{ij}^p, \quad (2.31)$$

then the only solution to the set of equations (2.30) is $\tilde{\mathbf{q}}_i = 0$ for $i \in \mathcal{N}$. Furthermore, if the scalar part $\tilde{\eta}_i$ is guaranteed to be strictly positive for $i \in \mathcal{N}$, the above result holds without any condition on the gains.

Lemma 2.5. Consider a group of n -rigid bodies, with the relative attitudes between the group members defined in (2.20). If the communication graph between spacecraft is a tree, then the only solution to the set of equations

$$\sum_{j=1}^n k_{ij}^p \mathbf{q}_{ij} = 0, \quad \text{for } i \in \mathcal{N} \quad (2.32)$$

is $\mathbf{q}_{ij} = 0$ for $i, j \in \mathcal{N}$, where k_{ij}^p are defined as in Lemma 2.4. Furthermore, if the scalar part η_i is strictly positive (or strictly negative) for $i \in \mathcal{N}$, then $\mathbf{q}_{ij} = 0$ for $i, j \in \mathcal{N}$ is the only solution to (2.32) for any connected undirected communication graph.

The proof of Lemma 2.4 and Lemma 2.5 are given respectively in Appendix A.1.1 and Appendix A.1.2.

Furthermore, to design a priori bounded control laws in this thesis, we define for any vector $\mathbf{x} = (x^1, x^2, x^3)^T \in \mathbb{R}^3$ the saturation function

$$\chi(\mathbf{x}) = \text{col}[\sigma(x^j)] \in \mathbb{R}^3 \quad (2.33)$$

and the diagonal matrix

$$h(\mathbf{x}) = \text{diag} \left[\frac{\partial \sigma(x^j)}{\partial x^j} \right], \quad (2.34)$$

for $j = 1, \dots, 3$, with $\sigma : \mathbb{R} \rightarrow \mathbb{R}$, is a strictly increasing continuously differentiable function satisfying the following properties:

P1. $\sigma(0) = 0$ and $x\sigma(x) > 0$ for $x \neq 0$,

P2. $|\sigma(x)| \leq \sigma_b$, with $\sigma_b > 0$, for $x \in \mathbb{R}$,

P3. $\frac{\partial\sigma(x)}{\partial x}$ is bounded, for $x \in \mathbb{R}$.

Examples of the function $\sigma(x)$ include: $\tanh(x)$, $\arctan(x)$ and $\frac{x}{\sqrt{1+x^2}}$. Note that property P3 can be verified from P1 and P2. The following stability result will be often used in the analysis of the proposed solutions in this thesis.

Lemma 2.6. *Consider the second order system*

$$\ddot{\boldsymbol{\theta}} = -k_p\chi(\boldsymbol{\theta}) - k_d\dot{\chi}(\dot{\boldsymbol{\theta}}) + \boldsymbol{\varepsilon}, \quad (2.35)$$

with $\boldsymbol{\theta} \in \mathbb{R}^3$, $\chi(\boldsymbol{\theta})$ is defined in (2.33) and k_p and k_d are positive scalars. If $\boldsymbol{\varepsilon}$ is bounded for all time and $\boldsymbol{\varepsilon} \rightarrow 0$, then $\boldsymbol{\theta}$ and $\dot{\boldsymbol{\theta}}$ are bounded and $\boldsymbol{\theta} \rightarrow 0$ and $\dot{\boldsymbol{\theta}} \rightarrow 0$.

The proof of this lemma is given in Appendix A.1.3.

Chapter 3

Output feedback attitude synchronization of spacecraft formation

This chapter presents unit-quaternion based coordinated attitude control schemes for a spacecraft formation, without velocity measurements. The proposed design approach is based on the introduction of auxiliary dynamical systems to generate the individual and relative damping terms in the absence of the actual angular velocities and relative angular velocities. Using different structures of these auxiliary systems, we present two output feedback design methods each with some advantages and limitations. Based on these design methods, we address two control problems, namely the simultaneous attitude alignment and trajectory tracking problem and the consensus-seeking problem without velocity measurement. The information flow between spacecraft is assumed to be fixed and undirected, and is modeled using undirected graphs. The results presented in this chapter are based on Abdessameud and Tayebi (2008*a,b*, 2009*a,b*).

3.1 Introduction

The problem of controlling the relative attitudes of formation flying spacecraft, or rigid bodies in general, has been the interest of many researchers in the last few years. Based on different control design approaches, several papers deal with this problem in the full state information case, *i.e.*, when spacecraft attitudes and angular velocities are available for feedback (see for example Scharf *et al.*, 2004; Wang *et al.*, 1999; Beard *et al.*, 2001; Vandyke and Hall, 2006; Ren, 2007*a*; Bai *et al.*, 2008; Dimarogonas *et al.*, 2009, and references therein). However, less work has been done when the angular velocities are not available for feedback. This problem is attractive in the case where spacecraft angular velocities are either imprecisely measured or not measured to relieve the necessity of onboard velocity sensors, leading to reduced cost and weight of participating spacecraft. In addition, the implementation of redundant velocity-free control laws will enhance the reliability of the system to possible sensors failure.

The lead filter approach proposed in Lizarralde and Wen (1996) was used in the work of Lawton and Beard (2002) to develop a local control law for multi-spacecraft attitude alignment without velocity measurements, assuming a ring communication

topology. This work has been extended to the case of a general undirected communication topology in Ren (2009) using the MRP representation of the attitude. In both works, the authors consider the case where the final angular velocity is zero, and the extension of the obtained results to the trajectory tracking case is not obvious. The two velocity-free control laws proposed in Caccavale and Villani (1999) have been extended to the attitude control of two spacecraft in a leader-follower architecture in Kristiansen *et al.* (2009), using a lead filter, and in Grøtli and Gravdahl (2008), using the combined observer-controller design, and uniform practical stability is shown.

In this chapter, we propose two output feedback design methods that rely on the auxiliary systems approach recently introduced in Tayebi (2008). The first method consists of associating an auxiliary dynamic system to each spacecraft and to each pair of spacecraft with a communication link in order to generate the necessary damping that would have been generated by the actual angular velocities and relative angular velocities. In the second approach, we use a single auxiliary system with higher order to relax some of the implementation problems of the first method. This approach reduces the communication requirement between spacecraft in the team as compared to the full state information case, which is an interesting feature especially for largely populated formations.

The above mentioned approaches have been successfully applied to two different control problems. The first problem consists of designing a control law that allows to achieve simultaneous attitude tracking and synchronization of a group of spacecraft without velocity measurements and without any restriction on the graph topology. This attitude tracking and synchronization scheme can be classified as a behavioral type in the sense that two different objectives (behaviors), namely tracking and synchronization, can be achieved simultaneously. A priority between the two objectives can be established through the choice of the control gains. We also show that the proposed control law can be simplified further by removing the condition on the gains as long as the graph topology is an undirected tree. This velocity-free result is quite similar to the results obtained in the full state information case (*i.e.*, with velocity measurement) in Ren (2007a), Vandyke and Hall (2006), Bai *et al.* (2008). The second problem solved in this chapter is the case where no leader and no reference trajectory are used to dictate the group objective, and it is required that the spacecraft align their attitudes with the same (not necessarily constant) angular velocity, under an undirected, connected and acyclic graph. The presented solutions are analyzed using Lyapunov arguments and some results from graph theory.

3.2 Problem formulation

We consider a group of n -spacecraft modeled as rigid bodies, with equations of motion of the i^{th} spacecraft given in (2.9)-(2.11), *i.e.*,

$$\dot{\mathbf{Q}}_i = \mathbf{T}(\mathbf{Q}_i)\boldsymbol{\omega}_i, \tag{3.1}$$

$$\mathbf{J}_{f_i}\dot{\boldsymbol{\omega}}_i = \boldsymbol{\Gamma}_i - \mathbf{S}(\boldsymbol{\omega}_i)\mathbf{J}_{f_i}\boldsymbol{\omega}_i, \tag{3.2}$$

where $\mathbf{T}(\mathbf{Q}_i)$ is given in (2.10) and $i \in \mathcal{N} := \{1, \dots, n\}$. We assume that only the absolute attitude of each spacecraft is available for feedback (precisely measured), and we aim to design control schemes that achieve the following two control objectives.

Simultaneous attitude tracking and synchronization: We assign to each spacecraft in the team a time-varying reference attitude represented by the unit-quaternion \mathbf{Q}_d , with the desired angular velocity denoted by $\boldsymbol{\omega}_d$. Also, we define the attitude tracking error $\tilde{\mathbf{Q}}_i$ in (2.13), which is governed by the dynamics (2.14)-(2.15), with $\mathbf{Q}_{d_i} = \mathbf{Q}_d$ and $\boldsymbol{\omega}_{d_i} = \boldsymbol{\omega}_d$ for all $i \in \mathcal{N}$. Our objective is to design a control scheme such that the following tasks are simultaneously achieved without angular velocity measurements

- All relative attitudes and angular velocities between the team members converge to zero, *i.e.*, $\mathbf{Q}_i \rightarrow \mathbf{Q}_j$ and $\boldsymbol{\omega}_i \rightarrow \boldsymbol{\omega}_j$, for all $i, j \in \mathcal{N}$.
- Each spacecraft tracks the desired trajectory, *i.e.*, $\mathbf{Q}_i \rightarrow \mathbf{Q}_d$ and $\boldsymbol{\omega}_i \rightarrow \boldsymbol{\omega}_d$.

Attitude synchronization without reference trajectory: We assume that no reference signal is available to any spacecraft, and we want to design a velocity-free synchronization scheme such that spacecraft align their attitudes, *i.e.*, $\mathbf{Q}_i \rightarrow \mathbf{Q}_j$ and $\boldsymbol{\omega}_i \rightarrow \boldsymbol{\omega}_j$, for all $i, j \in \mathcal{N}$, using only local information transmitted between neighbors among the group.

To design synchronization schemes, we assume that the information flow between spacecraft is modeled using the two weighted undirected graphs; $\mathcal{G}_p = (\mathcal{N}, \mathcal{E}, \mathcal{K}_p)$ and $\mathcal{G}_d = (\mathcal{N}, \mathcal{E}, \mathcal{K}_d)$, with \mathcal{N} , \mathcal{E} and $\mathcal{K}_\star = [k_{ij}^\star]$, with $\star \in \{p, d\}$, are defined as in section 2.5. It is clear that \mathcal{G}_p and \mathcal{G}_d have the same set of nodes and set of edges, and they differ only by the elements of the adjacency matrices $\mathcal{K}_{p,d}$ associated to every link of each graph respectively. Therefore, \mathcal{G}_p and \mathcal{G}_d will have the same properties, and both describe the communication graph between members of the team.

3.3 State feedback design

This section presents some existent results related to the attitude synchronization problem when the full state vector is available for feedback. In this case, several state

feedback control schemes that solve the simultaneous attitude synchronization and trajectory tracking of spacecraft formations have been proposed in the literature and can be found in Vandyke and Hall (2006), Ren (2007a), Bai *et al.* (2008) and Chung *et al.* (2009). In general, these control schemes are based on the coupled dynamics controller proposed in Lawton and Beard (2000), which involves two terms in order to achieve two different objectives/behaviors, and is given by

$$\mathbf{\Gamma}_i = \mathbf{\Gamma}_i^1 + \mathbf{\Gamma}_i^2, \quad (3.3)$$

where the first term aims to track a reference attitude to achieve the goal-seeking behavior, and the second is used to achieve the formation-keeping behavior.

The first term in (3.3) is constructed using only the individual spacecraft states so that tracking of the desired attitude is guaranteed. A possible attitude tracking controller in the full state information case can be considered as

$$\mathbf{\Gamma}_i^1 = \mathbf{S}(\boldsymbol{\omega}_i) \mathbf{J}_{f_i} \boldsymbol{\omega}_i - \mathbf{J}_{f_i} \mathbf{S}(\tilde{\boldsymbol{\omega}}_i) \mathbf{R}(\tilde{\mathbf{Q}}_i) \boldsymbol{\omega}_d + \mathbf{J}_{f_i} \mathbf{R}(\tilde{\mathbf{Q}}_i) \dot{\boldsymbol{\omega}}_d - k_i^p \tilde{\mathbf{q}}_i - k_i^v \tilde{\boldsymbol{\omega}}_i, \quad (3.4)$$

where k_i^p and k_i^d are strictly positive gains that are generally referred to as attitude tracking control gains, $\tilde{\mathbf{Q}}_i$ and $\tilde{\boldsymbol{\omega}}_i$ represent the attitude and angular velocity tracking errors and are defined respectively in (2.13) and (2.15), and $\tilde{\mathbf{q}}_i$ is the vector part of $\tilde{\mathbf{Q}}_i$.

To achieve formation-keeping, the second control term is constructed based on relative attitudes and relative angular velocities between any two neighboring spacecraft. Therefore, the nature of the information exchange will define the structure of this control action. Since the information flow is assumed fixed and undirected, a weighted combination of the relative errors between a spacecraft and all its neighbors will be used in the second term in (3.3). The following control law is proposed

$$\mathbf{\Gamma}_i^2 = - \sum_{j=1}^n \left(k_{ij}^p \mathbf{q}_{ij} + k_{ij}^d \boldsymbol{\omega}_{ij} \right), \quad (3.5)$$

where \mathbf{q}_{ij} is the vector part of the unit-quaternion \mathbf{Q}_{ij} given in (2.20) representing the relative attitude between the i^{th} and j^{th} spacecraft, $\boldsymbol{\omega}_{ij}$ represents the relative angular velocity defined in (2.22), and the gains k_{ij}^p and k_{ij}^d are respectively the $(i, j)^{th}$ entries of the adjacency matrices of the communication graphs \mathcal{G}_p and \mathcal{G}_d . Note that spacecraft attitudes and angular velocities must be transmitted between any pair of communicating spacecraft in the team to implement the above control action.

The asymptotic convergence of the error signals to zero can be shown using the undirected communication graph properties and Lyapunov arguments with the

following Lyapunov function

$$V = \sum_{i=1}^n \left(\frac{1}{2} \tilde{\boldsymbol{\omega}}_i^T \mathbf{J}_{f_i} \tilde{\boldsymbol{\omega}}_i + 2k_i^p (1 - \tilde{\eta}_i) + 2 \sum_{j=1}^n k_{ij}^p (1 - \eta_{ij}) \right), \quad (3.6)$$

leading to the negative semi-definite time-derivative

$$\dot{V} = - \sum_{i=1}^n k_i^d \tilde{\boldsymbol{\omega}}_i^T \tilde{\boldsymbol{\omega}}_i - \frac{1}{2} \sum_{i=1}^n \sum_{j=1}^n k_{ij}^d \boldsymbol{\omega}_{ij}^T \boldsymbol{\omega}_{ij}. \quad (3.7)$$

Then using Barbălat Lemma with the result of Lemma 2.4, the error signals $\tilde{\mathbf{q}}_i$, $\tilde{\boldsymbol{\omega}}_i$, \mathbf{q}_{ij} and $\boldsymbol{\omega}_{ij}$ can be shown to asymptotically converge to zero under the condition that the control gains are selected according to (2.31). The details of the proof are omitted as they follow in part the arguments of the proofs of the results presented in the next sections.

It should be noted from the above state feedback control scheme that the goal-seeking control law, $\boldsymbol{\Gamma}_i^1$ in (3.3), will be sufficient to ensure attitude synchronization to the desired trajectory when perfect individual tracking of each rigid body is achieved. However, it is possible that some members of the team have achieved tracking of the desired attitude while others are late (*e.g.*, external disturbances acting on some members of the team, or the team consists of a number of heterogenous rigid bodies and the initial attitude errors are different). In this case, the second term, $\boldsymbol{\Gamma}_i^2$, brings in transient performance improvement through synchronization. Moreover, under some conditions, priority between the two group behaviors can be assigned.

In the case where it is required that all spacecraft align their attitudes without assigning any reference trajectory, the following torque input has been shown to achieve attitude synchronization under the condition that the communication graph \mathcal{G}_p is a tree (Ren, 2007a),

$$\boldsymbol{\Gamma}_i = \mathbf{S}(\boldsymbol{\omega}_i) \mathbf{J}_{f_i} \boldsymbol{\omega}_i + \boldsymbol{\Gamma}_i^2, \quad (3.8)$$

with $\boldsymbol{\Gamma}_i^2$ given in (3.5). In this case, asymptotic convergence of the relative errors to zero can be shown using the Lyapunov function

$$V = \sum_{i=1}^n \left(\frac{1}{2} \boldsymbol{\omega}_i^T \mathbf{J}_{f_i} \boldsymbol{\omega}_i + 2 \sum_{j=1}^n k_{ij}^p (1 - \eta_{ij}) \right), \quad (3.9)$$

leading to the negative semi-definite time-derivative

$$\dot{V} = - \frac{1}{2} \sum_{i=1}^n \sum_{j=1}^n k_{ij}^d \boldsymbol{\omega}_{ij}^T \boldsymbol{\omega}_{ij}. \quad (3.10)$$

which shows, with the help of Barbălat Lemma and the result of Lemma 2.5, that $\dot{\omega}_i$, \mathbf{q}_{ij} and ω_{ij} converge to zero asymptotically for all $i, j \in \mathcal{N}$.

3.4 Auxiliary systems-based output feedback - First approach

To achieve attitude synchronization and remove the requirement of the angular velocity, we use the concept of auxiliary systems introduced in Tayebi (2008). We associate a unit-quaternion auxiliary system to each individual spacecraft, defined as follows:

$$\dot{\bar{\mathbf{Q}}}_i = \mathbf{T}(\bar{\mathbf{Q}}_i)\beta_i, \quad (3.11)$$

where $\bar{\mathbf{Q}}_i = (\bar{\mathbf{q}}_i^T, \bar{\eta}_i)^T$ and $\beta_i \in \mathbb{R}^3$ is the input of the auxiliary system (3.11), which will be designed later. In addition, we associate a unit-quaternion auxiliary system to each pair of spacecraft (i, j) , with a communication link, defined as follows:

$$\dot{\bar{\mathbf{Q}}}_{ij} = \mathbf{T}(\bar{\mathbf{Q}}_{ij})\beta_{ij}, \quad (3.12)$$

where $\bar{\mathbf{Q}}_{ij} = (\bar{\mathbf{q}}_{ij}^T, \bar{\eta}_{ij})^T$ and $\beta_{ij} \in \mathbb{R}^3$ is the input of the auxiliary system (3.12) to be designed later. The two above auxiliary systems can be initialized arbitrarily.

The mismatch between the absolute attitude of the i^{th} spacecraft and the output of the auxiliary system (3.11) is represented by the unit-quaternion $\mathbf{Q}_i^e = (\mathbf{q}_i^{eT}, \eta_i^e)^T$ and is defined as

$$\mathbf{Q}_i^e = \bar{\mathbf{Q}}_i^{-1} \odot \mathbf{Q}_i, \quad (3.13)$$

satisfying the unit-quaternion dynamics

$$\dot{\mathbf{Q}}_i^e = \mathbf{T}(\mathbf{Q}_i^e)\Omega_i, \quad (3.14)$$

$$\Omega_i = \omega_i - \mathbf{R}(\mathbf{Q}_i^e)\beta_i, \quad (3.15)$$

where $\mathbf{R}(\mathbf{Q}_i^e)$ is the rotation matrix related to \mathbf{Q}_i^e . Similarly, the unit-quaternion describing the discrepancy between the relative attitude error of the i^{th} and j^{th} spacecraft and the output of (3.12) is represented by the unit-quaternion $\mathbf{Q}_{ij}^e = (\mathbf{q}_{ij}^{eT}, \eta_{ij}^e)^T$ and is defined as

$$\mathbf{Q}_{ij}^e = \bar{\mathbf{Q}}_{ij}^{-1} \odot \mathbf{Q}_{ij}, \quad (3.16)$$

and obeys to the following dynamic equations

$$\dot{\mathbf{Q}}_{ij}^e = \mathbf{T}(\mathbf{Q}_{ij}^e)\Omega_{ij}, \quad (3.17)$$

$$\Omega_{ij} = \omega_{ij} - \mathbf{R}(\mathbf{Q}_{ij}^e)\beta_{ij}. \quad (3.18)$$

3.4.1 Attitude synchronization with time-varying reference trajectory

The objective in this section is to design the input control of each spacecraft allowing all members of the group to align their attitudes with a time-varying reference attitude, while maintaining the same relative attitude during formation maneuvers. To this end, we consider the control structure (3.3), with Γ_i^1 given by

$$\Gamma_i^1 = \mathbf{J}_{f_i} \mathbf{R}(\tilde{\mathbf{Q}}_i) \dot{\boldsymbol{\omega}}_d + \mathbf{S} \left(\mathbf{R}(\tilde{\mathbf{Q}}_i) \boldsymbol{\omega}_d \right) \mathbf{J}_{f_i} \mathbf{R}(\tilde{\mathbf{Q}}_i) \boldsymbol{\omega}_d - k_i^p \tilde{\mathbf{q}}_i - k_i^d \mathbf{q}_i^e, \quad (3.19)$$

where k_i^p and k_i^d are the strictly positive attitude tracking control gains. Note that the vector part of the unit-quaternion \mathbf{Q}_i^e defined in (3.13) is used in the control law instead of the actual angular-velocity tracking error. The tracking control scheme (3.19) has been developed in Tayebi (2008) and it was shown that almost global stability of the closed loop system is achieved.

For the formation-keeping objective, we propose the following control law for the i^{th} spacecraft

$$\Gamma_i^2 = - \sum_{j=1}^n k_{ij}^p \mathbf{q}_{ij} - \sum_{j=1}^n k_{ij}^d \left(\mathbf{q}_{ij}^e - \mathbf{R}(\mathbf{Q}_{ij}) \mathbf{q}_{ji}^e \right), \quad (3.20)$$

where \mathbf{q}_{ij}^e is the vector part of the unit-quaternion \mathbf{Q}_{ij}^e , given in (3.16), k_{ij}^p and k_{ij}^d are respectively the $(i, j)^{\text{th}}$ entries of the adjacency matrices of the communication graphs \mathcal{G}_p and \mathcal{G}_d .

Theorem 3.1. *Consider the spacecraft formation given in (3.1)-(3.2) with the control law (3.3), with (3.19)-(3.20), and let the inputs of the auxiliary systems (3.11) and (3.12) be respectively*

$$\boldsymbol{\beta}_i = \mathbf{R}(\mathbf{Q}_i^e)^T \mathbf{R}(\tilde{\mathbf{Q}}_i) \boldsymbol{\omega}_d + \lambda_i \mathbf{q}_i^e, \quad \boldsymbol{\beta}_{ij} = \lambda_{ij} \mathbf{q}_{ij}^e, \quad (3.21)$$

where λ_i and λ_{ij} are positive scalar gains. If the control gains are selected to satisfy condition (2.31), then all the signals are globally bounded and $\mathbf{q}_i \rightarrow \mathbf{q}_j \rightarrow \mathbf{q}_d$, $\boldsymbol{\omega}_i \rightarrow \boldsymbol{\omega}_j \rightarrow \boldsymbol{\omega}_d$ asymptotically, $\forall i, j \in \mathcal{N}$. Furthermore, if there exists a time $t_0 > 0$ such that $\tilde{\eta}_i > 0$, for all $t \geq t_0$ and $i \in \mathcal{N}$, then the same convergence results are obtained without condition (2.31).

Sketch of proof: From the definition of the angular velocity tracking error in (2.15), and exploiting the attitude dynamics with the properties of the vector cross product, the application of the torque input (3.3) with (3.19)-(3.20) results in the angular

velocity error dynamics

$$\tilde{\boldsymbol{\omega}}_i^T \mathbf{J}_{f_i} \dot{\tilde{\boldsymbol{\omega}}}_i = \tilde{\boldsymbol{\omega}}_i^T \left(-k_i^p \tilde{\mathbf{q}}_i - k_i^d \mathbf{q}_i^e - \sum_{j=1}^n \left(k_{ij}^p \mathbf{q}_{ij} + k_{ij}^d (\mathbf{q}_{ij}^e - \mathbf{R}(\mathbf{Q}_{ij}) \mathbf{q}_{ji}^e) \right) \right). \quad (3.22)$$

The proof of Theorem 3.1 follows from standard Lyapunov arguments, with the following positive definite Lyapunov function

$$\begin{aligned} V = & \sum_{j=1}^n \left(\frac{1}{2} \tilde{\boldsymbol{\omega}}_j^T I_{f_j} \tilde{\boldsymbol{\omega}}_j + 2k_j^p (1 - \tilde{\eta}_j) + 2k_j^d (1 - \eta_j^e) \right) \\ & + \sum_{j=1}^n \sum_{k=1}^n \left(k_{kj}^p (1 - \eta_{kj}) + 2k_{kj}^d (1 - \eta_{kj}^e) \right), \end{aligned} \quad (3.23)$$

leading to the following negative semi-definite time-derivative

$$\dot{V} = - \sum_{i=1}^n k_i^d \lambda_i (\mathbf{q}_i^e)^T \mathbf{q}_i^e - \sum_{i=1}^n \sum_{j=1}^n k_{ij}^d \lambda_{ij} (\mathbf{q}_{ij}^e)^T \mathbf{q}_{ij}^e, \quad (3.24)$$

which shows that $V(t) \leq V(0)$, and $\tilde{\boldsymbol{\omega}}_i$ is bounded. Invoking Barbălat Lemma, we conclude that $\mathbf{q}_i^e \rightarrow 0$ and $\mathbf{q}_{ij}^e \rightarrow 0$, which leads us to conclude that $\boldsymbol{\Omega}_i \rightarrow \tilde{\boldsymbol{\omega}}_i$ and $\boldsymbol{\Omega}_{ij} \rightarrow \boldsymbol{\omega}_{ij}$. Also, with the assumption that the desired angular velocity is bounded as well as its time-derivative, we show that $\boldsymbol{\Omega}_i \rightarrow 0$ and $\boldsymbol{\Omega}_{ij} \rightarrow 0$ using Barbălat Lemma. This leads to the conclusion that $\dot{\tilde{\boldsymbol{\omega}}}_i \rightarrow 0$, and the closed loop dynamics reduces to

$$k_i^p \tilde{\mathbf{q}}_i + \sum_{j=1}^n k_{ij}^p \mathbf{q}_{ij} = 0, \quad (3.25)$$

for $i \in \mathcal{N}$. The results of the theorem then follow using Lemma 2.4. A detailed proof of Theorem 3.1 is given in Appendix A.2.1. □

Remark 3.1. *The condition on the control gains (2.31) is restrictive in the sense that priority is given to the goal-seeking behavior over the formation-keeping behavior. This condition is not required if there exists a time $t_0 > 0$ such that $\tilde{\eta}_i > 0$ for all $t > t_0$ and $i \in \mathcal{N}$. To solve the relative attitude control problem in a leader-follower context, the authors in Kristiansen et al. (2009) assume that the scalar part $\tilde{\eta}_i$ is initially positive and does not change sign for all time. An analytical proof to this assumption is provided in the early work of Lawton and Beard (2002), under the condition that the systems initial states are selected within an attraction region. From a practical point of view, this assumption can always be satisfied, and the scalar parts of unit-*

quaternion are ensured to be positive for all $t \geq 0$ if one restricts the rotation angle to be in $[-\pi, \pi)$.

We can show that the above control law can be further simplified by allowing $k_i^p = 0$, under some conditions on the communication graph. The result is stated as follows:

Corollary 3.1. *Given the spacecraft formation (3.1)-(3.2) with the control law (3.3) with (3.19)-(3.20). Let $k_i^p = 0$, $k_i^d > 0$, and the inputs of the auxiliary systems (3.11) and (3.12) be given by (3.21). If the communication graph is a tree, then all the signals are globally bounded and $\tilde{\omega}_i \rightarrow 0$, $\mathbf{q}_i \rightarrow \mathbf{q}_j$ for all $i, j \in \mathcal{N}$. Furthermore, if there exists a time $t_0 > 0$ such that $\tilde{\eta}_i > 0$, (or $\tilde{\eta}_i < 0$), for all $t \geq t_0$ and $i \in \mathcal{N}$, then the above result holds for any connected undirected graph.*

Sketch of proof: Following the same steps of the proof of Theorem 3.1, with the same Lyapunov function candidate with $k_i^p = 0$, it can be shown that $\tilde{\omega}_i \rightarrow 0$, $\omega_{ij} \rightarrow 0$ and the closed loop dynamics reduces to

$$\sum_{j=1}^n k_{ij}^p \mathbf{q}_{ij} = 0, \tag{3.26}$$

for $i \in \mathcal{N}$. The results of the corollary are then deduced using Lemma 2.5. □

Remark 3.2. *Note that the result $\tilde{\omega}_i \rightarrow 0$ implies that the final angular velocity of each spacecraft is guaranteed to converge to the desired angular velocity expressed in the spacecraft body frame \mathcal{F}_i , i.e., $\mathbf{R}(\tilde{\mathbf{Q}}_i)\omega_d$.*

Remark 3.3. *The result in Corollary 3.1 extends the work of Ren (2007a) and Bai et al. (2008) to the velocity-free case, where similar results were obtained in the full state information case (i.e., with velocity measurement) under the same sufficient condition on the communication graph. Furthermore, when the desired angular velocity is zero, a similar result is obtained in Ren (2009) where the author considers the MRP representation for the attitude and proposes a passivity-based velocity-free control law that guarantees group-attitude alignment with any connected undirected graph. However, in addition to the singularity of the MRP representation, the extension of this passivity based scheme to the tracking control case is not obvious.*

An important advantage of using auxiliary systems is that the resulting control inputs are *a priori* bounded. In fact, we can see that the control law (3.31) consists of pure unit-quaternion feedback terms. Consequently, the control effort is bounded regardless of the angular velocities as follows

$$\|\mathbf{\Gamma}_i\| \leq \|\mathbf{J}_{f_i}\|(\varrho + \rho^2) + k_i^p + k_i^d + \sum_{j=1}^n (k_{ij}^p + 2k_{ij}^d), \tag{3.27}$$

with $\|\dot{\omega}_d\|_\infty \leq \varrho$ and $\|\omega_d\|_\infty \leq \rho$. Therefore, the designer can easily set the desired bounds on the control torques via an appropriate choice of the control gains. In addition, we can see that to implement the control law (3.20), communicating spacecraft should transmit their absolute attitudes and the vector parts of the unit-quaternion \mathbf{Q}_{ij}^e . Hence, the proposed control scheme in Theorem 3.1 does not increase the communication requirements as compared to the full state information case where both spacecraft absolute attitudes and angular velocities are transmitted through the communication channels. Fig.3.1 illustrates the implementation of the control law in Theorem 3.1.

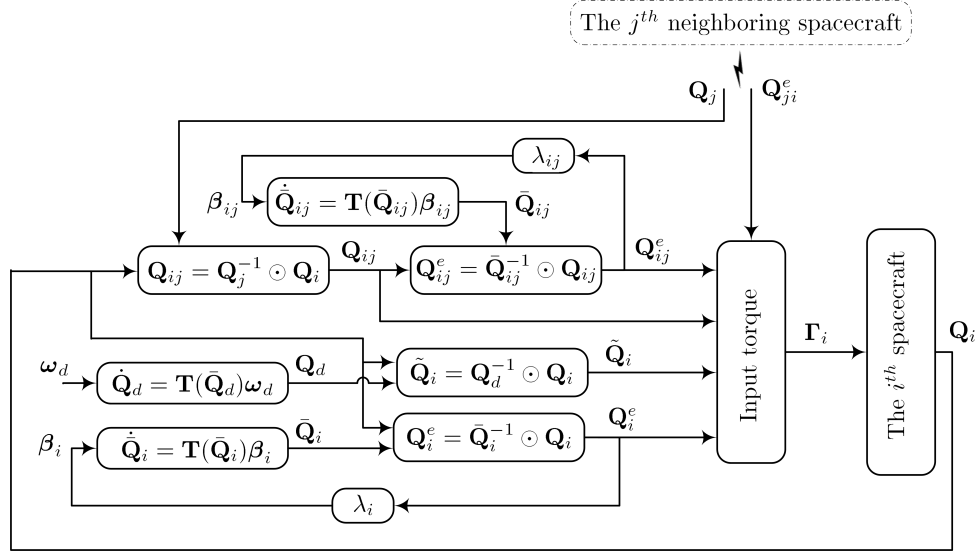


Figure 3.1: Implementation of the control law in Theorem 3.1.

Remark 3.4. *It can be verified that the synchronization control scheme presented above satisfies the reduction principle in that it applies to the attitude synchronization problem with constant (or zero) desired angular velocity. In addition, it can be easily extended to the case where spacecraft are required to maintain given non-zero relative attitudes during formation maneuvers.*

3.4.2 Attitude synchronization without reference assignment

In this subsection, we consider the case where it is desired that spacecraft align their attitudes and no reference trajectory is considered to dictate the behavior of the team. To this end, we consider the discrepancy between the error vectors \mathbf{Q}_i^e in (3.13) of

the i^{th} and j^{th} spacecraft represented by $\tilde{\mathbf{Q}}_{ij}^e = (\tilde{\mathbf{q}}_{ij}^e{}^T, \tilde{\eta}_{ij}^e)^T$, and is defined as

$$\tilde{\mathbf{Q}}_{ij}^e = \mathbf{Q}_j^e{}^{-1} \odot \mathbf{Q}_i^e, \quad (3.28)$$

satisfying the following dynamic equations

$$\dot{\tilde{\mathbf{Q}}}_{ij}^e = \mathbf{T}(\tilde{\mathbf{Q}}_{ij}^e)\tilde{\mathbf{\Omega}}_{ij}, \quad (3.29)$$

$$\tilde{\mathbf{\Omega}}_{ij} = \mathbf{\Omega}_i - \mathbf{R}(\tilde{\mathbf{Q}}_{ij}^e)\mathbf{\Omega}_j. \quad (3.30)$$

We propose the following control input for each spacecraft

$$\mathbf{\Gamma}_i = - \sum_{j=1}^n k_{ij}^p \mathbf{q}_{ij} - \sum_{j=1}^n k_{ij}^d \left(\mathbf{q}_{ij}^e - \mathbf{R}(\mathbf{Q}_{ij})\mathbf{q}_{ji}^e + \tilde{\mathbf{q}}_{ij}^e \right), \quad (3.31)$$

where $\tilde{\mathbf{q}}_{ij}^e$ is the vector part of the unit-quaternion $\tilde{\mathbf{Q}}_{ij}^e$ defined in (3.28) and the gains k_{ij}^p and k_{ij}^d are defined as in Theorem 3.1.

Theorem 3.2. *Consider the spacecraft formation given in (3.1)-(3.2) with the control law (3.31) and let the inputs of the auxiliary systems (3.11) and (3.12) be respectively*

$$\boldsymbol{\beta}_i = \lambda_i \mathbf{R}(\mathbf{Q}_i^e)^T \left(\sum_{j=1}^n k_{ij}^d \tilde{\mathbf{q}}_{ij}^e \right), \quad (3.32)$$

$$\boldsymbol{\beta}_{ij} = \lambda_{ij} \mathbf{q}_{ij}^e, \quad (3.33)$$

where λ_i and λ_{ij} are positive scalar gains. If the information flow graph is a tree, then all the signals are globally bounded and $\mathbf{q}_i \rightarrow \mathbf{q}_j$, $\boldsymbol{\omega}_i \rightarrow \boldsymbol{\omega}_j$ asymptotically, for all $i, j \in \mathcal{N}$. Furthermore, if there exists a time $t_0 > 0$ such that $\eta_i^e > 0$, (or $\eta_i^e < 0$), for all $t \geq t_0$ and $i \in \mathcal{N}$, then the above result holds for any connected undirected graph.

Sketch of proof: The results of the theorem are shown using the Lyapunov function

$$\begin{aligned} V = & \frac{1}{2} \sum_{i=1}^n \boldsymbol{\omega}_i^T \mathbf{J}_{f_i} \boldsymbol{\omega}_i + \sum_{i=1}^n \sum_{j=1}^n k_{ij}^p (1 - \eta_{ij}) \\ & + \sum_{i=1}^n \sum_{j=1}^n k_{ij}^d \left(2(1 - \eta_{ij}^e) + (1 - \tilde{\eta}_{ij}^e) \right), \end{aligned} \quad (3.34)$$

leading to the negative semi-definite time-derivative

$$\dot{V} = - \sum_{i=1}^n \sum_{j=1}^n k_{ij}^d \lambda_{ij} \mathbf{q}_{ij}^e{}^T \mathbf{q}_{ij}^e - \sum_{i=1}^n \lambda_i \left(\sum_{j=1}^n k_{ij}^d \tilde{\mathbf{q}}_{ij}^e \right)^T \left(\sum_{j=1}^n k_{ij}^d \tilde{\mathbf{q}}_{ij}^e \right). \quad (3.35)$$

Invoking Barbălat Lemma, we show that $\mathbf{q}_{ij}^e \rightarrow 0$, for $i, j \in \mathcal{N}$, and $\left(\sum_{j=1}^n k_{ij}^d \tilde{\mathbf{q}}_{ij}^e \right) \rightarrow 0$, for $i \in \mathcal{N}$. Next, the result of Lemma 2.5 is used to show that $\tilde{\mathbf{q}}_{ij}^e \rightarrow 0$ under the assumption that the communication graph is a tree. Also, it can be shown that $\tilde{\boldsymbol{\Omega}}_{ij} \rightarrow 0$ and $\tilde{\boldsymbol{\omega}}_{ij} \rightarrow 0$, from which we conclude by simple deductions that $\mathbf{q}_i \rightarrow \mathbf{q}_j$ and $\boldsymbol{\omega}_i \rightarrow \boldsymbol{\omega}_j$, for all $i, j \in \mathcal{N}$. The last part of the proof follows also the last part of the proof of Lemma 2.5. A detailed proof of Theorem 3.2 is given in Appendix A.2.2. \square

Remark 3.5. *It is important to mention that the proposed control scheme in Theorem 3.2 ensures that the spacecraft final angular velocities converge to a common bounded time-varying function. This can be seen from the proof of Theorem 3.2 where we can verify that the input torque of each spacecraft converges asymptotically to zero and the dynamics of the angular velocity at the limit satisfy*

$$\mathbf{J}_{f_i} \dot{\boldsymbol{\omega}}_i = -\mathbf{S}(\boldsymbol{\omega}_i) \mathbf{J}_{f_i} \boldsymbol{\omega}_i. \quad (3.36)$$

In the full state information case, a similar result has been obtained in Ren (2007a), where it has been shown that the control law given in (3.8) guarantees, under similar conditions on the communication graph as in Theorem 3.2, that attitude alignment is achieved with a constant common angular velocity. This was achieved by compensating the nonlinear term $\mathbf{S}(\boldsymbol{\omega}_i) \mathbf{J}_{f_i} \boldsymbol{\omega}_i$ in the control law as the angular velocities are available for feedback.

An important feature of the proposed control law in Theorem 3.2 is that it is independent of the spacecraft inertia matrices. This enhances the systems robustness to uncertainties and/or modeling errors. Furthermore, similar to the synchronization controller in section 3.4.1, the control effort (3.31) can be *a priori* bounded regardless of the angular velocities as

$$\|\boldsymbol{\Gamma}_i\| \leq \sum_{j=1}^n (k_{ij}^p + 3k_{ij}^d). \quad (3.37)$$

However, to implement the control law (3.31), neighboring spacecraft should transmit their absolute attitudes, the unit-quaternion \mathbf{Q}_i^e and the vector parts of the unit-quaternion \mathbf{Q}_{ij}^e .

It is worth noticing that the basic idea in the output feedback design approach in this section consists of associating an auxiliary dynamic system to each spacecraft

and to each pair of spacecraft with a communication link in order to generate the necessary damping that would have been generated by the actual angular velocities and relative angular velocities. As a result, to implement the control scheme in Theorem 3.1 and Theorem 3.2, it is required to use a number of auxiliary dynamical systems, for each spacecraft, which increases with the number of its neighbors, hence augmenting considerably the order of the system when the number of spacecraft in the formation is large. To solve this problem, we present in the next section a second approach to the design of output feedback attitude synchronization schemes that is based on auxiliary systems with higher order.

3.5 Auxiliary systems-based output feedback - Second approach

In this section, we present output feedback attitude synchronization schemes that require the association of a single auxiliary system to each spacecraft and achieve attitude synchronization using only spacecraft absolute attitudes. We associate the following auxiliary system to each spacecraft

$$\begin{cases} \dot{\bar{\mathbf{Q}}}_i &= \mathbf{T}(\bar{\mathbf{Q}}_i)\beta_i, \\ \dot{\bar{\boldsymbol{\beta}}}_i &= -\lambda_i\beta_i + \bar{\boldsymbol{\beta}}_i, \end{cases} \quad (3.38)$$

where $\bar{\mathbf{Q}}_i = (\bar{\mathbf{q}}_i^T, \bar{\eta}_i)^T$, λ_i is a strictly positive scalar gain and $\bar{\boldsymbol{\beta}}_i \in \mathbb{R}^3$ is an input to be designed later. The initial states $\bar{\mathbf{Q}}_i(0)$ and $\beta_i(0)$ can be selected arbitrarily. Note that the difference between the dynamic system (3.38) and the auxiliary system used in the previous section is the choice of the input β_i , which is defined in this section by a dynamic equation.

3.5.1 Attitude synchronization with time-varying reference

Using the auxiliary system (3.38), we represent the discrepancy between the i^{th} spacecraft attitude tracking error and the output of the auxiliary system (3.38) by the unit-quaternion $\tilde{\mathbf{Q}}_i^e = (\tilde{\mathbf{q}}_i^{e\ T}, \tilde{\eta}_i^e)^T$, defined by

$$\tilde{\mathbf{Q}}_i^e = \bar{\mathbf{Q}}_i^{-1} \odot \tilde{\mathbf{Q}}_i, \quad (3.39)$$

satisfying the unit-quaternion dynamics

$$\dot{\tilde{\mathbf{Q}}}_i^e = \mathbf{T}(\tilde{\mathbf{Q}}_i^e)\tilde{\boldsymbol{\Omega}}_i, \quad (3.40)$$

$$\tilde{\boldsymbol{\Omega}}_i = \tilde{\boldsymbol{\omega}}_i - \mathbf{R}(\tilde{\mathbf{Q}}_i^e)\beta_i, \quad (3.41)$$

where $\tilde{\boldsymbol{\omega}}_i$ is the angular velocity tracking error and $\mathbf{R}(\tilde{\mathbf{Q}}_i^e)$ is the rotation matrix related to $\tilde{\mathbf{Q}}_i^e$. We propose the following input torque for each spacecraft

$$\boldsymbol{\Gamma}_i = \mathbf{H}_i(\boldsymbol{\omega}_d, \dot{\boldsymbol{\omega}}_d, \boldsymbol{\beta}_i, \dot{\boldsymbol{\beta}}_i, \tilde{\mathbf{Q}}_i, \tilde{\mathbf{Q}}_i^e) - k_i^p \tilde{\mathbf{q}}_i - \sum_{j=1}^n k_{ij}^p \mathbf{q}_{ij}, \quad (3.42)$$

where the control gains are defined as in Theorem 3.1 and the nonlinear term $\mathbf{H}_i(\cdot)$ is given by

$$\begin{aligned} \mathbf{H}_i(\cdot) = & \mathbf{J}_{f_i} \left(\mathbf{R}(\tilde{\mathbf{Q}}_i) \dot{\boldsymbol{\omega}}_d + \mathbf{R}(\tilde{\mathbf{Q}}_i^e) \dot{\boldsymbol{\beta}}_i + \mathbf{S}(\mathbf{R}(\tilde{\mathbf{Q}}_i) \boldsymbol{\omega}_d) \mathbf{R}(\tilde{\mathbf{Q}}_i^e) \boldsymbol{\beta}_i \right) \\ & + \mathbf{S} \left(\mathbf{R}(\tilde{\mathbf{Q}}_i) \boldsymbol{\omega}_d + \mathbf{R}(\tilde{\mathbf{Q}}_i^e) \boldsymbol{\beta}_i \right) \mathbf{J}_{f_i} \left(\mathbf{R}(\tilde{\mathbf{Q}}_i) \boldsymbol{\omega}_d + \mathbf{R}(\tilde{\mathbf{Q}}_i^e) \boldsymbol{\beta}_i \right). \end{aligned} \quad (3.43)$$

Under the assumption that spacecraft absolute attitudes are transmitted between any two neighbors, the following result holds:

Theorem 3.3. *Consider the spacecraft formation given in (3.1)-(3.2) under the control law (3.42), and let the input of the dynamic system (3.38) be defined as*

$$\bar{\boldsymbol{\beta}}_i = -\mathbf{R}(\tilde{\mathbf{Q}}_i^e)^T \left(k_i^p \tilde{\mathbf{q}}_i + \sum_{j=1}^n k_{ij}^p \mathbf{q}_{ij} \right). \quad (3.44)$$

If the control gains satisfy condition (2.31), then all the signals are globally bounded and $\mathbf{q}_i \rightarrow \mathbf{q}_j \rightarrow \mathbf{q}_d$ and $\boldsymbol{\omega}_i \rightarrow \boldsymbol{\omega}_j \rightarrow \boldsymbol{\omega}_d$, for all $i, j \in \mathcal{N}$. Furthermore, if there exists a time $t_0 > 0$ such that $\tilde{\eta}_i > 0$, for all $t \geq t_0$ and $i \in \mathcal{N}$, then the same convergence results are obtained without condition (2.31).

Sketch of proof: First, we can show using some algebraic manipulations that the angular velocity error dynamics satisfy

$$\tilde{\boldsymbol{\Omega}}_i^T \mathbf{J}_{f_i} \dot{\tilde{\boldsymbol{\Omega}}}_i = \tilde{\boldsymbol{\Omega}}_i^T (\boldsymbol{\Gamma}_i - \mathbf{H}_i(\boldsymbol{\omega}_d, \dot{\boldsymbol{\omega}}_d, \boldsymbol{\beta}_i, \dot{\boldsymbol{\beta}}_i, \tilde{\mathbf{Q}}_i, \tilde{\mathbf{Q}}_i^e)), \quad (3.45)$$

with $\mathbf{H}_i(\cdot)$ is given in (3.43). The proof of Theorem 3.3 follows from Lyapunov arguments using the Lyapunov function

$$V = \frac{1}{2} \sum_{i=1}^n (\tilde{\boldsymbol{\Omega}}_i^T \mathbf{J}_{f_i} \tilde{\boldsymbol{\Omega}}_i + \boldsymbol{\beta}_i^T \boldsymbol{\beta}_i) + \sum_{i=1}^n 2k_i^p (1 - \tilde{\eta}_i) + \sum_{i=1}^n \sum_{j=1}^n k_{ij}^p (1 - \eta_{ij}), \quad (3.46)$$

leading to the negative semi-definite time-derivative

$$\dot{V} = - \sum_{i=1}^n \lambda_i \boldsymbol{\beta}_i^T \boldsymbol{\beta}_i. \quad (3.47)$$

Then, Invoking Barbălat Lemma, one can show that $\beta_i \rightarrow 0$ and $\dot{\beta}_i \rightarrow 0$, which in turns, from (3.38) and (3.44) with Lemma 2.4, implies that $\tilde{\mathbf{q}}_i \rightarrow 0$ and $\mathbf{q}_{ij} \rightarrow 0$. Then, it can be deduced from the boundedness of $\tilde{\omega}_i$ that $\tilde{\omega}_i \rightarrow 0$ and $\omega_{ij} \rightarrow 0$. The rest of the proof can be shown using Lemma 2.4. A detailed proof of Theorem 3.3 is given in Appendix A.2.3. □

Remark 3.6. *The control scheme presented in this section satisfies the reduction principle, however the results of Corollary 3.1 do not hold if the gain k_i^p is set to zero in (3.42).*

3.5.2 Attitude synchronization without reference assignment

The control scheme in section 3.4.2 is modified here to reduce the communication requirement between spacecraft. We associate to each spacecraft the auxiliary system (3.38) and let the mismatch between the absolute attitude of the i^{th} spacecraft and the output of the auxiliary system (3.38) be represented by the unit-quaternion $\mathbf{Q}_i^e = (\mathbf{q}_i^e{}^T, \eta_i^e)^T$ given in (3.13), governed by the dynamic equations (3.14)-(3.15). We propose the following velocity-free input torque

$$\Gamma_i = \mathbf{J}_{f_i} \mathbf{R}(\mathbf{Q}_i^e) \dot{\beta}_i + \mathbf{S}(\mathbf{R}(\mathbf{Q}_i^e) \beta_i) \mathbf{J}_{f_i} \mathbf{R}(\mathbf{Q}_i^e) \beta_i - \sum_{j=1}^n k_{ij}^p \mathbf{q}_{ij}, \quad (3.48)$$

for $i \in \mathcal{N}$, with the control gains being defined as in Theorem 3.1. Under the assumption that each spacecraft can transmit its absolute attitude, the following result holds:

Theorem 3.4. *Consider a spacecraft formation modeled in (3.1)-(3.2) with the control law (3.48). Let the input of the auxiliary system (3.38) be given as*

$$\bar{\beta}_i = -\mathbf{R}(\mathbf{Q}_i^e)^T \sum_{j=1}^n k_{ij}^p \mathbf{q}_{ij}. \quad (3.49)$$

Let the information flow graph be a tree. Then all the signals are globally bounded and $\mathbf{q}_i \rightarrow \mathbf{q}_j$, $\omega_i \rightarrow \omega_j$, for all $i, j \in \mathcal{N}$. Furthermore, if there exists a time $t_0 > 0$ such that $\eta_i(t) > 0$, (or $\eta_i(t) < 0$), for all $t \geq t_0$ and $i \in \mathcal{N}$, then the above results hold for any connected undirected communication graph.

Sketch of proof: The angular velocity error dynamics can be shown, in view of (3.45), to satisfy

$$\Omega_i^T \mathbf{J}_{f_i} \dot{\Omega}_i = \Omega_i^T \left(\Gamma_i - \mathbf{J}_{f_i} \mathbf{R}(\mathbf{Q}_i^e) \dot{\beta}_i - \mathbf{S}(\mathbf{R}(\mathbf{Q}_i^e) \beta_i) \mathbf{J}_{f_i} \mathbf{R}(\mathbf{Q}_i^e) \beta_i \right). \quad (3.50)$$

The result of Theorem 3.4 can be shown using the Lyapunov function

$$V = \frac{1}{2} \sum_{i=1}^n (\boldsymbol{\Omega}_j^T \mathbf{J}_{f_i} \boldsymbol{\Omega}_j + \boldsymbol{\beta}_j^T \boldsymbol{\beta}_j) + \sum_{i=1}^n \sum_{j=1}^n k_{ij}^p (1 - \eta_{ij}), \quad (3.51)$$

with the negative semi-definite time-derivative

$$\dot{V} = - \sum_{i=1}^n \lambda_i \boldsymbol{\beta}_i^T \boldsymbol{\beta}_i, \quad (3.52)$$

which allows to conclude, following similar arguments as in the proof of Theorem 3.3, that $\boldsymbol{\beta}_i \rightarrow 0$ and $\dot{\boldsymbol{\beta}}_i \rightarrow 0$, which in turns implies from (3.38) and (3.49) and Lemma 2.5 that $\mathbf{q}_i \rightarrow \mathbf{q}_j$ and $\boldsymbol{\omega}_i \rightarrow \boldsymbol{\omega}_j$ for $i, j \in \mathcal{N}$. A detailed proof of Theorem 3.4 is given in appendix A.2.4. □

Remark 3.7. Note that Remark 3.5 also applies for the result of Theorem 3.4.

The output feedback attitude synchronization schemes presented in this section improve the results proposed in section 3.4 in the sense that only spacecraft absolute attitudes are transmitted between neighboring spacecraft, and a single auxiliary system is implemented for each member of the team. Hence, the communication flow requirement is reduced and the order of the system is not affected by the communication topology between spacecraft. Fig.3.2 shows the implementation of the control law in Theorem 3.3. However, precise knowledge of the spacecraft inertia matrices is required in the control law (3.48), which cannot be extended in a straightforward manner to account for input torque saturations.

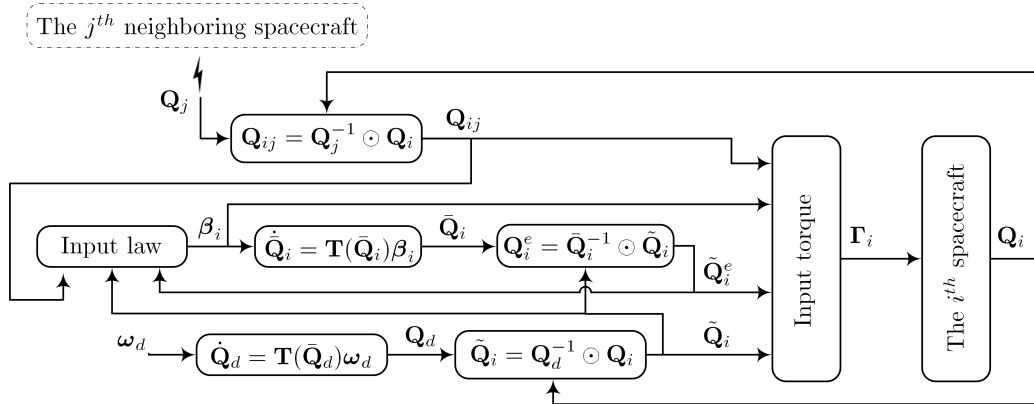


Figure 3.2: Implementation of the control law in Theorem 3.3.

3.6 Combined design

It can be seen from Corollary 3.1 that attitude alignment is achieved in the case where the desired angular velocity is zero, *i.e.*, $\mathbf{q}_i \rightarrow \mathbf{q}_j$ and $\boldsymbol{\omega}_i \rightarrow 0$. This result is not guaranteed using the second approach in section 3.5 as stated in Remark 3.6. This particular problem is considered in this section, where the two auxiliary systems proposed in the previous sections are used in the same control law to design the output feedback attitude synchronization controller. The difference between this method and the result of Corollary 3.1 is that only absolute attitudes are transmitted between neighboring spacecraft.

We propose the following control law

$$\boldsymbol{\Gamma}_i = \mathbf{J}_{f_i} \mathbf{R}(\mathbf{Q}_i^e) \dot{\boldsymbol{\beta}}_i + \mathbf{S}(\mathbf{R}(\mathbf{Q}_i^e) \boldsymbol{\beta}_i) \mathbf{J}_{f_i} \mathbf{R}(\mathbf{Q}_i^e) \boldsymbol{\beta}_i - k_i^v \tilde{\boldsymbol{\phi}}_i - \sum_{j=1}^n k_{ij}^p \mathbf{q}_{ij}, \quad (3.53)$$

where k_{ij}^p are defined as in Theorem 3.1 and the scalar gain k_i^v is defined such that $k_i^v > 0$ if $i \in \mathcal{I}$ and $k_i^v = 0$ otherwise, where the set $\mathcal{I} \neq \emptyset$ is a subset of \mathcal{N} . The unit quaternion \mathbf{Q}_i^e is defined in (3.13) with $\bar{\mathbf{Q}}_i$ being the output of the dynamic system (3.38), and $\tilde{\boldsymbol{\phi}}_i$ the vector part of the unit quaternion $\tilde{\boldsymbol{\Phi}}_i := (\tilde{\boldsymbol{\phi}}_i^T, \tilde{\zeta}_i)^T$, defined by

$$\tilde{\boldsymbol{\Phi}}_i = \boldsymbol{\Phi}_i^{-1} \odot \mathbf{Q}_i, \quad \text{for } i \in \mathcal{I}, \quad (3.54)$$

where the unit-quaternion $\boldsymbol{\Phi}_i$ is the output of the auxiliary system

$$\dot{\boldsymbol{\Phi}}_i = \mathbf{T}(\boldsymbol{\Phi}_i) \boldsymbol{\psi}_i, \quad \text{for } i \in \mathcal{I}, \quad (3.55)$$

and $\boldsymbol{\psi}_i \in \mathbb{R}^3$ is an input to be designed later. It is straightforward to verify that $\tilde{\boldsymbol{\Phi}}_i$ satisfies the dynamics

$$\dot{\tilde{\boldsymbol{\Phi}}}_i = \mathbf{T}(\tilde{\boldsymbol{\Phi}}_i) (\boldsymbol{\omega}_i - \mathbf{R}(\tilde{\boldsymbol{\Phi}}_i) \boldsymbol{\psi}_i). \quad (3.56)$$

The definition of the set \mathcal{I} indicates that the dynamic system (3.55) is implemented in only some spacecraft in the team (at least one spacecraft).

Theorem 3.5. *Consider a spacecraft formation modeled in (3.2) with the control law (3.53). Let the inputs of the auxiliary systems (3.38) and (3.55) be given respectively as*

$$\bar{\boldsymbol{\beta}}_i = -\mathbf{R}(\mathbf{Q}_i^e)^T \left(k_i^v \tilde{\boldsymbol{\phi}}_i + \sum_{j=1}^n k_{ij}^p \mathbf{q}_{ij} \right), \quad \boldsymbol{\psi}_i = \bar{\lambda}_i \tilde{\boldsymbol{\phi}}_i, \quad (3.57)$$

where $\bar{\lambda}_i$ are strictly positive scalar gains. Let the information flow graph be a tree. Then all the signals are globally bounded and $\mathbf{q}_i \rightarrow \mathbf{q}_j$, $\boldsymbol{\omega}_i \rightarrow 0$ for all $i, j \in \mathcal{N}$. Furthermore, if there exists a time $t_0 > 0$ such that $\eta_i(t) > 0$, (or $\eta_i(t) < 0$),

for all $t \geq t_0$ and $i \in \mathcal{N}$, then the above results hold for any connected undirected communication graph.

Sketch of proof: The proof of the theorem follows using the Lyapunov function

$$V = \frac{1}{2} \sum_{i=1}^n (\boldsymbol{\Omega}_i^T \mathbf{J}_{f_i} \boldsymbol{\Omega}_i + \boldsymbol{\beta}_i^T \boldsymbol{\beta}_i) + \sum_{i=1}^n \sum_{j=1}^n k_{ij}^p (1 - \eta_{ij}) + \sum_{i=1}^n 2k_i^v (1 - \zeta_i), \quad (3.58)$$

leading to the negative semi-definite time-derivative

$$\dot{V} = - \sum_{i=1}^n \lambda_i \boldsymbol{\beta}_i^T \boldsymbol{\beta}_i - \sum_{i=1}^n \bar{\lambda}_i k_i^v \tilde{\boldsymbol{\phi}}_i^T \tilde{\boldsymbol{\phi}}_i. \quad (3.59)$$

Then, Following similar arguments as in the proof of Theorem 3.4, from the first term in the right hand side of (3.59), we can conclude that $\mathbf{q}_i \rightarrow \mathbf{q}_j$ and $\boldsymbol{\omega}_i \rightarrow \boldsymbol{\omega}_j$, for all $i, j \in \mathcal{N}$. In addition, using similar steps as in the proof of Theorem 3.1, the last term in (3.59) leads to the conclusion that $\boldsymbol{\omega}_i \rightarrow 0$, for $i \in \mathcal{I}$. From the definition of the set \mathcal{I} and the above result, we conclude that $\boldsymbol{\omega}_i \rightarrow 0$, for $i \in \mathcal{N}$. A detailed proof of Theorem 3.5 is given in Appendix A.2.5. □

Remark 3.8. *The synchronization control law in this section can be extended in a straightforward manner to the trajectory tracking case.*

3.7 Simulation results

This section contains the results of simulations that illustrate the effectiveness of the proposed output feedback attitude synchronization schemes in this chapter. The simulations are conducted using MATLAB/SIMULINK. We consider a group of four spacecraft with inertia matrices $\mathbf{J}_{f_i} = \text{diag}[20, 20, 30]$ kg/m² for $i \in \mathcal{N} := \{1 \dots 4\}$, with initial conditions

$$\begin{aligned} \mathbf{Q}_1(0) &= (0, 0, 1, 0)^T, & \mathbf{Q}_2(0) &= (1, 0, 0, 0)^T, \\ \mathbf{Q}_3(0) &= (0, 1, 0, 0)^T, & \mathbf{Q}_4(0) &= (0, 0, \sin(-\pi/4), \cos(-\pi/4))^T, \\ \boldsymbol{\omega}_1(0) &= (-0.5, 0.5, -0.45)^T, & \boldsymbol{\omega}_2(0) &= (0.5, -0.3, 0.1)^T, \\ \boldsymbol{\omega}_3(0) &= (0.1, 0.6, -0.1)^T, & \boldsymbol{\omega}_4(0) &= (0.4, 0.4, -0.5)^T. \end{aligned}$$

In addition, the auxiliary systems (3.11), (3.12), (3.38) and (3.55) are initialized for all $i, j \in \mathcal{N}$ as

$$\bar{\mathbf{Q}}_i = \bar{\mathbf{Q}}_{ij} = \boldsymbol{\Phi}_i(0) = (1, 0, 0, 0)^T, \quad \dot{\boldsymbol{\beta}}_i = (0.1, 0.1, 0.1)^T. \quad (3.60)$$



Figure 3.3: Information flow graph

Attitude synchronization with reference trajectory: We consider the problem where spacecraft are required to align their attitudes while tracking a desired time-varying reference trajectory given by

$$\boldsymbol{\omega}_d = 0.5 \sin(0.1\pi t)(1, 1, 1)^T \text{ rad/sec}, \quad \dot{\mathbf{Q}}_d = \mathbf{T}(\mathbf{Q}_d)\boldsymbol{\omega}_d, \quad (3.61)$$

where $\mathbf{Q}_d(0) = (0, 0, 0, 1)^T$. We assume that the information flow between spacecraft is modeled by the two communication graphs \mathcal{G}_p and \mathcal{G}_d having the same sets of nodes and edges of the communication graph \mathcal{G}_1 in Fig. 3.3 with the set of edges $\mathcal{E}_1 = \{(1, 2), (1, 4), (2, 3), (2, 4)\}$. The adjacency matrices of \mathcal{G}_p and \mathcal{G}_d are given respectively by $\mathcal{K}_p = \text{col}[k_{ij}^p]$ and $\mathcal{K}_d = \text{col}[k_{ij}^d]$ with $k_{ij}^p = 1.5$ and $k_{ij}^d = 25$ for $(i, j) \in \mathcal{E}_1$, and are zero otherwise.

We implement the control schemes in Theorem 3.1 and Theorem 3.3 with the control gains given in table 3.1. Note that the control gains are selected such that condition (2.31) is satisfied. Fig.3.4-Fig.3.6 illustrate the obtained results, where spacecraft attitudes and angular velocities are respectively given by \mathbf{q}_i^j and $\boldsymbol{\omega}_i^j$, for $i \in \mathcal{N}$ and $i = d$ for the desired trajectory. We used the superscript j to denote the j^{th} component of a vector. It can be seen from these figures that the four spacecraft converge to the same specified trajectory in the two cases. As noted above, the control law in Theorem 3.3 is simpler to implement since only a single auxiliary system is needed in each spacecraft and only absolute attitudes are transmitted between members of the group. However, the control effort applied in this case is considerably larger than the applied control input when using the control scheme in Theorem 3.1, especially during the transient. This is mainly due to the presence of the term $\mathbf{H}_i(\cdot)$ in (3.42), which can take large values when the relative attitudes are large.

Attitude synchronization without reference trajectory: We implement the control schemes given in Theorem 3.2 and Theorem 3.4 with the control gains given in table 3.1, and the communication graph between spacecraft is modeled by the two undirected graphs \mathcal{G}_p and \mathcal{G}_d having the same sets of nodes and edges as the graph \mathcal{G}_2 in Fig.3.3 with the set of edges $\mathcal{E}_2 = \{(1, 2), (1, 4), (2, 3)\}$. The elements of

Table 3.1: Control gains

Theorem 3.1	$k_i^p = 30, k_i^d = 80, \lambda_i = 6, \text{ for } i \in \mathcal{N}, \lambda_{ij} = 5 \text{ for all } (i, j) \in \mathcal{E}_1$
Theorem 3.2	$\lambda_i = 6, \text{ for } i \in \mathcal{N}, \lambda_{ij} = 5, \text{ for all } i, j \in \mathcal{E}_2$
Theorem 3.3	$k_i^p = 10, \lambda_i = 6, \text{ for all } i \in \mathcal{N}$
Theorem 3.4	$\lambda_i = 6, \text{ for } i \in \mathcal{N}$
Theorem 3.5	$k_i^v = 20, \lambda_i = 6, \bar{\lambda}_i = 0.5$

the adjacency matrices $\mathcal{K}_p = \text{col}[k_{ij}^p]$ and $\mathcal{K}_d = \text{col}[k_{ij}^d]$ are such that $k_{ij}^p = 10$ and $k_{ij}^d = 20$ for $(i, j) \in \mathcal{E}_2$, and are zero otherwise. Note that the communication graph is connected and contains no cycles, *i.e.*, it is a tree. The obtained results are shown in Fig.3.7-Fig.3.9, where it is clear that spacecraft reach an agreement and converge to the same final time-varying attitude with the two attitude synchronization schemes. Note that the final attitude depends on the initial conditions and the weights assigned to each link of the communication graph. As a result, the agreement attitude (The final value) is different in the two cases.

The last simulations considered in this section concern the combined auxiliary systems design to solve the spacecraft attitude alignment problem with zero final angular velocity. We implement the control law proposed in Theorem 3.5 with the control gains given in table 3.1 and the information flow is described by the same communication graph \mathcal{G}_p as in the above example. The auxiliary system (3.55) is implemented only in the first spacecraft, *i.e.*, $\mathcal{I} = \{1\}$. Fig.3.10 illustrates the spacecraft angular velocities and attitudes in this case. It can be seen that since the angular velocity of the first spacecraft is driven to zero, the four spacecraft align their attitudes to the same final attitude with zero final angular velocity.

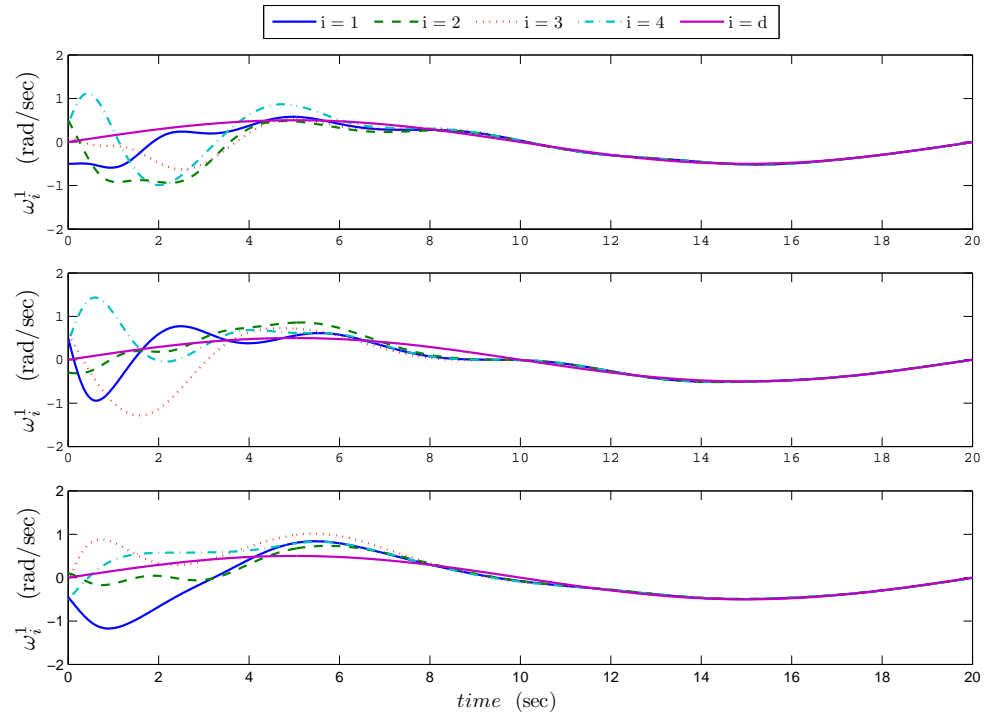
3.8 Concluding Remarks

In this chapter, we proposed output feedback design methods for the attitude synchronization problem of a group of rigid bodies (or spacecraft). Instrumental in our approach, the introduction of the so-called “auxiliary systems” (playing the role of velocity observers in a certain sense) allowing to generate the necessary damping in the absence of the actual spacecraft angular velocities and relative angular velocities. Two output feedback design methods are presented based on auxiliary systems of different structures. As discussed throughout this chapter, the two design methods provide similar solutions, each with some advantages and limitations. The main advantage with the first approach is the design of control schemes accounting for input torque saturations, whereas the advantage gained with the implementation of a auxiliary systems with higher order, the second approach, is to reduce the communication requirements between spacecraft in the team by using only spacecraft absolute attitudes in the control law. In addition, the latter method requires the implementation

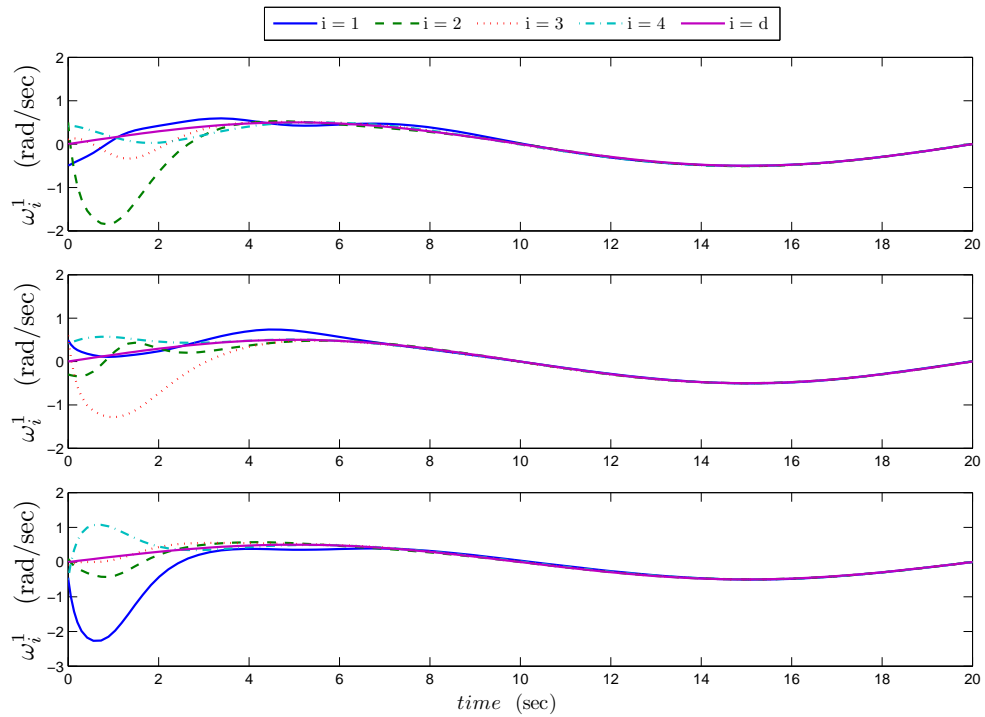
of only a single auxiliary system for each spacecraft to achieve the control objectives. However, the order of the system depends on the communication topology between spacecraft in the output feedback control schemes using the first approach. Both output feedback design methods achieve ‘almost’ global asymptotic stability results in the sense that the closed loop system has multiple equilibria, that represent the same physical configuration, but only one of them is an attractor (Bhat and Bernstein, 2000).

The two approaches have been used to solve two problems. The first problem addressed is the simultaneous attitude tracking and formation-keeping without angular velocity measurements (Theorem 3.1 and Theorem 3.3). One important requirement in these synchronization schemes is that the desired angular velocity must be available to all spacecraft. This can be achieved either by assuming that the reference velocity is a global information available to all spacecraft, or can be available to one spacecraft and then transmitted to all members of the group via communication channels. The extension of the above control law to the case where the desired angular velocity is available to only one or some spacecraft, and cannot be transmitted between members of the team, is not straightforward. This problem still presents some technical challenges even with angular velocity measurements. In the full state information case, a preliminary solution to this problem has been proposed in Bai *et al.* (2008) where a reference trajectory is assumed to be known to a single spacecraft (the leader), and assumed to be linearly parameterized in terms of some scalar time functions known by all spacecraft, and unknown constant coefficients. In the approach of Bai *et al.* (2008), some information on the reference velocity is still required to be available to all spacecraft and the type of reference trajectories is restricted. On the other hand, it has been shown in Ren (2007*b*) and Ren (2009) that in addition to the angular velocities, the rigid bodies accelerations are required in the control law to achieve attitude synchronization to a time-varying reference available to only some rigid bodies among the team acting as group leaders. In the case where the reference angular velocity is zero, we have proposed in Abdessameud and Tayebi (2008*a*) a velocity-free leader-follower scheme that achieves attitude synchronization under the condition that the communication graph between spacecraft is a tree and the desired constant attitude is available to a single leader.

In Theorem 3.2 and Theorem 3.4, we solved the attitude alignment problem in the case where no reference trajectory is considered to dictate the behavior of spacecraft and all members of the team are required to align their attitudes using only local information exchange. We have shown that spacecraft angular velocities are guaranteed to converge to a common bounded time-function. To drive the final angular velocity to zero using only relative attitude errors, we proposed in Theorem 3.5 a combined design that exploits the benefits of the two design approaches.



(a)



(a)

Figure 3.4: Spacecraft angular velocities: (a) Theorem 3.1, (b) Theorem 3.3.

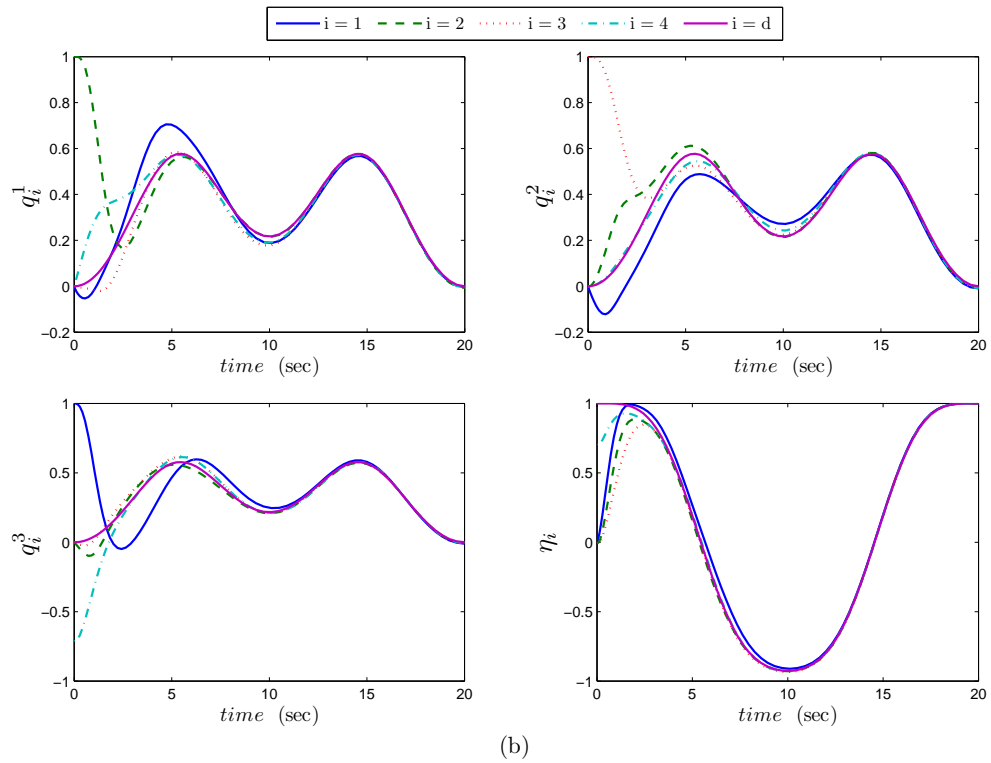
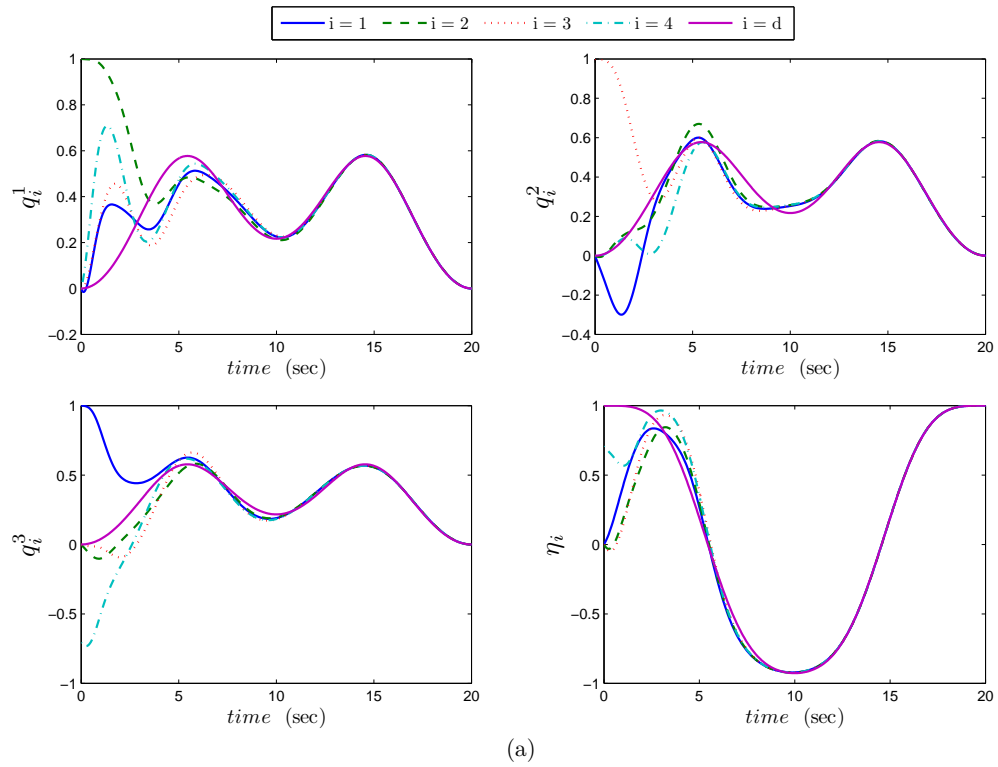
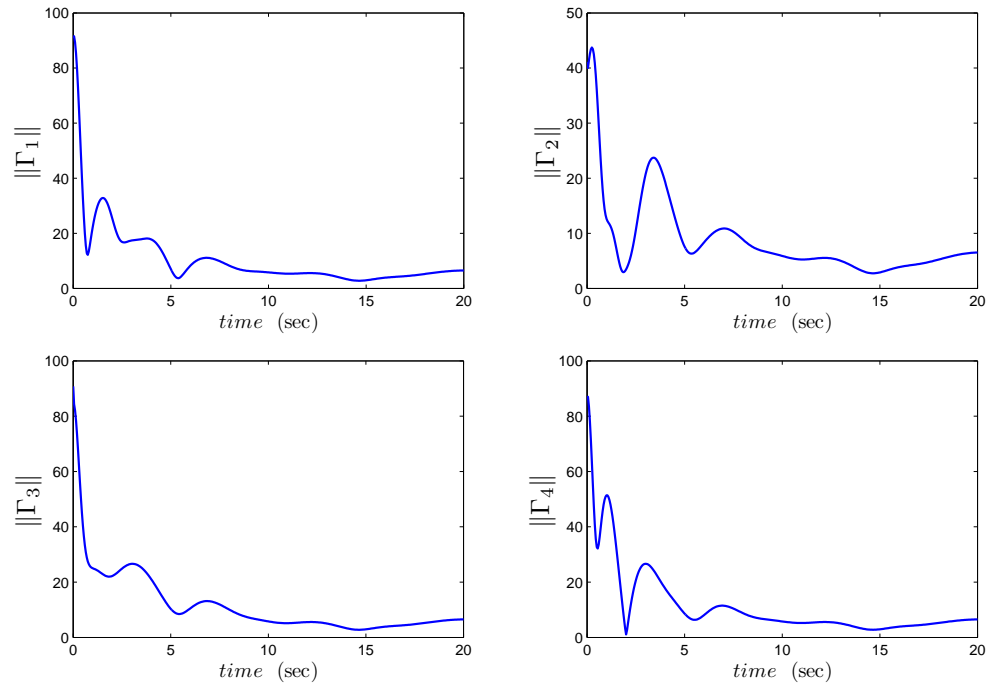
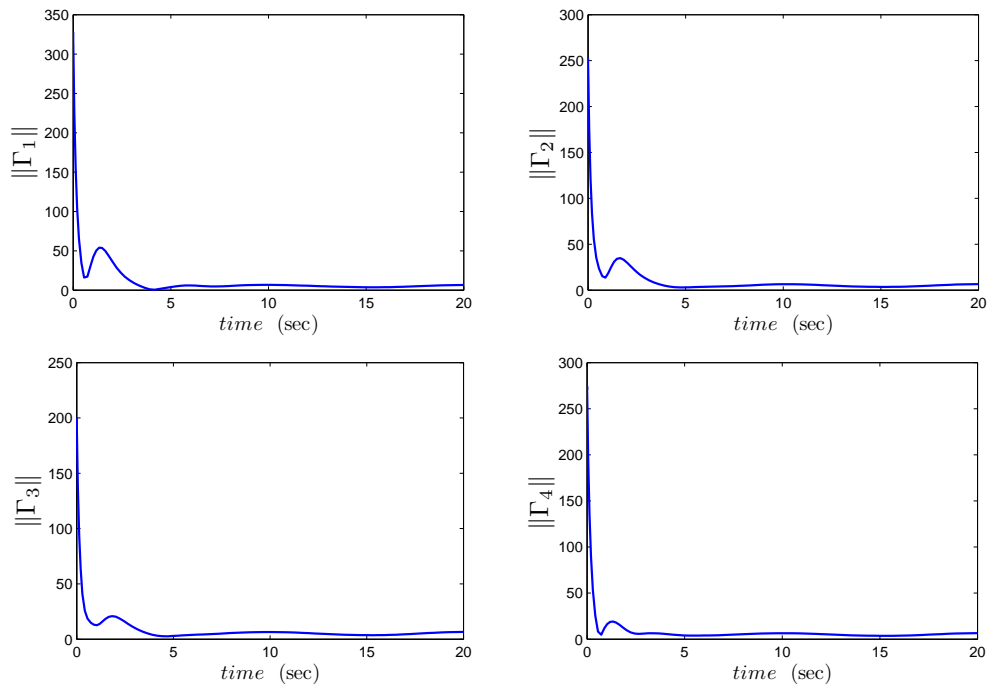


Figure 3.5: Spacecraft attitudes: (a) Theorem 3.1, (b) Theorem 3.3.

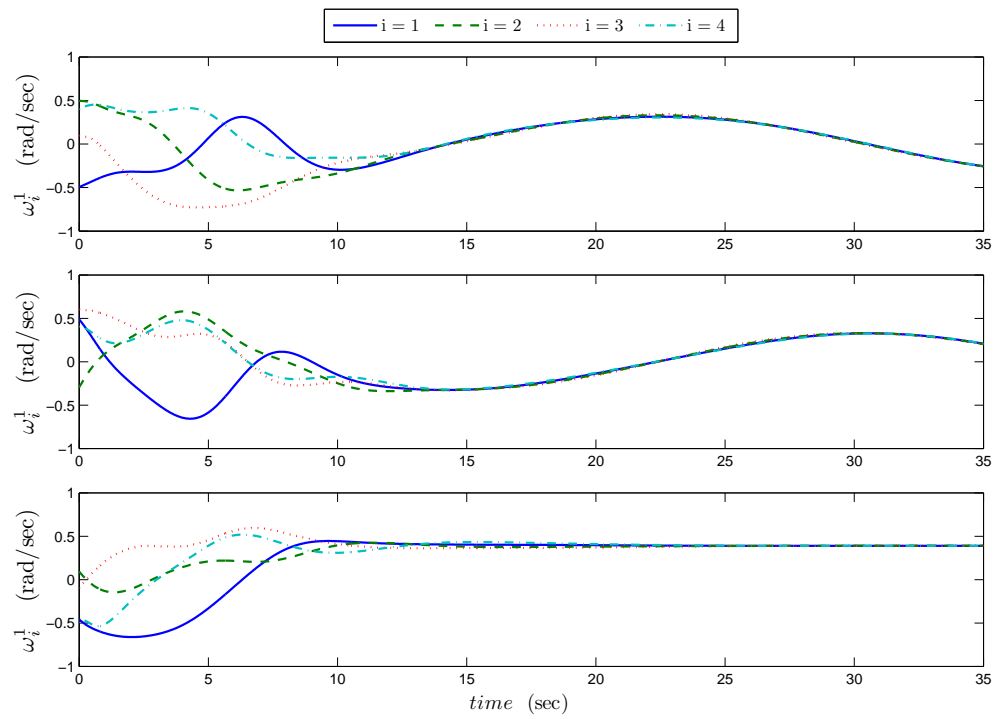


(a)

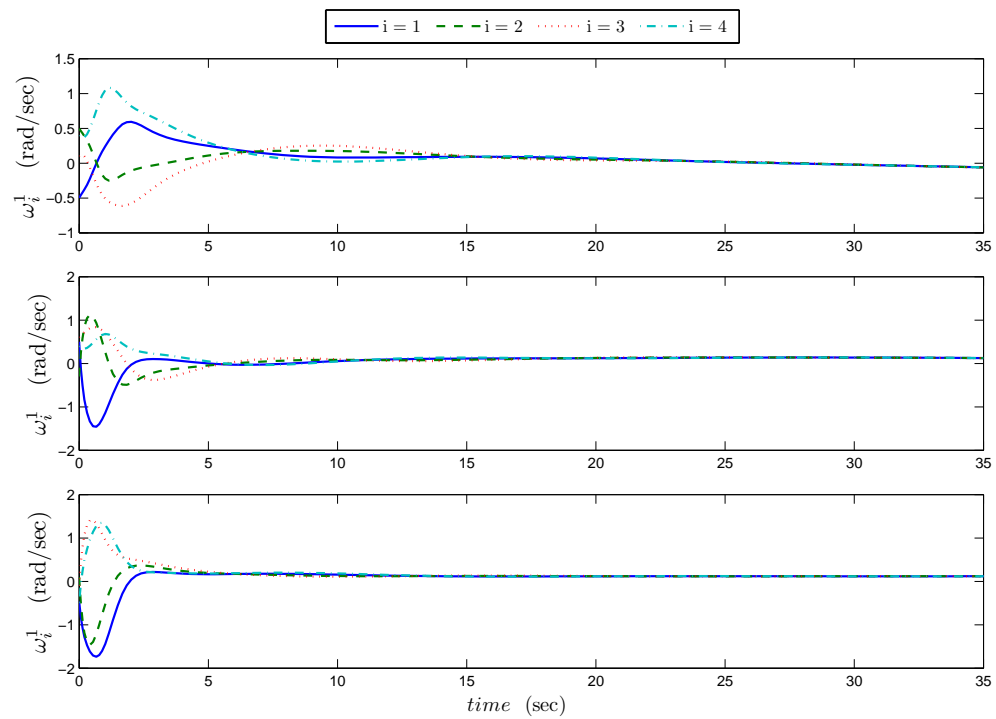


(b)

Figure 3.6: Norm of input torques: (a) Theorem 3.1, (b) Theorem 3.3.

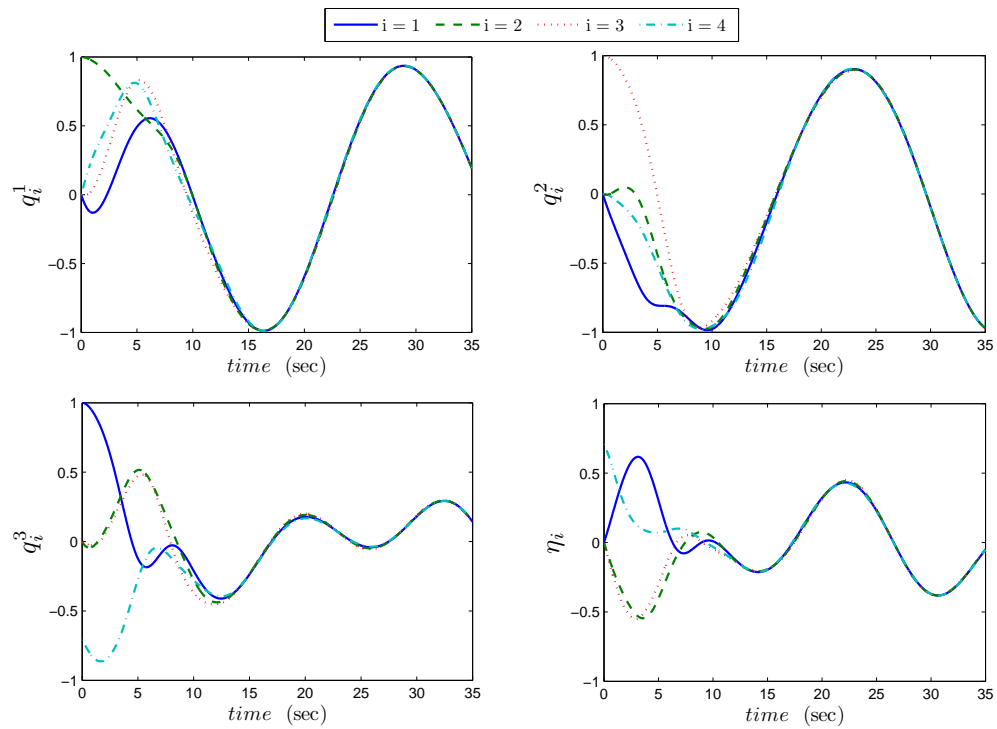


(a)

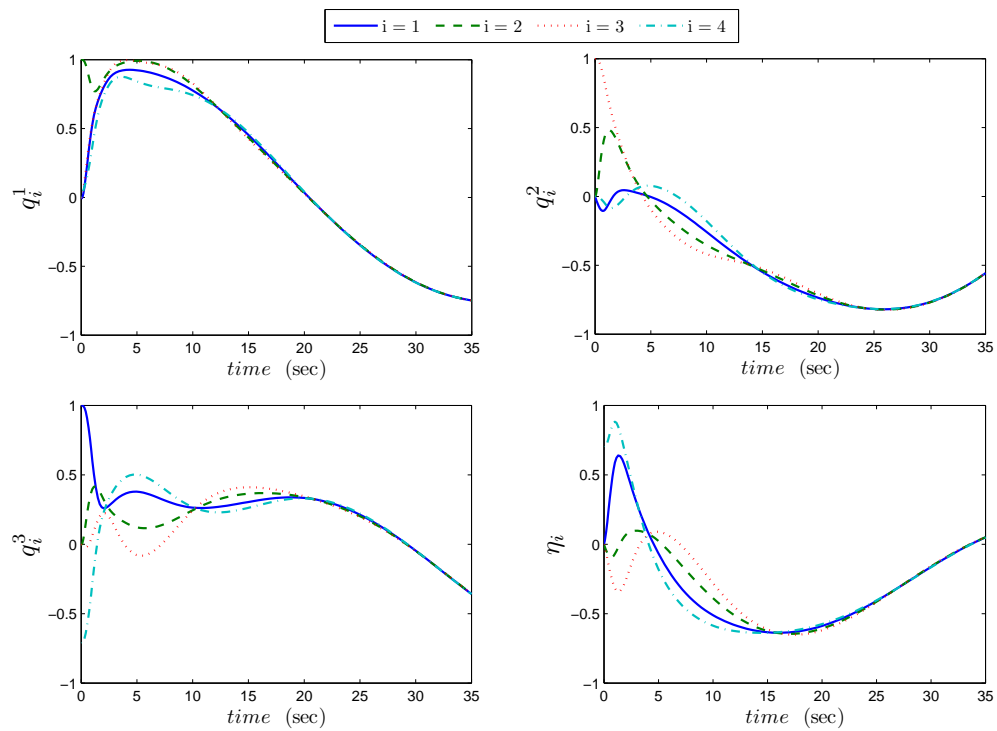


(a)

Figure 3.7: Spacecraft angular velocities: (a) Theorem 3.2, (b) Theorem 3.4.



(a)



(b)

Figure 3.8: Spacecraft attitudes: (a) Theorem 3.2, (b) Theorem 3.4.

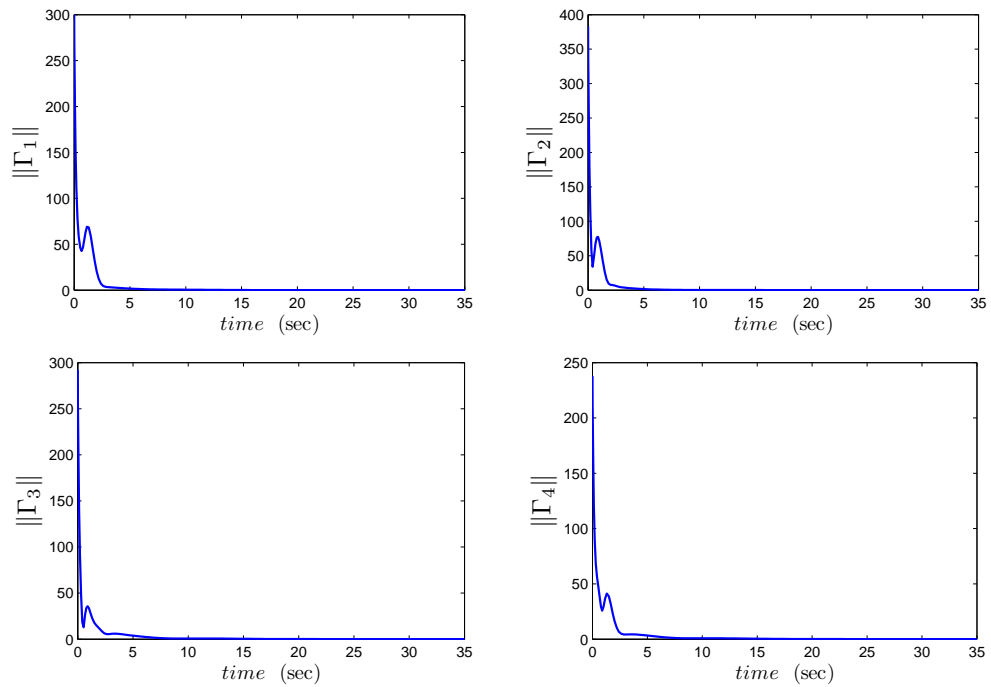
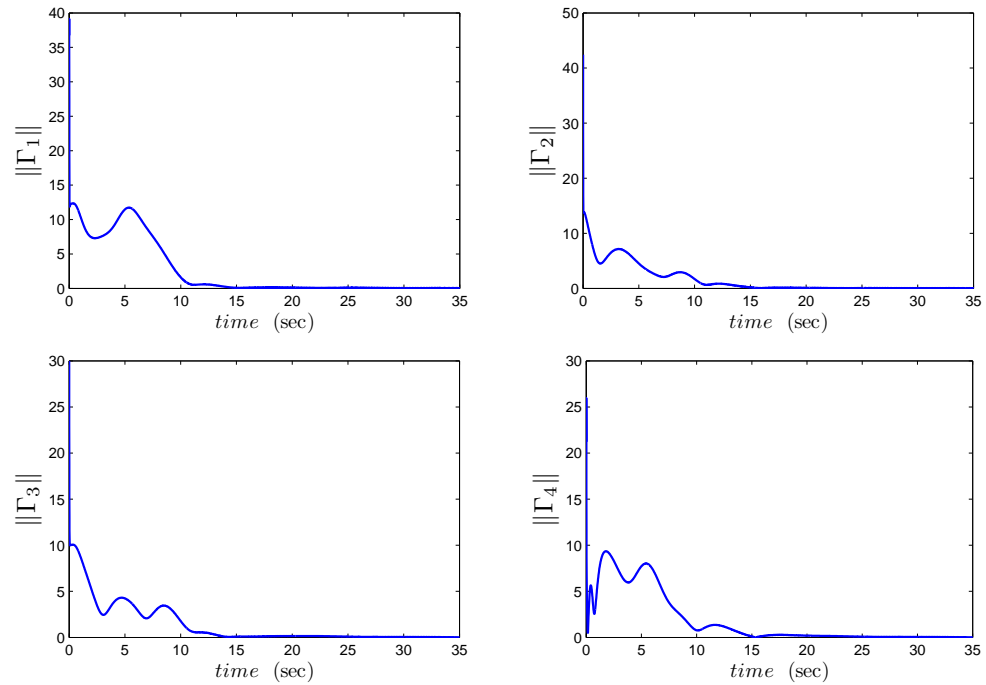
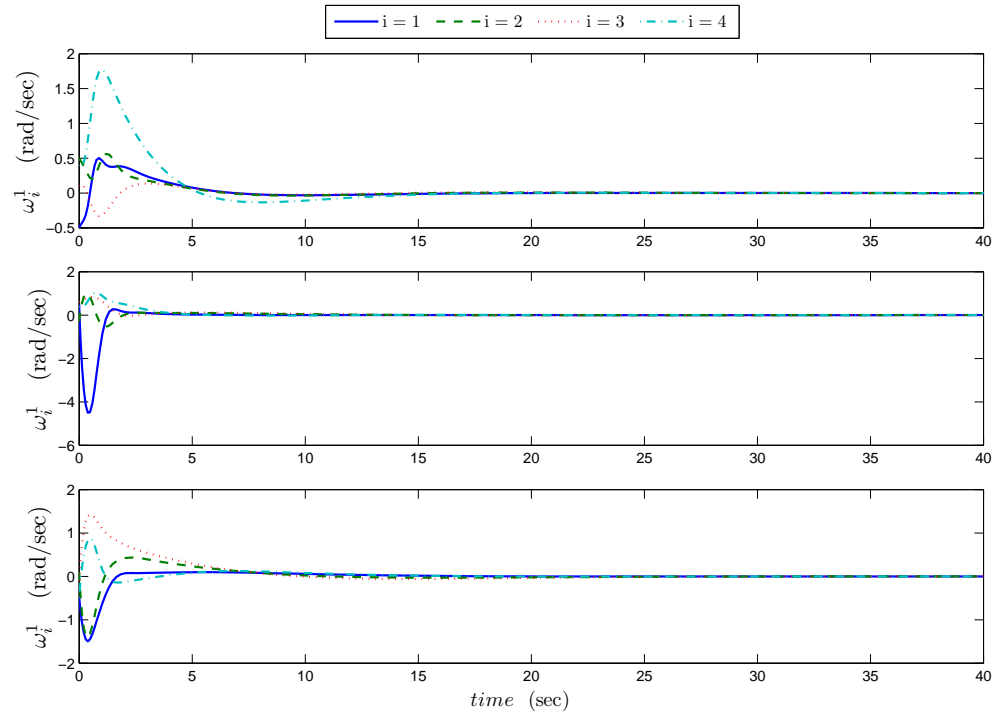
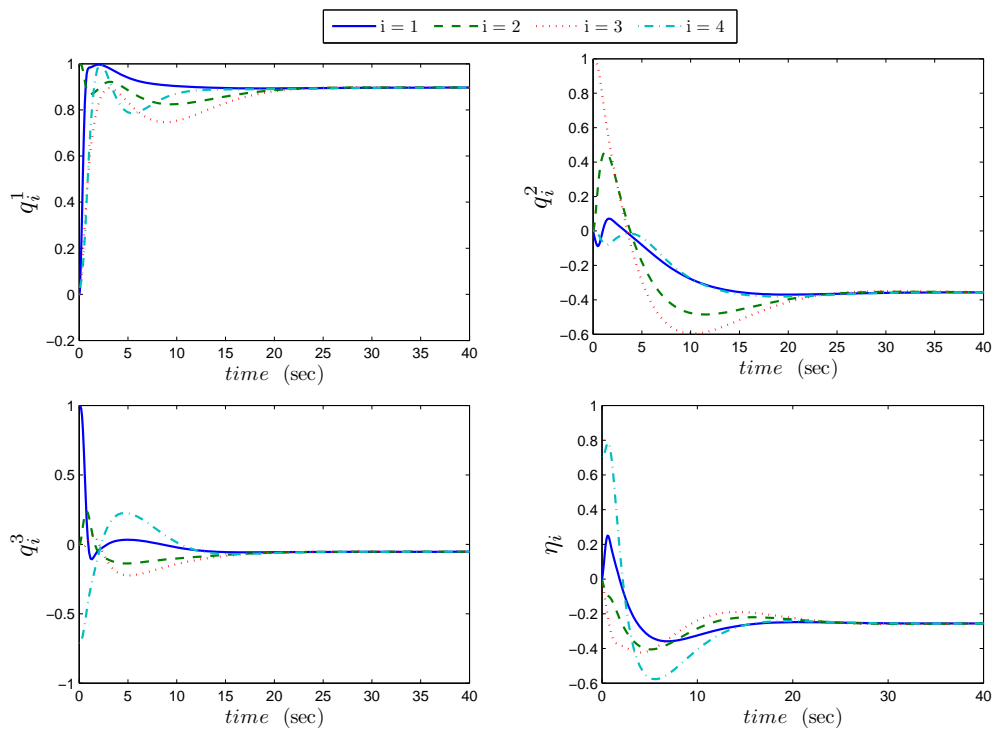


Figure 3.9: Norm of input torques: (a) Theorem 3.2, (b) Theorem 3.4.



(a)



(b)

Figure 3.10: Simulation results in case of Theorem 3.5: (a) Spacecraft angular velocities (b) Spacecraft attitudes

Chapter 4

Global trajectory tracking of VTOL UAVs

The trajectory tracking control problem, in $SE(3)$, of a single VTOL aircraft is discussed in this chapter. The main objective is to present a new control design methodology for this class of under-actuated systems that will constitute an important step towards the design of the formation control schemes discussed in the next chapters. Based on the unit-quaternion representation of the attitude, we propose a multistage constructive control design procedure, exploiting the cascade property of the translational and rotational dynamics. More precisely, we consider the force as a virtual control input for the translational dynamics, from which we extract the required (desired) system attitude and thrust achieving the control objective. Thereafter, the control torque is designed to drive the actual attitude to the desired one. Instrumental auxiliary systems are introduced to remove the requirement of the linear-velocity measurement and to achieve global asymptotic stability results of the overall closed loop system. The state feedback trajectory tracking control scheme proposed in this chapter is an adaptation of the work in Abdessameud and Tayebi (2009c) and the linear-velocity-free control scheme is reported in Abdessameud and Tayebi (2010a).

4.1 Introduction

VTOL-UAVs are suitable for a broad range of applications requiring stationary flights, and constitute an important class of thrust propelled UAVs. These vehicles are generally *under-actuated*. It is clear that one of the most important components for reliable autonomous flights is an efficient attitude control and stabilization scheme. In fact, this problem has been the focus of many researchers over the past years, resulting in a myriad of successful attitude controllers (see for example Wen and Kreutz-Delgado, 1991; Tayebi and McGillvray, 2006, and references therein). However, the position control of under-actuated VTOL vehicles in $SE(3)$ is more challenging than the attitude control problem as evidenced by the lack of global asymptotic stability results in the literature (Koo and Sastry, 1998; Frazzoli *et al.*, 2000; Pflimlin *et al.*, 2007; Madani and Benallegue, 2007; Kendoul *et al.*, 2006).

Due to the under-actuated nature of this class of systems, a common practice is to use the system attitude as a means to direct the thrust in order to control the system position and velocity. The authors in Hamel *et al.* (2002) and Pflimlin *et al.* (2007) proposed a hierarchical design procedure for the position control of

VTOL-UAVs. The idea consists of using the vehicle orientation and thrust as control variables to stabilize the vehicle position, and then apply a classical backstepping procedure to determine the torque-input capable of stabilizing the required orientation. In Hua *et al.* (2009), a similar control architecture is applied to solve the trajectory tracking problem, where the angular velocity is used as an intermediate variable instead of the orientation. In the work of Aguiar and Hespanha (2007), the tracking problem of a class of under-actuated systems, including VTOL UAVs, has been solved using a backstepping design procedure leading global practical stability results.

In this chapter, we present new solutions to the trajectory tracking problem of a single VTOL aircraft. We use an extraction algorithm that provides the necessary thrust and desired orientation of the aircraft, from an intermediary translational force (virtual input). The extracted thrust input is used to drive the translational dynamics of the aircraft, and the desired orientation is considered as a time-varying reference attitude to the rotational dynamics. This extraction algorithm provides non-singular solutions and leads to a multistage control design procedure for this class of systems. Global trajectory tracking control laws are designed following this procedure in the full state information case and in the case where the linear-velocity vector is not available for feedback. The latter problem is interesting from a practical point of view since good estimates of aircraft linear-velocities are generally obtained from the fusion of available measurements from accelerometers and high-quality GPS sensors. However, the GPS signal is not available in indoor and urban applications (structure/bridge inspection for example) due to signal blockage and attenuation. While the extraction algorithm presents several advantages, its application gives rise to some technical difficulties, which are particularly challenging in the partial state information case.

4.2 Problem formulation

The trajectory tracking problem of the class of under-actuated VTOL aircraft involves the design of the input thrust and the input torque such that the position of the aircraft converge to a time-varying desired trajectory. Our objective is to design trajectory tracking control schemes for a VTOL UAV governed by the dynamic model given in section 2.2, *i.e.*,

$$(\Sigma_1) : \begin{cases} \dot{\mathbf{p}} = \mathbf{v}, \\ \dot{\mathbf{v}} = g\hat{\mathbf{e}}_3 - \frac{\mathcal{I}}{m}\mathbf{R}(\mathbf{Q})^T\hat{\mathbf{e}}_3, \end{cases} \quad (4.1)$$

$$(\Sigma_2) : \begin{cases} \dot{\mathbf{Q}} = \frac{1}{2}\mathbf{T}(\mathbf{Q})\boldsymbol{\omega}, \\ \mathbf{J}_f\dot{\boldsymbol{\omega}} = \boldsymbol{\Gamma} - \mathbf{S}(\boldsymbol{\omega})\mathbf{J}_f\boldsymbol{\omega}. \end{cases} \quad (4.2)$$

More formally, we would like to design a global control law guaranteeing the asymptotic convergence to zero of the following position and linear-velocity tracking errors

$$\tilde{\mathbf{p}} = \mathbf{p} - \mathbf{p}_d, \quad \tilde{\mathbf{v}} := \dot{\tilde{\mathbf{p}}} = \mathbf{v} - \mathbf{v}_d, \quad (4.3)$$

where \mathbf{p}_d and \mathbf{v}_d are respectively the desired position and linear-velocity, with $\mathbf{v}_d = \dot{\mathbf{p}}_d$.

4.3 Controlling VTOL UAVs

To control the position of a VTOL aircraft, the orientation (attitude) of the system is generally used as a means to direct the thrust. In fact, to move the vehicle from one point to another, it is necessary to first determine the magnitude and direction of the thrust that must be applied to the translational dynamics. The direction of the thrust is equivalent to the orientation of the aircraft in the case of VTOL aircraft modeled in (4.1)-(4.2). In this section, we present a new control design approach for this class of under-actuated systems that relies on a non-singular extraction algorithm of the thrust and orientation of the aircraft.

4.3.1 Thrust and desired attitude extraction

The translational acceleration of the aircraft given in (4.1) can be rewritten as

$$\dot{\mathbf{v}} = \mathbf{F} - \frac{\mathcal{T}}{m} \left(\mathbf{R}(\mathbf{Q})^T - \mathbf{R}(\mathbf{Q}_d)^T \right) \hat{\mathbf{e}}_3, \quad (4.4)$$

with

$$\mathbf{F} := g\hat{\mathbf{e}}_3 - \frac{\mathcal{T}}{m} \mathbf{R}(\mathbf{Q}_d)^T \hat{\mathbf{e}}_3, \quad (4.5)$$

where the variable \mathbf{F} is an “intermediary” control input to the translational dynamics and $\mathbf{Q}_d = (\mathbf{q}_d, \eta_d)^T$ is the unit-quaternion representing the desired attitude of the aircraft, which will be determined through the control design.

It should be noted that the intermediary control input \mathbf{F} in (4.5) is written function of the input thrust and the desired attitude of the aircraft. The latter variables can be extracted from the expression of a defined intermediary input according to the results of the following lemma, which was initiated in the work of Roberts and Tayebi (2009).

Lemma 4.1. *Consider equation (4.5) and let the vector $\mathbf{F} := (\mu_1, \mu_2, \mu_3)^T$. It is always possible to extract the thrust magnitude and the desired system attitude from (4.5) as*

$$\mathcal{T} = m \|g\hat{\mathbf{e}}_3 - \mathbf{F}\|, \quad (4.6)$$

$$\eta_d = \sqrt{\frac{1}{2} + \frac{m(g - \mu_3)}{2\mathcal{T}}}, \quad \mathbf{q}_d = \frac{m}{2\mathcal{T}\eta_d} \begin{pmatrix} \mu_2 \\ -\mu_1 \\ 0 \end{pmatrix}, \quad (4.7)$$

under the condition that

$$\mathbf{F} \neq (0, 0, x), \text{ for } x \geq g. \quad (4.8)$$

In addition, if \mathbf{F} is differentiable, we can write the desired angular velocity of the aircraft as

$$\boldsymbol{\omega}_d = \Xi(\mathbf{F})\dot{\mathbf{F}}, \quad (4.9)$$

$$\Xi(\mathbf{F}) = \frac{1}{\gamma_1^2 \gamma_2} \begin{pmatrix} -\mu_1 \mu_2 & -\mu_2^2 + \gamma_1 \gamma_2 & \mu_2 \gamma_2 \\ \mu_1^2 - \gamma_1 \gamma_2 & \mu_1 \mu_2 & -\mu_1 \gamma_2 \\ \mu_2 \gamma_1 & -\mu_1 \gamma_1 & 0 \end{pmatrix}, \quad (4.10)$$

with $\gamma_1 = (\mathcal{T}/m)$ and $\gamma_2 = \gamma_1 + (g - \mu_3)$.

The proof of this Lemma is given in Appendix A.3.1.

4.3.2 Control design procedure

The extraction algorithm in Lemma 4.1 suggests a simple design procedure that provides an almost separate control design for the translational and rotational dynamics for the class of under-actuated systems under study. As a matter of fact, if one is able to design an appropriate intermediary control input \mathbf{F} that satisfies condition (4.8), the necessary input thrust and the desired attitude can be extracted respectively from the singularity-free expressions (4.6)-(4.7). The extracted value of the thrust will then be used as the input of the translational dynamics of the aircraft and the desired attitude will be considered as a reference input for the rotational dynamics. Then, the torque input can be designed to drive the attitude of the aircraft to the desired one. The design procedure that we will follow in the control of VTOL UAVs in this chapter is summarized as follows:

1. Consider the translational dynamics in (4.4), and design the *intermediary* control input \mathbf{F} satisfying (4.8),
2. Based on the result of Lemma 4.1, extract the necessary thrust \mathcal{T} and the desired attitude \mathbf{Q}_d . The magnitude of the thrust will be the input to the translational subsystem,
3. Consider \mathbf{Q}_d as a time-varying desired attitude, and design a torque input such that the aircraft attitude tracks the desired attitude, *i.e.*, the attitude tracking error $\tilde{\mathbf{Q}}$, defined in (2.13) converges asymptotically to zero.

Based on this procedure, the control of a single VTOL aircraft is schematically described in Fig. 4.1.

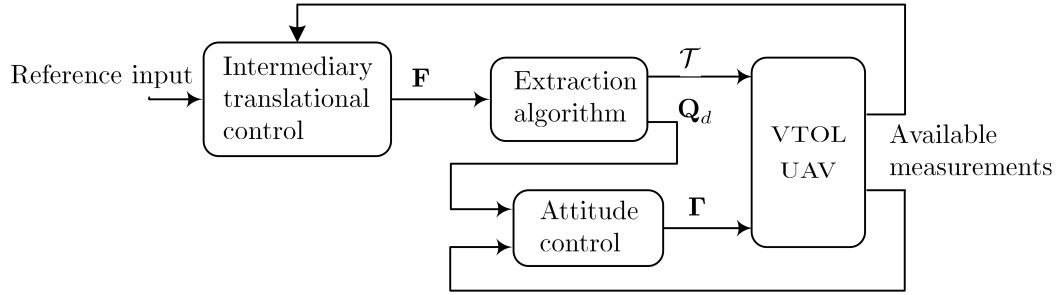


Figure 4.1: The control structure for a single VTOL aircraft

4.3.3 Intermediary control input constraints

It is important to mention that in view of (4.4), the translational dynamics of the aircraft are written as a linear system with the intermediary control \mathbf{F} as input, which must satisfy condition (4.8). It should be noticed that to satisfy this condition, it is sufficient to ensure that the third element of the intermediary control \mathbf{F} is bounded by an appropriate (known) value. In addition, the vector $\left(\frac{T}{m}(\mathbf{R}(\mathbf{Q})^T - \mathbf{R}(\mathbf{Q}_d)^T)\hat{e}_3\right)$ can be considered as a perturbation term to the translational dynamics. We can see from (4.4) and the extracted value of the thrust in (4.6) that the design of an *a priori* bounded intermediary control is sufficient to guarantee that this perturbation term is bounded.

Furthermore, we can see from Lemma 4.1 that the extracted desired attitude is time-varying. Therefore, the desired angular velocity, $\boldsymbol{\omega}_d$, and its time-derivative, $\dot{\boldsymbol{\omega}}_d$, are not necessarily zero, and the first step preceding the design of an attitude tracking control law will be to derive explicit expressions of these signals. From equation (4.9), we know that $\boldsymbol{\omega}_d$ and $\dot{\boldsymbol{\omega}}_d$ can be derived using the expressions of $\dot{\mathbf{F}}$ and $\ddot{\mathbf{F}}$. Consequently, the intermediary control input must be at least twice differentiable and the expressions of the first and second derivatives of \mathbf{F} must be function of available signals.

4.4 Trajectory tracking control of a single aircraft

A solution to the trajectory tracking problem of a single VTOL aircraft in the full state information case is presented in this section. We assume that the aircraft position, linear-velocity, attitude and angular velocity are available for feedback, and present a control scheme that provides global results in terms of the position¹.

1. We use the abusive notation “global in terms of the position” to emphasize that the results are guaranteed for any arbitrary initial conditions of the aircraft position and linear-velocity. Since attitude dynamics are involved, the obtained results are almost global.

4.4.1 Intermediary position control design

The first step is to determine an appropriate intermediary input for the translational dynamics subject to the constraints described in section 4.3.3. The velocity tracking error dynamics can be obtained from (4.3) and (4.4), using property 2.1, as

$$\dot{\tilde{\mathbf{v}}} = \mathbf{F} - \dot{\mathbf{v}}_d - \frac{2\mathcal{T}}{m}\mathbf{R}(\mathbf{Q})^T\mathbf{S}(\bar{\mathbf{q}})\tilde{\mathbf{q}}, \quad (4.11)$$

where $\tilde{\mathbf{q}}$ is the vector part of the unit-quaternion representing the attitude tracking error, defined in (2.13), and $\bar{\mathbf{q}}$ is given in (2.18). To achieve the trajectory tracking objective, we propose the following bounded intermediary input

$$\mathbf{F} = \dot{\mathbf{v}}_d - k_p\chi(\tilde{\mathbf{p}}) - k_d\chi(\tilde{\mathbf{v}}), \quad (4.12)$$

with k_p and k_d being positive scalar gains and the nonlinear function χ defined in (2.33). The intermediary input \mathbf{F} is guaranteed to be *a priori* bounded as

$$\|\mathbf{F}\| \leq \delta_d + \sigma_b\sqrt{3}(k_p + k_d), \quad (4.13)$$

with $\delta_d = \|\dot{\mathbf{v}}_d\|_\infty$ and σ_b is defined in property P2 in section 2.6. Before we proceed, we consider the following assumption.

Assumption 4.1. *The three first time-derivatives of the desired linear-velocity $\mathbf{v}_d(t)$ are bounded. The elements of the desired acceleration vector $\dot{\mathbf{v}}_d(t) := (\dot{v}_{d_1}, \dot{v}_{d_2}, \dot{v}_{d_3})^T$, and the positive control gains k_p and k_d should satisfy one of the following conditions:*

- (a) $\sigma_b(k_p + k_d) < |\dot{v}_{d_1}(t)|, \forall t \geq 0$,
- (b) $\sigma_b(k_p + k_d) < |\dot{v}_{d_2}(t)|, \forall t \geq 0$,
- (c) $|\dot{v}_{d_3}(t)| \leq \delta, \forall t \geq 0$, and $\sigma_b(k_p + k_d) \leq g - \delta$,
- (d) $\|\dot{\mathbf{v}}_d(t)\|_\infty \leq \bar{\delta}, \forall t \geq 0$, and $\sigma_b\sqrt{3}(k_p + k_d) \leq g - \bar{\delta}$.

with $\delta > 0$ and $0 \leq \bar{\delta} < g$.

It is straightforward to verify that if one of the cases of Assumption 4.1 is met, condition (4.8) is satisfied and the intermediary control \mathbf{F} can be used in the extraction algorithm given in Lemma 4.1. In fact, cases (a) and (b) ensure that $\mu_1 \neq 0$ and $\mu_2 \neq 0$ for all $t \geq 0$ respectively, case (c) is considered such that $\mu_3 < g$ for all $t \geq 0$, and finally, the more restrictive case (d) guarantees that $\|\mathbf{F}\| < g$ for all $t \geq 0$.

When condition (4.8) is satisfied for all time, the extracted value of the thrust \mathcal{T} , in (4.6), is guaranteed to be positive and *a priori* bounded as

$$\mathcal{T} \leq m \left(g + \delta_d + \sigma_b\sqrt{3}(k_p + k_d) \right) := \mathcal{T}_b, \quad (4.14)$$

with \mathcal{T}_b a positive constant. Also, the extracted desired attitude of the vehicle, \mathbf{Q}_d , is guaranteed to be realizable.

4.4.2 Attitude control design

Next, we consider the orientation dynamics and design a torque input for the aircraft that guarantees tracking of the desired attitude \mathbf{Q}_d given in (4.7). To this end, we need first to derive explicit expressions for the desired angular velocity and its time-derivative. After simple computations, the first and second time-derivatives of the intermediary control input can be obtained as

$$\dot{\mathbf{F}} = \ddot{\mathbf{v}}_d - k_p h(\tilde{\mathbf{p}}) \tilde{\mathbf{v}} - k_d h(\tilde{\mathbf{v}}) \dot{\tilde{\mathbf{v}}}, \quad (4.15)$$

and

$$\ddot{\mathbf{F}} = \mathbf{v}_d^{(3)} - k_p \dot{h}(\tilde{\mathbf{p}}) \tilde{\mathbf{v}} - \left(k_p h(\tilde{\mathbf{p}}) + k_d \dot{h}(\tilde{\mathbf{v}}) \right) \dot{\tilde{\mathbf{v}}} - k_d h(\tilde{\mathbf{v}}) \ddot{\tilde{\mathbf{v}}}, \quad (4.16)$$

where the diagonal matrix $h(\cdot)$ is defined in (2.34), and $\dot{h}(\cdot)$ is the time-derivative of $h(\cdot)$. Using the above expressions, the desired angular velocity of the aircraft can be explicitly evaluated from (4.9) and (4.15). In addition, we can see that $\dot{\tilde{\mathbf{v}}}$ can be obtained from the first time-derivative of (4.11), and hence the time-derivative of the desired angular velocity is completely known and is obtained from (4.9) as

$$\dot{\boldsymbol{\omega}}_d = \bar{\Xi}(\mathbf{F}, \dot{\mathbf{F}}) \dot{\mathbf{F}} + \Xi(\mathbf{F}) \ddot{\mathbf{F}}, \quad (4.17)$$

where $\bar{\Xi}(\mathbf{F}, \dot{\mathbf{F}})$ is the time-derivative of $\Xi(\mathbf{F})$ given in (4.10).

To design the attitude tracking control input, we introduce the following variable

$$\boldsymbol{\Omega} = \tilde{\boldsymbol{\omega}} - \boldsymbol{\beta}, \quad (4.18)$$

where $\tilde{\boldsymbol{\omega}}$ is the angular velocity tracking error defined in (2.15) and $\boldsymbol{\beta}$ is a design parameter to be determined later, and apply the following input torque for the aircraft

$$\boldsymbol{\Gamma} = \mathbf{H}(\boldsymbol{\omega}, \boldsymbol{\omega}_d, \dot{\boldsymbol{\omega}}_d) + \mathbf{J}_f \dot{\boldsymbol{\beta}} - k_q \tilde{\mathbf{q}} - k_\Omega \boldsymbol{\Omega}, \quad (4.19)$$

where k_q and k_Ω are positive scalar gains and

$$\mathbf{H}(\cdot) = \mathbf{S}(\boldsymbol{\omega}) \mathbf{J}_f \boldsymbol{\omega} - \mathbf{J}_f \mathbf{S}(\tilde{\boldsymbol{\omega}}) \mathbf{R}(\tilde{\mathbf{Q}}) \boldsymbol{\omega}_d + \mathbf{J}_f \mathbf{R}(\tilde{\mathbf{Q}}) \dot{\boldsymbol{\omega}}_d. \quad (4.20)$$

The design parameter $\boldsymbol{\beta}$ is used in the control law to ensure global stability results of the overall closed loop system.

4.4.3 Stability of the overall System

Our results in this part are stated in the following theorem.

Theorem 4.1. *Consider the VTOL-UAV modeled as in (4.1)-(4.2) and let the desired velocity \mathbf{v}_d and the controller gains k_p and k_d satisfy Assumption 4.1. Let the thrust input \mathcal{T} and the desired attitude \mathbf{Q}_d be given, respectively, by (4.6) and (4.7), with \mathbf{F} given in (4.12). Let the input torque of the aircraft be as in (4.19) with the variable $\boldsymbol{\beta}$ given by*

$$\boldsymbol{\beta} = -k_\beta \tilde{\mathbf{q}} + \frac{2\mathcal{T}}{k_q m} \mathbf{S}(\tilde{\mathbf{q}})^T \mathbf{R}(\mathbf{Q}) \tilde{\mathbf{v}}, \quad (4.21)$$

where k_β is a positive scalar gain. Then, starting from any initial conditions, all signals are bounded and $\tilde{\mathbf{p}} \rightarrow 0$, $\tilde{\mathbf{v}} \rightarrow 0$, $\tilde{\mathbf{q}} \rightarrow 0$ and $\tilde{\boldsymbol{\omega}} \rightarrow 0$.

Sketch of proof: First, we can see that with Assumption 4.1, the extraction condition (4.8) is satisfied and Lemma 4.1 can be used to derive the necessary thrust input and the desired attitude for the aircraft.

The angular velocity tracking error dynamics can be obtained from (2.15) and (4.2) as

$$\mathbf{J}_f \dot{\tilde{\boldsymbol{\omega}}} = \boldsymbol{\Gamma} - \mathbf{S}(\boldsymbol{\omega}) \mathbf{J}_f \boldsymbol{\omega} + \mathbf{J}_f \mathbf{S}(\tilde{\boldsymbol{\omega}}) \mathbf{R}(\tilde{\mathbf{Q}}) \boldsymbol{\omega}_d - \mathbf{J}_f \mathbf{R}(\tilde{\mathbf{Q}}) \dot{\boldsymbol{\omega}}_d, \quad (4.22)$$

and using (4.18) and (4.19)-(4.20) we can write

$$\mathbf{J}_f \dot{\tilde{\boldsymbol{\Omega}}} = -k_q \tilde{\mathbf{q}} - k_\Omega \tilde{\boldsymbol{\Omega}}. \quad (4.23)$$

The result of Theorem 4.1 can be shown using the Lyapunov function

$$V = \frac{1}{2} \tilde{\mathbf{v}}^T \tilde{\mathbf{v}} + k_p \sum_{j=1}^3 \int_0^{\tilde{p}^j} \sigma(s) ds + \frac{1}{2} \tilde{\boldsymbol{\Omega}}^T \mathbf{J}_f \tilde{\boldsymbol{\Omega}} + 2k_q(1 - \tilde{\eta}), \quad (4.24)$$

with $\tilde{\mathbf{p}} = (\tilde{p}^1, \tilde{p}^2, \tilde{p}^3)^T$ and σ being the saturation function defined in (2.33), leading to the negative semi-definite time-derivative

$$\dot{V} = -k_d \tilde{\mathbf{v}}^T \chi(\tilde{\mathbf{v}}) - k_\Omega \tilde{\boldsymbol{\Omega}}^T \tilde{\boldsymbol{\Omega}} - k_q k_\beta \tilde{\mathbf{q}}^T \tilde{\mathbf{q}}, \quad (4.25)$$

which indicates that $V(t) \leq V(0)$ and the vectors $\tilde{\mathbf{p}}$, $\tilde{\mathbf{v}}$ and $\tilde{\boldsymbol{\Omega}}$ are bounded, and leads us to conclude the boundedness of $\tilde{\boldsymbol{\omega}}$, $\dot{\tilde{\mathbf{v}}}$ and $\dot{\tilde{\boldsymbol{\Omega}}}$. Invoking Barbălat lemma, we conclude that $\tilde{\mathbf{v}} \rightarrow 0$, $\tilde{\mathbf{q}} \rightarrow 0$ and $\tilde{\boldsymbol{\omega}} \rightarrow 0$. Also, invoking Lemma 2.3, we conclude that $\dot{\tilde{\mathbf{v}}} \rightarrow 0$, leading to $\tilde{\mathbf{p}} \rightarrow 0$. Details of the proof of Theorem 4.1 are given in Appendix A.3.2. □

Remark 4.1. *The cases in Assumption (4.1) are natural restrictions of the desired trajectory for VTOL-UAVs. As shown in the proof of Theorem 4.1, the input \mathbf{F} will converge asymptotically to $\dot{\mathbf{v}}_d$. If the desired acceleration is selected as in one of the above cases, we will guarantee that $\dot{\mathbf{v}}_d \neq (0, 0, x)^T$ for all $x \geq g$, and condition (4.8) will be satisfied. This is a reasonable condition for this type of UAVs since, in normal*

operations, the vehicle is not allowed to land with an acceleration higher than or equal to the gravitational acceleration.

It is important to mention that the unit-quaternion representation of the attitude and the singularity-free extraction algorithm play an important role in achieving global trajectory tracking for the VTOL aircraft. In fact, the proposed design procedure allows the design of an *a priori* bounded intermediary control using standard control techniques based on nonlinear smooth saturation functions. Furthermore, the nonlinear perturbation term, which depends on the aircraft thrust and attitude tracking error, *i.e.*, \mathcal{T} and $\tilde{\mathbf{q}}$, is compensated using the linear-velocity tracking error in the design of the variable β . Note that the time-derivative of this variable, $\dot{\beta}$, is used in the input torque (4.19) and is derived by simple calculations as

$$\begin{aligned} \dot{\beta} = & \frac{-k_{\beta}}{2}(\tilde{\eta}\mathbf{I}_3 + \mathbf{S}(\tilde{\mathbf{q}}))\tilde{\omega} + \frac{2\mathcal{T}}{k_q m} \left(\mathbf{S}(\tilde{\mathbf{q}})^T \mathbf{R}(\mathbf{Q})\dot{\tilde{\mathbf{v}}} + \frac{d}{dt}(\mathbf{S}(\tilde{\mathbf{q}})^T \mathbf{R}(\mathbf{Q}))\tilde{\mathbf{v}} \right) \\ & + \frac{2m}{k_q \mathcal{T}}(g\hat{e}_3 - \mathbf{F})^T \dot{\mathbf{F}} \mathbf{S}(\tilde{\mathbf{q}})^T \mathbf{R}(\mathbf{Q})\tilde{\mathbf{v}}, \end{aligned} \quad (4.26)$$

with $\frac{d}{dt}(\mathbf{S}(\tilde{\mathbf{q}})^T \mathbf{R}(\mathbf{Q})) = \mathbf{S}(\dot{\tilde{\mathbf{q}}})^T \mathbf{R}(\mathbf{Q}) - \mathbf{S}(\tilde{\mathbf{q}})^T \mathbf{S}(\boldsymbol{\omega}) \mathbf{R}(\mathbf{Q})$. Note that β and $\dot{\beta}$ are computed using only available signals.

4.5 Design without linear-velocity measurements

A global trajectory tracking control scheme that removes the requirements of the linear-velocity is presented in this section. Similar to section 4.4, the first step in the control design is to determine an appropriate intermediary translational input subject to some constraints. In the case where the linear-velocity vector is not available for feedback, the first and second time-derivatives of any ‘classical’ output feedback scheme will be respectively function of the aircraft linear-velocity and linear-acceleration. To solve this problem, a new control structure is proposed for the intermediary translational input. The main idea is to implement an auxiliary system having an input with two terms. The first term, which is the intermediary control input of the aircraft, is constructed using the states of the auxiliary system through smooth saturation functions. The second term is designed using the aircraft states to achieve the trajectory tracking objective. This control structure leads to an *a priori* bounded intermediary control input that does not depend explicitly on the system states, which simplifies considerably the input torque design.

4.5.1 Intermediary position control design

Let us define the following auxiliary system

$$\ddot{\boldsymbol{\theta}} = \mathbf{F} - \mathbf{u} - \dot{\mathbf{v}}_d, \quad (4.27)$$

where $\boldsymbol{\theta} \in \mathbb{R}^3$ is an auxiliary variable and \mathbf{u} is an input to be determined later. Also, the variables $\boldsymbol{\theta}$ and $\dot{\boldsymbol{\theta}}$ can be initialized arbitrarily. We propose the following intermediary control input

$$\mathbf{F} = \dot{\mathbf{v}}_d - k_p \chi(\boldsymbol{\theta}) - k_d \chi(\dot{\boldsymbol{\theta}}), \quad (4.28)$$

where k_p, k_d are defined as in Theorem 4.1 and χ is defined in (2.33). We can see that the input \mathbf{F} is guaranteed to be bounded as in (4.13). Also, if the extraction condition (4.8) is satisfied, the extracted necessary thrust input \mathcal{T} is guaranteed to be bounded as in (4.14) and the extracted desired attitude \mathbf{Q}_d is realizable.

To design the auxiliary input \mathbf{u} , we define the following error variables

$$\boldsymbol{\xi} = \tilde{\mathbf{p}} - \boldsymbol{\theta}, \quad \mathbf{z} = \dot{\boldsymbol{\xi}} = \tilde{\mathbf{v}} - \dot{\boldsymbol{\theta}}, \quad (4.29)$$

where $\boldsymbol{\theta}$ is the output of the auxiliary system (4.27). Using (4.4) and (4.29) with property 2.1, the translational error dynamics can be shown to satisfy

$$\dot{\mathbf{z}} = \mathbf{u} - \frac{2\mathcal{T}}{m} \mathbf{R}(\mathbf{Q})^T \mathbf{S}(\bar{\mathbf{q}}) \tilde{\mathbf{q}}. \quad (4.30)$$

We propose the following partial state feedback input

$$\mathbf{u} = -k_r \boldsymbol{\xi} - k_v (\boldsymbol{\xi} - \boldsymbol{\psi}), \quad (4.31)$$

$$\dot{\boldsymbol{\psi}} = k_\psi (\boldsymbol{\xi} - \boldsymbol{\psi}), \quad (4.32)$$

where k_r, k_v and k_ψ are positive scalar gains and $\boldsymbol{\psi} \in \mathbb{R}^3$ can be initialized arbitrarily. The objective of this auxiliary input is to drive the error vectors $\boldsymbol{\xi}$ and \mathbf{z} to zero asymptotically without linear-velocity measurements. The block diagram in Fig.4.2 illustrates the implementation of the proposed intermediary control law in (4.28) with (4.27) and (4.31)-(4.32).

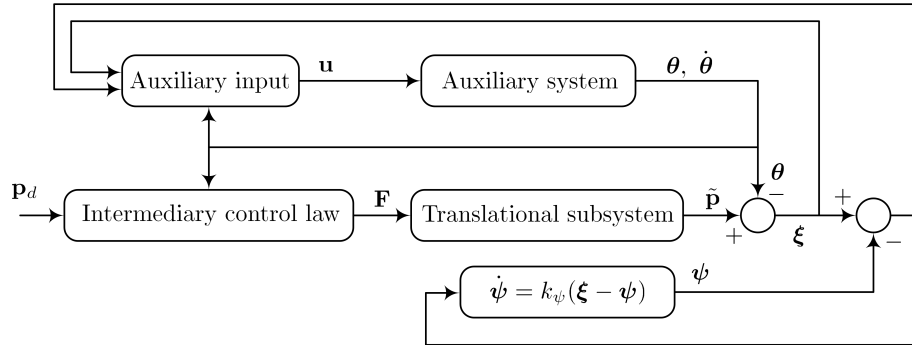


Figure 4.2: Intermediary control block diagram.

4.5.2 Attitude control design

Now, we consider the orientation dynamics and design a torque input for the vehicle that guarantees tracking of the desired attitude \mathbf{Q}_d given in (4.7). It is important to see that the first time-derivative of \mathbf{F} in (4.28) is obtained as

$$\dot{\mathbf{F}} = \ddot{\mathbf{v}}_d - k_p h(\boldsymbol{\theta}) \dot{\boldsymbol{\theta}} - k_d h(\dot{\boldsymbol{\theta}}) (\mathbf{F} - \dot{\mathbf{v}}_d - \mathbf{u}), \quad (4.33)$$

and is function of available signals. Therefore, the desired angular velocity, $\boldsymbol{\omega}_d$, derived in (4.9), does not depend on the linear-velocity vector. However, using (4.17) and the time-derivative of (4.33), the time-derivative of the desired angular velocity, $\dot{\boldsymbol{\omega}}_d$, will be given as

$$\dot{\boldsymbol{\omega}}_d = \boldsymbol{\Psi}_1 - \boldsymbol{\Psi}_2 \mathbf{z}, \quad (4.34)$$

where

$$\begin{aligned} \boldsymbol{\Psi}_1 = & \bar{\Xi}(\mathbf{F}, \dot{\mathbf{F}})(\mathbf{F}) \dot{\mathbf{F}} + \Xi(\mathbf{F}) \{ \mathbf{v}_d^{(3)} - k_p \dot{h}(\boldsymbol{\theta}) \dot{\boldsymbol{\theta}} - k_d h(\dot{\boldsymbol{\theta}}) (-k_v \dot{\boldsymbol{\psi}} - k_p h(\boldsymbol{\theta}) \dot{\boldsymbol{\theta}}) \\ & - (k_p h(\boldsymbol{\theta}) + k_d \dot{h}(\dot{\boldsymbol{\theta}}) - (k_d)^2 h(\dot{\boldsymbol{\theta}}) h(\ddot{\boldsymbol{\theta}})) (\mathbf{F} - \dot{\mathbf{v}}_d - \mathbf{u}) \}, \end{aligned} \quad (4.35)$$

$$\boldsymbol{\Psi}_2 = k_d (k_r + k_v) \Xi(\mathbf{F}) h(\dot{\boldsymbol{\theta}}). \quad (4.36)$$

From the angular velocity tracking error dynamics in (4.22), with (4.18) and (4.34), we can verify that

$$\mathbf{J}_f \dot{\boldsymbol{\Omega}} = \boldsymbol{\Gamma} - \bar{\mathbf{H}}(\boldsymbol{\omega}, \boldsymbol{\omega}_d, \boldsymbol{\Psi}_1) + \boldsymbol{\Upsilon} \mathbf{z} - \mathbf{J}_f \dot{\boldsymbol{\beta}}, \quad (4.37)$$

where

$$\bar{\mathbf{H}}(\cdot) = \mathbf{S}(\boldsymbol{\omega}) \mathbf{J}_f \boldsymbol{\omega} - \mathbf{J}_f \mathbf{S}(\tilde{\boldsymbol{\omega}}) \mathbf{R}(\tilde{\mathbf{Q}}) \boldsymbol{\omega}_d + \mathbf{J}_f \mathbf{R}(\tilde{\mathbf{Q}}) \boldsymbol{\Psi}_1, \quad (4.38)$$

and $\boldsymbol{\Omega} = (\tilde{\boldsymbol{\omega}} - \boldsymbol{\beta})$, $\boldsymbol{\Upsilon} = \mathbf{J}_f \mathbf{R}(\tilde{\mathbf{Q}}) \boldsymbol{\Psi}_2$, $\tilde{\mathbf{Q}}$ is given in (2.13), $\boldsymbol{\omega}_d$ is given in (4.9) with (4.33) and $\boldsymbol{\Psi}_1$ and $\boldsymbol{\Psi}_2$ are given respectively in (4.35)-(4.36). Note that the angular velocity error dynamics (4.37) depend on the vector \mathbf{z} , and hence on the aircraft linear-velocity, which is not available for feedback.

To design an input torque in (4.37) without linear-velocity measurements, the following nonlinear observer that generates estimates of the linear-velocity vector, $\hat{\mathbf{z}}$, is considered

$$\begin{cases} \dot{\hat{\mathbf{z}}} := \dot{\boldsymbol{\xi}} = \boldsymbol{\nu} - L_p \tilde{\boldsymbol{\xi}}, \\ \dot{\boldsymbol{\nu}} = \mathbf{u} - \frac{2\mathcal{T}}{m} \mathbf{R}(\mathbf{Q})^T \mathbf{S}(\bar{\mathbf{q}}) \tilde{\mathbf{q}} + \boldsymbol{\Upsilon}^T \boldsymbol{\Omega} - L_v^2 \tilde{\boldsymbol{\xi}}, \end{cases} \quad (4.39)$$

where $\tilde{\boldsymbol{\xi}} := (\hat{\boldsymbol{\xi}} - \boldsymbol{\xi})$ and L_p and L_v are strictly positive scalar gains. It should be noted that at this stage of the control design, all the signals required for the observer are well determined, namely \mathcal{T} , \mathbf{Q}_d and $\boldsymbol{\omega}_d$. Using the observed states, we propose

the following torque input for the rotational dynamics

$$\mathbf{\Gamma} = \bar{\mathbf{H}}(\boldsymbol{\omega}, \boldsymbol{\omega}_d, \boldsymbol{\Psi}_1) + \mathbf{J}_f \dot{\boldsymbol{\beta}} - k_q \tilde{\mathbf{q}} - k_\Omega \boldsymbol{\Omega} - \Upsilon \left(\hat{\mathbf{z}} + L_v \tilde{\boldsymbol{\xi}} \right), \quad (4.40)$$

with k_q, k_Ω being positive scalar gains and $\bar{\mathbf{H}}(\cdot)$ given in (4.38). The design of the vector $\boldsymbol{\beta}$ cannot rely on the estimated state $\hat{\mathbf{z}}$ since its time-derivative will give rise to the vector \mathbf{z} , which is not available for feedback.

4.5.3 Stability of the overall System

The following theorem states our results in this part.

Theorem 4.2. *Consider the VTOL-UAV modeled as in (4.1)-(4.2) and let the desired velocity \mathbf{v}_d and the controller gains k_p and k_d satisfy Assumption 4.1. Let the thrust input \mathcal{T} and the desired attitude \mathbf{Q}_d be given, respectively, by (4.6) and (4.7), with \mathbf{F} given by (4.28) with (4.27) and (4.31). Let the torque input be as in (4.40) with the observer (4.39) and the vector $\boldsymbol{\beta}$ given by*

$$\boldsymbol{\beta} = -k_\beta \tilde{\mathbf{q}} + \frac{2\mathcal{T}}{k_q m} \mathbf{S}(\bar{\mathbf{q}})^T \mathbf{R}(\mathbf{Q}) \left(\hat{\mathbf{z}} + L_p \tilde{\boldsymbol{\xi}} \right), \quad (4.41)$$

where k_ψ and k_β are positive scalar gains and $\bar{\mathbf{q}}$ is defined in (2.18). Pick the control and observer gains as follows

$$L_p - L_v > \sigma_1, \quad L_v^3 > \sigma_2, \quad k_q k_\beta > \frac{\mathcal{T}_b^2}{m^2} \left(\frac{1}{\sigma_1} + \frac{L_p^2}{\sigma_2} \right), \quad (4.42)$$

for some $\sigma_1 > 0, \sigma_2 > 0$, and \mathcal{T}_b given in (4.14). Then, starting from any initial conditions, all signals are bounded and $\tilde{\mathbf{p}} \rightarrow 0, \tilde{\mathbf{v}} \rightarrow 0, \tilde{\boldsymbol{\xi}} \rightarrow 0, \tilde{\mathbf{z}} \rightarrow 0, \tilde{\mathbf{q}} \rightarrow 0$ and $\tilde{\boldsymbol{\omega}} \rightarrow 0$.

Sketch of proof: Define the observation error vector as, $\tilde{\mathbf{z}} := \dot{\tilde{\boldsymbol{\xi}}} = \hat{\mathbf{z}} - \mathbf{z}$. The closed loop dynamics of the system are obtained as

$$\begin{aligned} \dot{\mathbf{z}} &= -k_r \boldsymbol{\xi} - k_v (\boldsymbol{\xi} - \boldsymbol{\psi}) - \frac{2\mathcal{T}}{m} \mathbf{R}(\mathbf{Q})^T \mathbf{S}(\bar{\mathbf{q}}) \tilde{\mathbf{q}}, \\ \mathbf{J}_f \dot{\boldsymbol{\Omega}} &= -k_q \tilde{\mathbf{q}} - k_\Omega \boldsymbol{\Omega} - \Upsilon \left(\tilde{\mathbf{z}} + L_v \tilde{\boldsymbol{\xi}} \right), \\ \dot{\tilde{\mathbf{z}}} &= -L_p \tilde{\mathbf{z}} - L_v^2 \tilde{\boldsymbol{\xi}} + \Upsilon^T \boldsymbol{\Omega}. \end{aligned}$$

The first part of the proof consists of using the Lyapunov function

$$V = \frac{1}{2} \left(\mathbf{z}^T \mathbf{z} + k_p \boldsymbol{\xi}^T \boldsymbol{\xi} + k_d (\boldsymbol{\xi} - \boldsymbol{\psi})^T (\boldsymbol{\xi} - \boldsymbol{\psi}) + \boldsymbol{\Omega}^T \mathbf{I}_f \boldsymbol{\Omega} + 4k_q (1 - \tilde{\eta}) \right) + \frac{1}{2} \left(\tilde{\mathbf{z}} + L_v \tilde{\boldsymbol{\xi}} \right)^T \left(\tilde{\mathbf{z}} + L_v \tilde{\boldsymbol{\xi}} \right) + \frac{1}{2} L_v L_p \tilde{\boldsymbol{\xi}}^T \tilde{\boldsymbol{\xi}}, \quad (4.43)$$

leading to the time-derivative that can be upper bounded as

$$\dot{V} \leq -k_d k_\psi \|\boldsymbol{\xi} - \boldsymbol{\psi}\|^2 - (L_p - L_v - \sigma_1) \|\tilde{\mathbf{z}}\|^2 - k_\Omega \|\boldsymbol{\Omega}\|^2 - (L_v^3 - \sigma_2) \|\tilde{\boldsymbol{\xi}}\|^2 - \left(k_q k_\beta - \frac{\mathcal{T}_b^2}{m^2} \left(\frac{1}{\sigma_1} + \frac{L_p^2}{\sigma_2} \right) \right) \|\tilde{\mathbf{q}}\|^2. \quad (4.44)$$

This indicates that $V(t) \leq V(0)$ and, by standard signal chasing, the signals \mathbf{z} , $\dot{\mathbf{z}}$, $\boldsymbol{\xi}$, $\boldsymbol{\psi}$, $\dot{\boldsymbol{\psi}}$, $\boldsymbol{\Omega}$, $\dot{\boldsymbol{\Omega}}$, $\tilde{\mathbf{z}}$, $\dot{\tilde{\mathbf{z}}}$, $\tilde{\boldsymbol{\xi}}$ and $\dot{\tilde{\boldsymbol{\xi}}}$ are bounded. Then, using the extended Barbălat Lemma (Lemma 2.3), we show that $\boldsymbol{\xi} \rightarrow 0$, $\mathbf{z} \rightarrow 0$, $\tilde{\boldsymbol{\xi}} \rightarrow 0$, $\tilde{\mathbf{z}} \rightarrow 0$, $\tilde{\mathbf{q}} \rightarrow 0$ and $\tilde{\boldsymbol{\omega}} \rightarrow 0$. The second part of the proof relies on the result of Lemma 2.6, where we can see that the dynamics of the variable $\boldsymbol{\theta}$ in (4.27) with (4.28) can be rewritten as in (2.35) with $\boldsymbol{\varepsilon} = -\mathbf{u}$. Using the above results, we know that the input \mathbf{u} in (4.31) is guaranteed to be globally bounded and converges asymptotically to zero. Hence the condition of Lemma 2.6 are satisfied and consequently $\boldsymbol{\theta} \rightarrow 0$ and $\dot{\boldsymbol{\theta}} \rightarrow 0$, which leads to the result of Theorem 4.2 using the error variables definition (4.29). The details of the proof of Theorem 4.2 are given in Appendix A.3.3. \square

Remark 4.2. *The role of the variable $\boldsymbol{\beta}$ in this section is not to compensate for the perturbation term appearing in the translational dynamics (as done in the Theorem 4.1), but it is used to dominate the effects of this term in closed loop using the vector $(\hat{\mathbf{z}} + L_p \tilde{\boldsymbol{\xi}})$. Note that this term is equal to the vector $\boldsymbol{\nu}$ given in (4.39), and therefore the time-derivative of $\boldsymbol{\beta}$ used in the torque input (4.40) does not depend of the linear-velocity information and, similarly to (4.26), is given by*

$$\dot{\boldsymbol{\beta}} = \frac{-k_\beta}{2} (\tilde{\eta} \mathbf{I}_3 + \mathbf{S}(\tilde{\mathbf{q}})) \tilde{\boldsymbol{\omega}} + \frac{2\mathcal{T}}{k_q m} \left(\mathbf{S}(\tilde{\mathbf{q}})^T \mathbf{R}(\mathbf{Q}) \dot{\boldsymbol{\nu}} + \frac{d}{dt} (\mathbf{S}(\tilde{\mathbf{q}})^T \mathbf{R}(\mathbf{Q})) \boldsymbol{\nu} \right) + \frac{2m}{k_q \mathcal{T}} (g \hat{\mathbf{e}}_3 - \mathbf{F})^T \dot{\mathbf{F}} \mathbf{S}(\tilde{\mathbf{q}})^T \mathbf{R}(\mathbf{Q}) \boldsymbol{\nu}, \quad (4.45)$$

where $\boldsymbol{\nu}$ and $\dot{\boldsymbol{\nu}}$ are defined in (4.39).

It is interesting to notice that the intermediary control design in this section is different from the full state information case. In fact, in addition to the partial state feedback design, we have introduced the auxiliary system (4.27) with the main objective is to modify (during the transient) the system trajectories. Instead of attempting to drive the tracking error vectors directly to zero, the auxiliary input \mathbf{u} is

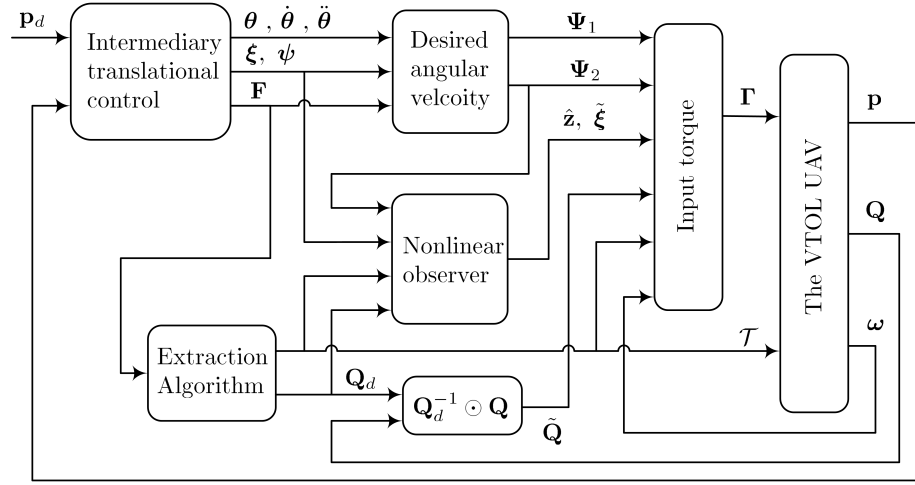


Figure 4.3: Implementation of the control scheme in Theorem 4.2.

designed without linear-velocity measurement to drive $\tilde{\mathbf{v}}$ and $\tilde{\mathbf{p}}$ to $\dot{\boldsymbol{\theta}}$ and $\boldsymbol{\theta}$ respectively. Once this is achieved, the auxiliary variables $\dot{\boldsymbol{\theta}}$ and $\boldsymbol{\theta}$ converge asymptotically to zero, achieving hence our control objective.

The main feature of this control structure is that the intermediary control input \mathbf{F} in (4.28) does not depend explicitly on the position tracking error. As a result, only the second time-derivative of the intermediary control depends on the linear-velocity, which was obviated using the nonlinear observer (4.39). The implementation of the control scheme in Theorem 4.2 is shown in Fig.4.3. It should be noted that without the introduction of the auxiliary system (4.27), the use of the position tracking error explicitly in the expression of \mathbf{F} results in $\boldsymbol{\omega}_d$ being function of the linear-velocity and $\dot{\boldsymbol{\omega}}_d$ being function of the linear-acceleration, which will make the control design more difficult.

4.6 Simulation results

In this section, simulation results are presented to illustrate the effectiveness of the proposed control schemes. Using SIMULINK, we consider a VTOL UAV modeled as a rigid body of mass $m = 3$ kg and with inertia matrix $\mathbf{J}_f = \text{diag}[0.13, 0.13, 0.04]$ kg.m² and the gravitational force is taken as $g = 9.8$ m/sec². The initial states of the aircraft are assumed to be

$$\begin{aligned} \mathbf{p}(0) &= (-2, 5, -1)^T, & \mathbf{v}(0) &= (0, 0, 0)^T, \\ \boldsymbol{\omega}(0) &= (0, 0, 0)^T, & \mathbf{q}(0) &= (0, 0, 0, 1)^T. \end{aligned}$$

Table 4.1: Control gains

	k_p	k_d	k_q	k_Ω	k_β	k_r	k_v	L_p	L_v	k_ψ
Theorem 4.1	0.3	0.5	40	30	10					
Theorem 4.2	1.5	1.5	40	30	40	0.3	0.5	1.5	0.8	1

The control objective is to track the desired trajectory given by

$$\mathbf{p}_d(t)^T = (10 \cos(0.1t + 2), 10 \sin(0.1t + 2.4), t) \text{ m.} \quad (4.46)$$

The two control schemes proposed in this chapter are implemented with the control gains given in table 4.1. Note that the gains are selected to satisfy case (c) of Assumption 4.1 and condition (4.42) in the case of Theorem 4.2.

In the case where the full state vector is available for feedback and the control scheme in Theorem 4.1 is implemented, Fig.4.4a and Fig.4.4b illustrate the three components of the obtained position and velocity tracking errors. Note that a superscript is introduced to differentiate between the three components of a vector, *e.g.* $\tilde{\mathbf{p}} = (\tilde{p}^1, \tilde{p}^2, \tilde{p}^3)^T$. Fig.4.4c shows the attitude tracking error and Fig.4.4d illustrates the desired and actual angular velocities of the aircraft. It is clear from these figures that asymptotic convergence to zero is guaranteed after few seconds. To illustrate the vehicle position tracking, a 3-D plot of the vehicle position with the desired trajectory is given in Fig.4.4e, as well as the projections of the curves in the different planes.

Similar plots are given in Fig.4.5 in the case where the linear-velocity is not available for feedback, and the control law in Theorem 4.2 is implemented with the auxiliary variables initialized as

$$\boldsymbol{\theta}(0) = \dot{\boldsymbol{\theta}}(0) = \hat{\boldsymbol{\xi}}(0) = \boldsymbol{\nu}(0) = (0, 0, 0)^T.$$

It can be seen that the control objective is attained without linear-velocity measurements.

4.7 Concluding remarks

In this chapter, we addressed the trajectory tracking problem of the class of VTOL UAVs in the full and partial state information cases. The control design relies on a singularity-free extraction algorithm that has enabled a separate translational and rotational control design. It is important to mention that a similar method, with a more general formulation of the extraction algorithm, has been used in Roberts and Tayebi (2009) to solve the trajectory tracking problem of the class of under-actuated systems under study with external disturbances.

The proposed tracking control law in the full state information case complements the literature in this field by providing global stability results which are rarely

obtained for this class of under-actuated systems. In this case, a global result has been obtained in Frazzoli *et al.* (2000) for the trajectory tracking problem, where the control is guaranteed to be smooth provided that the rotation angle of the attitude error is different from $\pi/2$. Also, the thrust input is defined as a solution to a second order differential equation. The authors in Frazzoli *et al.* (2000) first determine an optimal desired thrust input and desired orientation, then using the backstepping procedure, a thrust and input torque are determined. A conceptually similar approach has been considered in Hamel *et al.* (2002) to solve the stabilization problem. The main difference between the proposed approach and the work of Frazzoli *et al.* (2000) and Hamel *et al.* (2002), is the adopted singularity-free attitude extraction method (in terms of unit-quaternion) as well as the *a priori* boundedness of the intermediary translational control input and the system thrust. Note that since attitude dynamics are involved, the obtained results in this chapter are almost global however, the results are guaranteed with arbitrary position and linear-velocity initial conditions.

Furthermore, the proposed linear-velocity-free control scheme can be considered as a first solution to the problem under study. At the first stage of the control design, the requirement of the linear-velocity has been obviated with the introduction of new control variables reshaping the desired trajectory during the transient. In the second stage of the control design, a nonlinear observer has been used to design a linear-velocity-free control torque guaranteeing the tracking of the desired attitude derived at the first stage of the control design. The control design procedure proposed for VTOL UAVs as well as the idea of using the auxiliary system (4.27) constitute important tools in the design of formation control schemes in the next two chapters.

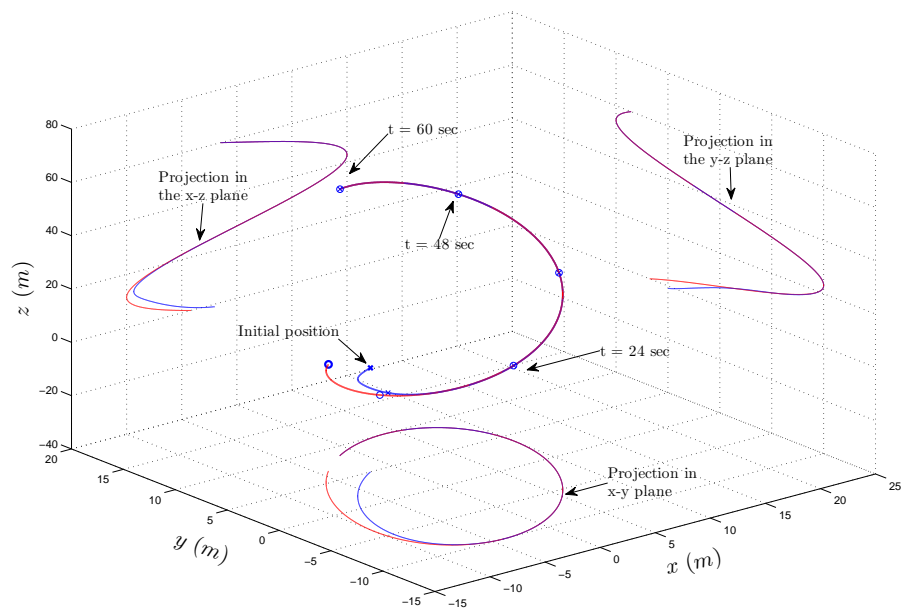
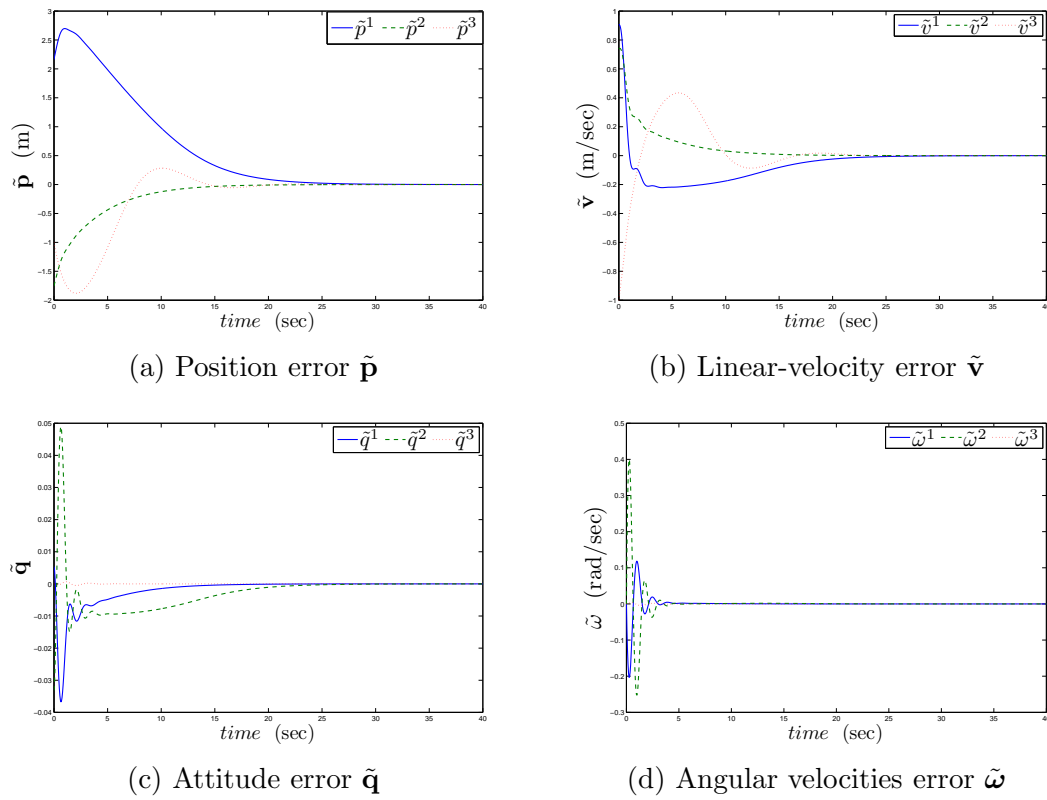
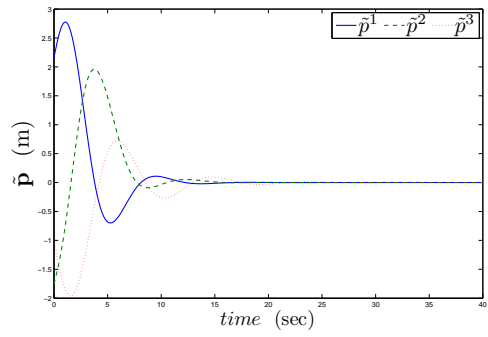
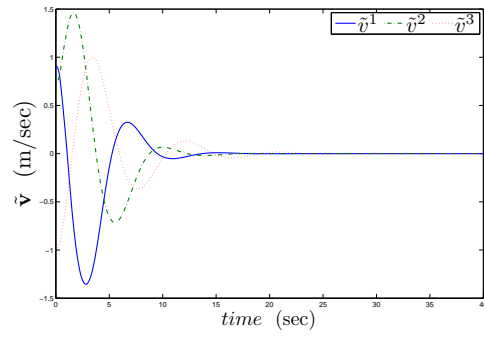


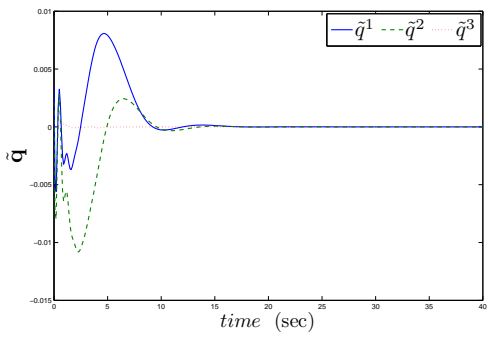
Figure 4.4: Simulation results in case of Theorem 4.1.



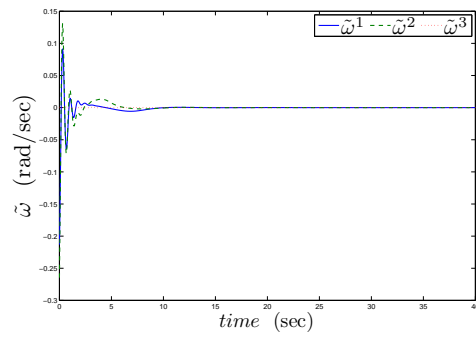
(a) Position error $\tilde{\mathbf{p}}$



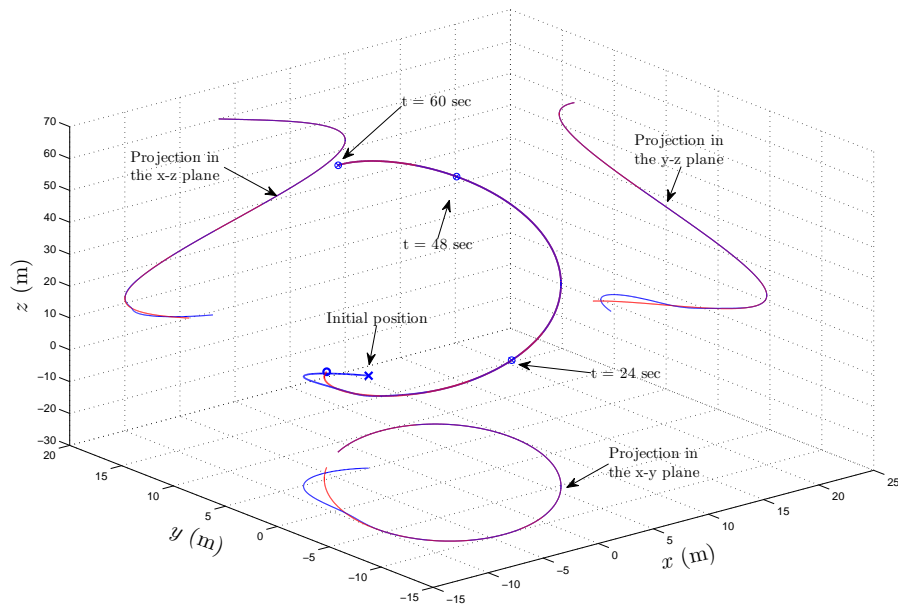
(b) Linear-velocity error $\tilde{\mathbf{v}}$



(c) Attitude error $\tilde{\mathbf{q}}$



(d) Angular velocities error $\tilde{\boldsymbol{\omega}}$



(e) System trajectory

Figure 4.5: Simulation results in case of Theorem 4.2.

Chapter 5

Formation control of VTOL UAVs

In this chapter, we consider the problem of steering a group of VTOL aircraft to a desired inter-vehicle formation pattern that translates with a prescribed reference linear-velocity. Following the control design methodology developed in the previous chapter, formation control schemes are proposed assuming a fixed and undirected communication topology between aircraft. The objectives of this chapter are to extend the trajectory tracking control schemes proposed for a single VTOL UAV to the formation control problem in the full and partial state information cases and achieve global stability results. The results presented in this chapter are based on Abdessameud and Tayebi (2009*c*, 2010*b,c*).

5.1 Introduction

This chapter is devoted to the formation control of a group of VTOL UAVs that are required to converge to a specified formation that translates with a predefined reference linear-velocity. A state feedback and two output feedback formation control schemes are proposed following the control design methodology presented in section 4.3. Based on local information exchange between neighboring vehicles, an intermediary control input for the translational dynamics of each aircraft is designed. Thereafter, the extraction algorithm in Lemma 4.1 is used to extract the magnitude of the necessary thrust input and the desired orientation (in terms of unit-quaternion) of the aircraft. The thrust input will be used to drive the translational dynamics, and the time-varying desired attitude will be considered as a reference input to be tracked by the individual rotational dynamics with an appropriate design of the torque input. As noted previously, the main challenge in using this control design procedure is related to satisfy the requirements of the extraction algorithm, which gives rise to some constraints on the intermediary control input.

Multiple vehicles subject to input constraints have been considered in the work of Lawton *et al.* (2003), where formation control strategies for multi-robot formation maneuvers are discussed. The authors presented two control schemes that respectively account for actuator saturations and consider the lack of relative velocity measurements. The communication flow between vehicles is restricted to a bidirectional ring, and the state feedback control law is constructed using smooth saturation functions of the relative states of robots. The author in Ren (2008) considered the same problems

in Lawton *et al.* (2003) in the context of consensus of double-integrator dynamics, and extended the results to a more general undirected communication topology. However, in both works, the velocity-free control laws do not take into consideration actuator saturations. Our proposed approach presents several advantages over the conventional methods when applied to VTOL UAVs in the full state information case, and enables the design of formation control schemes without linear-velocities measurements.

5.2 Problem formulation

The control problem is to design control schemes for a group of VTOL UAVs such that starting from any initial conditions, aircraft are steered to a desired inter-vehicle formation that translates with a prescribed reference linear-velocity. We consider a group of n -aircraft modeled as in (2.12)-(2.11), which can be rewritten, using similar steps as in (4.4) and property 2.1, as

$$(\Sigma_{1_i}) : \begin{cases} \dot{\mathbf{p}}_i = \mathbf{v}_i, \\ \dot{\mathbf{v}}_i = \mathbf{F}_i - \frac{2\mathcal{T}_i}{m_i} \mathbf{R}(\mathbf{Q}_i)^T \mathbf{S}(\bar{\mathbf{q}}_i) \tilde{\mathbf{q}}_i, \end{cases} \quad (5.1)$$

$$(\Sigma_{2_i}) : \begin{cases} \dot{\mathbf{Q}}_i = \mathbf{T}(\mathbf{Q}_i) \boldsymbol{\omega}_i, \\ I_{f_i} \dot{\boldsymbol{\omega}}_i = \boldsymbol{\Gamma}_i - \mathbf{S}(\boldsymbol{\omega}_i) I_{f_i} \boldsymbol{\omega}_i, \end{cases} \quad (5.2)$$

where \mathbf{F}_i is the intermediary control input defined in section 4.3, $\bar{\mathbf{q}}_i$ is defined in (2.18) and $\tilde{\mathbf{q}}_i$ is the vector part of the unit-quaternion representing the attitude tracking error given in (2.13) with \mathbf{Q}_{d_i} representing the desired attitude of the i^{th} aircraft and will be determined through the control design. We assume that the reference linear-velocity, \mathbf{v}_d , as well as its first, second and third derivatives are available to each aircraft in the team. We assume further that the communication flow between aircraft is fixed and undirected and is described by the weighted graph $\mathcal{G} = (\mathcal{N}, \mathcal{E}, \mathcal{K})$ defined in section 2.5.

Following the control design procedure described in section 4.3, our goal is to design the input thrust, \mathcal{T}_i , and the torque input, $\boldsymbol{\Gamma}_i$, for each aircraft such that

$$\mathbf{v}_i \rightarrow \mathbf{v}_d \quad \text{and} \quad (\mathbf{p}_i - \mathbf{p}_j) \rightarrow \boldsymbol{\delta}_{ij}, \quad (5.3)$$

for $i, j \in \mathcal{N}$, where $\boldsymbol{\delta}_{ij} \in \mathbb{R}^3$, satisfying $\boldsymbol{\delta}_{ij} = -\boldsymbol{\delta}_{ji}$, defines the desired constant offset between the i^{th} and j^{th} aircraft, and hence defines the formation pattern.

5.3 Formation control in the full state information case

We assume that the full state vector is available for feedback, *i.e.*, all aircraft are equipped with sufficient sensors that provide the aircraft positions, linear-velocities, angular velocities and orientation. The design of a formation control scheme follows the steps of the control design procedure presented in section 4.3.

We propose the following intermediary (virtual) input for each aircraft

$$\mathbf{F}_i = \dot{\mathbf{v}}_d - k_i^p \chi(\boldsymbol{\theta}_i) - k_i^d \chi(\dot{\boldsymbol{\theta}}_i), \quad (5.4)$$

$$\ddot{\boldsymbol{\theta}}_i = \mathbf{F}_i - \mathbf{u}_i - \dot{\mathbf{v}}_d, \quad (5.5)$$

where k_i^p and k_i^d are positive scalar gains and the function χ is defined in (2.33). The variables $\boldsymbol{\theta}_i$ and $\dot{\boldsymbol{\theta}}_i$ can be initialized arbitrarily and \mathbf{u}_i is an auxiliary input to be determined later. We define the following error variables

$$\boldsymbol{\xi}_i = \mathbf{p}_i - \boldsymbol{\theta}_i, \quad \mathbf{z}_i = \mathbf{v}_i - \mathbf{v}_d - \dot{\boldsymbol{\theta}}_i := \dot{\boldsymbol{\xi}}_i - \mathbf{v}_d, \quad (5.6)$$

for $i \in \mathcal{N}$. It should be noted from (5.4)-(5.5) that if the input \mathbf{u}_i is guaranteed to be globally bounded and converges asymptotically to zero, the variable $\boldsymbol{\theta}_i$ and its time-derivative are guaranteed to be bounded and converge asymptotically to zero by virtue of Lemma 2.6. Therefore, the formation control objective is attained when the auxiliary input is designed such that $\mathbf{z}_i \rightarrow 0$ and $(\boldsymbol{\xi}_i - \boldsymbol{\xi}_j) \rightarrow \boldsymbol{\delta}_{ij}$. To this end, we propose the following input for system (5.5)

$$\mathbf{u}_i = -k_i^v \mathbf{z}_i - \sum_{j=1}^n k_{ij} \boldsymbol{\xi}_{ij}, \quad (5.7)$$

where $\boldsymbol{\xi}_{ij} = (\boldsymbol{\xi}_i - \boldsymbol{\xi}_j - \boldsymbol{\delta}_{ij})$, k_i^v is a strictly positive scalar gain and k_{ij} is the $(i, j)^{th}$ entry of the weighted adjacency matrix \mathcal{K} of the communication graph, $\mathcal{G} = (\mathcal{N}, \mathcal{E}, \mathcal{K})$, characterizing the information flow between aircraft. Note that the intermediary control input \mathbf{F}_i in (5.4) is guaranteed to be bounded as

$$\|\mathbf{F}_i\| \leq \delta_d + \sigma_b \sqrt{3}(k_i^p + k_i^d), \quad (5.8)$$

with $\|\dot{\mathbf{v}}_d\| \leq \delta_d$ and σ_b is defined in property P2 in section 2.6. Therefore, the extraction condition (4.8) can be satisfied with a natural restriction on the desired linear-velocity and an appropriate choice of the gains k_i^p and k_i^d . As a result, the necessary thrust input and the desired attitude for each aircraft can be extracted according to Lemma 4.1.

Next, we consider the extracted value of the desired attitude \mathbf{Q}_{d_i} , given in

(4.7), as a time-varying reference attitude for the i^{th} aircraft. Using the expression of the intermediary control input in (5.4), explicit expressions for the desired angular velocity and its time-derivative of each aircraft can be obtained as

$$\boldsymbol{\omega}_{d_i} = \Xi(\mathbf{F}_i)\dot{\mathbf{F}}_i, \quad (5.9)$$

$$\dot{\boldsymbol{\omega}}_{d_i} = \bar{\Xi}(\mathbf{F}_i, \dot{\mathbf{F}}_i)\dot{\mathbf{F}}_i + \Xi(\mathbf{F}_i)\ddot{\mathbf{F}}_i, \quad (5.10)$$

where $\bar{\Xi}(\mathbf{F}_i, \dot{\mathbf{F}}_i)$ is the time-derivative of $\Xi(\mathbf{F}_i)$ given in (4.10), and

$$\dot{\mathbf{F}}_i = \ddot{\mathbf{v}}_d - k_i^p h(\boldsymbol{\theta}_i)\dot{\boldsymbol{\theta}}_i - k_i^d h(\dot{\boldsymbol{\theta}}_i)\ddot{\boldsymbol{\theta}}_i, \quad (5.11)$$

$$\ddot{\mathbf{F}}_i = \mathbf{v}_d^{(3)} - k_i^p \dot{h}(\boldsymbol{\theta}_i)\dot{\boldsymbol{\theta}}_i - \left(k_i^p h(\boldsymbol{\theta}_i) + k_i^d \dot{h}(\dot{\boldsymbol{\theta}}_i)\right)\ddot{\boldsymbol{\theta}}_i - k_i^d h(\dot{\boldsymbol{\theta}}_i)(\dot{\mathbf{F}}_i - \ddot{\mathbf{v}}_d - \dot{\mathbf{u}}_i), \quad (5.12)$$

where the diagonal matrix $h(\cdot)$ is defined in (2.34) and $\dot{h}(\cdot)$ is its time-derivative. We propose the following input torque for each aircraft

$$\boldsymbol{\Gamma}_i = \mathbf{H}_i(\boldsymbol{\omega}_i, \boldsymbol{\omega}_{d_i}, \dot{\boldsymbol{\omega}}_{d_i}, \tilde{\mathbf{Q}}_i) + \mathbf{J}_{f_i}\dot{\boldsymbol{\beta}}_i - k_i^q \tilde{\mathbf{q}}_i - k_i^\Omega(\tilde{\boldsymbol{\omega}}_i - \boldsymbol{\beta}_i), \quad (5.13)$$

$$\boldsymbol{\beta}_i = -k_i^\beta \tilde{\mathbf{q}}_i + \frac{2\mathcal{T}_i}{k_i^q m_i} \mathbf{S}(\tilde{\mathbf{q}}_i)^T \mathbf{R}(\mathbf{Q}_i) \mathbf{z}_i, \quad (5.14)$$

where k_i^q , k_i^Ω and k_i^β are positive scalar gains, $\tilde{\mathbf{q}}_i$ is the vector part of the unit-quaternion $\tilde{\mathbf{Q}}_i$ describing the attitude tracking error defined in (2.13), $\tilde{\boldsymbol{\omega}}_i$ is the angular velocity tracking error defined in (2.15),

$$\mathbf{H}_i(\cdot) = \mathbf{S}(\boldsymbol{\omega}_i)\mathbf{J}_{f_i}\boldsymbol{\omega}_i - \mathbf{J}_{f_i}\mathbf{S}(\tilde{\boldsymbol{\omega}}_i)\mathbf{R}(\tilde{\mathbf{Q}}_i)\boldsymbol{\omega}_{d_i} + \mathbf{J}_{f_i}\mathbf{R}(\tilde{\mathbf{Q}}_i)\dot{\boldsymbol{\omega}}_{d_i}, \quad (5.15)$$

and $\boldsymbol{\omega}_{d_i}$, $\dot{\boldsymbol{\omega}}_{d_i}$ are derived in (5.9)-(5.12) with

$$\dot{\mathbf{u}}_i = -k_i^v \left(\mathbf{u}_i - \frac{2\mathcal{T}_i}{m_i} \mathbf{R}(\mathbf{Q}_i)^T \mathbf{S}(\tilde{\mathbf{q}}_i) \tilde{\mathbf{q}}_i \right) - \sum_{j=1}^n k_{ij} (\mathbf{z}_i - \mathbf{z}_j). \quad (5.16)$$

Note that to implement the above control scheme, communicating aircraft need to transmit their variables $\boldsymbol{\xi}_i$ and \mathbf{z}_i . Our result is stated in the following theorem.

Theorem 5.1. *Consider the VTOL-UAVs modeled as in (5.1)-(5.2) and let the desired velocity \mathbf{v}_d and the controller gains k_i^p and k_i^d satisfy Assumption 4.1. For each aircraft, let the thrust input \mathcal{T}_i and the desired attitude \mathbf{Q}_{d_i} be extracted according to Lemma 4.1, and are given by (4.6) and (4.7) respectively, with \mathbf{F}_i given in (5.4) with (5.5) and (5.7). Let the input torque for each aircraft be given as in (5.13)-(5.14) and let the communication graph \mathcal{G} be connected. Then, starting from any initial conditions, the signals \mathbf{v}_i , $(\mathbf{p}_i - \mathbf{p}_j)$ and $\tilde{\boldsymbol{\omega}}_i$ are bounded and $\mathbf{v}_i \rightarrow \mathbf{v}_d$, $(\mathbf{p}_i - \mathbf{p}_j) \rightarrow \boldsymbol{\delta}_{ij}$, $\tilde{\mathbf{q}}_i \rightarrow 0$ and $\tilde{\boldsymbol{\omega}}_i \rightarrow 0$ for all $i, j \in \mathcal{N}$.*

Sketch of Proof: First, we can verify that if the desired trajectory and control gains are selected according to Assumption 4.1, the extraction condition (4.8) is always satisfied, and the results of Lemma 4.1 can be used to extract the necessary thrust and desired attitude, from (4.6) and (4.7) respectively, for each VTOL vehicle. The translational error dynamics can be obtained from (5.1) and (5.5)-(5.7) as

$$\dot{\mathbf{z}}_i = -k_i^v \mathbf{z}_i - \sum_{j=1}^n k_{ij} \boldsymbol{\xi}_{ij} - \frac{2\mathcal{T}_i}{m_i} \mathbf{R}(\mathbf{Q}_i)^T \mathbf{S}(\bar{\mathbf{q}}_i) \tilde{\mathbf{q}}_i. \quad (5.17)$$

In addition, the attitude tracking error dynamics are derived from (5.2) with (2.15) and (5.13) as

$$\mathbf{J}_{f_i} \dot{\boldsymbol{\Omega}}_i = -k_i^q \tilde{\mathbf{q}}_i - k_i^\Omega \boldsymbol{\Omega}_i, \quad (5.18)$$

with $\boldsymbol{\Omega}_i = (\tilde{\boldsymbol{\omega}}_i - \boldsymbol{\beta}_i)$. The proof of Theorem 5.1 follows from Lyapunov arguments using the positive definite Lyapunov function

$$V = \frac{1}{2} \sum_{i=1}^n \left(\mathbf{z}_i^T \mathbf{z}_i + \frac{1}{2} \sum_{j=1}^n k_{ij} \boldsymbol{\xi}_{ij}^T \boldsymbol{\xi}_{ij} + \boldsymbol{\Omega}_i^T \mathbf{J}_{f_i} \boldsymbol{\Omega}_i + 4(1 - \tilde{\eta}_i) \right), \quad (5.19)$$

leading to the negative semi-definite time-derivative

$$\dot{V} = \sum_{i=1}^n \left(-k_i^v \mathbf{z}_i^T \mathbf{z}_i - k_i^\Omega \boldsymbol{\Omega}_i^T \boldsymbol{\Omega}_i - k_i^q k_i^\beta \tilde{\mathbf{q}}_i^T \tilde{\mathbf{q}}_i \right). \quad (5.20)$$

Invoking Barbălat Lemma, we can show that $\mathbf{z}_i \rightarrow 0$, $\boldsymbol{\Omega}_i \rightarrow 0$ and $\tilde{\mathbf{q}}_i \rightarrow 0$, which leads us to conclude that $\tilde{\boldsymbol{\omega}}_i \rightarrow 0$. Also, invoking the extended Barbălat Lemma (Lemma 2.3), we show that $\dot{\mathbf{z}}_i \rightarrow 0$, and the translational dynamics (5.17) reduces to

$$\sum_{j=1}^n k_{ij} \boldsymbol{\xi}_{ij} = 0, \quad (5.21)$$

for $i \in \mathcal{N}$. Exploiting the properties of the undirected communication graph, we show that this last set of equations leads to $(\boldsymbol{\xi}_i - \boldsymbol{\xi}_j) \rightarrow \boldsymbol{\delta}_{ij}$, for all $i, j \in \mathcal{N}$. Next, the result of Lemma 2.6 is used to show that $\boldsymbol{\theta}_i$ and $\dot{\boldsymbol{\theta}}_i$ are bounded and converge asymptotically to zero, which leads to the results of the theorem. A detailed proof of Theorem 5.1 is given in Appendix A.4.1. □

Remark 5.1. *It is important to mention that the variable $\boldsymbol{\beta}_i$ is used in the input torque (5.13) to compensate for the perturbation term in the translational dynamics*

using the linear-velocity tracking error. Also, the time-derivative of this variable is required in the input torque and is given by

$$\begin{aligned} \dot{\boldsymbol{\beta}}_i = & \frac{-k_i^\beta}{2}(\tilde{\eta}_i \mathbf{I}_3 + \mathbf{S}(\tilde{\mathbf{q}}_i))\tilde{\boldsymbol{\omega}}_i + \frac{2\mathcal{T}_i}{k_i^q m_i} \left(\frac{d}{dt}(\mathbf{S}(\bar{\mathbf{q}}_i)^T \mathbf{R}(\mathbf{Q}_i))\mathbf{z}_i + \mathbf{S}(\bar{\mathbf{q}}_i)^T \mathbf{R}(\mathbf{Q}_i)\dot{\mathbf{z}}_i \right) \\ & + \frac{2m_i}{k_i^q \mathcal{T}_i} (g\hat{\mathbf{e}}_3 - \mathbf{F}_i)^T \dot{\mathbf{F}}_i \mathbf{S}(\bar{\mathbf{q}}_i)^T \mathbf{R}(\mathbf{Q}_i)\mathbf{z}_i \end{aligned} \quad (5.22)$$

with $\frac{d}{dt}(\mathbf{S}(\bar{\mathbf{q}}_i)^T \mathbf{R}(\mathbf{Q}_i)) = \mathbf{S}(\dot{\bar{\mathbf{q}}}_i)^T \mathbf{R}(\mathbf{Q}_i) - \mathbf{S}(\bar{\mathbf{q}}_i)^T \mathbf{S}(\boldsymbol{\omega}_i) \mathbf{R}(\mathbf{Q}_i)$. In Abdessameud and Tayebi (2009c), a different design for this variable is considered, where it has been shown that the effects of the perturbation term in the translational dynamics can be dominated with the choice of $\boldsymbol{\beta}_i = -k_i^\beta \tilde{\mathbf{q}}_i$ under some conditions on the control gains.

It should be noted that the formation control scheme in Theorem 5.1 is based on the introduction of an auxiliary system whose input is designed such that \mathbf{v}_i and $(\mathbf{p}_i - \mathbf{p}_j - \boldsymbol{\delta}_{ij})$ converge first to $(\mathbf{v}_d - \boldsymbol{\theta}_i)$ and $(\boldsymbol{\theta}_i - \boldsymbol{\theta}_j)$ respectively. Then, the variables $\boldsymbol{\theta}_i$ and $\dot{\boldsymbol{\theta}}_i$ are driven to zero asymptotically, leading to our original objective. A different design of the intermediary control input is possible using classical formation control methods. In fact, we can show that the formation control objective is achieved using the input

$$\mathbf{F}_i = \dot{\mathbf{v}}_d - k_i^v \chi(\mathbf{v}_i - \mathbf{v}_d) - \sum_{j=1}^n k_{ij} \chi(\mathbf{p}_{ij}), \quad (5.23)$$

with $\mathbf{p}_{ij} = (\mathbf{p}_i - \mathbf{p}_j - \boldsymbol{\delta}_{ij})$ and the control gains being defined as in Theorem 5.1, together with the torque input (5.13) with

$$\boldsymbol{\beta}_i = -k_i^\beta \tilde{\mathbf{q}}_i + \frac{2\mathcal{T}_i}{k_i^q m_i} \mathbf{S}(\bar{\mathbf{q}}_i)^T \mathbf{R}(\mathbf{Q}_i)(\mathbf{v}_i - \mathbf{v}_d), \quad (5.24)$$

and the desired angular velocity and its time-derivative are derived from (5.9)-(5.10) using the the first and second time-derivatives of the intermediary input (5.23).

It can be verified that \mathbf{F}_i in (5.23) is *a priori* bounded as

$$\|\mathbf{F}_i\| \leq \delta_d + \sigma_b \sqrt{3} \left(k_i^v + \sum_{j=1}^n k_{ij} \right), \quad (5.25)$$

which depends on the number of neighbors of each aircraft. Therefore, if the communication topology between aircraft is known in advance, we can satisfy condition (4.8) and use the thrust and attitude extraction algorithm in Lemma 4.1. However, when the number of neighbors of each aircraft is large, it is generally difficult to satisfy the extraction condition and achieve a good/acceptable system response. Moreover, the

first and second time-derivatives of (5.23) will be respectively function of the linear-velocities and linear-accelerations of neighboring aircraft. Hence, to implement the above control scheme, communicating aircraft need to transmit their positions, linear-velocities and linear-accelerations. Of course, aircraft linear-accelerations can be computed on-line and then transmitted through the communication channels, which will increase the communication requirement between aircraft.

The proposed control scheme in Theorem 5.1 presents several advantages over the above classical design. This can be seen from the proposed intermediary control input that does not depend *explicitly* on the systems states (linear-velocity tracking error vectors and relative positions). As a result, the upper bound of the intermediary control input, given in (5.8), does not depend on the number of neighbors of each aircraft. This is important since condition (4.8) can be easily satisfied without any consideration on the communication topology between aircraft. In addition, the extracted input thrust of each aircraft, given in (4.6), is guaranteed to be *a priori* bounded as

$$\mathcal{T}_i \leq m_i \left(g + \delta_d + \sqrt{3}\sigma_b(k_i^p + k_i^d) \right) := \mathcal{T}_i^b \quad (5.26)$$

with \mathcal{T}_i^b being a positive constant. In view of (5.26), the designer can set the maximum allowed input thrust for each aircraft without any *a priori* knowledge on the information flow between members of the team. Furthermore, the desired angular velocity and its time-derivative can be obtained using only available signals and communicating aircraft need to transmit only the variables ξ_j and z_j . The implementation of the control scheme in Theorem 5.1 is shown in Fig.5.1.

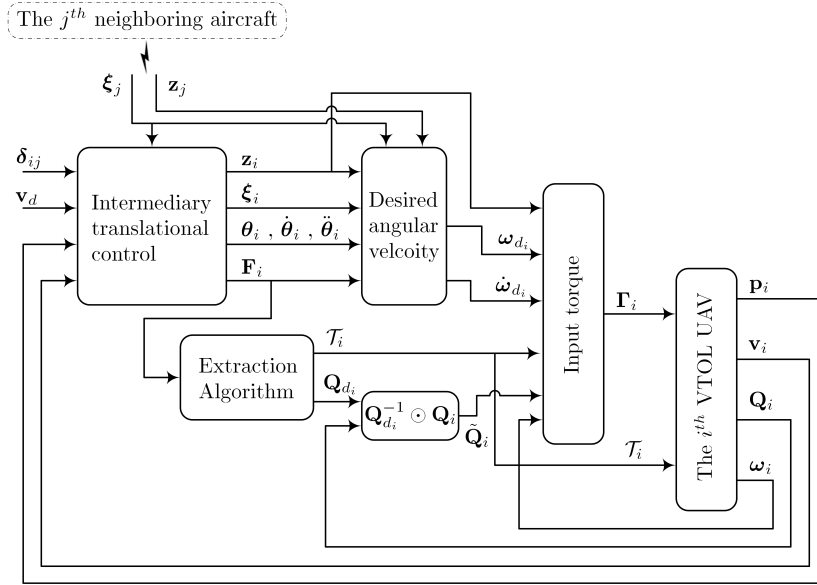


Figure 5.1: Implementation of the control scheme in Theorem 5.1.

5.4 Formation control without linear-velocity measurements

In this section, the formation control problem of VTOL aircraft without linear-velocity measurement is considered. Following the same design procedure as in section 5.3, we first consider the translational dynamics and design an appropriate linear-velocity-free intermediary control input for each aircraft. We propose the intermediary control input \mathbf{F}_i , given in (5.4)-(5.5), with the auxiliary input

$$\mathbf{u}_i = -k_i^v(\boldsymbol{\xi}_i - \boldsymbol{\psi}_i) - \sum_{j=1}^n k_{ij}\boldsymbol{\xi}_{ij}, \quad (5.27)$$

$$\dot{\boldsymbol{\psi}}_i = \mathbf{v}_d + k_i^\psi(\boldsymbol{\xi}_i - \boldsymbol{\psi}_i), \quad (5.28)$$

where $\boldsymbol{\xi}_{ij} = (\boldsymbol{\xi}_i - \boldsymbol{\xi}_j - \boldsymbol{\delta}_{ij})$, $\boldsymbol{\xi}_i$ is defined in (5.6), $\boldsymbol{\psi}_i$ can be initialized arbitrarily, k_i^v and k_{ij} are defined as in Theorem 5.1 and k_i^ψ is a strictly positive scalar gain. Note that \mathbf{F}_i is upper bounded as in (5.8), and hence we can use the result of Lemma 4.1 if condition (4.8) is satisfied. Also, an upper bound of the extracted value of the thrust \mathcal{T}_i , in (4.6), can be determined *a priori* as in (5.26).

To design an attitude tracking control input for the rotational dynamics, we need first to determine the desired angular velocity and its time-derivative from the extracted desired attitude. Using the above intermediary control design, explicit expressions of $\boldsymbol{\omega}_{d_i}$ and $\dot{\boldsymbol{\omega}}_{d_i}$ can be derived from (5.9)-(5.12) and

$$\dot{\mathbf{u}}_i = -k_i^v(\mathbf{z}_i + \mathbf{v}_d - \dot{\boldsymbol{\psi}}_i) - \sum_{j=1}^n k_{ij}(\mathbf{z}_i - \mathbf{z}_j). \quad (5.29)$$

where \mathbf{z}_i is defined in (5.6). It should be noted that the desired angular velocity $\boldsymbol{\omega}_{d_i}$ does not depend on the linear-velocity signal, and its time-derivative, $\dot{\boldsymbol{\omega}}_{d_i}$, can be expressed as

$$\dot{\boldsymbol{\omega}}_{d_i} = \boldsymbol{\Psi}_{1i} - \boldsymbol{\Psi}_{2i}(k_i^v\mathbf{z}_i + \sum_{j=1}^n k_{ij}(\mathbf{z}_i - \mathbf{z}_j)), \quad (5.30)$$

with

$$\begin{aligned} \boldsymbol{\Psi}_{1i} = & \bar{\Xi}(\mathbf{F}_i, \dot{\mathbf{F}}_i)\dot{\mathbf{F}}_i + \Xi(\mathbf{F}_i)\{\mathbf{v}_d^{(3)} - k_i^p\dot{h}(\boldsymbol{\theta}_i)\dot{\boldsymbol{\theta}}_i - k_i^d h(\dot{\boldsymbol{\theta}}) (k_v(\mathbf{v}_d - \dot{\boldsymbol{\psi}}_i) - k_i^p h(\boldsymbol{\theta}_i)\dot{\boldsymbol{\theta}}_i) \\ & - (k_i^p h(\boldsymbol{\theta}_i) + k_i^d \dot{h}(\boldsymbol{\theta}_i) - (k_i^d)^2 h(\dot{\boldsymbol{\theta}}_i)h(\boldsymbol{\theta}_i)) (\mathbf{F}_i - \dot{\mathbf{v}}_d - \mathbf{u}_i)\}, \end{aligned} \quad (5.31)$$

$$\boldsymbol{\Psi}_{2i} = k_i^d \Xi(\mathbf{F}_i)h(\dot{\boldsymbol{\theta}}_i). \quad (5.32)$$

Following similar steps as in section 4.5, the angular velocity error dynamics can be obtained as

$$\mathbf{J}_{f_i} \dot{\boldsymbol{\Omega}}_i = \boldsymbol{\Gamma}_i - \bar{\mathbf{H}}_i(\cdot) - \mathbf{J}_{f_i} \dot{\boldsymbol{\beta}}_i + \boldsymbol{\Upsilon}_i (k_i^v \mathbf{z}_i + \sum_{j=1}^n k_{ij} (\mathbf{z}_i - \mathbf{z}_j)), \quad (5.33)$$

where

$$\bar{\mathbf{H}}_i(\cdot) = \mathbf{S}(\boldsymbol{\omega}_i) \mathbf{J}_{f_i} \boldsymbol{\omega}_i - \mathbf{J}_{f_i} \mathbf{S}(\tilde{\boldsymbol{\omega}}_i) \mathbf{R}(\tilde{\mathbf{Q}}_i) \boldsymbol{\omega}_{d_i} + \mathbf{J}_{f_i} \mathbf{R}(\tilde{\mathbf{Q}}_i) \boldsymbol{\Psi}_{1i}, \quad (5.34)$$

$\boldsymbol{\Omega}_i = (\tilde{\boldsymbol{\omega}}_i - \boldsymbol{\beta}_i)$, $\boldsymbol{\Upsilon}_i = \mathbf{J}_{f_i} \mathbf{R}(\tilde{\mathbf{Q}}_i) \boldsymbol{\Psi}_{2i}$, $\tilde{\mathbf{Q}}_i$ is defined in (2.13), and $\boldsymbol{\omega}_{d_i}$ is obtained from (5.9) and (5.11). Note from (5.33) that the attitude error dynamics depend on the aircraft linear-velocities.

We propose the following input torque for each aircraft

$$\begin{aligned} \boldsymbol{\Gamma}_i = & \bar{\mathbf{H}}_i(\cdot) + \mathbf{J}_{f_i} \dot{\boldsymbol{\beta}}_i - k_i^q \tilde{\mathbf{q}}_i - k_i^\Omega \boldsymbol{\Omega}_i - k_i^v \boldsymbol{\Upsilon}_i (\hat{\mathbf{z}}_i + L_v \tilde{\boldsymbol{\xi}}_i - \mathbf{v}_d) \\ & - \boldsymbol{\Upsilon}_i \sum_{j=1}^n k_{ij} \left((\hat{\mathbf{z}}_i + L_v \tilde{\boldsymbol{\xi}}_i) - (\hat{\mathbf{z}}_j + L_v \tilde{\boldsymbol{\xi}}_j) \right), \end{aligned} \quad (5.35)$$

$$\boldsymbol{\beta}_i = -k_i^\beta \tilde{\mathbf{q}}_i + \frac{2\mathcal{T}_i}{k_i^q m_i} \mathbf{S}(\bar{\mathbf{q}}_i)^T \mathbf{R}(\mathbf{Q}_i) (\hat{\mathbf{z}}_i + L_p \tilde{\boldsymbol{\xi}}_i - \mathbf{v}_d), \quad (5.36)$$

where k_i^q , k_i^Ω , L_v and k_i^β are strictly positive scalar gains, $\tilde{\boldsymbol{\xi}}_i := (\hat{\boldsymbol{\xi}}_i - \boldsymbol{\xi}_i)$ and the variables $\hat{\mathbf{z}}_i$ and $\hat{\boldsymbol{\xi}}_i$ are the output of the dynamic system

$$\begin{cases} \hat{\mathbf{z}}_i := \hat{\boldsymbol{\xi}}_i = \boldsymbol{\nu}_i - L_p \tilde{\boldsymbol{\xi}}_i, \\ \dot{\boldsymbol{\nu}}_i = \mathbf{u}_i + \dot{\mathbf{v}}_d - \frac{2\mathcal{T}_i}{m_i} \mathbf{R}(\mathbf{Q}_i)^T \mathbf{S}(\bar{\mathbf{q}}_i) \tilde{\mathbf{q}}_i + k_i^v \boldsymbol{\Upsilon}_i^T \boldsymbol{\Omega}_i \\ \quad - L_v^2 \tilde{\boldsymbol{\xi}}_i + \sum_{j=1}^n k_{ij} \left(\boldsymbol{\Upsilon}_i^T \boldsymbol{\Omega}_i - \boldsymbol{\Upsilon}_j^T \boldsymbol{\Omega}_j \right), \end{cases} \quad (5.37)$$

with L_p being a strictly positive scalar gain. Our result is stated in the following theorem.

Theorem 5.2. *Consider the VTOL-UAVs modeled as in (5.1)-(5.2) and let the desired velocity \mathbf{v}_d and the controller gains k_i^p and k_i^d satisfy Assumption 4.1. For each aircraft, let the thrust input \mathcal{T}_i and the desired attitude \mathbf{Q}_{d_i} be given, respectively, by (4.6) and (4.7), with \mathbf{F}_i given by (5.4) with (5.5) and (5.27)-(5.28). Let the input torque for each aircraft be as in (5.35)-(5.37). Let the communication graph \mathcal{G} be connected. If the control gains satisfy*

$$L_p - L_v > \sigma_{1i} \frac{\mathcal{T}_i^b}{m_i}, \quad L_v^3 > \sigma_{2i} \frac{\mathcal{T}_i^b}{m_i}, \quad k_i^\beta k_i^q > \frac{\mathcal{T}_i^b}{m_i} \left(\frac{1}{\sigma_{1i}} + \frac{L_p^2}{\sigma_{2i}} \right), \quad (5.38)$$

for some $\sigma_{1i} > 0$, $\sigma_{2i} > 0$ and \mathcal{T}_i^b defined in (5.26), then starting from any initial

conditions, the signals \mathbf{v}_i , $(\mathbf{p}_i - \mathbf{p}_j)$ and $\tilde{\boldsymbol{\omega}}_i$ are bounded and $\mathbf{v}_i \rightarrow \mathbf{v}_d$, $(\mathbf{p}_i - \mathbf{p}_j) \rightarrow \boldsymbol{\delta}_{ij}$, $\tilde{\mathbf{q}}_i \rightarrow 0$ and $\tilde{\boldsymbol{\omega}}_i \rightarrow 0$ for all $i, j \in \mathcal{N}$.

Sketch of proof : Similar to the proof of Theorem 5.1, if Assumption 4.1 is satisfied, the results of Lemma 4.1 can be used to extract the necessary thrust and attitude for each VTOL aircraft. Also, following similar steps as in the proof of Theorem 5.1 and Theorem 4.2, the closed loop dynamics can be obtained as

$$\begin{aligned} \dot{\mathbf{z}}_i &= -k_i^v(\boldsymbol{\xi}_i - \boldsymbol{\psi}_i) - \sum_{j=1}^n k_{ij} \boldsymbol{\xi}_{ij} - \frac{2\mathcal{T}_i}{m_i} \mathbf{R}(\mathbf{Q}_i)^T \mathbf{S}(\tilde{\mathbf{q}}_i) \tilde{\mathbf{q}}_i, \\ \mathbf{J}_{f_i} \dot{\boldsymbol{\Omega}}_i &= -k_i^q \tilde{\mathbf{q}}_i - k_i^\Omega \boldsymbol{\Omega}_i - k_i^v \boldsymbol{\Upsilon}_i (\tilde{\mathbf{z}}_i + L_v \tilde{\boldsymbol{\xi}}_i) \\ &\quad - \boldsymbol{\Upsilon}_i \sum_{j=1}^n k_{ij} \left((\tilde{\mathbf{z}}_i + L_v \tilde{\boldsymbol{\xi}}_i) - (\tilde{\mathbf{z}}_j + L_v \tilde{\boldsymbol{\xi}}_j) \right), \\ \dot{\tilde{\mathbf{z}}}_i &= -L_p \tilde{\mathbf{z}}_i - L_v^2 \tilde{\boldsymbol{\xi}}_i + k_i^v \boldsymbol{\Upsilon}_i^T \boldsymbol{\Omega}_i + \sum_{j=1}^n k_{ij} \left(\boldsymbol{\Upsilon}_i^T \boldsymbol{\Omega}_i - \boldsymbol{\Upsilon}_j^T \boldsymbol{\Omega}_j \right). \end{aligned} \quad (5.39)$$

with $\tilde{\mathbf{z}}_i := \dot{\tilde{\boldsymbol{\xi}}}_i = (\dot{\boldsymbol{\xi}}_i - \dot{\boldsymbol{\xi}}_i)$. The results of the theorem can be shown using the Lyapunov function

$$\begin{aligned} V &= \frac{1}{2} \sum_{i=1}^n \left(\mathbf{z}_i^T \mathbf{z}_i + k_i^v (\boldsymbol{\xi}_i - \boldsymbol{\psi}_i)^T (\boldsymbol{\xi}_i - \boldsymbol{\psi}_i) \right) + \frac{1}{4} \sum_{i=1}^n \sum_{j=1}^n k_{ij} \boldsymbol{\xi}_{ij}^T \boldsymbol{\xi}_{ij} \\ &\quad + \frac{1}{2} \sum_{i=1}^n (\tilde{\mathbf{z}}_i + L_v \tilde{\boldsymbol{\xi}}_i)^T (\tilde{\mathbf{z}}_i + L_v \tilde{\boldsymbol{\xi}}_i) + \frac{1}{2} \sum_{i=1}^n L_v L_p \tilde{\boldsymbol{\xi}}_i^T \tilde{\boldsymbol{\xi}}_i \\ &\quad + \sum_{i=1}^n \left(\frac{1}{2} \boldsymbol{\Omega}_i^T \mathbf{J}_{f_i} \boldsymbol{\Omega}_i + k_i^q \tilde{\mathbf{q}}_i^T \tilde{\mathbf{q}}_i + k_i^q (1 - \tilde{\eta}_i)^2 \right), \end{aligned} \quad (5.40)$$

which leads to the negative semi-definite time-derivative that can be upper bounded as

$$\begin{aligned} \dot{V} &\leq - \sum_{i=1}^n k_i^\psi k_i^v \|\boldsymbol{\xi}_i - \boldsymbol{\psi}_i\|^2 - \sum_{i=1}^n (L_p - L_v - \sigma_{1i} \frac{\mathcal{T}_i^b}{m_i}) \|\tilde{\mathbf{z}}_i\|^2 - \sum_{i=1}^n (L_v^3 - \sigma_{2i} \frac{\mathcal{T}_i^b}{m_i}) \|\tilde{\boldsymbol{\xi}}_i\|^2 \\ &\quad - \sum_{i=1}^n k_i^\Omega \|\boldsymbol{\Omega}_i\|^2 - \sum_{i=1}^n \left(k_i^\beta k_i^q - \frac{\mathcal{T}_i^b}{m_i} \left(\frac{1}{\sigma_{1i}} + \frac{L_p^2}{\sigma_{2i}} \right) \right) \|\tilde{\mathbf{q}}_i\|^2, \end{aligned} \quad (5.41)$$

Invoking Barbălat Lemma, one can conclude that $(\boldsymbol{\xi}_i - \boldsymbol{\psi}_i) \rightarrow 0$, $\mathbf{z}_i \rightarrow 0$, $\tilde{\mathbf{z}}_i \rightarrow 0$, $\tilde{\boldsymbol{\xi}}_i \rightarrow 0$, $\tilde{\mathbf{q}}_i \rightarrow 0$, $\tilde{\boldsymbol{\omega}}_i \rightarrow 0$ and $(\boldsymbol{\xi}_i - \boldsymbol{\xi}_i) \rightarrow \boldsymbol{\delta}_{ij}$ for all $i, j \in \mathcal{N}$. With these results, we can show that $\boldsymbol{\theta}_i$ and $\dot{\boldsymbol{\theta}}_i$ are bounded and converge asymptotically to zero in view of

Lemma 2.6, which leads to the results of the theorem. Details of the proof of Theorem 5.2 are provided in Appendix A.4.2. \square

Remark 5.2. *Note that the role of the variable β_i in this section is not to compensate for the perturbation term appearing in the translational dynamics, but it is used to dominate the effects of this term in closed loop using the term $\nu_i = (\hat{\mathbf{z}}_i + L_p \tilde{\xi}_i)$ obtained from (5.37). In addition, we can see that the time-derivative of β_i does not depend on the linear-velocity and can be derived similar to (4.45) with the expression of $\dot{\nu}_i$ in (5.37).*

Similarly to the case of a single aircraft, the introduction of the auxiliary system (5.5) simplifies considerably the design of the formation control scheme without linear-velocity measurements. However, to implement the above control scheme, the terms ξ_i , $\Upsilon_i^T \Omega_i$, $\hat{\mathbf{z}}_i$ and $\hat{\xi}_i$ must be transmitted between each pair of communicating vehicles. Note that the last three terms are needed because the angular velocity error dynamics depend explicitly on the aircraft linear-velocity as well as the linear-velocity of its neighboring aircraft.

5.5 Design with reduced communication requirements

In this section, we extend the linear-velocity-free formation control scheme in Theorem 5.2 to reduce the communication requirements between aircraft. Let us consider the intermediary control input \mathbf{F}_i given in (5.4)-(5.5), *i.e.*,

$$\mathbf{F}_i = \dot{\mathbf{v}}_d - k_i^p \chi(\boldsymbol{\theta}_i) - k_i^d \chi(\dot{\boldsymbol{\theta}}_i), \quad (5.42)$$

$$\ddot{\boldsymbol{\theta}}_i = \mathbf{F}_i - \mathbf{u}_i - \dot{\mathbf{v}}_d, \quad (5.43)$$

where k_i^p and k_i^d are defined as in Theorem 5.1, the variables $\boldsymbol{\theta}_i$ and $\dot{\boldsymbol{\theta}}_i$ can be initialized arbitrarily, and \mathbf{u}_i is an input to be determined later. The intermediary control input can be upper bounded as in (5.8), and when the extraction condition (4.8) is satisfied, the necessary thrust and desired attitude can be extracted according to Lemma 4.1.

Moreover, we introduce the following additional auxiliary system

$$\ddot{\boldsymbol{\alpha}}_i = \mathbf{u}_i - \boldsymbol{\phi}_i - \frac{2\mathcal{T}_i}{m_i} \mathbf{R}(\mathbf{Q}_i)^T \mathbf{S}(\bar{\mathbf{q}}_i) \tilde{\mathbf{q}}_i, \quad (5.44)$$

where $\boldsymbol{\alpha}_i \in \mathbb{R}^3$ is an auxiliary variable, \mathbf{u}_i is the input of (5.5) and $\boldsymbol{\phi}_i$ is an additional auxiliary input. The variables $\boldsymbol{\alpha}_i$ and $\dot{\boldsymbol{\alpha}}_i$ can be initialized arbitrarily. With the above definitions, the control design problem is reduced to finding the appropriate inputs

\mathbf{u}_i and ϕ_i that achieve our control objectives. To this end, we redefine the error variables (5.6) as

$$\boldsymbol{\xi}_i = \mathbf{p}_i - \boldsymbol{\theta}_i - \boldsymbol{\alpha}_i, \quad \mathbf{z}_i = \dot{\boldsymbol{\xi}}_i - \mathbf{v}_d, \quad (5.45)$$

and propose the following input laws

$$\mathbf{u}_i = -L_i^p \boldsymbol{\alpha}_i - L_i^d \dot{\boldsymbol{\alpha}}_i, \quad (5.46)$$

$$\phi_i = -k_i^v (\boldsymbol{\xi}_i - \boldsymbol{\psi}_i) - \sum_{j=1}^n k_{ij} \boldsymbol{\xi}_{ij}, \quad (5.47)$$

$$\dot{\boldsymbol{\psi}}_i = \mathbf{v}_d + k_i^\psi (\boldsymbol{\xi}_i - \boldsymbol{\psi}_i), \quad (5.48)$$

where $\boldsymbol{\xi}_{ij} = (\boldsymbol{\xi}_i - \boldsymbol{\xi}_j - \boldsymbol{\delta}_{ij})$, k_i^v , k_i^ψ and k_{ij} are defined as in Theorem 5.2, L_i^p and L_i^d are positive scalar gains. The block diagram in Fig.5.2 illustrates the implementation of the proposed intermediary input in this section.

It should be noted that the time-derivative of \mathbf{u}_i can be determined explicitly using available signals as

$$\dot{\mathbf{u}}_i = -L_i^p \dot{\boldsymbol{\alpha}}_i - L_i^d \left(\mathbf{u}_i - \phi_i - \frac{2\mathcal{T}_i}{m_i} \mathbf{R}(\mathbf{Q}_i)^T \mathbf{S}(\bar{\mathbf{q}}_i) \tilde{\mathbf{q}}_i \right). \quad (5.49)$$

As a result, the desired angular velocity and its time-derivative, $\boldsymbol{\omega}_{d_i}$ and $\dot{\boldsymbol{\omega}}_{d_i}$, can be obtained from (5.9)-(5.12) with (5.49) and are function of only available signals. Therefore, a similar torque input used in the full state information case, (5.13), can

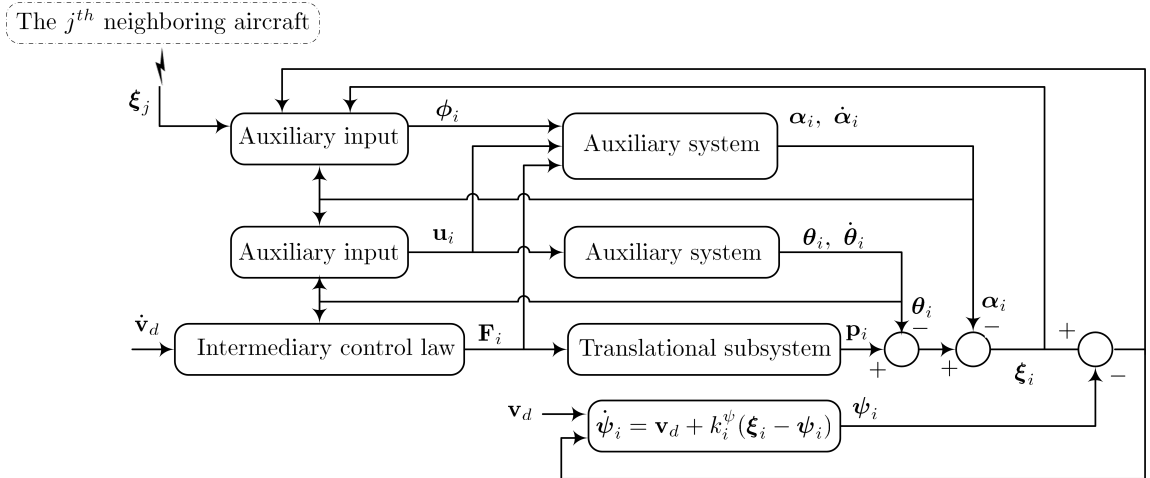


Figure 5.2: Intermediary control block diagram.

be applied

$$\mathbf{\Gamma}_i = \mathbf{H}_i(\cdot) + \mathbf{J}_{f_i} \dot{\boldsymbol{\beta}}_i - k_i^q \tilde{\mathbf{q}}_i - k_i^\Omega (\tilde{\boldsymbol{\omega}}_i - \boldsymbol{\beta}_i), \quad (5.50)$$

$$\boldsymbol{\beta}_i = k_i^\beta \tilde{\mathbf{q}}_i. \quad (5.51)$$

where $\mathbf{H}_i(\cdot)$ is given in (5.15) and $\boldsymbol{\omega}_d$ and $\dot{\boldsymbol{\omega}}_d$ are derived in (5.9)-(5.12) with (5.49). Our results in this section are summarized in the following theorem.

Theorem 5.3. *Consider the VTOL-UAVs modeled as in (5.1)-(5.2) and let the desired velocity \mathbf{v}_d and the controller gains k_p and k_d satisfy Assumption 4.1. Let the thrust input \mathcal{T}_i and the desired attitude \mathbf{Q}_{d_i} be given, respectively, by (4.6) and (4.7), with \mathbf{F}_i given by (5.42)-(5.44) and (5.46)-(5.48). Let the input torque be as in (5.50)-(5.51), and let the communication graph \mathcal{G} be connected. Then, starting from any initial conditions, the signals \mathbf{v}_i , $(\mathbf{p}_i - \mathbf{p}_j)$ and $\tilde{\boldsymbol{\omega}}_i$ are bounded and $\mathbf{v}_i \rightarrow \mathbf{v}_d$, $(\mathbf{p}_i - \mathbf{p}_j) \rightarrow \boldsymbol{\delta}_{ij}$, $\tilde{\mathbf{q}}_i \rightarrow 0$ and $\tilde{\boldsymbol{\omega}}_i \rightarrow 0$ for all $i, j \in \mathcal{N}$.*

Sketch of proof: The closed loop dynamics of the system can be derived as

$$\begin{aligned} \dot{\mathbf{z}}_i &= -k_i^v (\boldsymbol{\xi}_i - \boldsymbol{\psi}_i) - \sum_{j=1}^n k_{ij} \boldsymbol{\xi}_{ij}, \\ \mathbf{J}_{f_i} \dot{\boldsymbol{\Omega}}_i &= -k_i^q \tilde{\mathbf{q}}_i - k_i^\Omega \boldsymbol{\Omega}_i, \end{aligned} \quad (5.52)$$

with $\boldsymbol{\Omega}_i = (\tilde{\boldsymbol{\omega}}_i - \boldsymbol{\beta}_i)$. The proof of the theorem is based on the use of the following Lyapunov function

$$\begin{aligned} V &= \frac{1}{2} \sum_{i=1}^n \left(\mathbf{z}_i^T \mathbf{z}_i + k_i^v (\boldsymbol{\xi}_i - \boldsymbol{\psi}_i)^T (\boldsymbol{\xi}_i - \boldsymbol{\psi}_i) \right) + \frac{1}{4} \sum_{i=1}^n \sum_{j=1}^n k_{ij} \boldsymbol{\xi}_{ij}^T \boldsymbol{\xi}_{ij} \\ &\quad + \sum_{i=1}^n \left(\frac{1}{2} \boldsymbol{\Omega}_i^T \mathbf{J}_{f_i} \boldsymbol{\Omega}_i + k_i^q \tilde{\mathbf{q}}_i^T \tilde{\mathbf{q}}_i + k_i^q (1 - \tilde{\eta}_i)^2 \right), \end{aligned} \quad (5.53)$$

leading to the negative semi-definite time-derivative

$$\dot{V} = - \sum_{i=1}^n \left(k_i^\psi k_i^v (\boldsymbol{\xi}_i - \boldsymbol{\psi}_i)^T (\boldsymbol{\xi}_i - \boldsymbol{\psi}_i) - k_i^q k_i^\beta \tilde{\mathbf{q}}_i^T \tilde{\mathbf{q}}_i - k_i^\Omega \boldsymbol{\Omega}_i^T \boldsymbol{\Omega}_i \right). \quad (5.54)$$

Invoking Barbălat Lemma and Lemma 2.3, we conclude that $\tilde{\boldsymbol{\omega}}_i \rightarrow 0$, $\tilde{\mathbf{q}}_i \rightarrow 0$, $\mathbf{z}_i \rightarrow 0$ and $(\boldsymbol{\xi}_i - \boldsymbol{\xi}_j) \rightarrow \boldsymbol{\delta}_{ij}$ for all $i, j \in \mathcal{N}$. Next, we exploit the boundedness and convergence to zero of the above signals to show that the auxiliary variables $\boldsymbol{\alpha}_i$ and $\dot{\boldsymbol{\alpha}}_i$ are globally bounded and converge asymptotically to zero. This is shown by exploiting the dynamics of the auxiliary system (5.44), which describe the dynamics of a linear system with bounded and vanishing perturbation. Finally, the result of

Lemma 2.6 is used to conclude the results of the theorem. Detailed proof of Theorem 5.3 is given in Appendix A.4.3. \square

It is important to point out that the control scheme in this section is based on a conceptually similar design technique for the intermediary translational control law proposed in Theorem 5.1 and Theorem 5.2. In fact, the main idea is to first design the linear-velocity-free input \mathbf{u}_i to guarantee that \mathbf{v}_i and $(\mathbf{p}_i - \mathbf{p}_j - \boldsymbol{\delta}_{ij})$ converge respectively to $(\dot{\boldsymbol{\theta}}_i + \dot{\boldsymbol{\alpha}}_i)$ and $(\boldsymbol{\theta}_i - \boldsymbol{\theta}_j) + (\boldsymbol{\alpha}_i - \boldsymbol{\alpha}_j)$, for all $i, j \in \mathcal{N}$. Then, the variables $\boldsymbol{\alpha}_i$ and $\dot{\boldsymbol{\alpha}}_i$ are driven asymptotically to zero in view of the dynamics (5.44). Once this is achieved, the auxiliary variables $\boldsymbol{\theta}_i$ and $\dot{\boldsymbol{\theta}}_i$ are guaranteed to converge asymptotically to zero leading to our control objective.

The main feature of using the additional auxiliary system (5.44) is to account for the constraints of the intermediary translational input. In fact, the time-derivative of the auxiliary input \mathbf{u}_i can be derived explicitly and independently of the time-derivatives of the system states. As a result, only measurable signals are involved in the input torque removing hence the necessity of the nonlinear observer (5.37). Note that this does not reduce the order of the system. However, communicating aircraft need to transmit only their variables $\boldsymbol{\xi}_i$, which reduces the communication requirements between aircraft.

Furthermore, the perturbation term in the translational dynamics has been compensated in the dynamics of the auxiliary system (5.44). Note that without this compensation, the analysis would be different and a nonlinear observer would be needed to achieve the closed loop stability results. To illustrate this case, consider the auxiliary system (5.44) without the last term, *i.e.*, $\ddot{\boldsymbol{\alpha}}_i = \mathbf{u}_i - \boldsymbol{\phi}_i$. The translational error dynamics will be written as

$$\dot{\mathbf{z}}_i = -k_i^v(\boldsymbol{\xi}_i - \boldsymbol{\psi}_i) - \sum_{j=1}^n k_{ij} \boldsymbol{\xi}_{ij} - \frac{2T_i}{m_i} \mathbf{R}(\mathbf{Q}_i)^T \mathbf{S}(\bar{\mathbf{q}}_i) \tilde{\mathbf{q}}_i, \quad (5.55)$$

and the rotational error dynamics are governed by (5.52). Therefore, to guarantee the stability of the closed loop system, the variable $\boldsymbol{\beta}_i$ can be designed as in (5.36), with the following observer

$$\begin{cases} \dot{\hat{\mathbf{z}}}_i := \dot{\hat{\boldsymbol{\xi}}}_i = \boldsymbol{\nu}_i - L_p \tilde{\boldsymbol{\xi}}_i, \\ \dot{\boldsymbol{\nu}}_i = \boldsymbol{\phi}_i + \dot{\mathbf{v}}_d - \frac{2T_i}{m_i} \mathbf{R}(\mathbf{Q}_i)^T \mathbf{S}(\bar{\mathbf{q}}_i) \tilde{\mathbf{q}}_i - L_v^2 \tilde{\boldsymbol{\xi}}_i. \end{cases} \quad (5.56)$$

Then, following similar steps as in the proof of Theorem 5.2, the same results are obtained under condition (5.38).

Clearly, the second auxiliary system with compensation of the perturbation term can be used in the linear-velocity-free trajectory tracking control law in section 4.5 to simplify the analysis of the closed loop system and remove the conditions on

the control gains. This modification is not necessary in the state feedback formation control scheme in Theorem 5.1 since the same results will be achieved. However, in the cases where aircraft are constrained to transmit only their variables ξ_i or the time-derivative of the auxiliary input depends on unavailable signals, the second auxiliary system might be considered in the full state information case.

5.6 Simulation results

The proposed formation control laws in this chapter are tested by simulations on a group of four aircraft modeled as in (5.1)-(5.2), with mass $m_i = 3$ kg and identical inertia matrices $\mathbf{J}_{f_i} = \text{diag}[0.13, 0.13, 0.04]$ kg.m², for $i \in \mathcal{N} := \{1, \dots, 4\}$, with initial conditions

$$\begin{aligned} \mathbf{p}_1(0) &= (14, 0, 2)^T, & \mathbf{p}_2(0) &= (10, -1, 2)^T, \\ \mathbf{p}_3(0) &= (6, 0, -2)^T, & \mathbf{p}_4(0) &= (9, -4, 1)^T, \\ \mathbf{v}_1(0) &= (-0.1, 0.9, -0.1)^T, & \mathbf{v}_2(0) &= (-0.5, -0.8, 0.3)^T, \\ \mathbf{v}_3(0) &= (-0.2, 0.4, -0.4)^T, & \mathbf{v}_4(0) &= (0.8, -0.1, 0.1)^T, \\ \boldsymbol{\omega}_i(0) &= (0, 0, 0)^T, & \mathbf{q}_i(0) &= (0, 0, 0, 1)^T. \end{aligned}$$

The control objective is to guarantee that the four aircraft maintain a pre-defined formation pattern that translates with a desired linear-velocity given by

$$\mathbf{v}_d(t) = (\sin(0.1t), 0.5 \cos(0.1t), 1) \text{ m/sec.}$$

The desired formation pattern is a square parallel to the universal $x - y$ plane, and is defined by the vectors $\boldsymbol{\delta}_{ij}$ obtained from

$$\boldsymbol{\delta}_1 = \begin{pmatrix} 2 \\ 2 \\ 0 \end{pmatrix}, \quad \boldsymbol{\delta}_2 = \begin{pmatrix} -2 \\ 2 \\ 0 \end{pmatrix}, \quad \boldsymbol{\delta}_3 = \begin{pmatrix} -2 \\ -2 \\ 0 \end{pmatrix}, \quad \boldsymbol{\delta}_4 = \begin{pmatrix} 2 \\ -2 \\ 0 \end{pmatrix}, \quad (5.57)$$

with $\boldsymbol{\delta}_{ij} = (\boldsymbol{\delta}_i - \boldsymbol{\delta}_j)$. The information flow between aircraft is fixed, undirected and connected and is represented by the undirected graph having the set of edges: $\mathcal{E} = \{(1, 2), (1, 3), (2, 3), (2, 4)\}$, and the adjacency matrix $\mathcal{K} = \text{col}[k_{ij}]$, with k_{ij} is defined as in table 5.1 for $(i, j) \in \mathcal{E}$ and zero otherwise. The auxiliary systems (5.5) are initialized as

$$\boldsymbol{\theta}_i(0) = \dot{\boldsymbol{\theta}}_i(0) = (0, 0, 0)^T. \quad (5.58)$$

For all the proposed control schemes, we consider for simulations that the saturation function χ is defined in (2.33) with $\sigma(\cdot) = \tanh(\cdot)$, and $\sigma_b = 1$, and the control gains are selected according to table 5.1.

Table 5.1: Control gains

	k_i^v	k_i^p	k_i^d	k_i^β	k_i^q	k_i^Ω	k_i^ψ	L_i^p	L_i^d	k_{ij}
Theorem 5.1	5	1.5	1.5	20	20	20				2
Theorem 5.2	1.5	0.8	0.8	30	100	50	1			0.4
Theorem 5.3	1.5	0.8	0.8	30	100	50	1	0.8	0.8	0.4

First, we consider the results of Theorem 5.1. Note that the control gains are selected such that Assumption 4.1 is satisfied. Fig.5.3a illustrates the 3-D plot of the aircraft positions and Fig.5.3b shows the three components of the linear-velocity tracking error of each aircraft, with $\tilde{\mathbf{v}}_i = (\mathbf{v}_i - \mathbf{v}_d)$. From these figures, we can see that the four aircraft converge to the desired formation and track the desired linear-velocity.

The control scheme in Theorem 5.2 is considered next where the nonlinear observer (5.37) and the first-order filter (5.28) are initialized as follows

$$\tilde{\boldsymbol{\xi}}_i(0) = \boldsymbol{\nu}_i(0) = (0, 0, 0)^T, \quad \boldsymbol{\psi}_i(0) = (0, 1, -1)^T.$$

The control gains in this case are selected such that Assumption 4.1 and conditions (5.38) are satisfied. The obtained results are shown in Fig.5.4a and Fig.5.4b, where it is clear that our control objective is achieved without linear-velocity measurements.

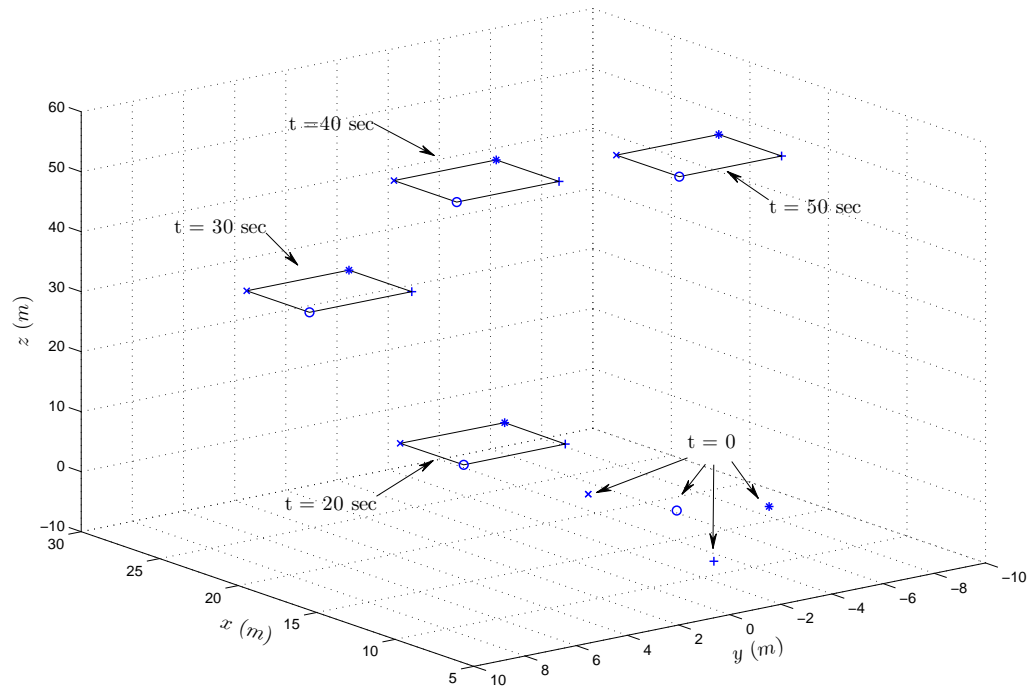
Finally, In Fig.5.5a and Fig.5.5b, we give plots of the aircraft positions and linear-velocities tracking error obtained when the control scheme in Theorem 5.3 is implemented with the auxiliary systems (5.44) initialized as: $\boldsymbol{\alpha}_i(0) = \dot{\boldsymbol{\alpha}}_i(0) = (0, 0, 0)^T$. We can notice that similar results are obtained as compared with Fig.5.4a and Fig.5.4b. However, the implementation of this control scheme is less complicated and reduces considerably the communication requirements between aircraft.

5.7 Concluding remarks

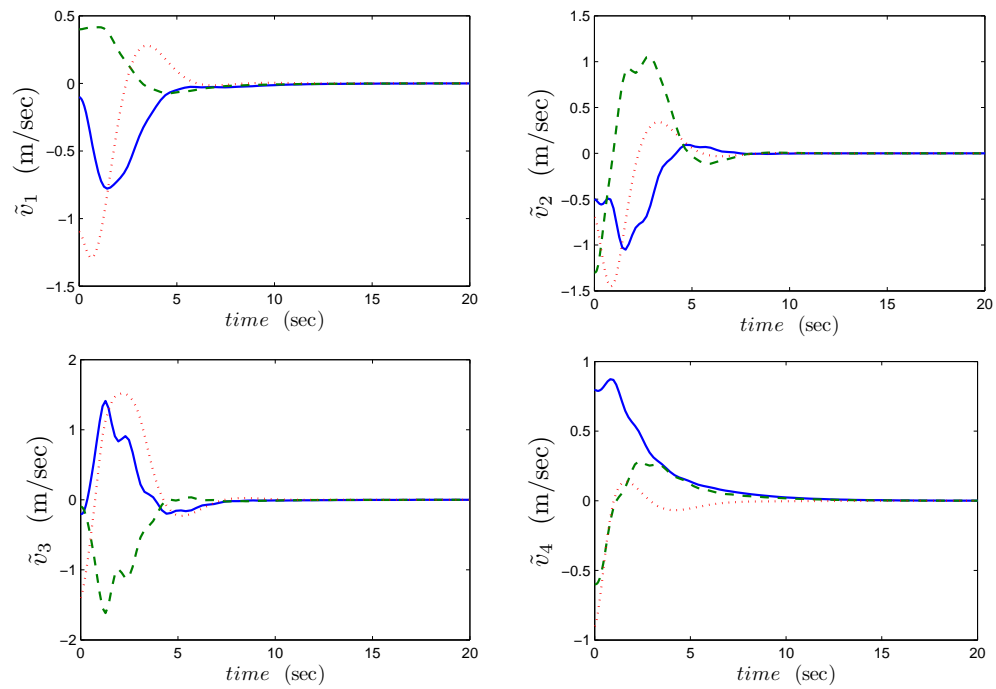
In this chapter, we addressed the formation control problem of multiple VTOL UAVs under a fixed and undirected communication topology. Based on the control design procedure developed in the previous chapter, we proposed state feedback and output feedback formation control schemes that achieve global stability results in terms of the position. The state feedback formation control scheme in Theorem 5.1 was shown to present several advantages when compared to conventional techniques applied to VTOL aircraft formations. These advantages can be summarized as follows. First, the extraction algorithm condition can be satisfied without any considerations on the communication topology between aircraft. This makes the design of the controller much simpler since appropriate control gains can be selected without an *a priori* knowledge on the number of aircraft interacting with each aircraft. In addition, the

designer can set limits of the applied thrust to each aircraft independently from the number of its neighbors. Second, the torque input design is considerably simplified since it involves only measurable signals. Third, the communication requirements between members of the team are reduced since only the variables ξ_i and \mathbf{z}_i are transmitted through the communication channels.

In Theorem 5.2, we proposed a linear-velocity-free formation control scheme. A partial state feedback and a nonlinear observer have been used to obviate the requirement of the linear-velocity measurements. Based on a conceptually similar approach, this result was extended in Theorem 5.3 to reduce the communication requirements between the group members. It should be mentioned that the output feedback solutions presented in this chapter can be applied to solve the consensus problem for multi-agent systems. In fact, using partial state feedback schemes based on similar auxiliary systems as (5.5), velocity-free solutions to the consensus problem of multiple vehicles modeled by double integrators subject to input constraints have been proposed in Abdessameud and Tayebi (2010*d*) and Abdessameud and Tayebi (2010*e*).

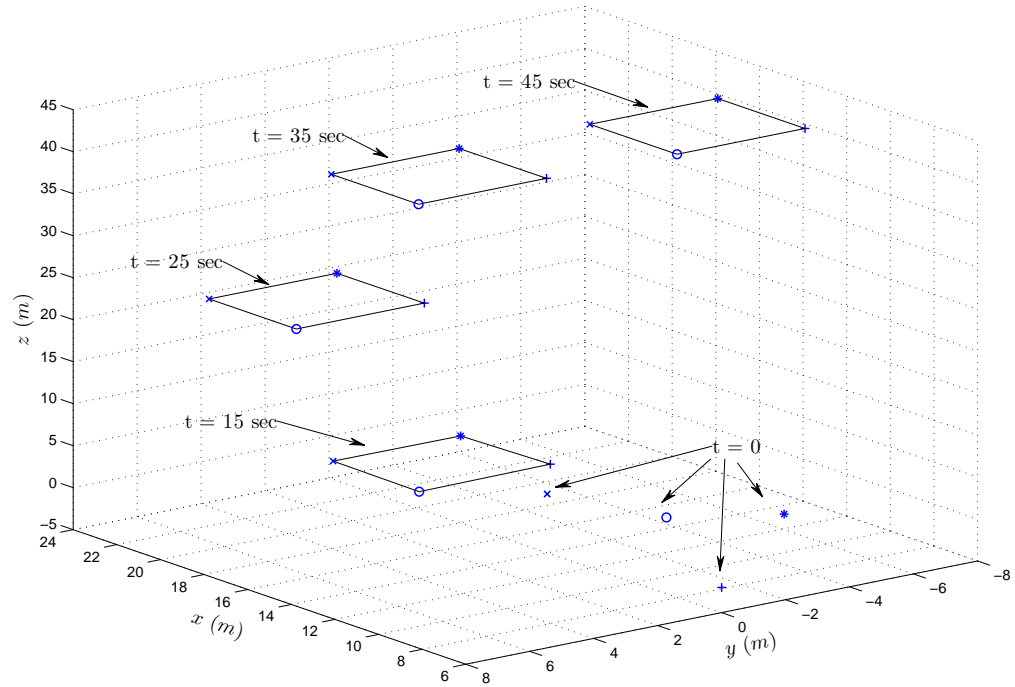


(a)

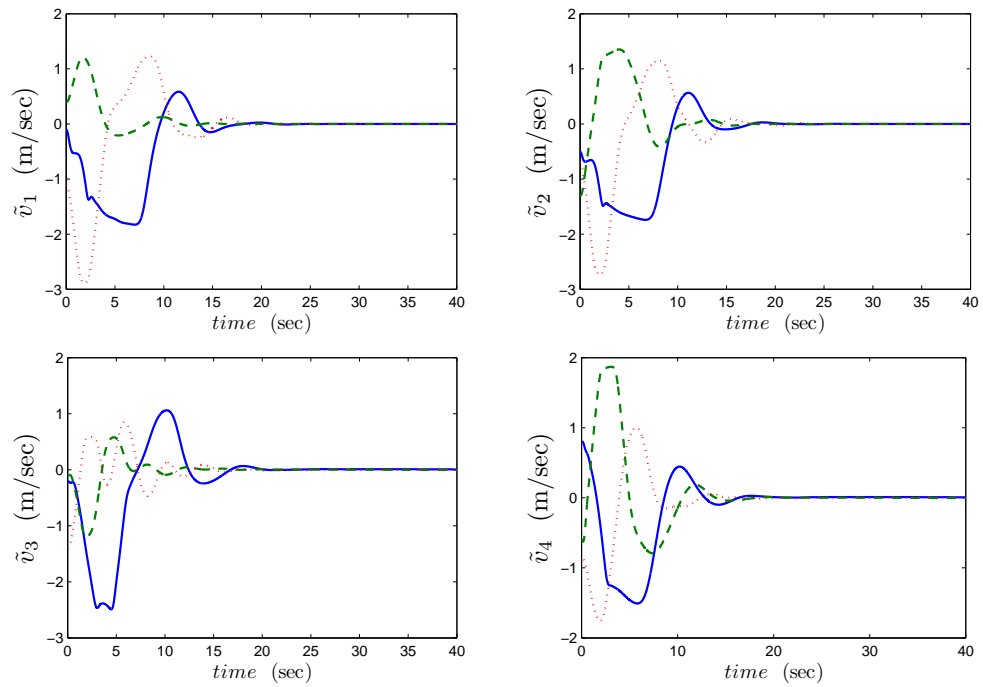


(b)

Figure 5.3: Simulation results in case of Theorem 5.1: (a) Systems trajectories (b) Linear-velocity error $\tilde{\mathbf{v}}_i$

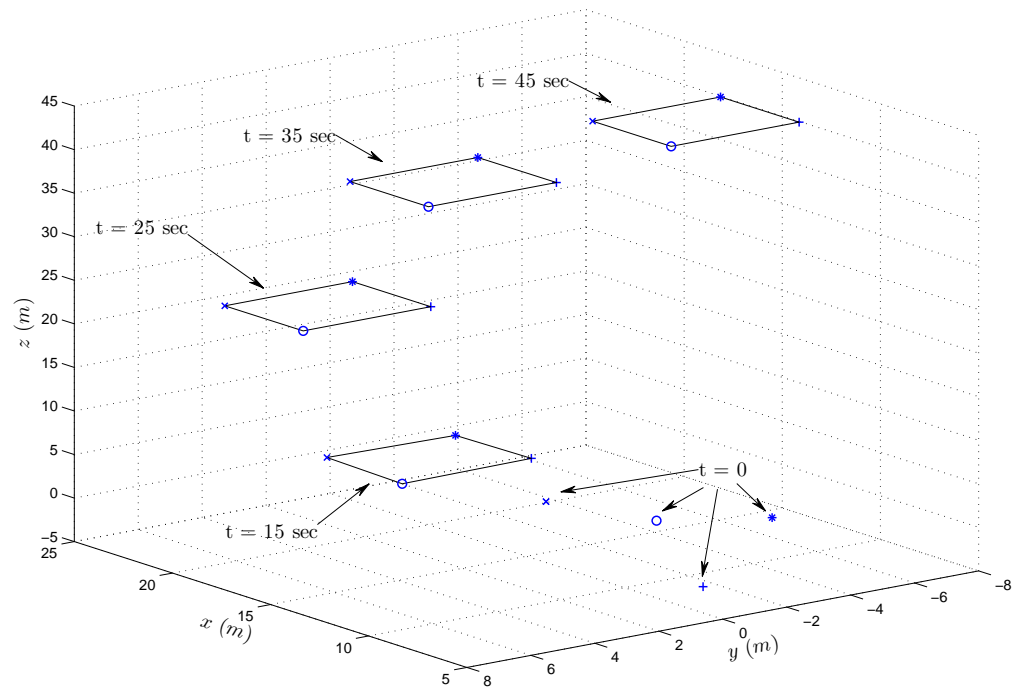


(a)

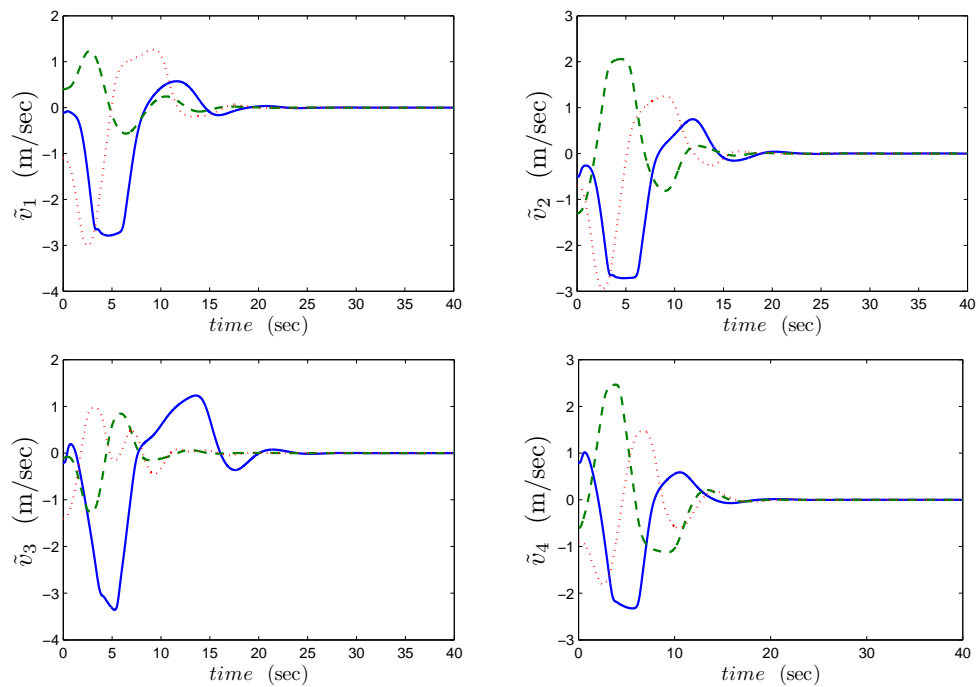


(b)

Figure 5.4: Simulation results in case of Theorem 5.2: (a) Systems trajectories (b) Linear-velocity error \tilde{v}_i



(a)



(b)

Figure 5.5: Simulation results in case of Theorem 5.3: (a) Systems trajectories (b) Linear-velocity error $\tilde{\mathbf{v}}_i$

Chapter 6

Formation control with communication delays

The problem of delays in the information exchange between aircraft is the focus of the present chapter. Four formation control schemes are presented in the full and partial state information cases with constant and time-varying communication delays. First, the effects of constant communication delays on the state feedback formation control scheme proposed in Theorem 5.1 are studied, and sufficient delay-dependent results are obtained. This control scheme is extended next to the cases of bounded time-varying and arbitrary constant communication delays. When the linear-velocity is not measured, a virtual vehicle approach is proposed to design an output feedback formation control scheme with constant communication delays. The results reported in this chapter are based on Abdessameud and Tayebi (2010*f,g*).

6.1 Introduction

Information exchange between vehicles plays a central role in the design of formation control schemes. In practical situations, this information transmission is often delayed. The effect of communication delays in multi-agent systems with second order dynamics has been extensively studied in recent years (Münz *et al.*, 2008; Seuret *et al.*, 2009; Hong-Yong *et al.*, 2010; Meng *et al.*, 2010, to cite a few) and sufficient conditions have been derived to achieve the stability of the system. In Münz *et al.* (2008), Seuret *et al.* (2009) and Meng *et al.* (2010) for example, Lyapunov-Krasovskii functionals have been used in the analysis of consensus algorithms of multi-agents with constant communication delays, and delay-dependent conditions have been derived. The authors in Hong-Yong *et al.* (2010) used the Nyquist stability criterion to study the stability and convergence of leader-following consensus algorithms in the presence of input and communication delays. In nonlinear systems, communication delays have also been considered in applications like spacecraft formation control (Chung *et al.*, 2009) and the synchronization of bilateral teleoperators (Polushin *et al.*, 2006; Chopra *et al.*, 2008; Nuño *et al.*, 2010). However, only few works have been done for nonlinear systems with nonlinear coupling that arises when control saturations are considered for example. In this context, the scattering variables formulation has been used in Chopra and Spong (2006) and an output synchronization scheme for passive nonlinear

systems with nonlinear coupling has been proposed. An important assumption in the above papers, however is that the full state vector is available for feedback. Despite the interesting results cited above, much work remains to be done to develop formation control algorithms for a group of vehicles with complex dynamics in the presence of communication delays and take into consideration the vehicles input constraints in the full and partial state information cases

In this chapter, we propose and analyze formation control schemes for a group of VTOL aircraft in the presence of communication delays. Similar to the previous chapter, the control design procedure presented in section 4.3 is considered. The state feedback formation control scheme proposed in Theorem 5.1 is considered first in the presence of constant communication delays, and sufficient delay-dependent conditions are derived. The implementation of this control law in the case where the communication delays are time-varying presents some technical difficulties. The challenge in this case is that the first time-derivative of the auxiliary input is function of non-available signals. This problem is solved by the implementation of a second auxiliary system and similar conditions are derived when the communication delays are bounded with bounded time-derivatives. Next, we propose a formation control scheme that achieves our control objectives with arbitrary constant communication delays. In the case where aircraft linear-velocities are not available for feedback, we propose a virtual vehicle approach to design an output feedback formation control scheme with delayed communication.

6.2 Problem formulation

The control objective in this chapter is to design formation control schemes for a group of aircraft, governed by the dynamics (5.1)-(5.2), such that, starting from any initial conditions, aircraft converge to a predefined formation with zero final linear-velocity. We assume that the information flow between aircraft is fixed and undirected, and is described by the weighted undirected graph $\mathcal{G} = (\mathcal{N}, \mathcal{E}, \mathcal{K})$. We further assume that each aircraft can sense its state with no delay, and the communication between two neighboring aircraft, the i^{th} and j^{th} aircraft, is delayed by τ_{ij} , where τ_{ij} is not necessarily equal to τ_{ji} .

With these assumptions, we aim to design an input thrust and torque for each aircraft such that

$$\mathbf{v}_i \rightarrow \mathbf{0} \quad \text{and} \quad \mathbf{p}_i - \mathbf{p}_j \rightarrow \boldsymbol{\delta}_{ij}, \quad (6.1)$$

for $i, j \in \mathcal{N}$, where $\boldsymbol{\delta}_{ij} \in \mathbb{R}^3$, satisfying $\boldsymbol{\delta}_{ij} = -\boldsymbol{\delta}_{ji}$, defines the formation pattern. We first consider this problem when the full state vector is available for feedback, and then we extend our results to remove the requirement of the linear-velocity measurements.

6.3 Delay-dependent formation control scheme

In this section, we study the effects of constant communication delays on the formation control law presented in section 5.3 with zero reference linear-velocity. In this case, the control scheme in Theorem 5.1 is equivalent to

$$\mathbf{F}_i = -k_i^p \chi(\boldsymbol{\theta}_i) - k_i^d \chi(\dot{\boldsymbol{\theta}}_i), \quad (6.2)$$

$$\ddot{\boldsymbol{\theta}}_i = \mathbf{F}_i - \mathbf{u}_i, \quad (6.3)$$

$$\mathbf{u}_i = -k_i^v \mathbf{z}_i - \sum_{j=1}^n k_{ij} (\boldsymbol{\xi}_i - \boldsymbol{\xi}_j(t - \tau_{ij}) - \boldsymbol{\delta}_{ij}), \quad (6.4)$$

where the control parameters are defined as in Theorem 5.1, the variable $\boldsymbol{\theta}_i \in \mathbb{R}^3$ can take arbitrary initial values, \mathbf{u}_i is an auxiliary input to (6.3), and the error variables $\boldsymbol{\xi}_i$ and \mathbf{z}_i are defined as

$$\boldsymbol{\xi}_i := \mathbf{p}_i - \boldsymbol{\theta}_i, \quad \mathbf{z}_i := \dot{\boldsymbol{\xi}}_i. \quad (6.5)$$

Note that the intermediary input (6.2) is guaranteed to be *a priori* bounded as

$$\|\mathbf{F}_i\| \leq \sigma_b \sqrt{3}(k_i^p + k_i^d) \quad (6.6)$$

where σ_b is defined in property P2 in section 2.6. Therefore, the requirements of the thrust and attitude extraction algorithm in Lemma 4.1 can be easily satisfied with an appropriate choice of the gains k_i^p and k_i^d , and without any consideration on the communication topology between aircraft. In addition, the extracted input thrust, given in (4.6), is guaranteed to be strictly positive and *a priori* bounded as

$$\mathcal{T}_i \leq m_i \left(g + \sigma_b \sqrt{3}(k_i^p + k_i^d) \right) := \mathcal{T}_i^b \quad (6.7)$$

with \mathcal{T}_i^b being a positive constant.

The torque input design follows the same steps as in section 5.3. We consider the extracted value of the desired attitude \mathbf{Q}_{d_i} , given in (4.7), as a time-varying reference attitude and derive explicit expressions of the desired angular velocity and its time-derivative, which can be obtained as in (5.9)-(5.10) with

$$\dot{\mathbf{F}}_i = -k_i^p h(\boldsymbol{\theta}_i) \dot{\boldsymbol{\theta}}_i - k_i^d h(\dot{\boldsymbol{\theta}}_i) (\mathbf{F}_i - \mathbf{u}_i), \quad (6.8)$$

$$\begin{aligned} \ddot{\mathbf{F}}_i = & -k_i^p \dot{h}(\boldsymbol{\theta}_i) \dot{\boldsymbol{\theta}}_i - \left(k_i^p h(\boldsymbol{\theta}_i) + k_i^d \dot{h}(\dot{\boldsymbol{\theta}}_i) \right) (\mathbf{F}_i - \mathbf{u}_i) \\ & - k_i^d \dot{h}(\dot{\boldsymbol{\theta}}_i) (\dot{\mathbf{F}}_i - \dot{\mathbf{u}}_i). \end{aligned} \quad (6.9)$$

It should be noted that the time-derivative of \mathbf{u}_i in (6.4) can be obtained as

$$\dot{\mathbf{u}}_i = -k_i^v \left(\mathbf{u}_i - \frac{2\mathcal{T}_i}{m_i} \mathbf{R}(\mathbf{Q}_i)^T \mathbf{S}(\bar{\mathbf{q}}_i) \tilde{\mathbf{q}}_i \right) - \sum_{j=1}^n k_{ij} (\mathbf{z}_i - \mathbf{z}_j(t - \tau_{ij})). \quad (6.10)$$

Therefore, we can see from (5.9)-(5.10) with (6.8)-(6.9) that only available signals are used to evaluate $\boldsymbol{\omega}_{d_i}$ and $\dot{\boldsymbol{\omega}}_{d_i}$, and the variables $\boldsymbol{\xi}_i$ and \mathbf{z}_i are transmitted between each pair of communicating aircraft in the team.

We consider the same input torque as in the communication delays-free case (5.13)-(5.14), *i.e.*,

$$\boldsymbol{\Gamma}_i = \mathbf{H}_i(\boldsymbol{\omega}_i, \boldsymbol{\omega}_{d_i}, \dot{\boldsymbol{\omega}}_{d_i}, \tilde{\mathbf{Q}}_i) + \mathbf{J}_{f_i} \dot{\boldsymbol{\beta}}_i - k_i^q \tilde{\mathbf{q}}_i - k_i^\Omega (\tilde{\boldsymbol{\omega}}_i - \boldsymbol{\beta}_i), \quad (6.11)$$

$$\boldsymbol{\beta}_i = -k_i^\beta \tilde{\mathbf{q}}_i + \frac{2\mathcal{T}_i}{k_i^q m_i} \mathbf{S}(\bar{\mathbf{q}}_i)^T \mathbf{R}(\mathbf{Q}_i) \mathbf{z}_i, \quad (6.12)$$

where the control variables and gains are defined as in Theorem 5.1 and the vector $\mathbf{H}_i(\cdot)$ is given in (5.15) with $\boldsymbol{\omega}_{d_i}$ and $\dot{\boldsymbol{\omega}}_{d_i}$ are defined in (5.9)-(5.10) and (6.8)-(6.10). Our results are stated in the following theorem .

Theorem 6.1. *Consider the VTOL-UAVs modeled as in (5.1)-(5.2). For each aircraft, let the thrust input \mathcal{T}_i and the desired attitude \mathbf{Q}_{d_i} be given, respectively, by (4.6) and (4.7), with \mathbf{F}_i given by (6.2)-(6.4). Let the input torque be as in (6.11)-(6.12). Let the controller gains satisfy*

$$\sqrt{3}\sigma_b \left(k_i^p + k_i^d \right) < g, \quad (6.13)$$

$$k_i^z = k_i^v - \frac{1}{2} \sum_{j=1}^n k_{ij} \left(\epsilon + \frac{\tau^2}{\epsilon} \right) > 0, \quad (6.14)$$

for some $\epsilon > 0$ and $\tau_{ij} \leq \tau$ for all $(i, j) \in \mathcal{E}$, and assume that the communication graph \mathcal{G} is connected. Then, starting from any initial conditions, the signals \mathbf{v}_i , $(\mathbf{p}_i - \mathbf{p}_j)$ and $\tilde{\boldsymbol{\omega}}_i$ are bounded and $\mathbf{v}_i \rightarrow 0$, $(\mathbf{p}_i - \mathbf{p}_j) \rightarrow \boldsymbol{\delta}_{ij}$, $\tilde{\mathbf{q}}_i \rightarrow 0$ and $\tilde{\boldsymbol{\omega}}_i \rightarrow 0$ for all $i, j \in \mathcal{N}$.

Sketch of proof: Notice first that if the control gains satisfy condition (6.13), we can always extract the thrust and the desired attitude from (4.6) and (4.7) respectively for each VTOL vehicle.

Similarly to the proof of Theorem 5.1, the translational and rotational error dynamics

can be obtained as in (5.17) and (5.18), *i.e.*,

$$\dot{\mathbf{z}}_i = -k_i^v \mathbf{z}_i - \sum_{j=1}^n k_{ij} \boldsymbol{\xi}_{ij} - \frac{2\mathcal{T}_i}{m_i} \mathbf{R}(\mathbf{Q}_i)^T \mathbf{S}(\bar{\mathbf{q}}_i) \tilde{\mathbf{q}}_i, \quad (6.15)$$

$$\mathbf{J}_{f_i} \dot{\boldsymbol{\Omega}}_i = -k_i^q \tilde{\mathbf{q}}_i - k_i^\Omega \boldsymbol{\Omega}_i, \quad (6.16)$$

with $\boldsymbol{\xi}_{ij} = (\boldsymbol{\xi}_i - \boldsymbol{\xi}_j(t - \tau_{ij}) - \boldsymbol{\delta}_{ij})$ and $\boldsymbol{\Omega}_i = (\tilde{\boldsymbol{\omega}}_i - \boldsymbol{\beta}_i)$. The results of Theorem 6.1 are shown using the Lyapunov-Krasovskii functional

$$V = V_{t_1} + V_{a_1} + V_{k_1}, \quad (6.17)$$

with

$$V_{t_1} = \frac{1}{2} \sum_{i=1}^n \left(\mathbf{z}_i^T \mathbf{z}_i + \frac{1}{2} \sum_{j=1}^n k_{ij} \bar{\boldsymbol{\xi}}_{ij}^T \bar{\boldsymbol{\xi}}_{ij} \right), \quad (6.18)$$

$$V_{a_1} = \sum_{i=1}^n \left(\frac{1}{2} \boldsymbol{\Omega}_i^T \mathbf{J}_{f_i} \boldsymbol{\Omega}_i + k_i^q \tilde{\mathbf{q}}_i^T \tilde{\mathbf{q}}_i + k_i^q (1 - \tilde{\eta}_i)^2 \right), \quad (6.19)$$

$$V_{k_1} = \sum_{i=1}^n \sum_{j=1}^n \frac{k_{ij}^T}{2\epsilon} \left(\int_{-\tau}^0 \int_{t+s}^t \mathbf{z}_j(\varrho)^T \mathbf{z}_j(\varrho) d\varrho ds \right), \quad (6.20)$$

where $\bar{\boldsymbol{\xi}}_{ij} = (\boldsymbol{\xi}_i - \boldsymbol{\xi}_j - \boldsymbol{\delta}_{ij})$, $\tau_{ij} \leq \tau$ for all $(i, j) \in \mathcal{E}$ and $\epsilon > 0$, which leads to the negative semi-definite time-derivative that can be upper bounded as

$$\dot{V} \leq \sum_{i=1}^n \left(-k_i^z \mathbf{z}_i^T \mathbf{z}_i - k_i^\Omega \boldsymbol{\Omega}_i^T \boldsymbol{\Omega}_i - k_i^q k_i^\beta \tilde{\mathbf{q}}_i^T \tilde{\mathbf{q}}_i \right) \quad (6.21)$$

with k_i^z given in (6.14). Invoking Barbălat Lemma we show that $\mathbf{z}_i \rightarrow 0$, $\tilde{\boldsymbol{\omega}}_i \rightarrow 0$ and $\tilde{\mathbf{q}}_i \rightarrow 0$. Also, invoking the extended Barbălat Lemma (Lemma 2.3), we show that $\dot{\mathbf{z}}_i \rightarrow 0$. Consequently, using the fact that $\mathbf{z}_i \rightarrow 0$, one can conclude that $(\boldsymbol{\xi}_i - \boldsymbol{\xi}_j) \rightarrow \boldsymbol{\delta}_{ij}$. The last part of the proof consist of showing that $\boldsymbol{\theta}_i$ and $\dot{\boldsymbol{\theta}}_i$ are bounded and converge to zero using the result of Lemma 2.6. A detailed proof of Theorem 6.1 is given in Appendix A.5.1. \square

Remark 6.1. Note that to satisfy condition (6.14), a good estimate of the value of τ , such that $\tau_{ij} \leq \tau$ for all $(i, j) \in \mathcal{E}$, must be known, which is a reasonable assumption from a practical point of view. In addition, we can see that the time-derivative of the variable $\boldsymbol{\beta}_i$ is required in the control input (6.11). Note that $\dot{\boldsymbol{\beta}}_i$ can be computed explicitly using available signals and is given in (5.22).

It is clear from the control structure (6.2)-(6.4) that the auxiliary input \mathbf{u}_i is designed independently from the boundedness constraint of the intermediary input. As a result, we were able to design an *a priori* bounded intermediary control input using linear coupling between neighboring aircraft, as can be seen from the definition of $\boldsymbol{\xi}_{ij}$. Consequently, Lyapunov-Krasovskii functionals have been successfully used in the analysis. This is not a trivial task using classical control techniques. For example, the classical formation control law given in (5.23) in this case is equivalent to

$$\mathbf{F}_i = -k_i^v \chi(\mathbf{v}_i) - \sum_{j=1}^n k_{ij} \chi(\mathbf{p}_i - \mathbf{p}_j(t - \tau_{ij}) - \boldsymbol{\delta}_{ij}). \quad (6.22)$$

It is clear that the stability analysis of the closed loop system would be difficult when using similar tools as in the proof of Theorem 6.1, due to the nonlinear interaction between aircraft through the function χ . In addition, the scattering variables formalism (Chopra and Spong, 2006) cannot be used since the time-derivatives of these variables will be required in the torque input design.

6.3.1 Extension to time-varying communication delays

In this subsection, we modify the control scheme (6.4) to achieve our control objectives in the case of time-varying communication delays. In this case, the main problem with the design (6.4) can be seen from the expression of $\dot{\boldsymbol{\omega}}_{d_i}$, given by (5.10) with (6.8)-(6.9). In fact, when the communication delays are time-varying, the vector $\dot{\mathbf{u}}_i$ is obtained as

$$\dot{\mathbf{u}}_i = -k_i^v \left(\mathbf{u}_i - \frac{2\mathcal{T}_i}{m_i} \mathbf{R}(\mathbf{Q}_i)^T \mathbf{S}(\bar{\mathbf{q}}_i) \tilde{\mathbf{q}}_i \right) - \sum_{j=1}^n k_{ij} (\mathbf{z}_i - (1 - \dot{\tau}_{ij}(t)) \mathbf{z}_j(t - \tau_{ij}(t))).$$

Therefore, the application of the above control scheme requires good knowledge of $\dot{\tau}_{ij}(t)$, which is not the case in general. To solve this problem, we propose the intermediary input \mathbf{F}_i given in (6.2)-(6.3) with the auxiliary input \mathbf{u}_i given by

$$\mathbf{u}_i = -L_i^p \boldsymbol{\alpha}_i - L_i^d \dot{\boldsymbol{\alpha}}_i, \quad (6.23)$$

where L_i^p and L_i^d are positive scalar gains and the vector $\boldsymbol{\alpha}_i \in \mathbb{R}^3$ is an auxiliary variable that can be initialized arbitrarily and is governed by

$$\ddot{\boldsymbol{\alpha}}_i = \mathbf{u}_i - \boldsymbol{\phi}_i - \frac{2\mathcal{T}_i}{m_i} \mathbf{R}(\mathbf{Q}_i)^T \mathbf{S}(\bar{\mathbf{q}}_i) \tilde{\mathbf{q}}_i, \quad (6.24)$$

with $\boldsymbol{\phi}_i \in \mathbb{R}^3$ being an additional input. We redefine the error signals in (6.5) as

$$\boldsymbol{\xi}_i = \mathbf{p}_i - \boldsymbol{\theta}_i - \boldsymbol{\alpha}_i, \quad \mathbf{z}_i := \dot{\boldsymbol{\xi}}_i \quad (6.25)$$

and propose the following design for the input of (6.24)

$$\phi_i = -k_i^v \mathbf{z}_i - \sum_{j=1}^n k_{ij} (\boldsymbol{\xi}_i - \boldsymbol{\xi}_j(t - \tau_{ij}(t)) - \boldsymbol{\delta}_{ij}), \quad (6.26)$$

with the control gains being defined as in Theorem 5.1. Note that the main advantage of the auxiliary system (6.24) is to allow the design of the input \mathbf{u}_i such that its time-derivative does not involve the time-derivative of the communication delays. In fact, from (6.24) and (6.23), we have

$$\dot{\mathbf{u}}_i = -L_i^p \dot{\boldsymbol{\alpha}}_i - L_i^d (\mathbf{u}_i - \phi_i - \frac{2\mathcal{T}_i}{m_i} \mathbf{R}(\mathbf{Q}_i)^T \mathbf{S}(\bar{\mathbf{q}}_i) \tilde{\mathbf{q}}_i), \quad (6.27)$$

and the vectors $\boldsymbol{\omega}_{d_i}$ and $\dot{\boldsymbol{\omega}}_{d_i}$, given in (5.9)-(5.10) with (6.8)-(6.9) and (6.27), can be evaluated using available signals. Furthermore, to implement the above control scheme, communicating aircraft need only to communicate the variables $\boldsymbol{\xi}_i$. Our results in this section are stated in the following theorem.

Theorem 6.2. *Consider the VTOL-UAVs modeled as in (5.1)-(5.2). For each aircraft, let the thrust input \mathcal{T}_i and the desired attitude \mathbf{Q}_{d_i} be given, respectively, by (4.6) and (4.7), with \mathbf{F}_i given by (6.2) with (6.3), (6.23)-(6.24) and (6.26). Let the input torque be given by (6.11) with the variable $\boldsymbol{\beta}_i$ is defined as in (5.51), i.e.,*

$$\boldsymbol{\beta}_i = k_i^\beta \tilde{\mathbf{q}}_i. \quad (6.28)$$

Let the controller gains satisfy condition (6.13) and

$$\bar{k}_i^z = k_i^v - \frac{1}{2} \sum_{j=1}^n k_{ij} (\epsilon + \frac{\bar{\tau}^2}{\epsilon}) > 0, \quad (6.29)$$

for some $\epsilon > 0$ and $\tau_{ij}(t) \leq \bar{\tau}$, for all $t > 0$ and $(i, j) \in \mathcal{E}$, and assume that the communication graph \mathcal{G} is connected. If the time-derivative of the communication delay, $\dot{\tau}_{ij}(t)$, is bounded for $(i, j) \in \mathcal{E}$, then starting from any initial conditions, the signals \mathbf{v}_i , $(\mathbf{p}_i - \mathbf{p}_j)$ and $\tilde{\boldsymbol{\omega}}_i$ are bounded and $\mathbf{v}_i \rightarrow 0$, $(\mathbf{p}_i - \mathbf{p}_j) \rightarrow \boldsymbol{\delta}_{ij}$, $\tilde{\mathbf{q}}_i \rightarrow 0$ and $\tilde{\boldsymbol{\omega}}_i \rightarrow 0$ for all $i, j \in \mathcal{N}$.

Sketch of proof : It is clear that if condition (6.13) is satisfied, the thrust input and the desired attitude can be extracted from the result of Lemma 4.1. The translational error dynamics in this case are obtained as

$$\dot{\mathbf{z}}_i = -k_i^v \mathbf{z}_i - \sum_{j=1}^n k_{ij} \boldsymbol{\xi}_{ij}, \quad (6.30)$$

and the angular velocity tracking error dynamics are given in (6.16). The proof of Theorem 6.2 is based on the following Lyapunov-Krasovskii functional

$$V = V_{t_1} + V_{a_1} + V_{k_2}, \quad (6.31)$$

where V_{t_1} and V_{a_1} are given respectively in (6.18) and (6.19) and

$$V_{k_2} = \frac{1}{2} \sum_{i=1}^n \sum_{j=1}^n \frac{k_{ij}}{\epsilon} \bar{\tau} \left(\int_{-\bar{\tau}}^0 \int_{t+s}^t \mathbf{z}_j(\varrho)^T \mathbf{z}_j(\varrho) d\varrho ds \right), \quad (6.32)$$

leading to the negative semi-definite time-derivative similar to (6.21). Following similar steps as in the proof of Theorem 6.1, we show that $\mathbf{z}_i \rightarrow 0$, $\tilde{\boldsymbol{\omega}}_i \rightarrow 0$, $\tilde{\mathbf{q}}_i \rightarrow 0$, and $(\boldsymbol{\xi}_i - \boldsymbol{\xi}_j) \rightarrow \boldsymbol{\delta}_{ij}$ for all $i, j \in \mathcal{N}$. Then, the variables $\boldsymbol{\alpha}_i$ and $\dot{\boldsymbol{\alpha}}_i$ are shown to be globally bounded and converge asymptotically to zero. This can be shown using the dynamics of the auxiliary system (6.24) with the fact that the signals $\boldsymbol{\phi}_i$ and $\tilde{\mathbf{q}}_i$ are bounded and converge asymptotically to zero. Finally, the results of the theorem are shown using Lemma 2.6. Details of the proof of Theorem 6.2 are given in Appendix A.5.2. □

Remark 6.2. Note that the perturbation term, $\left(\frac{2\mathcal{T}_i}{m_i} \mathbf{R}(\mathbf{Q}_i)^T \mathbf{S}(\bar{\mathbf{q}}_i) \tilde{\mathbf{q}}_i \right)$, has been compensated in the dynamics of the auxiliary system 6.24. In Abdessameud and Tayebi (2010g), the auxiliary system (6.24) is considered without this perturbation term, and the input variable $\boldsymbol{\beta}_i$ is selected as in (6.12). This does not change the results, however, the time-derivative of the perturbation term will be needed in the expression of $\dot{\boldsymbol{\beta}}_i$ in the torque input.

6.4 Delay-independent formation control design

The design of the translational input in the formation control schemes presented so far are based only on the relative positions of aircraft. In this section, we will show that the inclusion of the relative velocities in the control design will enable the design of a formation control scheme in the presence of arbitrary constant communication delays. For this purpose, we consider the intermediary control \mathbf{F}_i given by (6.2)-(6.3) and (6.24) and the auxiliary input \mathbf{u}_i given in (6.23) with the following input $\boldsymbol{\phi}_i$,

$$\begin{aligned} \boldsymbol{\phi}_i = & -k_i^v \mathbf{z}_i - k_i^v \lambda \sum_{j=1}^n k_{ij} (\boldsymbol{\xi}_i - \boldsymbol{\xi}_j(t - \tau_{ij}) - \boldsymbol{\delta}_{ij}) \\ & - 2\lambda \sum_{j=1}^n k_{ij} (\mathbf{z}_i - \mathbf{z}_j(t - \tau_{ij})), \end{aligned} \quad (6.33)$$

where the control gains are defined as in Theorem 5.1, λ is a positive scalar and the vectors $\boldsymbol{\xi}_i$ and \mathbf{z}_i are defined in (6.25).

Similarly to the previous section, we can see from (5.9)-(5.10) with (6.8)-(6.9) and (6.27) that $\boldsymbol{\omega}_{d_i}$ and $\dot{\boldsymbol{\omega}}_{d_i}$ can be evaluated using available signals and aircraft need only to communicate their variables $\boldsymbol{\xi}_i$ and \mathbf{z}_i . Therefore, the same input torque used in Theorem 6.2 can be applied to the rotational dynamics, and the following theorem holds:

Theorem 6.3. *Consider the VTOL-UAVs modeled as in (5.1)-(5.2). Let the thrust input \mathcal{T}_i and the desired attitude \mathbf{Q}_{d_i} be given, respectively, by (4.6) and (4.7), with \mathbf{F}_i given by (6.2) with (6.3), (6.23)-(6.24) and (6.33). Let the input torque be as in (6.11) with the vector $\boldsymbol{\beta}_i$ given as in (6.28). Let the controller gains satisfy condition (6.13), and assume that the communication graph \mathcal{G} is connected. Then, starting from any initial conditions, the signals \mathbf{v}_i , $(\mathbf{p}_i - \mathbf{p}_j)$ and $\tilde{\boldsymbol{\omega}}_i$ are bounded and $\mathbf{v}_i \rightarrow 0$, $(\mathbf{p}_i - \mathbf{p}_j) \rightarrow \boldsymbol{\delta}_{ij}$, $\tilde{\mathbf{q}}_i \rightarrow 0$ and $\tilde{\boldsymbol{\omega}}_i \rightarrow 0$ for all $i, j \in \mathcal{N}$.*

Sketch of proof: Similar to the proof of Theorem 6.1, Lemma 4.1 can be used to extract the necessary thrust and the desired attitude for each VTOL vehicle if condition (6.13) is satisfied. For analysis purposes, we define the new vector

$$\mathbf{r}_i = \mathbf{z}_i + \lambda \sum_{k=1}^n k_{ij} (\boldsymbol{\xi}_i - \boldsymbol{\xi}_j(t - \tau_{ij}) - \boldsymbol{\delta}_{ij}), \quad (6.34)$$

with time-derivative obtained from (5.1) and (6.25), using (6.3), (6.24) and (6.33), as

$$\dot{\mathbf{r}}_i = -k_i^y \mathbf{r}_i - \lambda \sum_{j=1}^n k_{ij} \mathbf{z}_{ij}. \quad (6.35)$$

where $\mathbf{z}_{ij} = (\mathbf{z}_i - \mathbf{z}_j(t - \tau_{ij}))$. Also, the attitude error dynamics are given in (6.16). The proof of the theorem is based on the use of the following Lyapunov-Krasovskii functional

$$\begin{aligned} V = & \frac{1}{2} \sum_{i=1}^n \mathbf{r}_i^T \mathbf{r}_i + \frac{1}{2} \sum_{i=1}^n \lambda \sum_{j=1}^n k_{ij} \int_{t-\tau_{ij}}^t \mathbf{z}_j^T \mathbf{z}_j ds \\ & + \frac{1}{2} \sum_{i=1}^n \lambda^2 \left(\sum_{j=1}^n k_{ij} \boldsymbol{\xi}_{ij} \right)^T \left(\sum_{j=1}^n k_{ij} \boldsymbol{\xi}_{ij} \right) + V_{a_1}, \end{aligned} \quad (6.36)$$

with V_{a_1} given in (6.19), which leads to the semi-definite time-derivative

$$\dot{V} = - \sum_{i=1}^n \left(k_i^v \mathbf{r}_i^T \mathbf{r}_i + k_i^\Omega \boldsymbol{\Omega}_i^T \boldsymbol{\Omega}_i + k_i^q k_i^\beta \tilde{\mathbf{q}}_i^T \tilde{\mathbf{q}}_i + \frac{1}{2} \sum_{j=1}^n \lambda k_{ij} \mathbf{z}_{ij}^T \mathbf{z}_{ij} \right). \quad (6.37)$$

Invoking Barbălat Lemma, we show that $\mathbf{r}_i \rightarrow 0$, $(\mathbf{z}_i - \mathbf{z}_j(t - \tau_{ij})) \rightarrow 0$, $\tilde{\boldsymbol{\omega}}_i \rightarrow 0$ and $\tilde{\mathbf{q}}_i \rightarrow 0$, for $i \in \mathcal{N}$. Then, invoking Lemma 2.3, we verify that $\dot{\mathbf{r}}_i \rightarrow 0$ and $\dot{\mathbf{z}}_i \rightarrow 0$, which leads us to conclude after some steps that $(\mathbf{z}_i - \mathbf{z}_j) \rightarrow 0$ and $(\boldsymbol{\xi}_i - \boldsymbol{\xi}_j) \rightarrow \boldsymbol{\delta}_{ij}$, for all $i, j \in \mathcal{N}$. The rest of the proof follows similar arguments as in the proof of Theorem 6.2, which consists of showing that the auxiliary variables $\boldsymbol{\alpha}_i$, $\dot{\boldsymbol{\alpha}}_i$, $\boldsymbol{\theta}_i$ and $\dot{\boldsymbol{\theta}}_i$ are bounded and converge to zero. A detailed proof of Theorem 6.3 is given in Appendix A.5.3. □

Remark 6.3. *The design of the input $\boldsymbol{\phi}_i$ in (6.33) can be considered as a generalization of the control law developed for bilateral teleoperators in Nuño et al. (2010) to the formation control of multiple aircraft.*

An important assumption made in the above formation control schemes is that the linear-velocity vectors are available for feedback, which is essential when using Lyapunov-Krasovskii functionals in this case. In the next section, we will show that using the auxiliary systems with a different design of the auxiliary inputs will enable us to remove the requirement of linear-velocity measurement and use Lyapunov-Krasovskii functionals in the analysis.

6.5 Virtual vehicle approach to the formation control problem

In this section, we propose a virtual vehicle approach to design a formation control scheme that removes the requirement of linear-velocity measurements in the presence of constant communication delays. The main idea in this approach is to associate a virtual vehicle to each aircraft with similar translational dynamics and an additional input. This input is designed so that the states of all virtual vehicles converge to the specified formation in the presence of communication delays. The advantage of this approach is that the states of the virtual vehicles, *i.e.*, virtual positions and virtual velocities, are internally synthesized and hence available.

We propose the following intermediary control input

$$\mathbf{F}_i = -k_i^p \chi(\boldsymbol{\theta}_i) - k_i^d \chi(\dot{\boldsymbol{\theta}}_i), \quad (6.38)$$

$$\ddot{\boldsymbol{\theta}}_i = \mathbf{F}_i - \mathbf{u}_i, \quad (6.39)$$

$$\ddot{\boldsymbol{\alpha}}_i = \mathbf{u}_i - \boldsymbol{\phi}_i - \frac{2\mathcal{T}_i}{m_i} \mathbf{R}(\mathbf{Q}_i)^T \mathbf{S}(\bar{\mathbf{q}}_i) \tilde{\mathbf{q}}_i, \quad (6.40)$$

$$\mathbf{u}_i = -k_i^v \dot{\boldsymbol{\alpha}}_i - \sum_{j=1}^n k_{ij} (\boldsymbol{\alpha}_i - \boldsymbol{\alpha}_j(t - \tau_{ij}) - \boldsymbol{\delta}_{ij}), \quad (6.41)$$

where $\boldsymbol{\phi}_i$ is an input vector to be designed latter and the control gains are defined as in Theorem 5.1. Note that the intermediary control structure is similar to (6.2)-(6.3) with (6.24) and the only difference is the design of the input \mathbf{u}_i . In fact, the auxiliary system (6.40) in this scheme describes the translational dynamics of a virtual system, associated to the i^{th} aircraft. The input \mathbf{u}_i is constructed based on the virtual vehicle velocity and position, $\dot{\boldsymbol{\alpha}}_i$ and $\boldsymbol{\alpha}_i$ respectively, to guarantee that all the virtual vehicles converge to the desired formation in the presence of communication delays *i.e.*, $(\boldsymbol{\alpha}_i - \boldsymbol{\alpha}_j) \rightarrow \boldsymbol{\delta}_{ij}$ and $\dot{\boldsymbol{\alpha}}_i \rightarrow 0$. The design of this input is motivated by the following preliminary result proved in Appendix A.5.4.

Lemma 6.1. *Consider n -vehicles modeled as*

$$\ddot{\boldsymbol{\alpha}}_i = -k_i^v \dot{\boldsymbol{\alpha}}_i - \sum_{j=1}^n k_{ij} (\boldsymbol{\alpha}_i - \boldsymbol{\alpha}_j(t - \tau_{ij}) - \boldsymbol{\delta}_{ij}) + \bar{\boldsymbol{\epsilon}}_i, \quad (6.42)$$

for $i \in \mathcal{N}$, where τ_{ij} is a constant communication delay between the i^{th} and j^{th} vehicles satisfying $\tau_{ij} \leq \tau$ for all $(i, j) \in \mathcal{E}$. Let the control gains k_i^v and k_{ij} satisfy condition (6.14), for some $\epsilon > 0$ and assume that the communication graph \mathcal{G} is connected. If the vector $\bar{\boldsymbol{\epsilon}}_i$ is bounded, such that $\|\bar{\boldsymbol{\epsilon}}_i\| \leq \bar{\epsilon}_i^b$, for all $t > 0$ and $i \in \mathcal{N}$, and converges asymptotically to zero, then $(\boldsymbol{\alpha}_i - \boldsymbol{\alpha}_j)$ and $\dot{\boldsymbol{\alpha}}_i$ are bounded and $\dot{\boldsymbol{\alpha}}_i \rightarrow 0$, $(\boldsymbol{\alpha}_i - \boldsymbol{\alpha}_j) \rightarrow \boldsymbol{\delta}_{ij}$, for all $i, j \in \mathcal{N}$.

The above lemma states that if the input $\boldsymbol{\phi}_i$ and the input torque are designed such that $\tilde{\mathbf{q}}_i$ and $\boldsymbol{\phi}_i$ are guaranteed to be bounded and converge asymptotically to zero, the virtual vehicles will converge to the prescribed formation with zero virtual velocity in the presence of communication delays. Therefore, the intermediary control design is reduced to determine an appropriate input $\boldsymbol{\phi}_i$, without linear-velocity measurements, such that each vehicle tracks the states of its corresponding virtual vehicle. To this end, we consider the following partial state feedback input

$$\boldsymbol{\phi}_i = -L_i^p \boldsymbol{\xi}_i - L_i^d (\boldsymbol{\xi}_i - \boldsymbol{\psi}_i), \quad (6.43)$$

$$\dot{\boldsymbol{\psi}}_i = L_i^\psi (\boldsymbol{\xi}_i - \boldsymbol{\psi}_i), \quad (6.44)$$

where L_i^p , L_i^d and L_i^ψ are positive scalar gains, the vector $\boldsymbol{\psi}_i \in \mathbb{R}^3$ is the output of the dynamic system (6.44) that can be initialized arbitrarily, and the error vector $\boldsymbol{\xi}_i$ is defined in (6.25), *i.e.*,

$$\boldsymbol{\xi}_i = \mathbf{p}_i - \boldsymbol{\theta}_i - \boldsymbol{\alpha}_i, \quad \mathbf{z}_i := \dot{\boldsymbol{\xi}}_i. \quad (6.45)$$

To complete the design of the input torque, notice first that the time-derivative of \mathbf{u}_i in (6.41) can be obtained as

$$\begin{aligned} \dot{\mathbf{u}}_i = & -k_i^v \left(\mathbf{u}_i - \boldsymbol{\phi}_i - \frac{2\mathcal{T}_i}{m_i} \mathbf{R}(\mathbf{Q}_i)^T \mathbf{S}(\bar{\mathbf{q}}_i) \tilde{\mathbf{q}}_i \right) \\ & - \sum_{j=1}^n k_{ij} (\dot{\boldsymbol{\alpha}}_i - \dot{\boldsymbol{\alpha}}_j(t - \tau_{ij})), \end{aligned} \quad (6.46)$$

and is function of available signals. Therefore, the desired angular velocity and its time-derivative given in (5.9)-(5.10) with (6.8)-(6.9) are explicitly known. However, to implement the above control scheme, neighboring aircraft must communicate the position and velocity of their corresponding virtual vehicles, *i.e.*, $\boldsymbol{\alpha}_i$ and $\dot{\boldsymbol{\alpha}}_i$. Note also that the perturbation term in the translational dynamics has been compensated in the dynamics of the virtual system (6.40). Therefore, the input torque for each aircraft can be considered similar to the previous section, and the following theorem holds:

Theorem 6.4. *Consider the VTOL-UAVs modeled as in (5.1)-(5.2). Let the thrust input \mathcal{T}_i and the desired attitude \mathbf{Q}_{d_i} be given, respectively, by (4.6) and (4.7), with \mathbf{F}_i given by (6.38)-(6.41) and (6.43)-(6.44). Let the input torque be given by (6.11) with (6.28). Let the controller gains satisfy conditions (6.13) and (6.14) for some $\epsilon > 0$ and $\tau_{ij} \leq \tau$, for all $(i, j) \in \mathcal{E}$, and assume that the communication graph is connected. Then, starting from any initial conditions, the signals \mathbf{v}_i , $(\mathbf{p}_i - \mathbf{p}_j)$ and $\tilde{\boldsymbol{\omega}}_i$ are bounded and $\mathbf{v}_i \rightarrow 0$, $(\mathbf{p}_i - \mathbf{p}_j) \rightarrow \boldsymbol{\delta}_{ij}$, $\tilde{\mathbf{q}}_i \rightarrow 0$ and $\tilde{\boldsymbol{\omega}}_i \rightarrow 0$ for all $i, j \in \mathcal{N}$.*

Sketch of proof: Similar to the proof of Theorem 6.1, the thrust input and desired attitude for each aircraft can be extracted if condition (6.13) is satisfied. The translational error dynamics can be obtained from (6.45) in view of (5.1), (6.39)-(6.40) and (6.43) is obtained as

$$\dot{\mathbf{z}}_i = -L_i^p \boldsymbol{\xi}_i - L_i^d (\boldsymbol{\xi}_i - \boldsymbol{\psi}_i), \quad (6.47)$$

Also, the attitude error dynamics are given similar to the proof of Theorem 6.1 in (6.16). The proof of the theorem consists of first showing that each vehicle converges to its corresponding virtual vehicle and the attitude tracking error converges to zero.

This is achieved using the following Lyapunov function

$$V = V_{t_2} + V_{a_1}, \quad (6.48)$$

where V_{a_1} is given in (6.19) and

$$V_{t_2} = \frac{1}{2} \sum_{i=1}^n \left(\mathbf{z}_i^T \mathbf{z}_i + L_i^p \boldsymbol{\xi}_i^T \boldsymbol{\xi}_i + L_i^d (\boldsymbol{\xi}_i - \boldsymbol{\psi}_i)^T (\boldsymbol{\xi}_i - \boldsymbol{\psi}_i) \right), \quad (6.49)$$

which leads to the negative semi-definite time-derivative

$$\dot{V} = \sum_{i=1}^n \left(-L_i^d L_i^\psi (\boldsymbol{\xi}_i - \boldsymbol{\psi}_i)^T (\boldsymbol{\xi}_i - \boldsymbol{\psi}_i) - k_i^\Omega \boldsymbol{\Omega}_i^T \boldsymbol{\Omega}_i - k_i^q k_i^\beta \tilde{\mathbf{q}}_i^T \tilde{\mathbf{q}}_i \right). \quad (6.50)$$

Following similar steps as in the proof of Theorem 4.2, we show that $\boldsymbol{\xi}_i \rightarrow 0$, $(\boldsymbol{\xi}_i - \boldsymbol{\psi}_i) \rightarrow 0$, $\mathbf{z}_i \rightarrow 0$, $\tilde{\mathbf{q}}_i \rightarrow 0$ and $\tilde{\boldsymbol{\omega}}_i \rightarrow 0$ for $i \in \mathcal{N}$. Then, the dynamics of the virtual system (6.40) with (6.41) can be rewritten as in (6.42) and the conditions of Lemma 6.1 are satisfied. As a result, the states of the virtual systems converge asymptotically to the predefined formation, *i.e.*, $\dot{\boldsymbol{\alpha}}_i \rightarrow 0$ and $(\boldsymbol{\alpha}_i - \boldsymbol{\alpha}_j) \rightarrow \boldsymbol{\delta}_{ij}$, for all $i, j \in \mathcal{N}$. Finally, we show using the results of Lemma 2.6 that $\boldsymbol{\theta}_i \rightarrow 0$ and $\tilde{\boldsymbol{\theta}}_i \rightarrow 0$, leading to the results of the theorem in view of the error definition (6.45). Detailed proof of Theorem 6.4 is given in Appendix A.5.5. □

6.6 Simulation result

In this section, we provide simulation results to demonstrate the effectiveness of the proposed control schemes. We consider a group of four aircraft modeled as in (5.1)-(5.2), with $m_i = 3$ kg, $I_{f_i} = \text{diag}[0.13, 0.13, 0.04]$ kg.m², for $i \in \mathcal{N} := \{1, \dots, 4\}$. The systems initial conditions as well as the desired formation pattern are the same considered in section 5.6. The information flow between aircraft is fixed, undirected and connected and is represented by the undirected graph having the set of edges: $\mathcal{E} = \{(1, 2), (1, 3), (2, 3), (2, 4)\}$, and the adjacency matrix $\mathcal{K} = \text{col}[k_{ij}]$, with $k_{ij} = 0.5$ for $(i, j) \in \mathcal{E}$ and zero otherwise. We assume that the communication between any two neighboring aircraft is delayed by τ_{ij} given in table 6.1. In addition, we consider the saturation function χ given in (2.33) with $\sigma(\cdot) = \tanh(\cdot)$, and the control gains are selected as in table 6.2.

First, we implement the control law in Theorem 6.1, with the control gains satisfying conditions (6.13) and (6.14), with $\tau = 0.3$ sec. The obtained results in this case are shown in Fig.6.1a and Fig.6.1b, which illustrate respectively the aircraft

Table 6.1: Communication delays

	τ_{1i}	τ_{2i}	τ_{3i}	τ_{4i}	$\tilde{\tau}_{1i}$	$\tilde{\tau}_{2i}$	$\tilde{\tau}_{3i}$	$\tilde{\tau}_{4i}$
Theorem 6.1&6.4	0.1	0.15	0.2	0.2				
Theorem 6.2					0.1	0.15	0.2	0.2
Theorem 6.3	0.5	0.8	0.6	0.9				

Table 6.2: Control gains

	k_i^v	k_i^p	k_i^d	k_i^β	k_i^q	k_i^Ω	L_i^p	L_i^d	λ	L_i^ψ
Theorem 6.1	3	1	1	40	40	40				
Theorem 6.2	3	1.5	1.5	50	80	80	1	1		
Theorem 6.3	5	1.5	1.5	50	80	80	1	1	0.25	
Theorem 6.4	2	1.5	1.5	40	80	80	0.5	5		5

positions and linear-velocities. We can see from these figures that our control objective is achieved in the presence of constant communication delays.

The control law in Theorem 6.2 is considered next with the following time-varying communication delays: $\tau_{ij}(t) = \tilde{\tau}_{ij}|\sin(0.5t)|$, with $\tilde{\tau}_{ij}$ given in table 6.1. The auxiliary systems (6.24) are initialized as $\alpha_i(0) = \dot{\alpha}_i(0) = (0, 0, 0)^T$. Fig.6.2a and Fig.6.2b show the obtained results in this case, which are similar to the results in Fig.6.1.

The obtained results when the control scheme in Theorem 6.3 is implemented, where the auxiliary systems (6.24) are initialized as above, are shown in Fig.6.3a and Fig.6.3b. Clearly, the formation control objective is achieved with arbitrary communication delays.

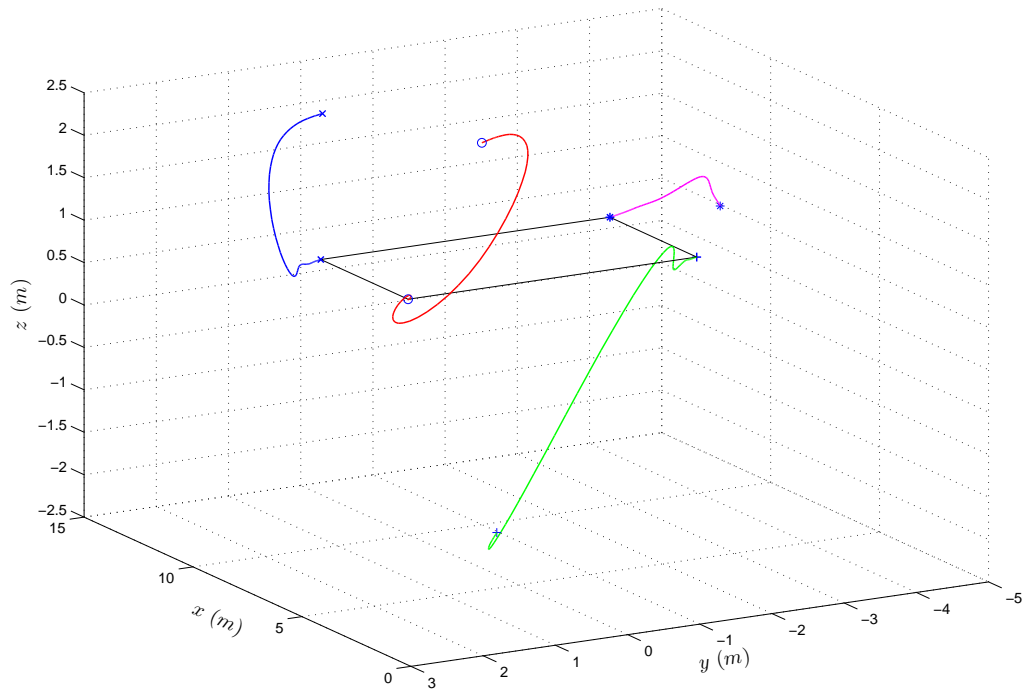
Finally, we consider the linear-velocity free formation control scheme proposed in Theorem 6.4, with the control gains and the communication delays are selected such that conditions (6.13)-(6.14) are satisfied. The auxiliary system (6.40) and (6.44) are initialized as $\psi_i(0) = (0, 1, -1)^T$, $\alpha_i(0) = \mathbf{p}_i(0)$ and $\dot{\alpha}_i(0) = 0$. We show the obtained results in Fig.6.4a and Fig.6.4b which validate the theoretical results proposed in Theorem 6.4.

6.7 Concluding remarks

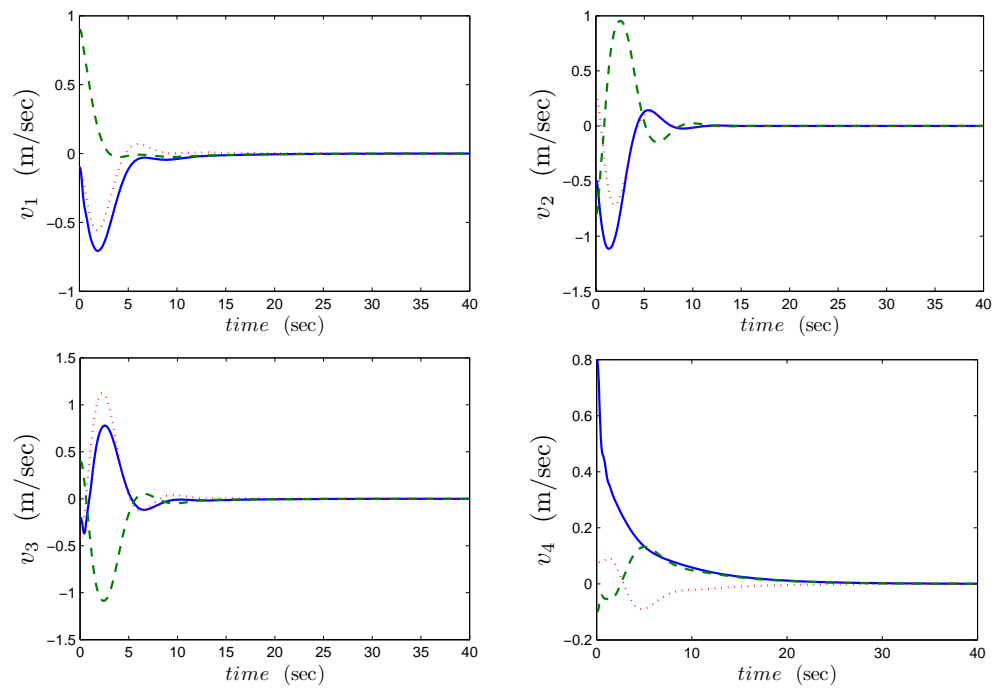
This chapter discussed formation control schemes for a team of VTOL UAVs in the presence of communication delays. The state feedback formation control law in Theorem 5.1 has been applied to the formation stabilization problem, *i.e.*, zero final linear-velocity, with delayed communication and sufficient delay-dependent conditions have been derived guaranteeing the formation objectives. This control scheme

has been modified using a second auxiliary system to handle time-varying communication delays and to achieve the formation control objective with arbitrary constant communication delays. In the output feedback case, some of the auxiliary systems have been attributed the role of virtual vehicles that are designed to achieve the formation requirements. The aircraft translational control objective is then reduced to achieve tracking of the virtual vehicles without linear-velocity measurements.

The auxiliary systems, acting in some situations as virtual systems, have been shown to be crucial in the design of control laws for systems with input constraints under constant and time-varying communication delays. This control approach can be applied to multi-agent systems with double integrator dynamics and constitutes on its own right a new contribution in this research area. The proposed virtual vehicle approach has been considered in Abdessameud and Tayebi (2010*h*) to solve the Rendezvous problem of double-integrators in the presence of delayed communication with input constraints and remove the requirements of velocity measurements.

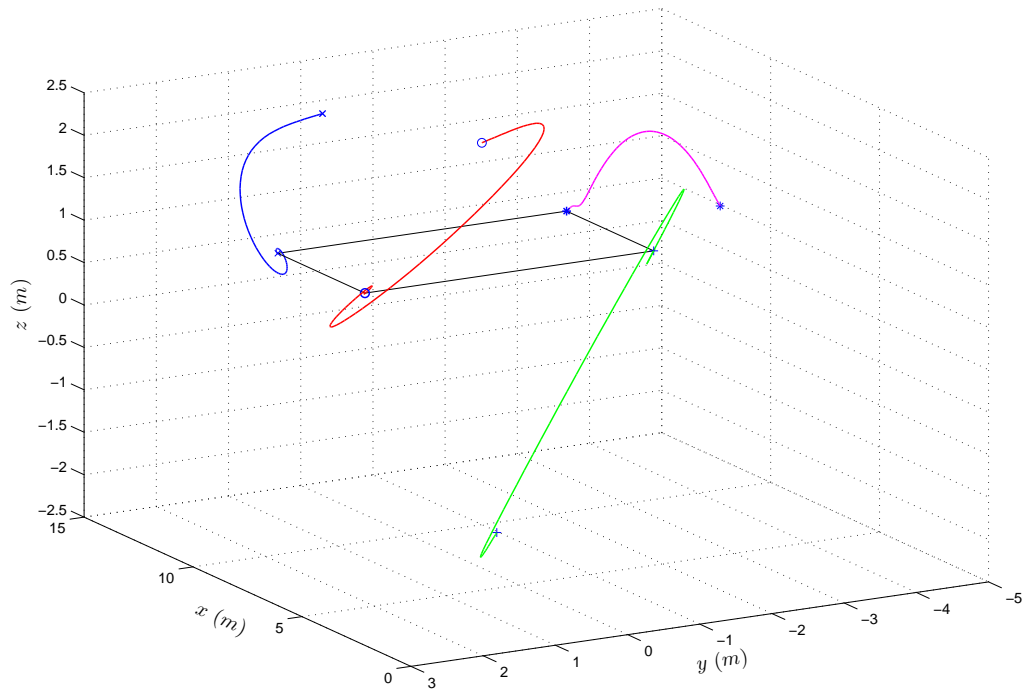


(a)

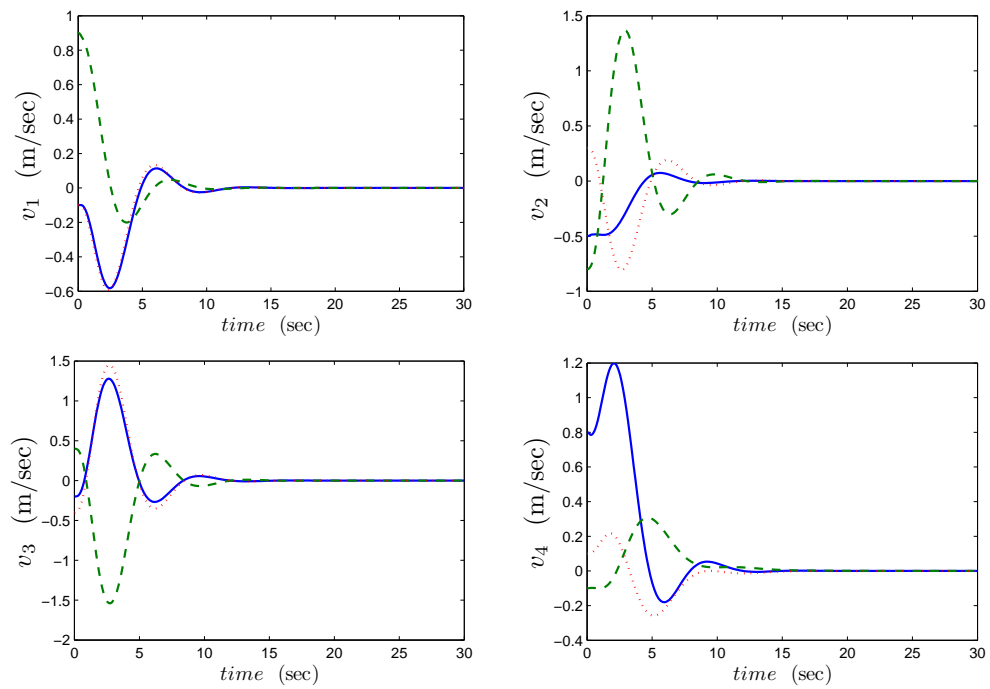


(b)

Figure 6.1: Simulation results in case of Theorem 6.1: (a) Systems trajectories (b) Aircraft linear velocities

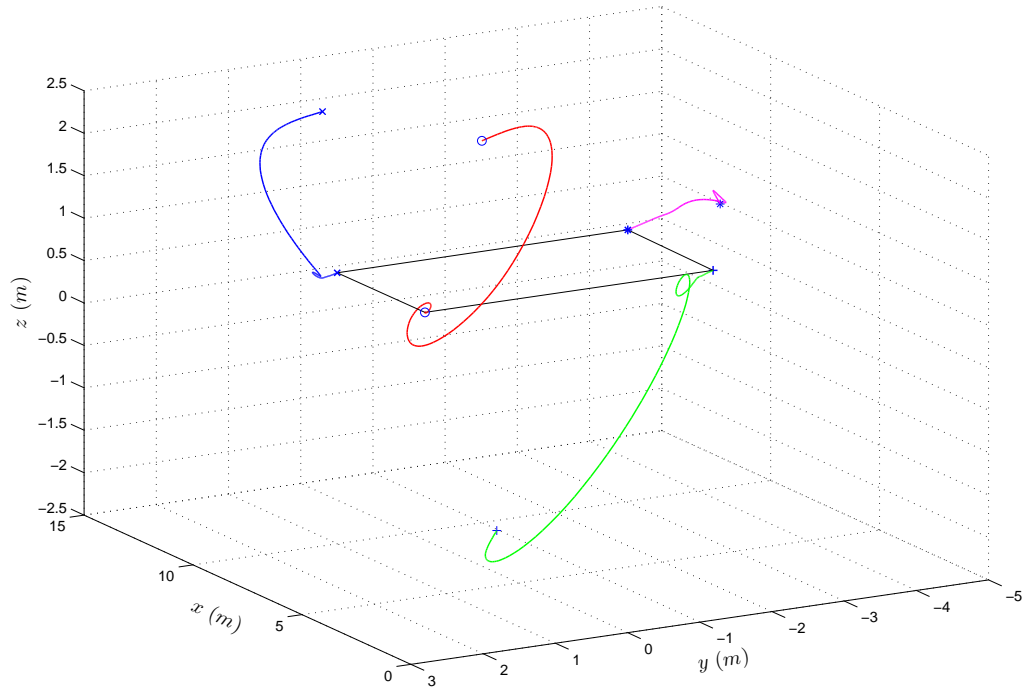


(a)

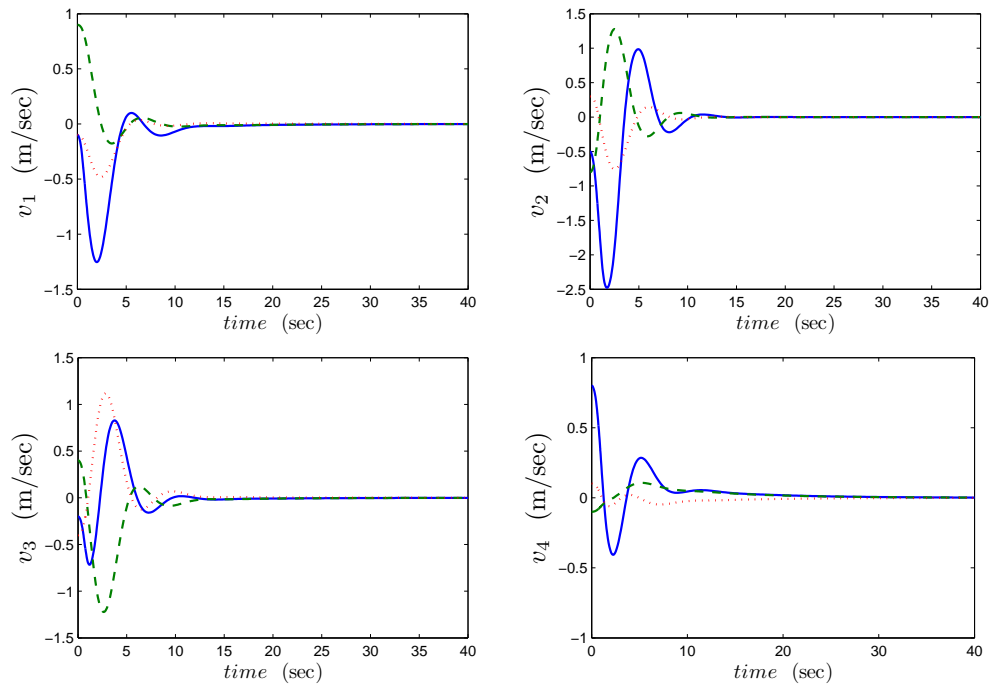


(b)

Figure 6.2: Simulation results in case of Theorem 6.2: (a) Systems trajectories (b) Aircraft linear velocities

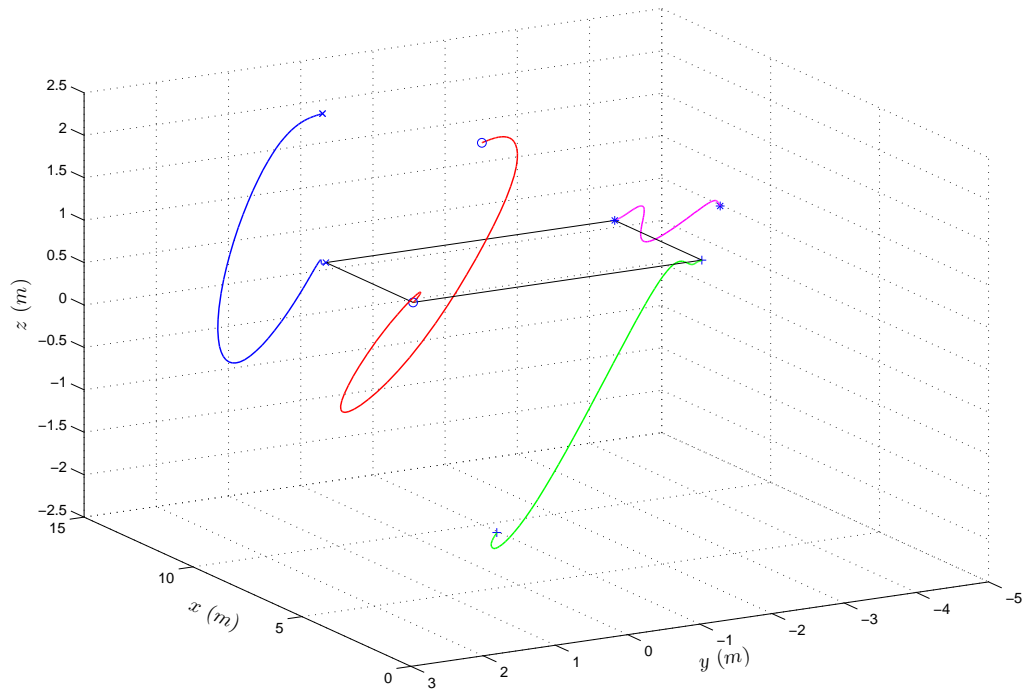


(a)

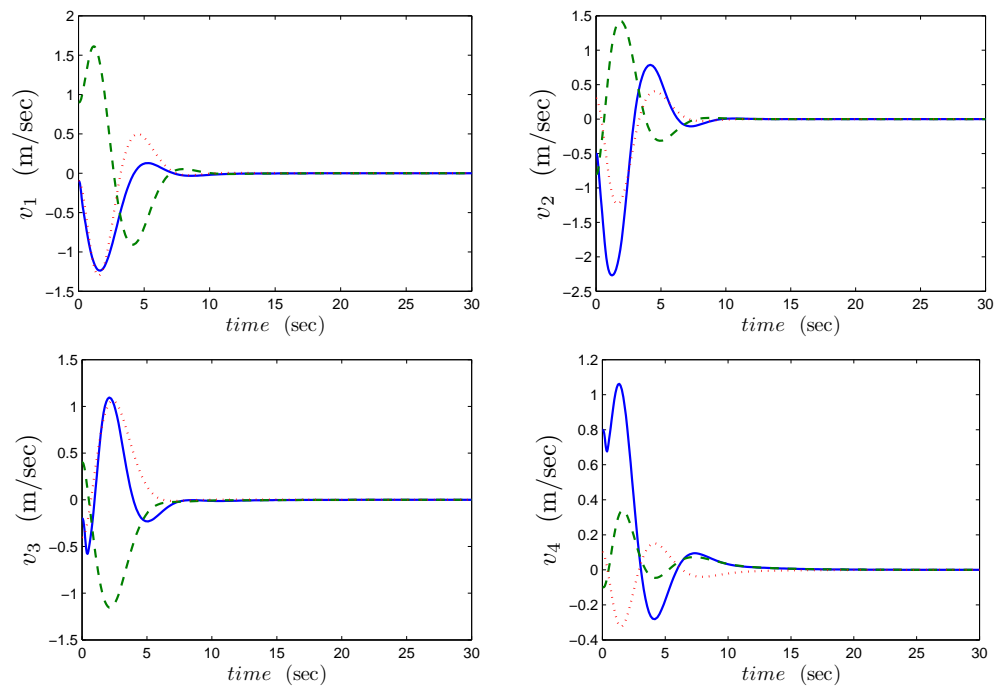


(b)

Figure 6.3: Simulation results in case of Theorem 6.3: (a) Systems trajectories (b) Aircraft linear velocities



(a)



(b)

Figure 6.4: Simulation results in case of Theorem 6.4: (a) Systems trajectories (b) Aircraft linear velocities

Chapter 7

Conclusion

In this thesis, we explored two topics relevant to the coordinated motion control of multiple aerial vehicles. The first is the output feedback attitude synchronization of a group of rigid bodies (or spacecraft in particular), and the second is the position coordination (formation control) in $SE(3)$ of a class of under-actuated VTOL aircraft.

In the framework of attitude synchronization, we proposed two different output feedback control design methods using auxiliary systems allowing to generate the necessary damping in the absence of the actual spacecraft angular velocities and relative angular velocities. The differences between these two methods are given in terms of the concept and the resulted implementation requirements rather than in terms of their performances. Based on these methods, we proposed attitude synchronization schemes without velocity measurements guaranteeing simultaneous group synchronization and trajectory tracking. One limitation of these schemes, which is shared with the existent state-feedback controllers, is that the desired reference trajectory is required for each spacecraft in the team. When the reference trajectory is available to only some spacecraft acting as leaders, and it is not transmitted between spacecraft in the team, the design of a control scheme in this case without angular velocity measurements is still an unsolved problem, for which a leader-follower approach can be used as part of a good research topic. The second control problem considered in this part is to drive all spacecraft to achieve consensus in their final attitudes. We have shown that the spacecraft angular velocities converge to a common bounded time-varying function. The prediction of this final angular velocity, and ideally the final attitude, is an important and challenging topic that is worth consideration in a future work. The main features of the proposed output feedback attitude alignment schemes, which differentiate them from existent output-feedback solutions in the literature, is that they can handle time-varying trajectories and achieve almost global asymptotic stability results.

To design control laws for the class of under-actuated VTOL aircraft, a new design methodology has been developed based on the unit-quaternion representation and a singularity-free attitude extraction algorithm (presented in section 4.3). Based on this design method, solutions to the state and output feedback trajectory tracking and formation control problems of VTOL aircraft have been proposed. Also, control schemes achieving the same results in the presence of constant and time-varying communication delays have been studied in the full and partial state information cases. To deal with the constraints in the aircraft inputs, we have adopted a new

control structure based on auxiliary systems. To the best of the author's knowledge, this work can be considered as the first dealing with the control of VTOL UAVs in the cases described above.

The effectiveness of the proposed control schemes have been demonstrated through simulation results. It should be mentioned that these simulations are illustrative and the control parameters are not necessarily optimal in the sense of performance, energy consumption or transient behavior.

In all the presented coordinated control schemes in this thesis, we have assumed that the communication flow between members of the team is fixed and undirected. In practice, the communication between vehicles can be constrained to be directed, and might be subject to uncertainties or corruption due to environmental conditions. The extension of the proposed control schemes to directed communication topologies, which is possibly time varying/switching, is an important future research topic. Furthermore, although thoroughly discussed in the case of VTOL UAVs, the communication time delay is still a challenging problem in the attitude synchronization of spacecraft formations due to the nonlinear expression of the relative attitude error resulting from the use of the unit-quaternion multiplication. A possible solution to this problem might be to consider the MRP representation of the attitude, which defines the relative attitudes using linear differences.

There are still several issues related to the control of the class of under-actuated VTOL aircraft, and the proposed solutions in this work constitute a good platform for several future extensions. One of the challenging problems in this area is to consider the coupling between the translational and rotational dynamics. This coupling exists in some types of aircraft where the vectored thrust produces a moment in addition to a translational force. This coupling is usually expressed by the aircraft torque input that affects the linear acceleration of the system and is discussed by some authors such as Hauser *et al.* (1992); Olfati-Saber (2002) and Pflimlin *et al.* (2007). This issue is still an open problem for the class of under-actuated systems considered here since no complete solution has been reported in the literature. Another problem that is of a particular importance in flying robots is to consider the external disturbances such as the effects of wind gusts. In this context, the authors in Roberts and Tayebi (2009) proposed an adaptive trajectory tracking control scheme for a single VTOL UAV in the presence of constant unknown disturbances. The application of this work to the formation control problem is not straightforward due to the requirement of the second derivative of the intermediary control law in the input torque design. Another problem is related to the attitude measurements, since the absolute attitude is assumed to be precisely known in the proposed solutions. In general, the attitude of a rigid body is obtained via an estimation algorithm relying on inertial vector measurements provided by an inertial measurement unit (IMU) equipped with accelerometers, magnetometers and gyroscopes. Therefore, a research topic in perspective is to directly incorporate the actual vector measurements in the design of motion coordination schemes (see for instance Tayebi *et al.* (2010)).

Furthermore, a practical problem in multi-vehicles motion coordination, which is not discussed in this work, is the collision avoidance between members of the team, and/or the environment, while converging to the desired final configuration. This problem is generally solved using potential functions that grow unbounded if two vehicles (or more) enter a predefined collision region or are near an obstacle. The main difficulty in the application of this technique, in our case, is that the intermediary control input needs to be a priori bounded and satisfy the requirements of the attitude extraction algorithm condition. The collision problem is not an issue in the attitude synchronization of spacecraft formations since no translational motion is assigned to spacecraft and it is assumed that spacecraft are far enough from each other so that they do not collide due to rotation manoeuvres.

Bibliography

- Abdessameud, A. and Tayebi, A. (2008a). Attitude synchronization of a spacecraft formation without velocity measurement. In *Proceedings of the 47th IEEE Conference on Decision and Control*, 3719–3724.
- Abdessameud, A. and Tayebi, A. (2008b). Decentralized attitude alignment control of spacecraft within a formation without angular velocity measurements. In *Proceedings of the 17th IFAC World Congress*, 1766–1771.
- Abdessameud, A. and Tayebi, A. (2009a). Attitude synchronization of a group of spacecraft without velocity measurements. *IEEE Transactions on Automatic Control*, 54(11), 2642–2648.
- Abdessameud, A. and Tayebi, A. (2009b). On the coordinated attitude alignment of a group of spacecraft without velocity measurements. In *Proceedings of the 48th IEEE Conference on Decision and Control*, 1476–1481.
- Abdessameud, A. and Tayebi, A. (2009c). Formation control of VTOL UAVs. In *Proceedings of the 48th Conference on Decision and Control*, 3454–3459.
- Abdessameud, A. and Tayebi, A. (2010a). Global trajectory tracking control of VTOL-UAVs without linear velocity measurements. *Automatica*, 46(6), 1053–1059.
- Abdessameud, A. and Tayebi, A. (2010b). Formation control of VTOL UAVs without linear-velocity measurements. In *Proceedings of the American Control Conference*, 2107–2112.
- Abdessameud, A. and Tayebi, A. (2010c). Motion coordination of a group of vertical take-off and landing aircraft. (Submitted).
- Abdessameud, A. and Tayebi, A. (2010d). On consensus algorithms for double-integrator dynamics without velocity measurements and with input constraints. *Systems and Control Letters*, 59, 812–821.
- Abdessameud, A. and Tayebi, A. (2010e). Velocity-free consensus algorithms for double-integrator dynamics with input saturations constraints. In *Proceedings of the 49th Conference on Decision and Control (to appear)*.
- Abdessameud, A. and Tayebi, A. (2010f). Formation control of VTOL unmanned aerial vehicles with communication delays. (Submitted).

- Abdessameud, A. and Tayebi, A. (2010g). Formation stabilization of VTOL UAVs subject to communication delays. In *Proceedings of the 49th Conference on Decision and Control (to appear)*.
- Abdessameud, A. and Tayebi, A. (2010h). Consensus of double-integrator multi-agents under communication delays—The partial state feedback case. Submitted to *The American Control conference, 2011*.
- Aguiar, A.P. and Hespanha, J.P. (2007). Trajectory-tracking and path-following of underactuated autonomous vehicles with parametric modeling uncertainty. *IEEE Transactions on Automatic Control*, 52(8), 1362–1379.
- Akella, M.R. (2001). Rigid body attitude tracking without angular velocity feedback. *Systems and Control Letters*, 42(4), 321–326.
- Anderson, B., Fidan, B., Yu, C., and Walle, D. (2008). UAV formation control: Theory and application. *Recent Advances in Learning and Control*, 15–33.
- Antonelli, G. and Chiaverini, S. (2006). Kinematic control of platoons of autonomous vehicles. *IEEE Transactions on Robotics*, 22(6), 1285–1292.
- Arcak, M. (2007). Passivity as a design tool for group coordination. *IEEE Transactions on Automatic Control*, 52(8), 1380–1390.
- Arrichiello, F., Chiaverini, S., and Fossen, T.I. (2006). Formation control of underactuated surface vessels using the null-space-based behavioral control. In *Proceedings of the International Conference on Intelligent Robots and Systems*.
- Bai, H., Arcak, M., and Wen, J. (2008). Rigid body attitude coordination without inertial frame information. *Automatica*, 44(12), 3170–3175.
- Balch, T. and Arkin, R.C. (1998). Behavior-based formation control for multirobot teams. *IEEE Transactions on Robotics and Automation*, 14, 926–939.
- Beard, R.W., Lawton, J., and Hadaegh, F.Y. (2001). A coordination architecture for spacecraft formation control. *IEEE Transactions on Control Systems Technology*, 9(6), 777–790.
- Beard, R.W., McLain, T.W., Goodrich, M., and Anderson, E.P. (2002). Coordinated target assignment and intercept for unmanned air vehicles. *IEEE Transactions on Robotics and Automation*, 18(6), 911–922.
- Beard, R. and Hadaegh, F. (1998). Constellation templates: an approach to autonomous formation flying. In *World Automation Congress*, 1771–1776.

- Benzemrane, K., Santosuosso, G., and Damm, G. (2007). Unmanned aerial vehicle speed estimation via nonlinear adaptive observers. In *Proceedings of the American Control Conference*, 985–990.
- Berghuis, H. and Nijmeijer, H. (1993a). A passivity approach to controller-observer design for robots. *IEEE Transactions on Robotics and Automation*, 9(6), 740–754.
- Berghuis, H. and Nijmeijer, H. (1993b). Global regulation of robots using only position measurements. *Systems and Control Letters*, 21(4), 289–293.
- Bhat, S.P. and Bernstein, D.S. (2000). Topological obstruction to continuous global stabilization of rotational motion and the unwinding phenomenon. *Systems and Control Letters*, 39(1), 63–70.
- Bondhus, A.K., Pettersen, K.Y., and Nijmeijer, H. (2005). Master-slave synchronization of robot manipulators: Experimental results. In *Proceedings of the 16th IFAC World Congress*.
- Caccavale, F., Chiacchio, P., and Chiaverini, S. (1998). A quaternion-based regulator for cooperative manipulators. In *Proceedings of the IEEE International Conference on Control Applications*, 557–561.
- Caccavale, F. and Villani, L. (1999). Output feedback control for attitude tracking. *Systems and Control Letters*, 38(2), 91–98.
- Chevron, T., Hamel, T., Mahony, R., and Baldwin, G. (2007). Robust nonlinear fusion of inertial and visual data for position, velocity and attitude estimation of UAV. In *Proceedings of the IEEE International Conference on Robotics and Automation*, 2010–2016.
- Chopra, N. and Spong, M. (2006). Passivity-based control of multi-agent systems. *Advances in Robot Control: From Everyday Physics to Human-Like Movements*, 107–134.
- Chopra, N., Spong, M., and Lozano, R. (2008). Synchronization of bilateral teleoperators with time delay. *Automatica*, 44(8), 2142–2148.
- Chung, S.J., Ahsun, U., and Slotine, J.J.E. (2009). Application of synchronization to formation flying spacecraft: Lagrangian approach. *Journal of Guidance, Control and Dynamics*, 32(2), 512–526.
- Costic, B.T., Dawson, D.M., Queiroz, M.S.d., and Kapila, V. (2001). A quaternion-based adaptive attitude tracking controller without velocity measurements. *AIAA Journal of Guidance, Control and Dynamics*, 24(6).
- Cullen, J.M., Shaw, E., and Baldwin, H.A. (1965). Methods for measuring the three-dimensional structure of fish schools. *Animal Behavior*, 13, 534–543.

- Desai, J. (2002). A graph theoretic approach for modeling mobile robot team formations. *Journal of Robotic Systems*, 19(11), 511–525.
- Dimarogonas, D., Tsiotras, P., and Kyriakopoulos, K. (2009). Leader-follower cooperative attitude control of multiple rigid bodies. *Systems and Control Letters*, 58(6), 429–435.
- Do, K.D., Jiang, Z.P., and Pan, J. (2003). On global tracking control of a VTOL aircraft without velocity measurements. *IEEE Transactions on Automatic Control*, 48(12), 2212–2217.
- Egerstedt, M., Hu, X., and Stotsky, A. (2001). Control of mobile platforms using a virtual vehicle approach. *IEEE Transactions on Automatic Control*, 46(11), 1777–1782.
- Eklund, J.M., Sprinkle, J., and Sastry, S. (2005). Implementing and testing a nonlinear model predictive tracking controller for aerial pursuit/evasion games on a fixed wing aircraft. In *Proceedings of the American Control Conference*, 1509–1514.
- Fahimi, F. (2008). Full formation control for autonomous helicopter groups. *Robotica*, 26(02), 143–156.
- Fax, J.A. and Murray, R.M. (2004). Information flow and cooperative control of vehicle formations. *IEEE Transactions on Automatic Control*, 49(9), 1465–1476.
- Fragopoulos, D. and Innocenti, M. (2004). Stability considerations in quaternion attitude control using discontinuous lyapunov functions. *IEE Proceedings Control Theory and Applications*, 151(3), 253–258.
- Frazzoli, E., Dahleh, M.A., and Feron, E. (2000). Trajectory tracking control design for autonomous helicopters using a backstepping algorithm. In *Proceedings of the of the American Control Conference*, 4102–4107.
- Freund, E. and Rossmann, J. (2003). The basic ideas of a proven dynamic collision avoidance approach for multi-robot manipulator systems. In *Proceedings of the International Conference on Intelligent Robots and Systems*.
- Giulietti, F., Pollini, L., and Innocenti, M. (2000). Autonomous formation flight. *IEEE Control Systems Magazine*, 20(66), 34–44.
- Grøtli, E.I. and Gravdahl, J.T. (2008). Output attitude tracking of a formation of spacecraft. In *Proceedings of the 17th IFAC World Congress*, 2137–2143.
- Gu, Y., Seanor, B., Campa, G., Napolitano, M.R., Rowe, L., Gururajan, S., and Wan, S. (2006). Design and flight testing evaluation of formation control laws. *IEEE Transactions on Control Systems Technology*, 14(6), 1105–1112.

- Hadaegh, F.Y., Lu, W.M., and Wang, P.K.C. (1998). Adaptive control of formation flying spacecraft for interferometry. In *IFAC Conference on Large Scale Systems*, 97–102.
- Hamel, T., Mahony, R., Lozano, R., and Ostrowski, J. (2002). Dynamic modelling and configuration stabilization for an x4-flyer. In *Proceedings of the 15th IFAC World Congress*.
- Hauser, J., Sastry, S., and Meyer, G. (1992). Nonlinear control design for slightly non-minimum phase systems: Applications to V/Stol aircraft. *Automatica*, 28(4), 665–679.
- Hong-Yong, Y., Xun-Lin, Z., and Si-Ying, Z. (2010). Consensus of second-order delayed multi-agent systems with leader-following. *European Journal of Control*, 15, 1–12.
- Hu, X., Alarcón, D.F., and Gustavi, T. (2003). Sensor-based navigation coordination for mobile robots. In *Proceedings of the 42nd IEEE Conference on Decision and Control*, 6375–6380.
- Hua, M., Hamel, T., Morin, P., and Samson, C. (2009). A control approach for thrust-propelled underactuated vehicles and its application to VTOL drones. *IEEE Transactions on Automatic Control*, 54(8), 1837–1853.
- Ihle, I.A.F., Jouffroy, J., and Fossen, T.I. (2004). Nonlinear formation control of marine craft with experimental results. In *Proceedings of the IEEE Conference on Decision and Control*.
- Ihle, I.A.F., Jouffroy, J., and Fossen, T.I. (2005). Formation control of marine surface craft using lagrange multipliers. In *Proceedings of the joint 44th IEEE Conference on Decision and Control, and the European Control Conference*.
- Jadbabaie, A., Lin, J., and Morse, A.S. (2003). Coordination of groups of mobile autonomous agents using nearest neighbour rules. *IEEE Transactions on Automatic Control*, 48(6), 988–1001.
- Jungnickel, D. (2005). *Graphs, networks and algorithms*, volume 5. Springer: Berlin.
- Kaminer, I., Pascoal, A., Hallberg, E., and Silvestre, C. (1998). Trajectory tracking for autonomous vehicles: An integrated approach to guidance and control. *Journal of Guidance, Control, and Dynamics*, 21(1), 29–38.
- Kang, W. and Yeh, H. (2002). Co-ordinated attitude control of multi-satellite systems. *International Journal of Robust and Nonlinear Control*, 12(2-3), 185–205.

- Kendoul, F., Lara, D., Fantoni, I., and Lozano, R. (2006). Nonlinear control for systems with bounded inputs: Real-time embedded control applied to UAVs. In *Proceedings of the 45th IEEE Conference on Decision and Control*, 5888–5893.
- Khalil, H. (2002). *Nonlinear systems*. Prentice hall, third edition edition.
- Khatib, O. (1986). Real-time obstacle avoidance for manipulators and mobile robots. *International Journal on Robotic Research*, 5(1), 90–99.
- Koo, T. and Sastry, S. (1998). Output tracking control design of a helicopter model based on approximate linearization. In *Proceedings of the 37th Conference on Decision and Control*, 3635–3640.
- Krishna, K.M. and Hexmoor, H. (2004). Reactive collision avoidance of multiple moving agents by cooperation and conflict propagation. In *Proceedings of the IEEE International Conference on Robotics and Automation*.
- Kristiansen, R., Loría, A., Chaillet, A., and Nicklasson, P. (2009). Spacecraft relative rotation tracking without angular velocity measurements. *Automatica*, 45(3), 750–756.
- Kyrkjebø, E., Panteley, E., Chaillet, A., and Pettersen, K.Y. (2006). Virtual vehicle approach to underway replenishment. *Group Coordination and Cooperative Control (K. Y. Pettersen, J. T. Gravdahl and H. Nijmeijer, Eds.)*. Vol. 336 of *Lecture Notes in Control and Information Sciences*. Springer Verlag., 171–189.
- Lawton, J. and Beard, R.W. (2000). Elementary attitude formation maneuver via leader-following and behaviour-based control. In *Proceedings of the AIAA Guidance, Navigation and Control Conference*.
- Lawton, J., Young, B.J., and Beard, R.W. (2000). A decentralized approach to elementary formation maneuvers. In *Proceedings of the IEEE International Conference on Robotics and Automation*, 2728–2733.
- Lawton, J. and Beard, R.W. (2002). Synchronized multiple spacecraft rotations. *Automatica*, 38(8), 1359–1364.
- Lawton, J., Beard, R.W., and Young, B. (2003). A decentralized approach to formation maneuvers. *IEEE Transactions on Robotics and Automation*, 19(6), 933–941.
- Lee, D. and Spong, M. (2006). Agreement with non-uniform information delays. In *Proceedings of the American Control Conference*, 756–761.
- Lee, D. and Spong, M.W. (2007). Stable flocking of multiple inertial agents on balanced graphs. *IEEE Transactions on Automatic Control*, 52(8), 1469–1475.

- Lewis, M. and Tan, K. (1997). High precision formation control of mobile robots using virtual structures. *Autonomous Robots*, 4(1), 387–403.
- Lindensmith, C. (2003). Technology plan for the Terrestrial Planet Finder. *JPL Publication*, 03–007.
- Lissaman, P.B.S. and Shollenberger, C.A. (1970). Formation flight of birds. *Science*, 168, 1003–1005.
- Lizarralde, F., Wen, J.T., and Hsu, L. (1995). Quaternion-based coordinated control of a subsea mobile manipulator with only position measurements. In *Proceedings of the 42nd IEEE Conference on Decision and Control*.
- Lizarralde, F. and Wen, J.T. (1996). Attitude control without angular velocity measurement: A passivity approach. *IEEE Transactions on Automatic Control*, 41(3), 468–472.
- Madani, T. and Benallegue, A. (2007). Backstepping control with exact 2-sliding mode estimation for a quadrotor unmanned aerial vehicle. In *Proceedings of the 2007 IEEE/RSJ international conference on intelligent robots and systems*, 141–146.
- May, R.M. (1979). Flight formations in geese and other birds. *Nature*, 282, 778–780.
- Meng, Z., Yu, W., and Ren, W. (2010). Discussion on: “Consensus of second-order delayed multi-agent systems with leader-following”. *European Journal of Control*, 2, 200–205.
- Mesbahi, M. and Hadaegh, F.Y. (2001). Formation flying of multiple spacecraft via graphs, matrix inequalities, and switching. *AIAA Journal of Guidance, Control, and Dynamics*, 24(2), 369–377.
- Moshtagh, N. and Jadbabaie, A. (2007). Distributed geodesic control laws for flocking of nonholonomic agents. *IEEE Transactions on Automatic Control*, 52(4), 681–686.
- Münz, U., Papachristodoulou, A., and Allgöwer, F. (2008). Delay-dependent rendezvous and flocking of large scale multi-agent systems with communication delays. In *Proceedings of the 47th Conference on Decision and Control*, 2038–2043.
- Münz, U., Papachristodoulou, A., and Allgöwer, F. (2010). Delay robustness in consensus problems. *Automatica*, 46(8), 1252–1265.
- Nuño, E., Ortega, R., and Basañez, L. (2010). An adaptive controller for nonlinear teleoperators. *Automatica*, 46(1), 155–159.

- Ögren, P., Fiorelli, E., and Leonard, N.E. (2004). Cooperative control of mobile sensor networks: Adaptive gradient climbing in a distributed environment. *IEEE Transactions on Automatic Control*, 49(8), 1292–1302.
- Olfati-Saber, R. (2002). Global configuration stabilization for the VTOL aircraft with strong input coupling. *IEEE Transactions on Automatic Control*, 47(11), 1949–1952.
- Olfati-Saber, R. and Murray, R. (2004). Consensus problems in networks of agents with switching topology and time-delays. *IEEE Transactions on Automatic Control*, 49(9), 1520–1533.
- Olfati-Saber, R. (2006). Flocking for multi-agent dynamic systems: Algorithms and theory. *IEEE Transactions on Automatic Control*, 51(3), 401–420.
- Olfati-Saber, R., Fax, J.A., and Murray, R.M. (2007). Consensus and cooperation in networked multi-agent systems. *Proceedings of the IEEE*, 95(1), 215–233.
- Pfifflin, J.M., Soures, P., and Hamel, T. (2007). Position control of a ducted fan VTOL UAV in crosswind. *International Journal of Control*, 80(5), 666–683.
- Polushin, I., Tayebi, A., and Marquez, H. (2006). Control schemes for stable teleoperation with communication delay based on IOS small gain theorem. *Automatica*, 42(6), 905–915.
- Ren, W. and Beard, R.W. (2002). Virtual structure based spacecraft formation control with formation feedback. In *AIAA Guidance, Navigation, and Control Conference*, 2002–4963.
- Ren, W. (2004). Consensus seeking, formation keeping, and trajectory tracking in multiple vehicle cooperative control. PhD thesis. Brigham Young University.
- Ren, W. and Beard, R.W. (2004). Decentralized scheme for spacecraft formation flying via the virtual structure approach. *AIAA Journal of Guidance, Control, and Dynamics*, 27(1), 73–82.
- Ren, W. (2007a). Distributed attitude alignment in spacecraft formation flying. *International journal of adaptive control and signal processing*, 21, 95–113.
- Ren, W. (2007b). Formation keeping and attitude alignment for spacecraft through local interactions. *Journal of Guidance, Control, and Dynamics*, 30(2), 633–638.
- Ren, W., Beard, R.W., and Atkins, E.M. (2007). Information consensus in multivehicle cooperative control: Collective group behavior through local interaction. *IEEE Control Systems Magazine*, 27(2), 71–82.

- Ren, W. (2008). On consensus algorithms for double-integrator dynamics. *IEEE Transactions on Automatic Control*, 53(6), 1503–1509.
- Ren, W. (2009). Distributed leaderless consensus algorithms for networked Euler–Lagrange systems. *International Journal of Control*, 82(11), 2137–2149.
- Roberts, A. and Tayebi, A. (2009). Adaptive position tracking of VTOL-UAVs. In *Proceedings of the 48th IEEE Conference on Decision and Control*, 5233–5238.
- Rodriguez-Angeles, A. and Nijmeijer, H. (2004). Mutual synchronization of robots via estimated state feedback: A cooperative approach. *IEEE Transactions on Control Systems Technology*, 12(4), 542–554.
- Rondon, E., Salazar, S., Escareno, J., and Lozano, R. (2009). Vision-based position control of a two-rotor VTOL miniUAV. *IEEE Transactions on Automatic Control*, 57, 49–64.
- Saffarian, M. and Fahimi, F. (2009). Non-Iterative nonlinear model predictive approach applied to the control of helicopters’ group formation. *Robotics and Autonomous Systems*, 57(6-7), 749–757.
- Salcudean, S. (1991). A globally convergent angular velocity observer for rigid body motion. *IEEE Transactions on Automatic Control*, 36(12), 1493–1497.
- Scharf, D.P., Hadeagh, F.Y., and Ploen, S.R. (2004). A survey of spacecraft formation flying guidance and control (part II): control. In *Proceeding of the 2004 American Control Conference*, 2976–2985.
- Seiler, P., Pant, A., and Hedrick, J.K. (2004). String instabilities in formation flight: Limitations due to integral constraints. *Journal of Dynamic Systems, Measurement, and Control*, 126(4), 873–879.
- Seuret, A., Dimarogonas, D., and Johansson, K. (2009). Consensus of double integrator multi-agents under communication delay. In *The 8th IFAC Workshop on Time Delay Systems*.
- Shuster, M.D. (1993). A survey of attitude representations. *Journal of Astronautical Sciences*, 41(4), 435–517.
- Singla, P., Subbarao, K., and Junkins, J.L. (2006). Adaptive output feedback control for spacecraft rendezvous and docking under measurement uncertainty. *Journal of Guidance, Control, and Dynamics*, 29(4), 892–902.
- Slotine, J. and Li, W. (1991). *Applied nonlinear control*. Prentice Hall. New Jersey, US.

- Spears, W.M., Spears, D.F., and Heil, R. (2004). A formal analysis of potential energy in a multi-agent system. *Formal approaches to agent-based systems. Lecture Notes in computer science*, 131–145.
- Stilwell, D.J. and Bishop, B.E. (2000). Platoons of underwater vehicles; communication, feedback and decentralized control. *IEEE Control Systems Magazine*, 20(6), 45–52.
- Sugar, T. and Kumar, V. (1998). Decentralized control of cooperating mobile manipulators. In *Proceedings of the IEEE International Conference on Robotics and Automation*.
- Sun, Y. and Wang, L. (2009). Consensus of multi-agent systems in directed networks with nonuniform time-varying delays. *IEEE Transactions on Automatic Control*, 54(7), 1607–1613.
- Tafazoli, S. (2009). A study of on-orbit spacecraft failures. *Acta Astronautica*, 64(2-3), 195–205.
- Tanner, H.G., Jadbabaie, A., and Pappas, G.J. (2003). Coordination of multiple autonomous vehicles. In *Proceedings of the IEEE Mediterranean Conference on Control and Automation*.
- Tanner, H.G., Jadbabaie, A., and Pappas, G.J. (2007). Flocking in fixed and switching networks. *IEEE Transactions on Automatic Control*, 52(5), 863–868.
- Tayebi, A. and McGilvray, S. (2006). Attitude stabilization of a quadrotor aircraft. *IEEE Transactions on Control Systems Technology*, 14, 562–571.
- Tayebi, A. (2008). Unit-quaternion based output feedback for the attitude tracking problem. *IEEE Transactions on Automatic Control*, 53(6), 1516–1520.
- Tayebi, A., Roberts, A., and Benallegue, A. (2010). Inertial measurements based dynamic attitude estimation and velocity-free attitude stabilization. Submitted to *The American Control conference, 2011*.
- Tsiotras, P. (1998). Further results on the attitude control problem. *IEEE Transactions on Automatic Control*, 34(11), 1597–1600.
- Vandyke, M.C. and Hall, C.D. (2006). Decentralized coordinated attitude control within a formation of spacecraft. *Journal of Guidance, Control and Dynamics*, 29(5), 1101–1109.
- Wang, P. and Hadaegh, F. (1996). Coordination and control of multiple microspacecraft moving in formation. *The Journal of the Astronautical Sciences*, 44, 315–355.

-
- Wang, P., Hadaegh, F., and Lau, K. (1999). Synchronized formation rotation and attitude control of multiple free-flying spacecraft. *Journal of Guidance, Control, and Dynamics*, 22, 28–35.
- Wang, W. and Slotine, J. (2006). Contraction analysis of time-delayed communications and group cooperation. *IEEE Transactions on Automatic Control*, 51(4), 712–717.
- Wen, J.T.Y. and Kreutz-Delgado, K. (1991). The attitude control problem. *IEEE Transactions on Automatic Control*, 36, 1148–1162.
- Wiehs, D. (1973). Hydromechanics of fish schooling. *Nature*, 241, 290–291.
- Yamaguchi, H. (1999). A cooperative hunting behavior by mobile-robot troops. *The International Journal of Robotics Research*, 18(9), 931–940.
- Young, B., Beard, R.W., and Kelsey, J. (2001). A control scheme for improving multi-vehicle formation maneuvers. In *Proceedings of the American Control Conference*, 704–709.
- Yun, X., Alptekin, G., and Albayrak, O. (1997). Line and circle formation of distributed physical mobile robots. *Journal of Robotic Systems*, 14(2), 63–76.

Appendix A

Detailed proofs

A.1 Preliminaries

A.1.1 Proof of Lemma 2.4

First, from (2.13) and (2.20), we can write

$$\begin{aligned}\mathbf{Q}_{ij} &= \mathbf{Q}_j^{-1} \odot \mathbf{Q}_d \odot \mathbf{Q}_d^{-1} \odot \mathbf{Q}_i \\ &= \tilde{\mathbf{Q}}_j^{-1} \odot \tilde{\mathbf{Q}}_i.\end{aligned}\tag{A.1}$$

Then, using the definition of the quaternion multiplication (2.7), equation (2.30) can be rewritten as

$$k_i^p \tilde{\mathbf{q}}_i + \sum_{j=1}^n k_{ij}^p (\tilde{\eta}_j \tilde{\mathbf{q}}_i - \tilde{\eta}_i \tilde{\mathbf{q}}_j - \mathbf{S}(\tilde{\mathbf{q}}_j) \tilde{\mathbf{q}}_i) = 0,\tag{A.2}$$

for $i \in \mathcal{N}$, which is equivalent to

$$\left(k_i^p + \sum_{j=1}^n k_{ij}^p \tilde{\eta}_j \right) \tilde{\mathbf{q}}_i - \tilde{\eta}_i \sum_{j=1}^n k_{ij}^p \tilde{\mathbf{q}}_j = -\mathbf{S}(\tilde{\mathbf{q}}_i) \sum_{j=1}^n k_{ij}^p \tilde{\mathbf{q}}_j,\tag{A.3}$$

for $i \in \mathcal{N}$. Following Lawton and Beard (2002) and Ren (2007a), multiplying both sides of (A.3) by the vector: $\left(\mathbf{S}(\tilde{\mathbf{q}}_i) \sum_{j=1}^n k_{ij}^p \tilde{\mathbf{q}}_j \right)^T$, leads to

$$\|\mathbf{S}(\tilde{\mathbf{q}}_i) \sum_{j=1}^n k_{ij}^p \tilde{\mathbf{q}}_j\|^2 = 0,\tag{A.4}$$

from which equation (A.3) is equivalent to

$$\left(k_i^p + \sum_{j=1}^n k_{ij}^p \tilde{\eta}_j \right) \tilde{\mathbf{q}}_i - \sum_{j=1}^n k_{ij}^p \tilde{\eta}_i \tilde{\mathbf{q}}_j = 0,\tag{A.5}$$

for $i \in \mathcal{N}$. This last set of equations can be rewritten in matrix form, using the Kronecker product \otimes , as

$$(\mathbf{M} \otimes \mathbf{I}_3) \mathbf{Q}_r = 0, \quad (\text{A.6})$$

where $\mathbf{Q}_r \in \mathbb{R}^{3n}$ is the column vector composed of all the vectors $\tilde{\mathbf{q}}_i$, for $i \in \mathcal{N}$, and the matrix $\mathbf{M} = [m_{ij}] \in \mathbb{R}^{n \times n}$ is given by

$$m_{ii} = k_i^p + \sum_{j=1}^n k_{ij}^p \tilde{\eta}_j, \quad m_{ij} = -k_{ij}^p \tilde{\eta}_i. \quad (\text{A.7})$$

A necessary and sufficient condition for equation (A.6) to have a unique solution is that the matrix \mathbf{M} has full rank. From equations (A.7), the matrix \mathbf{M} is strictly diagonally dominant if

$$|m_{ii}| > \sum_{j=1, j \neq i}^n |m_{ij}|, \quad (\text{A.8})$$

therefore,

$$|k_i^p + \sum_{j=1}^n k_{ij}^p \tilde{\eta}_j| > \sum_{j=1, j \neq i}^n |k_{ij}^p \tilde{\eta}_i|, \quad (\text{A.9})$$

which yields

$$|k_i^p + \sum_{j=1}^n k_{ij}^p \tilde{\eta}_j| > |\tilde{\eta}_i| \sum_{j=1, j \neq i}^n k_{ij}^p. \quad (\text{A.10})$$

Taking $\tilde{\eta}_i = 1$ and $\tilde{\eta}_j = -1$, we have

$$|k_i^p - \sum_{j=1}^n k_{ij}^p| > \sum_{j=1, j \neq i}^n k_{ij}^p. \quad (\text{A.11})$$

Hence, if condition (2.31) is satisfied, the matrix \mathbf{M} is strictly diagonally dominant, which implies that the only solution of (A.6) is $\mathbf{Q}_r = 0$, that is $\tilde{\mathbf{q}}_i = 0$ for $i \in \mathcal{N}$. Furthermore, we can see from equation (A.10) that the matrix \mathbf{M} is strictly diagonally dominant if the scalar parts $\tilde{\eta}_i$ for $i \in \mathcal{N}$ are strictly positive for all time. Therefore, if $\tilde{\eta}_i$ is guaranteed to be strictly positive, the only solution to (2.30) is $\tilde{\mathbf{q}}_i = 0$ for $i \in \mathcal{N}$ without any condition on the gains.

A.1.2 Proof of Lemma 2.5

We have the set of equations

$$\sum_{j=1}^n k_{ij}^p \mathbf{q}_{ij} = 0, \quad \text{for } i \in \mathcal{N}, \quad (\text{A.12})$$

with \mathbf{q}_{ij} is the vector part of the unit-quaternion representing the relative attitude between two rigid-bodies (or spacecraft) with a communication link. Note that the information flow between rigid-bodies is described by the undirected graph \mathcal{G}_p . To analyze the set of equations (A.12), we assign directions to the graph \mathcal{G}_p , by considering one of the nodes (spacecraft) to be the positive end of the link, and obtain the directed graph $\tilde{\mathcal{G}}_p = (\mathcal{N}, \tilde{\mathcal{E}}, \mathcal{K}_p)$, with $\tilde{\mathcal{E}}$ being the set of ordered edges of this graph. The positive end of a link can be chosen arbitrarily, since a bi-directional information flow is assumed. Let $m = |\tilde{\mathcal{E}}|$ be the total number of edges in the graph $\tilde{\mathcal{G}}_p$, which is equal to the number of undirected links in \mathcal{G}_p , *i.e.*, $|\mathcal{E}|$. With this direction assignment, and the assumption that the communication graph \mathcal{G}_p is a tree, the obtained directed graph $\tilde{\mathcal{G}}_p$ is weakly connected and acyclic, and $m = n - 1$.

The weighted incidence matrix of $\tilde{\mathcal{G}}_p$ is $\mathbf{D} = [d_{ij}] \in \mathbb{R}^{n \times n-1}$, which can be rewritten as

$$d_{i\mathcal{X}(u,v)} = \begin{cases} +k_{uv}^p & \text{if node } i \text{ is the positive end of link } (u, v), \\ -k_{uv}^p & \text{if node } i \text{ is the negative end of link } (u, v), \\ 0 & \text{otherwise,} \end{cases} \quad (\text{A.13})$$

where $\mathcal{X}^{(u,v)} : \tilde{\mathcal{E}} \rightarrow \{1, \dots, n-1\}$ is a function that associates a unique number from the set $\{1, \dots, n-1\}$ to each link $(u, v) \in \tilde{\mathcal{E}}$.

Let $\mathbf{Q}_u \in \mathbb{R}^{3(n-1)}$ be the column vector stack constructed from all \mathbf{q}_{ij} , $\forall (i, j) \in \tilde{\mathcal{E}}$. Using the fact that $\mathbf{q}_{ij} = -\mathbf{q}_{ji}$, the set of equations (A.12) can be written in matrix form as

$$(\mathbf{D} \otimes \mathbf{I}_3) \mathbf{Q}_u = 0, \quad (\text{A.14})$$

where \otimes denotes the kronecker product. Since $\tilde{\mathcal{G}}_p$ is weakly connected and acyclic, the incidence matrix \mathbf{D} is full column rank by Property 2.2. Hence, the only solution of (A.14) is $\mathbf{Q}_u = 0$, that is $\mathbf{q}_{ij} = 0, \forall (i, j) \in \tilde{\mathcal{E}}$. Further, since the graph is connected, each spacecraft communicates with at least one other spacecraft, we conclude that $\mathbf{q}_{ij} \rightarrow 0$, and $\mathbf{R}(\mathbf{Q}_{ij}) \rightarrow \mathbf{I}_3$, for $i, j \in \mathcal{N}$.

To show the second part of the Lemma, we use the definition of the inverse unit-quaternion (2.6) with (2.7) and (2.20) to rewrite equation (A.12) as

$$\sum_{j=1}^n k_{ij}^p (\eta_j \mathbf{q}_i - \eta_i \mathbf{q}_j + \mathbf{S}(\mathbf{q}_i) \mathbf{q}_j) = 0, \quad \text{for } i \in \mathcal{N}. \quad (\text{A.15})$$

We then multiply both sides of the above equations by \mathbf{q}_i^T and take the sum over i , to get

$$\sum_{i=1}^n \sum_{j=1}^n k_{ij}^p \mathbf{q}_i^T (\eta_j \mathbf{q}_i - \eta_i \mathbf{q}_j) = 0, \quad (\text{A.16})$$

which, in view of (2.2), is equivalent to

$$\sum_{i=1}^n \sum_{j=1}^n k_{ij}^p \eta_j (1 - \eta_i^2) - \sum_{i=1}^n \sum_{j=1}^n k_{ij}^p \eta_i \mathbf{q}_i^T \mathbf{q}_j = 0. \quad (\text{A.17})$$

Using the definition of unit-quaternion multiplication, we can verify that: $\eta_i \eta_j + \mathbf{q}_i^T \mathbf{q}_j = \eta_{ij}$, where η_{ij} is the scalar part of the unit-quaternion \mathbf{Q}_{ij} . Hence, this last equation can be rewritten as

$$\sum_{i=1}^n \sum_{j=1}^n k_{ij}^p \eta_i = \sum_{i=1}^n \sum_{j=1}^n k_{ij}^p \eta_i \eta_{ij}, \quad (\text{A.18})$$

which is equivalent to

$$\sum_{i=1}^n \sum_{j=1}^n k_{ij}^p \eta_i (1 - \eta_{ij}) = 0. \quad (\text{A.19})$$

Therefore, it is clear that if η_i is guaranteed to be strictly positive (or strictly negative), for $i \in \mathcal{N}$, the only solution to (2.32) is $\eta_{ij} = 1$, that is $\mathbf{q}_{ij} = 0$ for all $(i, j) \in \mathcal{E}$, and if the undirected communication graph is connected, this is verified for all $i, j \in \mathcal{N}$.

A.1.3 Proof of Lemma 2.6

Consider the Lyapunov function candidate

$$W = \frac{1}{2} \dot{\boldsymbol{\theta}}^T \dot{\boldsymbol{\theta}} + k_p \sum_{j=1}^3 \int_0^{\boldsymbol{\theta}^j} \sigma(s) ds, \quad (\text{A.20})$$

with $\boldsymbol{\theta} = (\boldsymbol{\theta}^1, \boldsymbol{\theta}^2, \boldsymbol{\theta}^3)^T$, which can be verified to be radially unbounded from the definition of σ . The time-derivative of W along (2.35) is given as

$$\begin{aligned} \dot{W} &= \dot{\boldsymbol{\theta}}^T (-k_p \chi(\boldsymbol{\theta}) - k_d \chi(\dot{\boldsymbol{\theta}}) + \boldsymbol{\varepsilon}) + k_p \dot{\boldsymbol{\theta}}^T \chi(\boldsymbol{\theta}) \\ &= -\dot{\boldsymbol{\theta}}^T (k_d \chi(\dot{\boldsymbol{\theta}}) - \boldsymbol{\varepsilon}) \\ &\leq -\sum_{j=1}^3 |\dot{\boldsymbol{\theta}}^j| (k_d \sigma(|\dot{\boldsymbol{\theta}}^j|) - |\boldsymbol{\varepsilon}^j|), \end{aligned} \quad (\text{A.21})$$

with $\boldsymbol{\varepsilon} = (\boldsymbol{\varepsilon}^1, \boldsymbol{\varepsilon}^2, \boldsymbol{\varepsilon}^3)^T$, where we have used the property; $x\sigma(x) = |x|\sigma(|x|)$, for any $x \in \mathbb{R}$. First of all, let us show that $\boldsymbol{\theta}$ and $\dot{\boldsymbol{\theta}}$ cannot escape in finite time. In fact,

from (A.21) it is clear that $\dot{W} \leq \|\dot{\boldsymbol{\theta}}\| \|\boldsymbol{\varepsilon}\|$. Using the fact that $\|\dot{\boldsymbol{\theta}}\|^2 \leq 2W$, we have $\dot{W} \leq \varepsilon_b \sqrt{W}$, with $\sqrt{2}\|\boldsymbol{\varepsilon}\| \leq \varepsilon_b$, which can be rewritten as

$$\frac{dW}{\sqrt{W}} \leq \varepsilon_b dt. \quad (\text{A.22})$$

Integrating the last inequality over the interval $[t_0, t]$ yields

$$2 \left(\sqrt{W(t)} - \sqrt{W(t_0)} \right) \leq \varepsilon_b (t - t_0), \quad (\text{A.23})$$

which shows that W cannot go to infinity in finite time.

Now, we will show the boundedness and convergence of $\boldsymbol{\theta}$ and $\dot{\boldsymbol{\theta}}$ to zero. It is easily seen that the right hand side of (A.21) is negative as long as

$$\sigma(|\dot{\boldsymbol{\theta}}^j|) > \frac{|\boldsymbol{\varepsilon}^j|}{k_d}, \quad \text{for } j = 1, 2, 3. \quad (\text{A.24})$$

Due to the fact that σ is bounded, inequality (A.24) cannot be satisfied when $|\boldsymbol{\varepsilon}^j| > \sigma_b k_d$, for $j = 1, 2, 3$, where σ_b is defined in property P2 in section 2.6. However, since $\boldsymbol{\varepsilon}$ is bounded and converges asymptotically to zero, it is clear that there exists a finite time t_1 such that $|\boldsymbol{\varepsilon}^j| \leq \sigma_b k_d$ for all $t \geq t_1$. Note that $\boldsymbol{\theta}$ and $\dot{\boldsymbol{\theta}}$ remain bounded on the interval $[0, t_1]$ as there is no finite-escape time. Consequently, for all $t \geq t_1$, one can conclude that $\dot{W} < 0$, and $\boldsymbol{\theta}$ and $\dot{\boldsymbol{\theta}}$ are bounded outside the set

$$\mathcal{S} = \left\{ \dot{\boldsymbol{\theta}} \mid \sigma(|\dot{\boldsymbol{\theta}}^j|) \leq \frac{|\boldsymbol{\varepsilon}^j|}{k_d}, \text{ for } j = 1, 2, 3 \right\}.$$

Since $\sigma(|\cdot|)$ is a class \mathcal{K} function, $\dot{\boldsymbol{\theta}}$ is ultimately bound to reach the set \mathcal{S} and will be driven to zero as $\boldsymbol{\varepsilon} \rightarrow 0$. Finally, invoking Lemma 2.3 (the extended Barbălat Lemma), together with the fact that $\boldsymbol{\varepsilon}$ and $\dot{\boldsymbol{\theta}}$ are bounded and converge to zero as t goes to infinity, one can show that $\boldsymbol{\theta} \rightarrow 0$.

A.2 Attitude synchronization

A.2.1 Proof of Theorem 3.1

From the definition of the angular velocity tracking error (2.15) and (2.8) we have

$$\dot{\tilde{\boldsymbol{\omega}}}_i = \dot{\boldsymbol{\omega}}_i - \mathbf{R}(\tilde{\mathbf{Q}}_i) \dot{\boldsymbol{\omega}}_d + \mathbf{S}(\tilde{\boldsymbol{\omega}}_i) \mathbf{R}(\tilde{\mathbf{Q}}_i) \boldsymbol{\omega}_d. \quad (\text{A.25})$$

Using the attitude dynamics, the time-derivative of the above equation gives

$$\begin{aligned} \mathbf{J}_{f_i} \dot{\tilde{\boldsymbol{\omega}}}_i = & \boldsymbol{\Gamma}_i - \mathbf{S} \left(\tilde{\boldsymbol{\omega}}_i - \mathbf{R}(\tilde{\mathbf{Q}}_i) \boldsymbol{\omega}_d \right) \mathbf{J}_{f_i} \left(\tilde{\boldsymbol{\omega}}_i - \mathbf{R}(\tilde{\mathbf{Q}}_i) \boldsymbol{\omega}_d \right) \\ & - \mathbf{J}_{f_i} \mathbf{R}(\tilde{\mathbf{Q}}_i) \dot{\boldsymbol{\omega}}_d - \mathbf{J}_{f_i} \mathbf{S} \left(\mathbf{R}(\tilde{\mathbf{Q}}_i) \boldsymbol{\omega}_d \right) \tilde{\boldsymbol{\omega}}_i, \end{aligned} \quad (\text{A.26})$$

which, after some algebraic manipulations, can be rewritten as

$$\begin{aligned} \mathbf{J}_{f_i} \dot{\tilde{\boldsymbol{\omega}}}_i = & \boldsymbol{\Gamma}_i - \mathbf{S}(\tilde{\boldsymbol{\omega}}_i) \mathbf{J}_{f_i} \left(\tilde{\boldsymbol{\omega}}_i - \mathbf{R}(\tilde{\mathbf{Q}}_i) \boldsymbol{\omega}_d \right) - \mathbf{J}_{f_i} \mathbf{R}(\tilde{\mathbf{Q}}_i) \dot{\boldsymbol{\omega}}_d \\ & - \left(\mathbf{S} \left(\mathbf{R}(\tilde{\mathbf{Q}}_i) \boldsymbol{\omega}_d \right) \mathbf{J}_{f_i} + \mathbf{J}_{f_i} \mathbf{S} \left(\mathbf{R}(\tilde{\mathbf{Q}}_i) \boldsymbol{\omega}_d \right) \mathbf{J}_{f_i} \right) \tilde{\boldsymbol{\omega}}_i. \end{aligned} \quad (\text{A.27})$$

Since $\mathbf{J}_{f_i} = \mathbf{J}_{f_i}^T > 0$, it is clear that $\left(\mathbf{S} \left(\mathbf{R}(\tilde{\mathbf{Q}}_i) \boldsymbol{\omega}_d \right) \mathbf{J}_{f_i} + \mathbf{J}_{f_i} \mathbf{S} \left(\mathbf{R}(\tilde{\mathbf{Q}}_i) \boldsymbol{\omega}_d \right) \mathbf{J}_{f_i} \right)$ is skew symmetric, and therefore, we can write

$$\tilde{\boldsymbol{\omega}}_i^T \mathbf{J}_{f_i} \dot{\tilde{\boldsymbol{\omega}}}_i = \tilde{\boldsymbol{\omega}}_i^T \left(\boldsymbol{\Gamma}_i - \mathbf{J}_{f_i} \mathbf{R}(\tilde{\mathbf{Q}}_i) \dot{\boldsymbol{\omega}}_d - \mathbf{S} \left(\mathbf{R}(\tilde{\mathbf{Q}}_i) \boldsymbol{\omega}_d \right) \mathbf{J}_{f_i} \mathbf{R}(\tilde{\mathbf{Q}}_i) \boldsymbol{\omega}_d \right). \quad (\text{A.28})$$

Therefore, using the control input (3.3) with (3.19) and (3.20), we obtain

$$\tilde{\boldsymbol{\omega}}_i^T \mathbf{J}_{f_i} \dot{\tilde{\boldsymbol{\omega}}}_i = \tilde{\boldsymbol{\omega}}_i^T \left(-k_i^p \tilde{\mathbf{q}}_i - k_i^d \mathbf{q}_i^e \right) - \sum_{j=1}^n \tilde{\boldsymbol{\omega}}_i^T \left(k_{ij}^p \mathbf{q}_{ij} + k_{ij}^d \left(\mathbf{q}_{ij}^e - \mathbf{R}(\mathbf{Q}_{ij}) \mathbf{q}_{ij}^e \right) \right). \quad (\text{A.29})$$

Consider the following Lyapunov function candidate

$$\begin{aligned} V = & \sum_{j=1}^n \left(\frac{1}{2} \tilde{\boldsymbol{\omega}}_i^T I_{f_i} \tilde{\boldsymbol{\omega}}_i + k_i^p \left(\tilde{\mathbf{q}}_i^T \tilde{\mathbf{q}}_i + (1 - \tilde{\eta}_i)^2 \right) + k_i^d \left(\left(\mathbf{q}_i^e \right)^T \mathbf{q}_i^e + (1 - \eta_i^e)^2 \right) \right) \\ & + \frac{1}{2} \sum_{i=1}^n \sum_{j=1}^n \left(k_{ij}^p \left(\mathbf{q}_{ij}^T \mathbf{q}_{ij} + (1 - \eta_{ij})^2 \right) + 2k_{ij}^d \left(\left(\mathbf{q}_{ij}^e \right)^T \mathbf{q}_{ij}^e + (1 - \eta_{ij}^e)^2 \right) \right), \end{aligned} \quad (\text{A.30})$$

which can be rewritten using the unity constraint (2.2) as

$$\begin{aligned} V = & \sum_{j=1}^n \left(\frac{1}{2} \tilde{\boldsymbol{\omega}}_i^T I_{f_i} \tilde{\boldsymbol{\omega}}_i + 2k_i^p (1 - \tilde{\eta}_i) + 2k_i^d (1 - \eta_i^e) \right) \\ & + \sum_{i=1}^n \sum_{j=1}^n \left(k_{ij}^p (1 - \eta_{ij}) + 2k_{ij}^d (1 - \eta_{ij}^e) \right). \end{aligned} \quad (\text{A.31})$$

The time-derivative of V using equations (2.14), (2.21), (3.14) and (3.17) gives

$$\begin{aligned} \dot{V} &= \sum_{j=1}^n \left(\tilde{\omega}_i^T \mathbf{J}_{f_i} \dot{\tilde{\omega}}_i + k_i^p \tilde{\omega}_i^T \tilde{\mathbf{q}}_i + k_i^d \boldsymbol{\Omega}_i^T \mathbf{q}_i^e \right) \\ &\quad + \sum_{i=1}^n \sum_{j=1}^n \left(\frac{1}{2} k_{ij}^p \boldsymbol{\omega}_{ij}^T \mathbf{q}_{ij} + k_{ij}^d \boldsymbol{\Omega}_{ij}^T \mathbf{q}_{ij}^e \right). \end{aligned} \quad (\text{A.32})$$

Using (A.29) with (2.15) and (3.15) yields

$$\begin{aligned} \dot{V} &= \sum_{i=1}^n k_i^d \left(\mathbf{R}(\tilde{\mathbf{Q}}_i) \boldsymbol{\omega}_d - \mathbf{R}(\mathbf{Q}_i^e) \boldsymbol{\beta}_i \right)^T \mathbf{q}_i^e \\ &\quad - \sum_{i=1}^n \sum_{j=1}^n \tilde{\omega}_i^T \left(k_{ij}^p \mathbf{q}_{ij} + k_{ij}^d \left(\mathbf{q}_{ij}^e - \mathbf{R}(\mathbf{Q}_{ij}) \mathbf{q}_{ji}^e \right) \right) \\ &\quad + \sum_{i=1}^n \sum_{j=1}^n \left(\frac{1}{2} k_{ij}^p \boldsymbol{\omega}_{ij}^T \mathbf{q}_{ij} + k_{ij}^d \boldsymbol{\Omega}_{ij}^T \mathbf{q}_{ij}^e \right). \end{aligned} \quad (\text{A.33})$$

Since spacecraft are required to align their attitudes to the same desired angular velocity, the relative attitude and relative angular velocity between the i^{th} and j^{th} spacecraft can be expressed as in (A.1) and, accordingly, the relative angular velocity can be expressed as

$$\boldsymbol{\omega}_{ij} = \tilde{\omega}_i - \mathbf{R}(\mathbf{Q}_{ij}) \tilde{\omega}_j, \quad (\text{A.34})$$

which can be easily verified using the definition of the angular velocity tracking error given in (2.15). Using equation (A.34), we can write

$$\begin{aligned} \frac{1}{2} \sum_{i=1}^n \sum_{j=1}^n k_{ij}^p \boldsymbol{\omega}_{ij}^T \mathbf{q}_{ij} &= \frac{1}{2} \sum_{i=1}^n \sum_{j=1}^n k_{ij}^p \tilde{\omega}_i^T \mathbf{q}_{ij} - \frac{1}{2} \sum_{i=1}^n \sum_{j=1}^n k_{ij}^p \tilde{\omega}_j^T \mathbf{R}(\mathbf{Q}_{ij})^T \mathbf{q}_{ij} \\ &= \frac{1}{2} \sum_{i=1}^n \sum_{j=1}^n k_{ij}^p \tilde{\omega}_i^T \mathbf{q}_{ij} - \frac{1}{2} \sum_{j=1}^n \sum_{i=1}^n k_{ji}^p \tilde{\omega}_i^T \mathbf{q}_{ji} \\ &= \sum_{i=1}^n \sum_{j=1}^n k_{ij}^p \tilde{\omega}_i^T \mathbf{q}_{ij}, \end{aligned} \quad (\text{A.35})$$

where we have used equations (2.24)-(2.25) with the properties of the undirected communication graph, *i.e.*, $k_{ij}^p = k_{ji}^p$. Similarly, using the expression of $\boldsymbol{\Omega}_{ij}$, given in

(3.18), with (2.24), (2.28) and (A.34), we get

$$\begin{aligned}
\sum_{i=1}^n \sum_{j=1}^n k_{ij}^d \boldsymbol{\Omega}_{ij}^T \mathbf{q}_{ij}^e &= \sum_{i=1}^n \sum_{j=1}^n k_{ij}^d \left(\tilde{\boldsymbol{\omega}}_i - \mathbf{R}(\mathbf{Q}_{ij}) \tilde{\boldsymbol{\omega}}_j - \mathbf{R}(\mathbf{Q}_{ij}^e) \boldsymbol{\beta}_{ij} \right)^T \mathbf{q}_{ij}^e \\
&= \sum_{i=1}^n \sum_{j=1}^n k_{ij}^d \tilde{\boldsymbol{\omega}}_i^T \mathbf{q}_{ij}^e - \sum_{j=1}^n \sum_{i=1}^n k_{ji}^d \tilde{\boldsymbol{\omega}}_i^T \mathbf{R}(\mathbf{Q}_{ji})^T \mathbf{q}_{ji}^e \\
&\quad - \sum_{i=1}^n \sum_{j=1}^n k_{ij}^d \boldsymbol{\beta}_{ij}^T \mathbf{R}(\mathbf{Q}_{ij}^e)^T \mathbf{q}_{ij}^e \\
&= \sum_{i=1}^n \sum_{j=1}^n k_{ij}^d \tilde{\boldsymbol{\omega}}_i^T \left(\mathbf{q}_{ij}^e - \mathbf{R}(\mathbf{Q}_{ij}) \mathbf{q}_{ji}^e \right) \\
&\quad - \sum_{i=1}^n \sum_{j=1}^n k_{ij}^d \boldsymbol{\beta}_{ij}^T \mathbf{R}(\mathbf{Q}_{ij}^e)^T \mathbf{q}_{ij}^e. \tag{A.36}
\end{aligned}$$

From the above relations, equation (A.33) can be rewritten as

$$\dot{V} = \sum_{i=1}^n k_i^d \left(\mathbf{R}(\tilde{\mathbf{Q}}_i) \boldsymbol{\omega}_d - \mathbf{R}(\mathbf{Q}_i^e) \boldsymbol{\beta}_i \right)^T \mathbf{q}_i^e - \sum_{i=1}^n \sum_{j=1}^n k_{ij}^d \boldsymbol{\beta}_{ij}^T \mathbf{q}_{ij}^e. \tag{A.37}$$

Finally, using equations (3.21), the time-derivative of V is obtained as

$$\dot{V} = - \sum_{i=1}^n k_i^d \lambda_i (\mathbf{q}_i^e)^T \mathbf{q}_i^e - \sum_{i=1}^n \sum_{j=1}^n k_{ij}^d \lambda_{ij} (\mathbf{q}_{ij}^e)^T \mathbf{q}_{ij}^e, \tag{A.38}$$

which implies that $V(t) \leq V(0)$, and $\tilde{\boldsymbol{\omega}}_i$ is globally bounded. Note that $\tilde{\mathbf{Q}}_i$, \mathbf{Q}_i^e , \mathbf{Q}_{ij} and \mathbf{Q}_{ij}^e are naturally bounded vectors from the definition of unit-quaternion. Hence, we conclude that $\boldsymbol{\beta}_i$ and $\boldsymbol{\beta}_{ij}$ are bounded, and consequently, we have $\boldsymbol{\Omega}_i$ and $\boldsymbol{\Omega}_{ij}$ are bounded. This leads us to conclude that $\dot{\mathbf{q}}_i^e$ and $\dot{\mathbf{q}}_{ij}^e$ are bounded. Therefore, we have \ddot{V} is bounded, and invoking Barbălat lemma we conclude that $\mathbf{q}_i^e \rightarrow 0$ and $\mathbf{q}_{ij}^e \rightarrow 0$, which implies that $\boldsymbol{\beta}_i \rightarrow \mathbf{R}(\mathbf{Q}_i^e)^T \mathbf{R}(\tilde{\mathbf{Q}}_i) \boldsymbol{\omega}_d$, $\boldsymbol{\beta}_{ij} \rightarrow 0$, $\mathbf{R}(\mathbf{Q}_i^e) \rightarrow \mathbf{I}_3$ and $\mathbf{R}(\mathbf{Q}_{ij}^e) \rightarrow \mathbf{I}_3$. As a result, we conclude from (3.15) and (3.18) that $\boldsymbol{\Omega}_i \rightarrow \tilde{\boldsymbol{\omega}}_i$ and $\boldsymbol{\Omega}_{ij} \rightarrow \boldsymbol{\omega}_{ij}$. Note that the above results are valid for $i \in \mathcal{N}$ and $(i, j) \in \mathcal{E}$. Since the communication graph is assumed to be connected, *i.e.*, each spacecraft communicates with at least one other spacecraft in the team, the obtained results are true for all $i, j \in \mathcal{N}$. Now, since $\boldsymbol{\omega}_d$ is bounded, one can show that $\ddot{\mathbf{Q}}_i^e$ and $\ddot{\mathbf{Q}}_{ij}^e$ are bounded, and hence $\dot{\mathbf{Q}}_i^e \rightarrow 0$ and $\dot{\mathbf{Q}}_{ij}^e \rightarrow 0$, which in turns, from (3.14) and (3.17), implies that $\boldsymbol{\Omega}_i \rightarrow 0$ and $\boldsymbol{\Omega}_{ij} \rightarrow 0$. As a result, we conclude that $\tilde{\boldsymbol{\omega}}_i \rightarrow 0$ and $\boldsymbol{\omega}_{ij} \rightarrow 0$. Furthermore, one

can easily verify that $\ddot{\tilde{\boldsymbol{\omega}}}_i$ is bounded since $\ddot{\boldsymbol{\omega}}_d$ is bounded, and so we conclude that $\dot{\tilde{\boldsymbol{\omega}}}_i \rightarrow 0$.

Using the above results, the angular velocity tracking error dynamics (A.27), with (3.3) and (3.19) and (3.20), reduces to

$$k_i^p \tilde{\mathbf{q}}_i + \sum_{j=1}^n k_{ij}^p \mathbf{q}_{ij} = 0, \quad \text{for } i \in \mathcal{N}. \quad (\text{A.39})$$

From the result of Lemma 2.4, we have $\tilde{\mathbf{q}}_i = 0$ is the only solution to (A.39) if the control gains are selected according to (2.31). Hence, we conclude that $\mathbf{q}_i \rightarrow \mathbf{q}_j \rightarrow \mathbf{q}_d$. Moreover, since $\tilde{\boldsymbol{\omega}}_i \rightarrow 0$, $\boldsymbol{\omega}_{ij} \rightarrow 0$, $\mathbf{R}(\tilde{\mathbf{Q}}_i) \rightarrow \mathbf{I}_3$ and $\mathbf{R}(\mathbf{Q}_{ij}) \rightarrow \mathbf{I}_3$, we conclude that $\boldsymbol{\omega}_i \rightarrow \boldsymbol{\omega}_j \rightarrow \boldsymbol{\omega}_d$, $\forall i, j \in \mathcal{N}$.

Furthermore, note that equation (A.39) holds when t tends to infinity. Therefore, we conclude from Lemma 2.4 that the above result holds without any condition if there exists a time $t_0 > 0$, such that $\tilde{\eta}_i(t) > 0$ for $t > t_0$ and $i \in \mathcal{N}$.

A.2.2 Proof of Theorem 3.2

Consider the following Lyapunov function candidate

$$\begin{aligned} V = & \frac{1}{2} \sum_{i=1}^n \boldsymbol{\omega}_i^T \mathbf{J}_{f_i} \boldsymbol{\omega}_i + \sum_{i=1}^n \sum_{j=1}^n k_{ij}^p (1 - \eta_{ij}) \\ & + \sum_{i=1}^n \sum_{j=1}^n k_{ij}^d \left(2(1 - \eta_{ij}^e) + (1 - \tilde{\eta}_{ij}^e) \right). \end{aligned} \quad (\text{A.40})$$

Note that the elements of the unit-quaternion \mathbf{Q}_{ij} satisfy the relation: $2(1 - \eta_{ij}) = \mathbf{q}_{ij}^T \mathbf{q}_{ij} + (1 - \eta_{ij})^2$, which holds for the elements of the unit-quaternion \mathbf{Q}_{ij}^e and $\tilde{\mathbf{Q}}_{ij}^e$. The time-derivative of V evaluated along the system trajectories, using (3.2), (3.17) (2.21) and (3.29), gives

$$\begin{aligned} \dot{V} = & \sum_{i=1}^n \boldsymbol{\omega}_i^T \boldsymbol{\Gamma}_i + \frac{1}{2} \sum_{i=1}^n \sum_{j=1}^n k_{ij}^p \boldsymbol{\omega}_{ij}^T \mathbf{q}_{ij} \\ & + \sum_{i=1}^n \sum_{j=1}^n k_{ij}^d \left(\boldsymbol{\Omega}_{ij}^T \mathbf{q}_{ij}^e + \frac{1}{2} \tilde{\boldsymbol{\Omega}}_{ij}^T \tilde{\mathbf{q}}_{ij}^e \right). \end{aligned} \quad (\text{A.41})$$

Using the definition of the unit-quaternion (3.28), with the properties of the rotation

matrix, the following relations can be verified similarly to (2.24) and (2.25)

$$\mathbf{R}(\tilde{\mathbf{Q}}_{ji}^e)^T = \mathbf{R}(\tilde{\mathbf{Q}}_{ij}^e), \quad (\text{A.42})$$

$$\tilde{\mathbf{q}}_{ji}^e = -\tilde{\mathbf{q}}_{ij}^e = -\mathbf{R}(\tilde{\mathbf{Q}}_{ji}^e) \tilde{\mathbf{q}}_{ij}^e. \quad (\text{A.43})$$

Also, from the expression of $\tilde{\mathbf{\Omega}}_{ij}$ in (3.30), and following similar steps as in (A.35), we can verify that

$$\frac{1}{2} \sum_{j=1}^n \sum_{i=1}^n k_{ij}^d \tilde{\mathbf{\Omega}}_{ij}^T \tilde{\mathbf{q}}_{ij}^e = \sum_{i=1}^n \sum_{j=1}^n k_{ij}^d \mathbf{\Omega}_i^T \tilde{\mathbf{q}}_{ij}^e. \quad (\text{A.44})$$

Applying the input torque (3.31) with relations (A.35), (A.36) and (A.44), yields

$$\dot{V} = \sum_{i=1}^n \sum_{j=1}^n \left(-k_{ij}^d \beta_i^T \mathbf{R}(\mathbf{Q}_i^e)^T \tilde{\mathbf{q}}_{ij}^e - k_{ij}^d \beta_{ij}^T \mathbf{q}_{ij}^e \right), \quad (\text{A.45})$$

which, in view of (3.32) and (3.33), leads to the negative semi-definite time-derivative

$$\begin{aligned} \dot{V} = & - \sum_{i=1}^n \sum_{j=1}^n k_{ij}^d \lambda_{ij} \mathbf{q}_{ij}^e{}^T \mathbf{q}_{ij}^e \\ & - \sum_{i=1}^n \lambda_i \left(\sum_{j=1}^n k_{ij}^d \tilde{\mathbf{q}}_{ij}^e \right)^T \left(\sum_{j=1}^n k_{ij}^d \tilde{\mathbf{q}}_{ij}^e \right), \end{aligned} \quad (\text{A.46})$$

and we can conclude that $\boldsymbol{\omega}_i$ is globally bounded. Note that \mathbf{Q}_{ij} , $\tilde{\mathbf{Q}}_{ij}^e$, $\tilde{\mathbf{Q}}_{ij}^e$ are bounded from the definition of unit-quaternion. Also, we can see from (3.30) and (3.18) respectively that $\tilde{\mathbf{\Omega}}_{ij}$ and $\mathbf{\Omega}_{ij}$ are bounded, which in turns, from (3.29) and (3.17), implies that $\tilde{\mathbf{q}}_{ij}^e$ and \mathbf{q}_{ij}^e are bounded respectively. Invoking Barbălat Lemma, we conclude that $\mathbf{q}_{ij}^e \rightarrow 0$, for all $i, j \in \mathcal{N}$, and

$$\sum_{j=1}^n k_{ij}^d \tilde{\mathbf{q}}_{ij}^e \rightarrow 0, \quad \text{for } i \in \mathcal{N}, \quad (\text{A.47})$$

which implies that $\beta_i \rightarrow 0$ and $\beta_{ij} \rightarrow 0$, allowing to conclude that $\mathbf{\Omega}_{ij} \rightarrow \boldsymbol{\omega}_{ij}$ and $\mathbf{\Omega}_i \rightarrow \boldsymbol{\omega}_i$. In order to determine the solutions of (A.47), notice that the set of equations (A.47) are similar to (2.32) in Lemma 2.5. Therefore, the same steps as in the proof of Lemma 2.5 can be used to the communication graph \mathcal{G}_d to conclude that the only solution to (A.47) is $\tilde{\mathbf{q}}_{ij}^e \rightarrow 0$, for all $i, j \in \mathcal{N}$, under the assumption that the communication graph is a tree. As a result, we conclude that $\mathbf{R}(\tilde{\mathbf{Q}}_{ij}^e) = \mathbf{I}_3$.

Furthermore, we can show that $\ddot{\tilde{\mathbf{Q}}}_{ij}^e$ and $\ddot{\mathbf{Q}}_{ij}^e$ are bounded, which leads us to conclude that $\dot{\mathbf{q}}_{ij}^e \rightarrow 0$ and $\dot{\tilde{\mathbf{q}}}_{ij}^e \rightarrow 0$, in virtue of Barbălat Lemma, and hence $\mathbf{\Omega}_{ij} \rightarrow 0$ and $\tilde{\mathbf{\Omega}}_{ij} \rightarrow 0$. Since $\mathbf{\Omega}_{ij} \rightarrow \boldsymbol{\omega}_{ij}$ and from (3.30), it is straightforward to conclude that

$$\begin{cases} \boldsymbol{\omega}_{ij} \rightarrow 0, & \text{and} \\ \mathbf{\Omega}_i - \mathbf{R}(\tilde{\mathbf{Q}}_{ij}^e)\mathbf{\Omega}_j \rightarrow 0 \end{cases} \Rightarrow \mathbf{\Omega}_i \rightarrow \mathbf{\Omega}_j. \quad (\text{A.48})$$

Hence, from (2.22) and the fact that $\mathbf{\Omega}_i \rightarrow \boldsymbol{\omega}_i$, we have

$$\begin{cases} \boldsymbol{\omega}_i \rightarrow \mathbf{R}(\mathbf{Q}_{ij})\boldsymbol{\omega}_j, & \text{and} \\ \boldsymbol{\omega}_i \rightarrow \boldsymbol{\omega}_j, \end{cases} \quad (\text{A.49})$$

which leads us to conclude that $\mathbf{R}(\mathbf{Q}_{ij}) \rightarrow \mathbf{I}_3$, that is $\mathbf{q}_i \rightarrow \mathbf{q}_j$ and $\boldsymbol{\omega}_i \rightarrow \boldsymbol{\omega}_j$, for all $i, j \in \mathcal{N}$.

In addition, note that equation (A.47) holds when time tends to infinity. Therefore, if there exists a time $t_0 > 0$, such that $\eta_i^e(t) > 0$, (or $\eta_i^e(t) < 0$), for $t > t_0$, the same steps of the proof of Lemma 2.5 can be used to show that the only solution to (A.47) is $\tilde{\mathbf{q}}_{ij}^e = 0$ for all $i, j \in \mathcal{N}$, for any connected graph, and the same above convergence results are obtained.

A.2.3 Proof of Theorem 3.3

The error dynamics for the i^{th} spacecraft can be written, using (3.2) and (3.41), as

$$\begin{aligned} \mathbf{J}_{f_i} \dot{\tilde{\mathbf{\Omega}}}_i &= \mathbf{\Gamma}_i - \mathbf{S}(\boldsymbol{\omega}_i)\mathbf{J}_{f_i}\boldsymbol{\omega}_i - \mathbf{J}_{f_i} \left(\mathbf{S}(\mathbf{R}(\tilde{\mathbf{Q}}_i)\boldsymbol{\omega}_d)\tilde{\boldsymbol{\omega}}_i + \mathbf{R}(\tilde{\mathbf{Q}}_i)\dot{\boldsymbol{\omega}}_d \right) \\ &\quad - \mathbf{J}_{f_i} \left(\mathbf{S}(\mathbf{R}(\tilde{\mathbf{Q}}_i^e)\boldsymbol{\beta}_i)\tilde{\mathbf{\Omega}}_i + \mathbf{R}(\tilde{\mathbf{Q}}_i^e)\dot{\boldsymbol{\beta}}_i \right). \end{aligned} \quad (\text{A.50})$$

Using similar steps as in the proof of Theorem 3.1, and equations (2.15) with (3.41), and after some algebraic manipulations using the cross product properties and the fact that $\mathbf{J}_{f_i} = \mathbf{J}_{f_i}^T > 0$, we can show that

$$\tilde{\mathbf{\Omega}}_i^T \mathbf{J}_{f_i} \dot{\tilde{\mathbf{\Omega}}}_i = \tilde{\mathbf{\Omega}}_i^T \left(\mathbf{\Gamma}_i - \mathbf{H}_i(\boldsymbol{\omega}_d, \dot{\boldsymbol{\omega}}_d, \boldsymbol{\beta}_i, \dot{\boldsymbol{\beta}}_i, \tilde{\mathbf{Q}}_i, \tilde{\mathbf{Q}}_i^e) \right), \quad (\text{A.51})$$

with $\mathbf{H}_i(\cdot)$ is given in (3.43). Therefore, applying the input torque (3.42) results in the error dynamics satisfying

$$\tilde{\mathbf{\Omega}}_i^T \mathbf{J}_{f_i} \dot{\tilde{\mathbf{\Omega}}}_i = \tilde{\mathbf{\Omega}}_i^T \left(-k_i^p \tilde{\mathbf{q}}_i - \sum_{j=1}^n k_{ij}^p \mathbf{q}_{ij} \right). \quad (\text{A.52})$$

Consider the following Lyapunov function candidate

$$V = \frac{1}{2} \sum_{i=1}^n (\tilde{\boldsymbol{\Omega}}_i^T \mathbf{J}_{f_i} \tilde{\boldsymbol{\Omega}}_i + \boldsymbol{\beta}_i^T \boldsymbol{\beta}_i) + \sum_{i=1}^n 2k_i^p (1 - \tilde{\eta}_i) + \sum_{i=1}^n \sum_{j=1}^n k_{ij}^p (1 - \eta_{ij}). \quad (\text{A.53})$$

The time-derivative of V evaluated along (A.52) is obtained as

$$\begin{aligned} \dot{V} = & \sum_{i=1}^n \tilde{\boldsymbol{\Omega}}_i^T (-k_i^p \tilde{\mathbf{q}}_i - \sum_{j=1}^n k_{ij}^p \mathbf{q}_{ij}) + \sum_{i=1}^n \boldsymbol{\beta}_i^T \dot{\boldsymbol{\beta}}_i \\ & + \sum_{i=1}^n \tilde{\boldsymbol{\omega}}_i^T \left(k_i^p \tilde{\mathbf{q}}_i + \sum_{j=1}^n k_{ij}^p \mathbf{q}_{ij} \right), \end{aligned} \quad (\text{A.54})$$

where we have used equations (A.34) and (A.35) to obtain the last term in the above equation. Therefore, the definition of $\tilde{\boldsymbol{\Omega}}_i$ in (3.41), with (3.38) and (3.44), yield to

$$\dot{V} = - \sum_{i=1}^n \lambda_i \boldsymbol{\beta}_i^T \boldsymbol{\beta}_i, \quad (\text{A.55})$$

which is negative semi-definite and we conclude that $\tilde{\boldsymbol{\Omega}}_i, \boldsymbol{\beta}_i$ are bounded, and consequently $\tilde{\boldsymbol{\omega}}_i$ is bounded, for $i \in \mathcal{N}$. Since the vectors $\tilde{\mathbf{q}}_i$ and \mathbf{q}_{ij} are bounded by the definition of unit-quaternion, we know from (3.38) with (3.44) that $\dot{\boldsymbol{\beta}}_i$ is bounded for $i \in \mathcal{N}$. Therefore, we conclude that \dot{V} is bounded. Invoking Barbălat Lemma, we conclude that $\boldsymbol{\beta}_i \rightarrow 0$ for $i \in \mathcal{N}$.

In addition, we can see from the time-derivative of (3.44) that $\dot{\boldsymbol{\beta}}_i$ is bounded. This can be easily verified knowing that $\tilde{\boldsymbol{\omega}}_i, \tilde{\boldsymbol{\Omega}}_i$ and $\dot{\boldsymbol{\beta}}_i$ are bounded. Invoking Barbălat Lemma, we conclude that $\dot{\boldsymbol{\beta}}_i \rightarrow 0$, which implies that

$$k_i^p \tilde{\mathbf{q}}_i + \sum_{j=1}^n k_{ij}^p \mathbf{q}_{ij} \rightarrow 0. \quad (\text{A.56})$$

for $i \in \mathcal{N}$. Then, we conclude from Lemma 2.4 that the only solution to (A.56) is $\tilde{\mathbf{q}}_i = 0$ if condition (2.31) is satisfied. Consequently, we conclude that $\mathbf{q}_i \rightarrow \mathbf{q}_j \rightarrow \mathbf{q}_d$. Moreover, since $\dot{\tilde{\boldsymbol{\Omega}}}_i$ is bounded, from (A.50) with (3.42), we know that $\dot{\tilde{\boldsymbol{\omega}}}_i$ is bounded, and hence $\ddot{\tilde{\mathbf{q}}}_i$ is bounded. Invoking Barbălat Lemma, we conclude that $\ddot{\tilde{\mathbf{q}}}_i \rightarrow 0$, which in turns implies that $\tilde{\boldsymbol{\omega}}_i \rightarrow 0$. As a result, we conclude that $\boldsymbol{\omega}_i \rightarrow \boldsymbol{\omega}_j \rightarrow \boldsymbol{\omega}_d$, for all $i, j \in \mathcal{N}$. The rest of the proof follows from the last part of Lemma 2.4.

A.2.4 Proof of Theorem 3.4

The dynamics of the error vector defined in (3.15) can be written as

$$\mathbf{J}_{f_i} \dot{\boldsymbol{\Omega}}_i = \boldsymbol{\Gamma}_i - \mathbf{S}(\boldsymbol{\omega}_i) \mathbf{J}_{f_i} \boldsymbol{\omega}_i - \mathbf{J}_{f_i} \left(\mathbf{S}(\mathbf{R}(\tilde{\mathbf{Q}}_i^e) \boldsymbol{\beta}_i) \boldsymbol{\Omega}_i + \mathbf{R}(\tilde{\mathbf{Q}}_i^e) \dot{\boldsymbol{\beta}}_i \right). \quad (\text{A.57})$$

Using similar steps as in the proof of Theorem 3.1, and after some algebraic manipulations using the cross product properties and the fact that $\mathbf{J}_{f_i} = \mathbf{J}_{f_i}^T > 0$, the dynamics of the angular velocity vector satisfy

$$\boldsymbol{\Omega}_i^T \mathbf{J}_{f_i} \dot{\boldsymbol{\Omega}}_i = \boldsymbol{\Omega}_i^T \left(\boldsymbol{\Gamma}_i - \mathbf{J}_{f_i} \mathbf{R}(\mathbf{Q}_i^e) \dot{\boldsymbol{\beta}}_i - \mathbf{S}(\mathbf{R}(\mathbf{Q}_i^e) \boldsymbol{\beta}_i) \mathbf{J}_{f_i} \mathbf{R}(\mathbf{Q}_i^e) \boldsymbol{\beta}_i \right). \quad (\text{A.58})$$

Consider the following Lyapunov function candidate

$$V = \frac{1}{2} \sum_{i=1}^n (\boldsymbol{\Omega}_i^T \mathbf{J}_{f_i} \boldsymbol{\Omega}_i + \boldsymbol{\beta}_i^T \boldsymbol{\beta}_i) + \sum_{i=1}^n \sum_{j=1}^n k_{ij}^p (1 - \eta_{ij}). \quad (\text{A.59})$$

The time-derivative of V in (A.59) evaluated along the system dynamics (A.58) with (2.21) and (3.48) is given by

$$\dot{V} = \sum_{i=1}^n \sum_{j=1}^n \left(-k_{ij}^p \boldsymbol{\Omega}_i^T \mathbf{q}_{ij} + \frac{1}{2} k_{ij}^p \mathbf{q}_{ij}^T \boldsymbol{\omega}_{ij} \right) + \sum_{i=1}^n \boldsymbol{\beta}_i^T \dot{\boldsymbol{\beta}}_i. \quad (\text{A.60})$$

Applying (3.49), with relations (2.22) and a similar relation to (A.35), yield

$$\dot{V} = - \sum_{i=1}^n \lambda_i \boldsymbol{\beta}_i^T \boldsymbol{\beta}_i, \quad (\text{A.61})$$

which is negative semi-definite. Therefore, following similar steps as in the proof of Theorem 3.3, we can show that $\boldsymbol{\Omega}_i$, $\boldsymbol{\beta}_i$ and $\boldsymbol{\omega}_i$ are bounded, for $i \in \mathcal{N}$, and invoking Barbălat Lemma, we conclude that $\boldsymbol{\beta}_i \rightarrow 0$ and $\dot{\boldsymbol{\beta}}_i \rightarrow 0$ for $i \in \mathcal{N}$. As a result, the input (3.49) reduces to

$$\sum_{j=1}^n k_{ij}^p \mathbf{q}_{ij} \rightarrow 0, \quad (\text{A.62})$$

for $i \in \mathcal{N}$. Then, if the communication graph is a tree, we know by Lemma 2.5 that the only solution to (A.62) is $\mathbf{q}_{ij} = 0$, for all $i, j \in \mathcal{N}$. As a result, we know that $\mathbf{q}_i \rightarrow \mathbf{q}_j$ for all $i, j \in \mathcal{N}$. Furthermore, since $\dot{\boldsymbol{\Omega}}_i$ is bounded, from (A.57) with (3.48), we know that $\dot{\boldsymbol{\omega}}_i$ is bounded, and from Barbălat Lemma, we conclude that $\boldsymbol{\omega}_i \rightarrow \boldsymbol{\omega}_j$ for all $i, j \in \mathcal{N}$. The last part of the proof follows similar arguments as in the last part of the proof of Theorem 3.2 using the result of Lemma 2.5.

A.2.5 Proof of Theorem 3.5

Similar to the proof of Theorem 3.4, the dynamics of Ω_i in (A.57) can be expressed, using (3.53), as

$$\Omega_i^T \mathbf{J}_{f_i} \dot{\Omega}_i = \Omega_i^T \left(-k_i^v \tilde{\phi}_i - \sum_{j=1}^n k_{ij}^p \mathbf{q}_{ij} \right). \quad (\text{A.63})$$

Consider the following Lyapunov function candidate

$$V = \frac{1}{2} \sum_{i=1}^n (\Omega_i^T \mathbf{J}_{f_i} \Omega_i + \beta_i^T \beta_i) + \sum_{i=1}^n \sum_{j=1}^n k_{ij}^p (1 - \eta_{ij}) + \sum_{i=1}^n 2k_i^v (1 - \zeta_i). \quad (\text{A.64})$$

Following similar steps as in the proof of Theorem 3.4 and using (3.56) with (3.13), the time-derivative of V is obtained as

$$\begin{aligned} \dot{V} = & - \sum_{i=1}^n k_i^v \Omega_i^T \tilde{\phi}_i + \sum_{i=1}^n \dot{\beta}_i^T \beta_i + \sum_{i=1}^n \sum_{j=1}^n k_{ij}^p \mathbf{q}_{ij}^T \mathbf{R}(\mathbf{Q}_i^e) \beta_i \\ & + \sum_{i=1}^n k_i^v \tilde{\phi}_i^T (\Omega_i + \mathbf{R}(\mathbf{Q}_i^e) \beta_i - \mathbf{R}(\tilde{\Phi}_i) \psi_i). \end{aligned} \quad (\text{A.65})$$

Then, applying the input vectors (3.57) yields

$$\dot{V} = - \sum_{i=1}^n \lambda_i \beta_i^T \beta_i - \sum_{i=1}^n \bar{\lambda}_i k_i^v \tilde{\phi}_i^T \tilde{\phi}_i, \quad (\text{A.66})$$

which leads us to conclude that Ω_i and β_i are bounded, and consequently, we can see from (3.56) and (3.15) that $\dot{\tilde{\Phi}}_i$ is bounded. Note that ψ_i is bounded from (3.57). Following similar arguments in the proof of Theorem 3.1 and Theorem 3.4, we conclude that $\beta_i \rightarrow 0$, $\dot{\beta}_i \rightarrow 0$ for $i \in \mathcal{N}$ and $\tilde{\phi}_i \rightarrow 0$ for $i \in \mathcal{I}$.

Therefore, the second equation in (3.38) with (3.57) reduces to (A.62) and we conclude from Lemma 2.5 that $\mathbf{q}_i \rightarrow \mathbf{q}_j$ for all $i, j \in \mathcal{N}$ if the communication graph is a tree. Also, similar to the proof of Theorem 3.4, we can verify that $\dot{\omega}_i$ is bounded and we conclude in virtue of Barbălat Lemma that $\omega_i \rightarrow \omega_j$ for all $i, j \in \mathcal{N}$.

Exploiting the above results, we can verify that $\ddot{\tilde{\Phi}}_i$ is bounded for $i \in \mathcal{I}$. Invoking Barbălat Lemma again leads us to conclude that $\tilde{\Phi}_i \rightarrow 0$ for $i \in \mathcal{I}$, since we have already shown that $\tilde{\phi}_i \rightarrow 0$ for $i \in \mathcal{I}$. As a result, we conclude from (3.56) that $\omega_i \rightarrow 0$ for $i \in \mathcal{I}$, and since we have shown above that $\omega_i \rightarrow \omega_j$ for all $i, j \in \mathcal{N}$, we conclude that $\omega_i \rightarrow 0$ for $i \in \mathcal{N}$. The last part of the proof follows from the result of Lemma 2.5.

A.3 Trajectory tracking of VTOL aircraft

A.3.1 Proof of Lemma 4.1

From equation (4.5), we have

$$\mathbf{R}(\mathbf{Q}_d)^T \hat{\mathbf{e}}_3 = \frac{m}{\mathcal{T}} (g\hat{\mathbf{e}}_3 - \mathbf{F}), \quad (\text{A.67})$$

since the left hand side of the above equation is a unit vector, from the definition of the rotation matrix, it is natural to choose the thrust input \mathcal{T} as in (4.6) to obtain

$$\mathbf{R}(\mathbf{Q}_d)^T \hat{\mathbf{e}}_3 = \frac{g\hat{\mathbf{e}}_3 - \mathbf{F}}{\|g\hat{\mathbf{e}}_3 - \mathbf{F}\|}. \quad (\text{A.68})$$

Let $\mathbf{Q}_d = (q_{d1}, q_{d2}, q_{d3}, \eta_d)^T$. Using (2.4), equation (A.67) is equivalent to

$$\begin{pmatrix} 2q_{d1}q_{d3} + 2\eta_d q_{d2} \\ 2q_{d2}q_{d3} - 2\eta_d q_{d1} \\ 1 - 2(q_{d1}^2 + q_{d2}^2) \end{pmatrix} = \frac{m}{\mathcal{T}} \begin{pmatrix} -\mu_1 \\ -\mu_2 \\ g - \mu_3 \end{pmatrix}, \quad (\text{A.69})$$

from which it is clear that there are multiple solutions for the desired attitude \mathbf{Q}_d . One possible solution can be obtained by fixing one of the above variables. A simple choice consists of picking $q_{d3} = 0$ which means that the desired axis of rotation is orthogonal to the $\hat{\mathbf{e}}_3$ -axis. In view of the unity constraint (2.2), we can rewrite (A.69) as

$$\begin{pmatrix} \eta_d q_{d2} \\ -\eta_d q_{d1} \\ \eta_d^2 - \frac{1}{2} \end{pmatrix} = \frac{m}{2\mathcal{T}} \begin{pmatrix} -\mu_1 \\ -\mu_2 \\ g - \mu_3 \end{pmatrix}, \quad (\text{A.70})$$

and we can derive one solution of η_d , q_{d1} and q_{d2} as given in (4.7), which are always defined under the condition that $\eta_d \neq 0$ and $\mathcal{T} \neq 0$. We can see that $\mathcal{T} = 0$ only if $\mathbf{F} = (0, 0, g)$, and $\eta_d = 0$ only if

$$(g - \mu_3) = -\frac{\mathcal{T}}{m} = -\|g\hat{\mathbf{e}}_3 - \mathbf{F}\| \quad (\text{A.71})$$

which is only possible if: $\mathbf{F} = (0, 0, x)$, with $x \geq g$, from which we obtain condition (4.8).

The desired angular velocity vector $\boldsymbol{\omega}_d$ is given by

$$\boldsymbol{\omega}_d = 2 \begin{pmatrix} \eta_d \mathbf{I}_3 + \mathbf{S}(\mathbf{q}_d) \\ -\mathbf{q}_d^T \end{pmatrix}^T \dot{\mathbf{Q}}_d. \quad (\text{A.72})$$

Hence, taking the time-derivative of (4.7) we can write

$$\dot{\eta}_d = \frac{(g - \mu_3)}{4\eta_d\gamma_1^3} \begin{pmatrix} -\mu_1 & -\mu_2 & \frac{-(\mu_1^2 + \mu_2^2)}{(g - \mu_3)} \end{pmatrix} \dot{\mathbf{F}}, \quad (\text{A.73})$$

$$\dot{\mathbf{q}}_d = \frac{1}{\eta_d^3\gamma_1^4} \begin{pmatrix} -\mu_1\mu_2\gamma_3 & -\mu_2^2\gamma_3 + 4\eta_d^2\gamma_3^3 & \mu_2\gamma_2^2 \\ \mu_1^2\gamma_3 - 4\eta_d^2\gamma_3^3 & \mu_1\mu_2\gamma_3 & -\mu_1\gamma_2^2 \\ 0 & 0 & 0 \end{pmatrix} \dot{\mathbf{F}}, \quad (\text{A.74})$$

with $\gamma_1 = \sqrt{(g - \mu_3)^2 + \mu_1^2 + \mu_2^2}$, $\gamma_2 = \gamma_1 + (g - \mu_3)$ and $\gamma_3 = 2\gamma_1 + (g - \mu_3)$. From this, and using (A.72) we obtain the expression of $\boldsymbol{\omega}_d$ in terms of the elements of the intermediary control input as given in (4.9) with (4.10), and this ends the proof.

A.3.2 Proof of Theorem 4.1

First, we can see that with Assumption 4.1, the extraction condition (4.8) is satisfied and Lemma (4.1) can be used to derive the necessary thrust input and the desired attitude for the aircraft.

The translational dynamics given in (4.11) can be rewritten in view of (4.19) as

$$\dot{\tilde{\mathbf{v}}} = -k_p\chi(\tilde{\mathbf{p}}) - k_v\chi(\tilde{\mathbf{v}}) - \frac{2\mathcal{T}}{m}\mathbf{R}(\mathbf{Q})^T\mathbf{S}(\tilde{\mathbf{q}})\tilde{\mathbf{q}}. \quad (\text{A.75})$$

In addition, using (4.18), we have

$$\dot{\tilde{\boldsymbol{\Omega}}} = \dot{\boldsymbol{\omega}} - \mathbf{R}(\tilde{\mathbf{Q}})\dot{\boldsymbol{\omega}}_d + \mathbf{S}(\tilde{\boldsymbol{\omega}})\mathbf{R}(\tilde{\mathbf{Q}})\boldsymbol{\omega}_d - \dot{\tilde{\boldsymbol{\beta}}}, \quad (\text{A.76})$$

which, using the rotational dynamics (4.2), leads to the following rotational error dynamics

$$\mathbf{J}_f\dot{\tilde{\boldsymbol{\Omega}}} = \boldsymbol{\Gamma} - \mathbf{H}(\boldsymbol{\omega}, \boldsymbol{\omega}_d, \dot{\boldsymbol{\omega}}_d, \tilde{\mathbf{Q}}) - \mathbf{J}_f\dot{\tilde{\boldsymbol{\beta}}}, \quad (\text{A.77})$$

with $\mathbf{H}(\cdot)$ is given in (4.20). Therefore, applying the input torque (4.19) leads us to write

$$\mathbf{J}_f\dot{\tilde{\boldsymbol{\Omega}}} = -k_q\tilde{\mathbf{q}} - k_\Omega\tilde{\boldsymbol{\Omega}}. \quad (\text{A.78})$$

Consider the following Lyapunov function candidate

$$V = \frac{1}{2}\tilde{\mathbf{v}}^T\tilde{\mathbf{v}} + k_p\sum_{j=1}^3\int_0^{\tilde{p}^j}\sigma(s)ds + \frac{1}{2}\tilde{\boldsymbol{\Omega}}^T\mathbf{J}_f\tilde{\boldsymbol{\Omega}} + 2k_q(1 - \tilde{\eta}), \quad (\text{A.79})$$

with $\tilde{\mathbf{p}} = (\tilde{p}^1, \tilde{p}^2, \tilde{p}^3)^T$ and σ is the saturation function defined in (2.33). The time-derivative of V evaluated along (A.75) and (A.78), using (2.14), is obtained as

$$\begin{aligned} \dot{V} = & \tilde{\mathbf{v}}^T \left(-k_p \chi(\tilde{\mathbf{p}}) - k_d \chi(\tilde{\mathbf{v}}) - \frac{2\mathcal{T}}{m} \mathbf{R}(\mathbf{Q})^T \mathbf{S}(\bar{\mathbf{q}}) \tilde{\mathbf{q}} \right) + k_p \tilde{\mathbf{v}}^T \chi(\tilde{\mathbf{p}}) \\ & + \mathbf{\Omega}^T (-k_q \tilde{\mathbf{q}} - k_\Omega \mathbf{\Omega}) + k_q \tilde{\mathbf{q}}^T \tilde{\boldsymbol{\omega}}, \end{aligned} \quad (\text{A.80})$$

which, in view of (4.18), gives

$$\dot{V} = -k_d \tilde{\mathbf{v}}^T \chi(\tilde{\mathbf{v}}) - k_\Omega \mathbf{\Omega}^T \mathbf{\Omega} + \left(k_q \boldsymbol{\beta} - \frac{2\mathcal{T}}{m} \mathbf{R}(\mathbf{Q})^T \mathbf{S}(\bar{\mathbf{q}}) \tilde{\mathbf{q}} \right)^T \tilde{\mathbf{q}}. \quad (\text{A.81})$$

Finally, using (4.21) we obtain

$$\dot{V} = -k_d \tilde{\mathbf{v}}^T \chi(\tilde{\mathbf{v}}) - k_\Omega \mathbf{\Omega}^T \mathbf{\Omega} - k_q k_\beta \tilde{\mathbf{q}}^T \tilde{\mathbf{q}}, \quad (\text{A.82})$$

which is negative semi-definite, and we conclude that $\tilde{\mathbf{v}}$, $\tilde{\mathbf{p}}$ and $\mathbf{\Omega}$ are bounded, and consequently $\tilde{\boldsymbol{\omega}}$ and $\dot{\tilde{\mathbf{q}}}_i$ are bounded. Note that $\tilde{\mathbf{q}}$ is naturally bounded from the definition of unit-quaternion. In addition, we know that $\dot{\tilde{\mathbf{v}}}$ and $\dot{\mathbf{\Omega}}$ are bounded in view of (A.75) and (A.78) respectively. As a result, we conclude that \dot{V} is bounded. Invoking Barbălat Lemma, we can conclude that $\tilde{\mathbf{q}} \rightarrow 0$, $\tilde{\mathbf{v}} \rightarrow 0$ and $\mathbf{\Omega} \rightarrow 0$, which leads us to conclude from (4.18) and (4.21) that $\tilde{\boldsymbol{\omega}} \rightarrow 0$. Furthermore, Invoking the extended Barbălat Lemma (Lemma 2.3), we conclude that $\dot{\tilde{\mathbf{v}}} \rightarrow 0$ since $\chi(\tilde{\mathbf{p}})$ is uniformly continuous, *i.e.*, $\frac{d}{dt} \chi(\tilde{\mathbf{p}}) = h(\tilde{\mathbf{p}}) \dot{\tilde{\mathbf{v}}}$ is bounded, where the diagonal matrix $h(\cdot)$ is given in (2.34) and contains bounded elements in view of property P3 in section 2.6. As a result, the translational tracking error dynamics in (A.75) will reduce to $-k_p \tilde{\mathbf{p}} = 0$, which leads us to conclude that $\tilde{\mathbf{p}} \rightarrow 0$.

To complete the proof, we need to show that the input torque in (4.19) is bounded. Exploiting the above boundedness results, we can easily show that $\boldsymbol{\Gamma}$ is bounded if $\boldsymbol{\omega}_d$, $\dot{\boldsymbol{\omega}}_d$ and $\dot{\boldsymbol{\beta}}$ are bounded. By taking the time-derivative of (4.21), we can easily show that $\frac{d}{dt} (\mathbf{S}(\bar{\mathbf{q}})^T \mathbf{R}(\mathbf{Q}))$ is bounded if $\boldsymbol{\omega}$, $\tilde{\boldsymbol{\omega}}$ are bounded, and we know that $\dot{\boldsymbol{\beta}}$ is bounded if \mathcal{T} and $\boldsymbol{\omega}_d$ are bounded. As a result, $\boldsymbol{\Gamma}$ is bounded if $\dot{\mathcal{T}}$, $\boldsymbol{\omega}_d$ and $\dot{\boldsymbol{\omega}}_d$ are bounded. Using the above boundedness results, it is clear that $\dot{\mathbf{F}}$ and $\ddot{\mathbf{F}}$ are bounded, and $\mathbf{F} \rightarrow \dot{\mathbf{v}}_d$, $\dot{\mathbf{F}} \rightarrow \ddot{\mathbf{v}}_d$ and $\ddot{\mathbf{v}} \rightarrow \mathbf{v}_d^{(3)}$, where $\ddot{\mathbf{v}}_d$ and $\mathbf{v}_d^{(3)}$ are, respectively, the third and fourth derivatives of the desired trajectory, which are assumed to be bounded. Hence, using (4.6), (4.9), (4.10), (4.15)-(4.17) and Assumption 4.1, we conclude that $\dot{\mathcal{T}}$, $\boldsymbol{\omega}_d$ and $\dot{\boldsymbol{\omega}}_d$ are bounded, and this ends the proof.

A.3.3 Proof of Theorem 4.2

First, it is easy to check that if the desired trajectory and the controller gains k_p and k_d satisfy Assumption 4.1, condition (4.8) is always satisfied, and hence it is always

possible to extract the magnitude of the thrust and the desired attitude from (4.6) and (4.7) respectively for the VTOL vehicle.

The translational error dynamics are given in (4.30). Let us define the observation error vector as, $\tilde{\mathbf{z}} := \dot{\tilde{\boldsymbol{\xi}}} = (\hat{\mathbf{z}} - \mathbf{z})$. Applying the torque input (4.40) in (4.37), we obtain the closed loop dynamics

$$\mathbf{J}_f \dot{\boldsymbol{\Omega}} = -k_q \tilde{\mathbf{q}} - k_\Omega \boldsymbol{\Omega} - \boldsymbol{\Upsilon} \left(\tilde{\mathbf{z}} + L_v \tilde{\boldsymbol{\xi}} \right), \quad (\text{A.83})$$

and the observation error dynamics can be obtained in view of (4.30) and (4.39) as

$$\dot{\tilde{\mathbf{z}}} = -L_p \tilde{\mathbf{z}} - L_v^2 \tilde{\boldsymbol{\xi}} + \boldsymbol{\Upsilon}^T \boldsymbol{\Omega}. \quad (\text{A.84})$$

Consider first the following Lyapunov function candidate

$$V = V_t + V_a. \quad (\text{A.85})$$

with

$$V_t = \frac{1}{2} \left(\mathbf{z}^T \mathbf{z} + k_p \boldsymbol{\xi}^T \boldsymbol{\xi} + k_d (\boldsymbol{\xi} - \boldsymbol{\psi})^T (\boldsymbol{\xi} - \boldsymbol{\psi}) \right), \quad (\text{A.86})$$

and

$$\begin{aligned} V_a = & \frac{1}{2} \left(\tilde{\mathbf{z}} + L_v \tilde{\boldsymbol{\xi}} \right)^T \left(\tilde{\mathbf{z}} + L_v \tilde{\boldsymbol{\xi}} \right) + \frac{1}{2} L_v L_p \tilde{\boldsymbol{\xi}}^T \tilde{\boldsymbol{\xi}} \\ & + \frac{1}{2} \boldsymbol{\Omega}^T \mathbf{I}_f \boldsymbol{\Omega} + 2k_q (1 - \tilde{\eta}). \end{aligned} \quad (\text{A.87})$$

The time-derivative of V_t is obtained, using (4.30) with (4.31)-(4.32), as

$$\begin{aligned} \dot{V}_t = & \mathbf{z}^T \left(-\frac{2T}{m} \mathbf{R}(\mathbf{Q})^T \mathbf{S}(\bar{\mathbf{q}}) \tilde{\mathbf{q}} - k_p \boldsymbol{\xi} - k_d (\boldsymbol{\xi} - \boldsymbol{\psi}) \right) \\ & + \mathbf{z}^T (k_p \boldsymbol{\xi} + k_d (\boldsymbol{\xi} - \boldsymbol{\psi})) - k_d \dot{\boldsymbol{\psi}}^T (\boldsymbol{\xi} - \boldsymbol{\psi}) \\ = & -\frac{2T}{m} \mathbf{z}^T \mathbf{R}(\mathbf{Q})^T \mathbf{S}(\bar{\mathbf{q}}) \tilde{\mathbf{q}} - k_d k_\psi (\boldsymbol{\xi} - \boldsymbol{\psi})^T (\boldsymbol{\xi} - \boldsymbol{\psi}). \end{aligned} \quad (\text{A.88})$$

In addition, in view of (A.83) and (A.84) with (2.14) and (4.41), the time-derivative of V_a is given as

$$\begin{aligned} \dot{V}_a = & - (L_p - L_v) \tilde{\mathbf{z}}^T \tilde{\mathbf{z}} - L_v^3 \tilde{\boldsymbol{\xi}}^T \tilde{\boldsymbol{\xi}} + (\tilde{\mathbf{z}} + L_v \tilde{\boldsymbol{\xi}})^T \boldsymbol{\Gamma}^T \boldsymbol{\Omega} \\ & + \boldsymbol{\Omega}^T \left(-k_q \tilde{\mathbf{q}} - k_\Omega \boldsymbol{\Omega} - \boldsymbol{\Gamma} \left(\tilde{\mathbf{z}} + L_v \tilde{\boldsymbol{\xi}} \right) \right) + k_q \tilde{\mathbf{q}}^T (\boldsymbol{\Omega} + \boldsymbol{\beta}) \\ = & - (L_p - L_v) \tilde{\mathbf{z}}^T \tilde{\mathbf{z}} - L_v^3 \tilde{\boldsymbol{\xi}}^T \tilde{\boldsymbol{\xi}} \\ & - k_\Omega \boldsymbol{\Omega}^T \boldsymbol{\Omega} - k_q k_\beta \tilde{\mathbf{q}}^T \tilde{\mathbf{q}} + \frac{2T}{m} \tilde{\mathbf{q}}^T \mathbf{S}(\bar{\mathbf{q}})^T \mathbf{R}(\mathbf{Q}) (\hat{\mathbf{z}} + L_p \tilde{\boldsymbol{\xi}}). \end{aligned} \quad (\text{A.89})$$

Therefore, the time-derivative of V evaluated along the closed loop dynamics is obtained as

$$\begin{aligned} \dot{V} = & -k_d k_\psi (\boldsymbol{\xi} - \boldsymbol{\psi})^T (\boldsymbol{\xi} - \boldsymbol{\psi}) - (L_p - L_v) \tilde{\mathbf{z}}^T \tilde{\mathbf{z}} - L_v^3 \tilde{\boldsymbol{\xi}}^T \tilde{\boldsymbol{\xi}} \\ & - k_\Omega \boldsymbol{\Omega}^T \boldsymbol{\Omega} - k_q k_\beta \tilde{\mathbf{q}}^T \tilde{\mathbf{q}} + \frac{2\mathcal{T}}{m} \tilde{\mathbf{q}}^T \mathbf{S}(\bar{\mathbf{q}})^T \mathbf{R}(\mathbf{Q})(\tilde{\mathbf{z}} + L_p \tilde{\boldsymbol{\xi}}). \end{aligned} \quad (\text{A.90})$$

Using the fact that $\|\mathbf{R}(\mathbf{Q})^T \mathbf{S}(\bar{\mathbf{q}})\| \leq 1$ and $L_p > L_v$ from (4.42), the following upper bound of \dot{V} is obtained

$$\begin{aligned} \dot{V} \leq & -k_d k_\psi \|\boldsymbol{\xi} - \boldsymbol{\psi}\|^2 - (L_p - L_v - \sigma_1) \|\tilde{\mathbf{z}}\|^2 - k_\Omega \|\boldsymbol{\Omega}\|^2 \\ & - (L_v^3 - \sigma_2) \|\tilde{\boldsymbol{\xi}}\|^2 - \left(k_q k_\beta - \frac{\mathcal{T}_b^2}{m^2} \left(\frac{1}{\sigma_1} + \frac{L_p^2}{\sigma_2} \right) \right) \|\tilde{\mathbf{q}}\|^2, \end{aligned} \quad (\text{A.91})$$

where \mathcal{T}_b is given in (4.14), and we have used young's inequality, *i.e.*, for any real numbers a and b , we have $2ab \leq a^2/\sigma + \sigma b^2$, for some $\sigma > 0$. Therefore, \dot{V} is negative semi-definite if condition (4.42) is satisfied. Hence, we can conclude that \mathbf{z} , $\boldsymbol{\xi}$, $\boldsymbol{\psi}$, $\boldsymbol{\Omega}$, $\tilde{\mathbf{z}}$ and $\tilde{\boldsymbol{\xi}}$ are bounded. Consequently, $\dot{\boldsymbol{\theta}}$, $\dot{\boldsymbol{\psi}}$, $\dot{\mathbf{z}}$ and $\dot{\tilde{\mathbf{z}}}$ are bounded. Also, we can see that $(\dot{\boldsymbol{\xi}} - \dot{\boldsymbol{\psi}})$ is bounded.

Since $\tilde{\mathbf{q}}$ is bounded, we can verify from (4.41) that $\boldsymbol{\beta}$ is bounded, and hence $\tilde{\boldsymbol{\omega}} = (\boldsymbol{\Omega} + \boldsymbol{\beta})$ is bounded, which leads us to conclude that $\dot{\tilde{\mathbf{q}}}$ is bounded. In addition, we can verify that $\dot{\boldsymbol{\Omega}}$ is bounded from (A.83). As a result, \dot{V} is bounded. Invoking Barbălat lemma, we conclude that $(\boldsymbol{\xi} - \boldsymbol{\psi}) \rightarrow 0$, $\tilde{\boldsymbol{\xi}} \rightarrow 0$, $\tilde{\mathbf{z}} \rightarrow 0$, $\boldsymbol{\Omega} \rightarrow 0$ and $\tilde{\mathbf{q}} \rightarrow 0$, and therefore we have $\mathbf{R}(\tilde{\mathbf{Q}}) \rightarrow I_3$ and $\tilde{\eta} \rightarrow \pm 1$.

Using the above results, we know that $(\dot{\boldsymbol{\xi}} - \dot{\boldsymbol{\psi}}) = \dot{\mathbf{z}} - k_\psi (\boldsymbol{\xi} - \boldsymbol{\psi})$ is bounded, and since we have shown that $(\boldsymbol{\xi} - \boldsymbol{\psi}) \rightarrow 0$, we conclude by virtue of Barbălat lemma that $(\dot{\boldsymbol{\xi}} - \dot{\boldsymbol{\psi}}) \rightarrow 0$. Consequently, we have $\dot{\boldsymbol{\xi}} = \dot{\mathbf{z}} \rightarrow 0$, since $\dot{\boldsymbol{\psi}} = k_\psi (\boldsymbol{\xi} - \boldsymbol{\psi}) \rightarrow 0$. Also, since \mathbf{z} and $\tilde{\mathbf{z}}$ converge to zero, it is clear that $\dot{\tilde{\mathbf{z}}}$ tends to zero, and with the limit of $\tilde{\boldsymbol{\xi}}$, one can conclude that $\boldsymbol{\nu} \rightarrow 0$, and consequently, $\boldsymbol{\beta} \rightarrow 0$ implying that $\tilde{\boldsymbol{\omega}} \rightarrow 0$.

Exploiting the above boundedness results, and since $\tilde{\mathbf{q}} \rightarrow 0$ and $(\boldsymbol{\xi} - \boldsymbol{\psi}) \rightarrow 0$, we can conclude from the translational error dynamics (4.30) with (4.31) that $\dot{\mathbf{z}} \rightarrow 0$ by invoking the extended version of Barbălat lemma (Lemma 2.3). Hence, we conclude from (4.30) that $\boldsymbol{\xi} \rightarrow 0$ and consequently $\boldsymbol{\psi} \rightarrow 0$.

The second part of the proof consist of showing the boundedness and convergence of $\tilde{\mathbf{p}}$ and $\tilde{\mathbf{v}}$. Note that the dynamics of the auxiliary variable θ in (4.27) can be rewritten using (4.28) as

$$\ddot{\boldsymbol{\theta}} = -k_p \chi(\boldsymbol{\theta}) - k_d \chi(\dot{\boldsymbol{\theta}}) - \mathbf{u}, \quad (\text{A.92})$$

which is equivalent to (2.35) with $\boldsymbol{\varepsilon} = -\mathbf{u} = (k_r \boldsymbol{\xi} + k_v (\boldsymbol{\xi} - \boldsymbol{\psi}))$. Exploiting the above results, we can verify that \mathbf{u} is bounded and converges to zero asymptotically. Therefore, we conclude from the result of Lemma 2.6 that $\boldsymbol{\theta}$ and $\dot{\boldsymbol{\theta}}$ are bounded and

converge asymptotically to zero, and as a result, $\tilde{\mathbf{p}}$ and $\tilde{\mathbf{v}}$ are bounded and converge asymptotically to zero. The rest of the proof is similar to the proof of Theorem 4.1.

A.4 Formation control of VTOL UAVs

A.4.1 proof of Theorem 5.1

First, it is easy to check that if the desired trajectory and the controller gains k_i^p and k_i^d satisfy Assumption 4.1, condition (4.8) is always satisfied, and hence it is always possible to extract the magnitude of the thrust and the desired attitude from (4.6) and (4.7) respectively for each VTOL vehicle.

The translational error dynamics can be written, using (5.1), (5.5)-(5.6) as

$$\dot{\mathbf{z}}_i = \mathbf{u}_i - \frac{2\mathcal{T}_i}{m_i} \mathbf{R}(\mathbf{Q}_i)^T \mathbf{S}(\bar{\mathbf{q}}_i) \tilde{\mathbf{q}}_i. \quad (\text{A.93})$$

For the rotational dynamics, we define the variable

$$\boldsymbol{\Omega}_i = \tilde{\boldsymbol{\omega}}_i - \boldsymbol{\beta}_i, \quad (\text{A.94})$$

The time-derivative of $\boldsymbol{\Omega}_i$ can be obtained using (2.8) and (2.15) as

$$\dot{\boldsymbol{\Omega}}_i = \dot{\boldsymbol{\omega}}_i - \mathbf{R}(\tilde{\mathbf{Q}}_i) \dot{\boldsymbol{\omega}}_{d_i} + \mathbf{S}(\tilde{\boldsymbol{\omega}}_i) \mathbf{R}(\tilde{\mathbf{Q}}_i) \boldsymbol{\omega}_{d_i} - \dot{\boldsymbol{\beta}}_i. \quad (\text{A.95})$$

Using the rotational dynamics (5.2), we can write

$$\mathbf{J}_{f_i} \dot{\boldsymbol{\Omega}}_i = \boldsymbol{\Gamma}_i - \mathbf{H}_i(\boldsymbol{\omega}_i, \boldsymbol{\omega}_{d_i}, \dot{\boldsymbol{\omega}}_{d_i}, \tilde{\mathbf{Q}}_i) - \mathbf{J}_{f_i} \dot{\boldsymbol{\beta}}_i, \quad (\text{A.96})$$

with $\mathbf{H}_i(\cdot)$ is given in (5.15). Consider the following Lyapunov function candidate

$$V = \frac{1}{2} \sum_{i=1}^n \left(\mathbf{z}_i^T \mathbf{z}_i + \frac{1}{2} \sum_{j=1}^n k_{ij} \boldsymbol{\xi}_{ij}^T \boldsymbol{\xi}_{ij} + \boldsymbol{\Omega}_i^T \mathbf{J}_{f_i} \boldsymbol{\Omega}_i + 2k_i^q \left(\tilde{\mathbf{q}}_i^T \tilde{\mathbf{q}}_i + (1 - \tilde{\eta}_i)^2 \right) \right). \quad (\text{A.97})$$

Note that $\left(\tilde{\mathbf{q}}_i^T \tilde{\mathbf{q}}_i + (1 - \tilde{\eta}_i)^2 \right) = 2(1 - \tilde{\eta}_i)$. The time-derivative of V evaluated along the closed loop dynamics (A.93) and (A.96), using (2.14), is obtained as

$$\begin{aligned} \dot{V} = & \sum_{i=1}^n \mathbf{z}_i^T \left(\mathbf{u}_i - \frac{2\mathcal{T}_i}{m_i} \mathbf{R}(\mathbf{Q}_i)^T \mathbf{S}(\bar{\mathbf{q}}_i) \tilde{\mathbf{q}}_i \right) + \frac{1}{2} \sum_{i=1}^n \sum_{j=1}^n k_{ij} \mathbf{z}_{ij}^T \boldsymbol{\xi}_{ij} \\ & + \sum_{i=1}^n k_i^q \tilde{\mathbf{q}}_i^T (\boldsymbol{\Omega}_i + \boldsymbol{\beta}_i) + \sum_{i=1}^n \boldsymbol{\Omega}_i^T \left(\boldsymbol{\Gamma}_i - \mathbf{H}_i(\cdot) - \mathbf{J}_{f_i} \dot{\boldsymbol{\beta}}_i \right), \end{aligned} \quad (\text{A.98})$$

with $\mathbf{z}_{ij} = (\mathbf{z}_i - \mathbf{z}_j)$. Using the properties of the undirected communication graph, *i.e.*, $k_{ij} = k_{ji}$, and the relation $\boldsymbol{\xi}_{ij} = -\boldsymbol{\xi}_{ji}$, we can show that

$$\begin{aligned} \frac{1}{2} \sum_{i=1}^n \sum_{j=1}^n k_{ij} \mathbf{z}_{ij}^T \boldsymbol{\xi}_{ij} &= \frac{1}{2} \sum_{i=1}^n \sum_{j=1}^n k_{ij} \mathbf{z}_i^T \boldsymbol{\xi}_{ij} - \frac{1}{2} \sum_{j=1}^n \sum_{i=1}^n k_{ji} \mathbf{z}_i^T \boldsymbol{\xi}_{ji} \\ &= \sum_{i=1}^n \sum_{j=1}^n k_{ij} \mathbf{z}_i^T \boldsymbol{\xi}_{ij}. \end{aligned} \quad (\text{A.99})$$

Applying the input control (5.7) and (5.13), we obtain

$$\dot{V} = \sum_{i=1}^n \left(\mathbf{z}_i^T \left(-k_i^v \mathbf{z}_i - \frac{2\mathcal{T}_i}{m_i} \mathbf{R}(\mathbf{Q}_i)^T \mathbf{S}(\tilde{\mathbf{q}}_i) \tilde{\mathbf{q}}_i \right) - k_i^\Omega \boldsymbol{\Omega}_i^T \boldsymbol{\Omega}_i + k_i^q \tilde{\mathbf{q}}_i^T \boldsymbol{\beta}_i \right), \quad (\text{A.100})$$

which using (5.14) yields to the negative semi-definite time-derivative

$$\dot{V} = \sum_{i=1}^n \left(-k_i^v \mathbf{z}_i^T \mathbf{z}_i - k_i^\Omega \boldsymbol{\Omega}_i^T \boldsymbol{\Omega}_i - k_i^q k_i^\beta \tilde{\mathbf{q}}_i^T \tilde{\mathbf{q}}_i \right). \quad (\text{A.101})$$

Therefore, we conclude that \mathbf{z}_i and $\boldsymbol{\Omega}_i$ are bounded for $i \in \mathcal{N}$ and $\boldsymbol{\xi}_{ij}$ is bounded for all $(i, j) \in \mathcal{E}$. Note that $\tilde{\mathbf{q}}_i$ is naturally bounded from the definition of unit-quaternion. Also, since the communication graph is assumed to be connected, we know that $\boldsymbol{\xi}_{ij}$ is bounded for all $i, j \in \mathcal{N}$. Furthermore, we can see from (5.5) and (A.93) that $\dot{\mathbf{z}}_i$ and $\ddot{\boldsymbol{\theta}}_i$ are bounded for $i \in \mathcal{N}$.

From equation (5.14), we know that $\boldsymbol{\beta}_i$ is bounded since $\tilde{\mathbf{q}}_i$ and \mathbf{z}_i are bounded, and hence $\tilde{\boldsymbol{\omega}}_i$ is bounded from (A.94), which leads us to conclude that $\check{\tilde{\mathbf{q}}}_i$ is bounded from (2.14). In addition, from equation (A.96) with (5.13), we can conclude that $\dot{\boldsymbol{\Omega}}_i$ is bounded. As a result, \dot{V} is bounded. Invoking Barbălat lemma we conclude that $\mathbf{z}_i \rightarrow 0$, $\boldsymbol{\Omega}_i \rightarrow 0$ and $\tilde{\mathbf{q}}_i \rightarrow 0$, and therefore, $\tilde{\boldsymbol{\omega}}_i \rightarrow 0$, for $i \in \mathcal{N}$.

Using the above boundedness and convergence results, we can see that $\boldsymbol{\xi}_{ij}$ is uniformly continuous since \mathbf{z}_i is bounded and δ_{ij} is a constant. Invoking the extended Barbălat lemma (Lemma 2.3), we conclude from (A.93) that $\dot{\mathbf{z}}_i \rightarrow 0$, for $i \in \mathcal{N}$. Then, the closed loop translational dynamics (A.93) with (5.7) reduce to

$$\sum_{j=1}^n k_{ij} (\boldsymbol{\xi}_i - \boldsymbol{\xi}_j - \boldsymbol{\delta}_{ij}) = 0, \quad (\text{A.102})$$

for $i \in \mathcal{N}$. Multiplying both sides of the above set of equations by $(\boldsymbol{\xi}_i - \boldsymbol{\delta}_i)$, and

taking the sum over i , we obtain the equivalent relation

$$\sum_{i=1}^n \sum_{j=1}^n k_{ij} (\boldsymbol{\xi}_i - \boldsymbol{\delta}_i)^T (\boldsymbol{\xi}_i - \boldsymbol{\xi}_j - \boldsymbol{\delta}_{ij}) = 0, \quad (\text{A.103})$$

where the constant vector $\boldsymbol{\delta}_i$ can be regarded as the desired position of the i^{th} aircraft with respect to the center of the formation. It is then clear that $\boldsymbol{\delta}_{ij} = (\boldsymbol{\delta}_i - \boldsymbol{\delta}_j)$. Using similar steps as in (A.99), we can show that

$$\sum_{i=1}^n \sum_{j=1}^n k_{ij} (\boldsymbol{\xi}_i - \boldsymbol{\delta}_i)^T (\boldsymbol{\xi}_i - \boldsymbol{\xi}_j - \boldsymbol{\delta}_{ij}) = \frac{1}{2} \sum_{i=1}^n \sum_{j=1}^n k_{ij} \boldsymbol{\xi}_{ij}^T \boldsymbol{\xi}_{ij} = 0, \quad (\text{A.104})$$

from which we conclude that $(\boldsymbol{\xi}_i - \boldsymbol{\xi}_j) \rightarrow \boldsymbol{\delta}_{ij}$, for all $(i, j) \in \mathcal{E}$. Since the communication graph is assumed to be connected, we conclude that $(\boldsymbol{\xi}_i - \boldsymbol{\xi}_j) \rightarrow \boldsymbol{\delta}_{ij}$, for all $i, j \in \mathcal{N}$.

Exploiting the above results, we know that the input \mathbf{u}_i , given in (5.7), is globally bounded and converges asymptotically to zero. Hence, the dynamics of $\boldsymbol{\theta}_i$ in (5.5) can be rewritten as

$$\ddot{\boldsymbol{\theta}}_i = -k_i^p \chi(\boldsymbol{\theta}_i) - k_i^d \chi(\dot{\boldsymbol{\theta}}_i) - \mathbf{u}_i, \quad (\text{A.105})$$

which is equivalent to (2.35) with $\boldsymbol{\varepsilon}_i = -\mathbf{u}_i$. Therefore, the conditions of Lemma 2.6 are satisfied and we conclude that $\boldsymbol{\theta}_i$ and $\dot{\boldsymbol{\theta}}_i$ are bounded and $\boldsymbol{\theta}_i \rightarrow 0$, $\dot{\boldsymbol{\theta}}_i \rightarrow 0$ for $i \in \mathcal{N}$. As a result, we conclude from (5.6) that $(\mathbf{v}_i - \mathbf{v}_d) \rightarrow 0$ and $(\mathbf{p}_i - \mathbf{p}_j) \rightarrow \boldsymbol{\delta}_{ij}$, for all $i, j \in \mathcal{N}$.

To complete the proof, we need to verify that the torque input for each aircraft is bounded. From (5.13), we can see that $\boldsymbol{\Gamma}_i$ is bounded if $\boldsymbol{\omega}_{d_i}$, $\dot{\boldsymbol{\omega}}_{d_i}$ and $\dot{\mathcal{T}}_i$ are bounded. Using the above boundedness results, it is clear that $\dot{\mathbf{F}}_i$ and $\ddot{\mathbf{F}}_i$ are bounded and $\mathbf{F}_i \rightarrow \dot{\mathbf{v}}_d$, $\dot{\mathbf{F}}_i \rightarrow \ddot{\mathbf{v}}_d$ and $\ddot{\mathbf{F}}_i \rightarrow \mathbf{v}_d^{(3)}$, for $i \in \mathcal{N}$. Note that $\ddot{\mathbf{v}}_d$ and $\mathbf{v}_d^{(3)}$ are assumed to be bounded. In addition, from (4.6), we can write

$$\dot{\mathcal{T}}_i = \frac{m_i^2}{\mathcal{I}_i} (g\hat{\mathbf{e}}_3 - \mathbf{F}_i)^T \dot{\mathbf{F}}_i. \quad (\text{A.106})$$

Hence, from the expressions of $\boldsymbol{\omega}_{d_i}$ and $\dot{\boldsymbol{\omega}}_{d_i}$, given in (5.9)-(5.12), and in view of Assumption 4.1, we can conclude that $\boldsymbol{\omega}_{d_i}$, $\dot{\boldsymbol{\omega}}_{d_i}$ and $\dot{\mathcal{T}}_i$ are bounded for $i \in \mathcal{N}$.

A.4.2 Proof of Theorem 5.2

Similar to the proof of Theorem 5.1, if the desired trajectory and the controller gains k_i^p and k_i^d satisfy Assumption 4.1, it is always possible to extract the magnitude of the thrust and the desired attitude from (4.6) and (4.7) respectively.

The translational error dynamics can be obtained similar to (A.93). Let us define the error vector: $\tilde{\mathbf{z}}_i := \dot{\tilde{\boldsymbol{\xi}}}_i = (\dot{\tilde{\boldsymbol{\xi}}}_i - \dot{\boldsymbol{\xi}}_i)$, which, using (5.6), can be rewritten as

$$\tilde{\mathbf{z}}_i = \hat{\mathbf{z}}_i - \mathbf{z}_i - \mathbf{v}_d. \quad (\text{A.107})$$

Applying the input torque (5.35) in (5.33), using (A.107), we obtain the angular velocity error dynamics

$$\begin{aligned} \mathbf{J}_{f_i} \dot{\boldsymbol{\Omega}}_i &= -k_i^q \tilde{\mathbf{q}}_i - k_i^\Omega \boldsymbol{\Omega}_i - k_i^v \boldsymbol{\Upsilon}_i (\tilde{\mathbf{z}}_i + L_v \tilde{\boldsymbol{\xi}}_i) \\ &\quad - \boldsymbol{\Upsilon}_i \sum_{j=1}^n k_{ij} \left((\tilde{\mathbf{z}}_i + L_v \tilde{\boldsymbol{\xi}}_i) - (\tilde{\mathbf{z}}_j + L_v \tilde{\boldsymbol{\xi}}_j) \right), \end{aligned} \quad (\text{A.108})$$

for $i \in \mathcal{N}$. In addition, the dynamics of $\tilde{\mathbf{z}}_i$ can be determined using (5.6), (5.37) and (A.107), as

$$\dot{\tilde{\mathbf{z}}}_i = -L_p \tilde{\mathbf{z}}_i - L_v^2 \tilde{\boldsymbol{\xi}}_i + k_i^v \boldsymbol{\Upsilon}_i^T \boldsymbol{\Omega}_i + \sum_{j=1}^n k_{ij} \left(\boldsymbol{\Upsilon}_i^T \boldsymbol{\Omega}_i - \boldsymbol{\Upsilon}_j^T \boldsymbol{\Omega}_j \right). \quad (\text{A.109})$$

Consider the following Lyapunov function candidate

$$\begin{aligned} V &= \frac{1}{2} \sum_{i=1}^n \left(\mathbf{z}_i^T \mathbf{z}_i + k_i^v (\boldsymbol{\xi}_i - \boldsymbol{\psi}_i)^T (\boldsymbol{\xi}_i - \boldsymbol{\psi}_i) \right) + \frac{1}{4} \sum_{i=1}^n \sum_{j=1}^n k_{ij} \boldsymbol{\xi}_{ij}^T \boldsymbol{\xi}_{ij} \\ &\quad + \frac{1}{2} \sum_{i=1}^n (\tilde{\mathbf{z}}_i + L_v \tilde{\boldsymbol{\xi}}_i)^T (\tilde{\mathbf{z}}_i + L_v \tilde{\boldsymbol{\xi}}_i) + \frac{1}{2} \sum_{i=1}^n L_v L_p \tilde{\boldsymbol{\xi}}_i^T \tilde{\boldsymbol{\xi}}_i \\ &\quad + \sum_{i=1}^n \left(\frac{1}{2} \boldsymbol{\Omega}_i^T \mathbf{J}_{f_i} \boldsymbol{\Omega}_i + k_i^q \tilde{\mathbf{q}}_i^T \tilde{\mathbf{q}}_i + k_i^q (1 - \tilde{\eta}_i)^2 \right). \end{aligned} \quad (\text{A.110})$$

The time-derivative of V evaluated along the closed loop dynamics (A.93) with (5.27),

(A.108) and (A.109) is obtained as

$$\begin{aligned}
\dot{V} = & \sum_{i=1}^n \mathbf{z}_i^T \left(-\frac{2\mathcal{T}_i}{m_i} \mathbf{z}_i^T \mathbf{R}(\mathbf{Q}_i)^T \mathbf{S}(\tilde{\mathbf{q}}_i) \tilde{\mathbf{q}}_i - k_i^v (\boldsymbol{\xi}_i - \boldsymbol{\psi}_i) - \sum_{j=1}^n k_{ij} \boldsymbol{\xi}_{ij} \right) \\
& + \sum_{i=1}^n \sum_{j=1}^n k_{ij} \mathbf{z}_i^T \boldsymbol{\xi}_{ij} + \sum_{i=1}^n \left(k_i^v (\mathbf{z}_i + \mathbf{v}_d - \boldsymbol{\psi}_i)^T (\boldsymbol{\xi}_i - \boldsymbol{\psi}_i) \right) \\
& + \sum_{i=1}^n \left(\tilde{\mathbf{z}}_i + L_v \tilde{\boldsymbol{\xi}}_i \right)^T \left(-(L_p - L_v) \tilde{\mathbf{z}}_i - L_v^2 \tilde{\boldsymbol{\xi}}_i + k_i^v \boldsymbol{\Upsilon}_i^T \boldsymbol{\Omega}_i \right) \\
& + \sum_{i=1}^n \sum_{j=1}^n k_{ij} \left(\tilde{\mathbf{z}}_i + L_v \tilde{\boldsymbol{\xi}}_i \right)^T \left(\boldsymbol{\Upsilon}_i^T \boldsymbol{\Omega}_i - \boldsymbol{\Upsilon}_j^T \boldsymbol{\Omega}_j \right) + \sum_{i=1}^n L_v L_p \tilde{\boldsymbol{\xi}}_i^T \tilde{\mathbf{z}}_i^T \\
& + \sum_{i=1}^n k_i^q \tilde{\mathbf{q}}_i^T \boldsymbol{\beta}_i + \sum_{i=1}^n \boldsymbol{\Omega}_i^T \left(-k_i^\Omega \boldsymbol{\Omega}_i - k_i^v \boldsymbol{\Upsilon}_i (\tilde{\mathbf{z}}_i + L_v \tilde{\boldsymbol{\xi}}_i) \right) \\
& - \sum_{i=1}^n \sum_{j=1}^n k_{ij} \boldsymbol{\Omega}_i^T \boldsymbol{\Upsilon}_i \left(\left(\tilde{\mathbf{z}}_i + L_v \tilde{\boldsymbol{\xi}}_i \right) - \left(\tilde{\mathbf{z}}_j + L_v \tilde{\boldsymbol{\xi}}_j \right) \right), \tag{A.111}
\end{aligned}$$

where we have used relation (A.99). Since the communication flow is undirected, we can verify that

$$\begin{aligned}
& \sum_{i=1}^n \sum_{j=1}^n k_{ij} \left(\tilde{\mathbf{z}}_i + L_v \tilde{\boldsymbol{\xi}}_i \right)^T \left(\boldsymbol{\Upsilon}_i^T \boldsymbol{\Omega}_i - \boldsymbol{\Upsilon}_j^T \boldsymbol{\Omega}_j \right) \\
& = \sum_{i=1}^n \sum_{j=1}^n k_{ij} \boldsymbol{\Omega}_i^T \boldsymbol{\Upsilon}_i \left(\left(\tilde{\mathbf{z}}_i + L_v \tilde{\boldsymbol{\xi}}_i \right) - \left(\tilde{\mathbf{z}}_j + L_v \tilde{\boldsymbol{\xi}}_j \right) \right). \tag{A.112}
\end{aligned}$$

Then, using (5.28), (5.36) with (A.107) yields

$$\begin{aligned}
\dot{V} = & - \sum_{i=1}^n k_i^\psi k_i^v (\boldsymbol{\xi}_i - \boldsymbol{\psi}_i)^T (\boldsymbol{\xi}_i - \boldsymbol{\psi}_i) - \sum_{i=1}^n (L_p - L_v) \tilde{\mathbf{z}}_i^T \tilde{\mathbf{z}}_i - \sum_{i=1}^n L_v^3 \tilde{\boldsymbol{\xi}}_i^T \tilde{\boldsymbol{\xi}}_i \\
& - \sum_{i=1}^n k_i^q k_i^\beta \tilde{\mathbf{q}}_i^T \tilde{\mathbf{q}}_i - \sum_{i=1}^n k_i^\Omega \boldsymbol{\Omega}_i^T \boldsymbol{\Omega}_i + \sum_{i=1}^n \frac{2\mathcal{T}_i}{m_i} \tilde{\mathbf{q}}_i^T \mathbf{S}(\tilde{\mathbf{q}}_i)^T \mathbf{R}(\mathbf{Q}_i) \left(\tilde{\mathbf{z}}_i + L_p \tilde{\boldsymbol{\xi}}_i \right), \tag{A.113}
\end{aligned}$$

which can be upper bounded as

$$\begin{aligned} \dot{V} \leq & - \sum_{i=1}^n k_i^\psi k_i^v \|\xi_i - \psi_i\|^2 - \sum_{i=1}^n L_v^3 \|\tilde{\xi}_i\|^2 - \sum_{i=1}^n (L_p - L_v) \|\tilde{z}_i\|^2 - \sum_{i=1}^n k_i^\beta k_i^q \|\tilde{\mathbf{q}}_i\|^2 \\ & - \sum_{i=1}^n k_i^\Omega \|\Omega_i\|^2 + \sum_{i=1}^n \frac{\mathcal{T}_i^b}{m_i} \left(\frac{1}{\sigma_{1i}} + \frac{L_p^2}{\sigma_{2i}} \right) \|\tilde{\mathbf{q}}_i\|^2 + \sum_{i=1}^n \frac{\mathcal{T}_i^b}{m_i} \left(\sigma_{1i} \|\tilde{z}_i\|^2 + \sigma_{2i} \|\tilde{\xi}_i\|^2 \right), \end{aligned} \quad (\text{A.114})$$

for some $\sigma_{1i} > 0$ and $\sigma_{2i} > 0$, where we have used (5.26), the fact that $L_p > L_v$ from (5.38), the relation $\|\mathbf{R}(\mathbf{Q}_i)^T \mathbf{S}(\tilde{\mathbf{q}}_i)\| \leq 1$ and young's inequality to obtain this last inequality. Finally, we obtain

$$\begin{aligned} \dot{V} \leq & - \sum_{i=1}^n k_i^\psi k_i^v \|\xi_i - \psi_i\|^2 - \sum_{i=1}^n (L_p - L_v - \sigma_{1i} \frac{\mathcal{T}_i^b}{m_i}) \|\tilde{z}_i\|^2 - \sum_{i=1}^n (L_v^3 - \sigma_{2i} \frac{\mathcal{T}_i^b}{m_i}) \|\tilde{\xi}_i\|^2 \\ & - \sum_{i=1}^n k_i^\Omega \|\Omega_i\|^2 - \sum_{i=1}^n \left(k_i^\beta k_i^q - \frac{\mathcal{T}_i^b}{m_i} \left(\frac{1}{\sigma_{1i}} + \frac{L_p^2}{\sigma_{2i}} \right) \right) \|\tilde{\mathbf{q}}_i\|^2, \end{aligned} \quad (\text{A.115})$$

which is negative semi-definite if the control gains are selected according to (5.38). Therefore, we conclude that \mathbf{z}_i , $(\xi_i - \psi_i)$, \tilde{z}_i , $\tilde{\xi}_i$, Ω_i and $\tilde{\mathbf{q}}_i$ are bounded for $i \in \mathcal{N}$, and ξ_{ij} is bounded for all $i, j \in \mathcal{N}$ (since the communication graph is connected).

Consequently, we know that $\ddot{\theta}_i$, $\dot{\mathbf{z}}_i$, $\dot{\tilde{z}}_i$, ν_i , $\dot{\psi}_i$ and β_i are bounded for $i \in \mathcal{N}$.

From the closed loop dynamics (A.108), we can see that $\tilde{\Omega}_i$ is bounded. Also, since $\tilde{\omega}_i = \Omega_i + \beta_i$ is bounded, we have $\tilde{\mathbf{q}}_i$ is bounded from (2.14). Hence, we can conclude that \dot{V} is bounded. Invoking Barbălat Lemma, we conclude that $(\xi_i - \psi_i) \rightarrow 0$, $\tilde{z}_i \rightarrow 0$, $\tilde{\xi}_i \rightarrow 0$, $\tilde{\mathbf{q}}_i \rightarrow 0$ and $\Omega_i \rightarrow 0$.

Since $(\xi_i - \psi_i) \rightarrow 0$, we know from (5.28) that $\dot{\psi}_i \rightarrow \mathbf{v}_d$. Also, we can verify that $(\dot{\xi}_i - \dot{\psi}_i)$ is bounded from the boundedness of $\dot{\mathbf{z}}_i$ and $(\xi_i - \psi_i)$. Invoking Barbălat Lemma, we conclude that $(\dot{\xi}_i - \dot{\psi}_i) \rightarrow 0$. Consequently, we have $\dot{\xi}_i \rightarrow \mathbf{v}_d$ and, from (5.6), $\mathbf{z}_i \rightarrow 0$. In addition, since \mathbf{z}_i and \tilde{z}_i converge to zero, we have $\hat{\mathbf{z}}_i \rightarrow \mathbf{v}_d$, and consequently $\beta_i \rightarrow 0$, from (5.36), and $\tilde{\omega}_i \rightarrow 0$. Note that the above results hold for $i \in \mathcal{N}$.

To this point, since $\tilde{\mathbf{q}}_i$ and $(\xi_i - \psi_i)$ converge to zero asymptotically and ξ_{ij} is uniformly continuous, we can use Lemma 2.3 to conclude that $\dot{\mathbf{z}}_i \rightarrow 0$ and the closed loop (A.93) with (5.27) reduces to (A.102). Then using the same arguments as in the proof of Theorem 5.1, we conclude that $(\xi_i - \xi_j) \rightarrow \delta_{ij}$, for all $i, j \in \mathcal{N}$.

Exploiting the above results, we know that the dynamics of the variable θ_i in (5.5) can be rewritten as in (2.35) with: $\varepsilon_i = -\mathbf{u}_i$, where \mathbf{u}_i is given in (5.27) and is globally bounded and converges asymptotically to zero. Hence, from Lemma 2.6, we conclude that θ_i and $\dot{\theta}_i$ are bounded and $\theta_i \rightarrow 0$ and $\dot{\theta}_i \rightarrow 0$, for $i \in \mathcal{N}$. As a result, we conclude from (5.6) that \mathbf{v}_i and $(\mathbf{p}_i - \mathbf{p}_j)$ are bounded and $(\mathbf{v}_i - \mathbf{v}_d) \rightarrow 0$ and

$(\mathbf{p}_i - \mathbf{p}_j) \rightarrow \boldsymbol{\delta}_{ij}$ for all $i, j \in \mathcal{N}$. The rest of the proof is similar to the proof of Theorem 5.1.

A.4.3 Proof of Theorem 5.3

Similar to the proof of Theorem 5.1, if Assumption 4.1 is satisfied, the result of Lemma 2.6 can be used to extract the magnitude of the thrust and the desired attitude for each VTOL aircraft.

The translational error dynamics can be written from (5.1) and (5.45), using the intermediary control input expressed by (5.42)-(5.44) with (5.46)-(5.47), as

$$\dot{\mathbf{z}}_i = -k_i^v(\boldsymbol{\xi}_i - \boldsymbol{\psi}_i) - \sum_{j=1}^n k_{ij} \boldsymbol{\xi}_{ij}. \quad (\text{A.116})$$

The attitude tracking error dynamics can be derived following the same steps in the proof of Theorem 5.1 as

$$\mathbf{J}_{f_i} \dot{\boldsymbol{\Omega}}_i = -k_i^q \tilde{\mathbf{q}}_i - k_i^\Omega \boldsymbol{\Omega}_i, \quad (\text{A.117})$$

and $\boldsymbol{\Omega}_i = (\tilde{\boldsymbol{\omega}}_i - \boldsymbol{\beta}_i)$. To proof the result of the theorem, we first consider the following Lyapunov function candidate

$$\begin{aligned} V = & \frac{1}{2} \sum_{i=1}^n \left(\mathbf{z}_i^T \mathbf{z}_i + k_i^v (\boldsymbol{\xi}_i - \boldsymbol{\psi}_i)^T (\boldsymbol{\xi}_i - \boldsymbol{\psi}_i) \right) + \frac{1}{4} \sum_{i=1}^n \sum_{j=1}^n k_{ij} \boldsymbol{\xi}_{ij}^T \boldsymbol{\xi}_{ij} \\ & + \sum_{i=1}^n \left(\frac{1}{2} \boldsymbol{\Omega}_i^T \mathbf{J}_{f_i} \boldsymbol{\Omega}_i + k_i^q \tilde{\mathbf{q}}_i^T \tilde{\mathbf{q}}_i + k_i^q (1 - \tilde{\eta}_i)^2 \right). \end{aligned} \quad (\text{A.118})$$

The time-derivative of V evaluated along the closed loop dynamics (A.116)-(A.117), using (2.14), gives

$$\begin{aligned} \dot{V} = & \sum_{i=1}^n \mathbf{z}_i^T \left(-k_i^v (\boldsymbol{\xi}_i - \boldsymbol{\psi}_i) - \sum_{j=1}^n k_{ij} \boldsymbol{\xi}_{ij} \right) + \sum_{i=1}^n \left(k_i^v (\mathbf{z}_i + \mathbf{v}_d - \boldsymbol{\psi}_i)^T (\boldsymbol{\xi}_i - \boldsymbol{\psi}_i) \right) \\ & + \sum_{i=1}^n \sum_{j=1}^n k_{ij} \mathbf{z}_i^T \boldsymbol{\xi}_{ij} + \sum_{i=1}^n \left(k_i^q \tilde{\mathbf{q}}_i^T \boldsymbol{\beta}_i - k_i^\Omega \boldsymbol{\Omega}_i^T \boldsymbol{\Omega}_i \right), \end{aligned} \quad (\text{A.119})$$

where we have used relation (A.99). Then, using (5.28) and (5.51) leads to the

negative semi-definite time-derivative

$$\dot{V} = - \sum_{i=1}^n \left(k_i^\psi k_i^v (\boldsymbol{\xi}_i - \boldsymbol{\psi}_i)^T (\boldsymbol{\xi}_i - \boldsymbol{\psi}_i) - k_i^q k_i^\beta \tilde{\mathbf{q}}_i^T \tilde{\mathbf{q}}_i - k_i^\Omega \boldsymbol{\Omega}_i^T \boldsymbol{\Omega}_i \right). \quad (\text{A.120})$$

Therefore, we conclude that \mathbf{z}_i , $(\boldsymbol{\xi}_i - \boldsymbol{\psi}_i)$, $\boldsymbol{\Omega}_i$ and $\boldsymbol{\xi}_{ij}$ are bounded for all $i, j \in \mathcal{N}$, which leads us to conclude that $\tilde{\boldsymbol{\omega}}_i$, $\dot{\mathbf{z}}_i$, $\dot{\boldsymbol{\psi}}_i$ and $\dot{\boldsymbol{\Omega}}_i$ are bounded signals. Invoking Barbălat Lemma, we conclude that $(\boldsymbol{\xi}_i - \boldsymbol{\psi}_i) \rightarrow 0$, $\tilde{\mathbf{q}}_i \rightarrow 0$ and $\tilde{\boldsymbol{\omega}}_i \rightarrow 0$ for $i \in \mathcal{N}$. Using similar arguments as in the proof of Theorem 5.2, we can show that $\mathbf{z}_i \rightarrow 0$ and $\dot{\mathbf{z}}_i \rightarrow 0$, which in turn leads us to conclude that $(\boldsymbol{\xi}_i - \boldsymbol{\xi}_j) \rightarrow \boldsymbol{\delta}_{ij}$ for all $i, j \in \mathcal{N}$. Next, we can see that the dynamics of the variable $\boldsymbol{\alpha}_i$ in (5.44) can be rewritten as

$$\ddot{\boldsymbol{\alpha}}_i = -L_i^p \boldsymbol{\alpha}_i - L_i^d \dot{\boldsymbol{\alpha}}_i + \boldsymbol{\epsilon}_i, \quad \text{for } i \in \mathcal{N}, \quad (\text{A.121})$$

with

$$\boldsymbol{\epsilon}_i = \left(k_i^v (\boldsymbol{\xi}_i - \boldsymbol{\psi}_i) + \sum_{j=1}^n k_{ij} \boldsymbol{\xi}_{ij} - \frac{2\mathcal{T}_i}{m_i} \mathbf{R}(\mathbf{Q}_i)^T \mathbf{S}(\bar{\mathbf{q}}_i) \tilde{\mathbf{q}}_i \right),$$

which is, in view of the above results, globally bounded and converges asymptotically to zero. It can be seen that (A.121) describes the dynamics of a double-integrator with a bounded and vanishing input perturbation, and hence we can verify that $\boldsymbol{\alpha}_i$, $\dot{\boldsymbol{\alpha}}_i$ are globally bounded and $\boldsymbol{\alpha}_i \rightarrow 0$ and $\dot{\boldsymbol{\alpha}}_i \rightarrow 0$. Finally, the dynamics of $\boldsymbol{\theta}_i$ in (5.43) with (5.42) and (5.46)-(5.47) will be equivalent to (2.35) in Lemma 2.6, with $\boldsymbol{\epsilon}_i = (L_i^p \boldsymbol{\alpha}_i + L_i^d \dot{\boldsymbol{\alpha}}_i)$, which is bounded and converges asymptotically to zero.

Then, using the results of Lemma 2.6, we conclude that $\boldsymbol{\theta}_i$ and $\dot{\boldsymbol{\theta}}_i$ are bounded and $\boldsymbol{\theta}_i \rightarrow 0$, $\dot{\boldsymbol{\theta}}_i \rightarrow 0$, for $i \in \mathcal{N}$, and consequently, we conclude from the error vectors definition (5.45) that the vectors \mathbf{v}_i and $(\mathbf{p}_i - \mathbf{p}_j)$ are bounded and $(\mathbf{v}_i - \mathbf{v}_d) \rightarrow 0$, $(\mathbf{p}_i - \mathbf{p}_j) \rightarrow \boldsymbol{\delta}_{ij}$, for all $i, j \in \mathcal{N}$. The rest of the proof is similar to the proof of Theorem 5.1.

A.5 Formation control with delayed communication

A.5.1 Proof of Theorem 6.1

First, we can see that if the control gains are selected according to (6.13), the extraction condition (4.8) will be always satisfied, in view of (5.8). Therefore, it is always possible to extract the magnitude of the thrust and the desired attitude from (4.6) and (4.7) respectively for each VTOL vehicle.

The translational error dynamics can be determined from (5.1) and (6.5) using the intermediary control input (6.2)-(6.4) as

$$\dot{\mathbf{z}}_i = -k_i^v \mathbf{z}_i - \sum_{j=1}^n k_{ij} \boldsymbol{\xi}_{ij} - \frac{2\mathcal{T}_i}{m_i} \mathbf{R}(\mathbf{Q}_i)^T \mathbf{S}(\bar{\mathbf{q}}_i) \tilde{\mathbf{q}}_i, \quad (\text{A.122})$$

with $\boldsymbol{\xi}_{ij} = (\boldsymbol{\xi}_i - \boldsymbol{\xi}_j(t - \tau_{ij}) - \boldsymbol{\delta}_{ij})$. The attitude error dynamics are obtained similar to the proof of Theorem 5.1 as

$$\mathbf{J}_{f_i} \dot{\boldsymbol{\Omega}}_i = -k_i^q \tilde{\mathbf{q}}_i - k_i^\Omega \boldsymbol{\Omega}_i, \quad (\text{A.123})$$

with $\boldsymbol{\Omega}_i = (\tilde{\boldsymbol{\omega}}_i - \boldsymbol{\beta}_i)$. Consider the following Lyapunov-Krasovskii functional candidate

$$V = V_{t_1} + V_{a_1} + V_{k_1}, \quad (\text{A.124})$$

with

$$V_{t_1} = \frac{1}{2} \sum_{i=1}^n \left(\mathbf{z}_i^T \mathbf{z}_i + \frac{1}{2} \sum_{j=1}^n k_{ij} \bar{\boldsymbol{\xi}}_{ij}^T \bar{\boldsymbol{\xi}}_{ij} \right), \quad (\text{A.125})$$

$$V_{a_1} = \sum_{i=1}^n \left(\frac{1}{2} \boldsymbol{\Omega}_i^T \mathbf{J}_{f_i} \boldsymbol{\Omega}_i + k_i^q \tilde{\mathbf{q}}_i^T \tilde{\mathbf{q}}_i + k_i^q (1 - \tilde{\eta}_i)^2 \right), \quad (\text{A.126})$$

$$V_{k_1} = \sum_{i=1}^n \sum_{j=1}^n \frac{k_{ij} \tau}{2\epsilon} \left(\int_{-\tau}^0 \int_{t+s}^t \mathbf{z}_j(\varrho)^T \mathbf{z}_j(\varrho) d\varrho ds \right), \quad (\text{A.127})$$

where $\bar{\boldsymbol{\xi}}_{ij} = (\boldsymbol{\xi}_i - \boldsymbol{\xi}_j - \boldsymbol{\delta}_{ij})$, $\tau_{ij} \leq \tau$ for all $(i, j) \in \mathcal{E}$ and $\epsilon > 0$. The time-derivative of V_{t_1} in view of (A.122) gives

$$\begin{aligned} \dot{V}_{t_1} &= \sum_{i=1}^n \mathbf{z}_i^T \left(-\frac{2\mathcal{T}_i}{m_i} \mathbf{R}(\mathbf{Q}_i)^T \mathbf{S}(\bar{\mathbf{q}}_i) \tilde{\mathbf{q}}_i - k_i^v \mathbf{z}_i - \sum_{j=1}^n k_{ij} \boldsymbol{\xi}_{ij} \right) \\ &\quad + \frac{1}{2} \sum_{i=1}^n \sum_{j=1}^n k_{ij} (\mathbf{z}_i - \mathbf{z}_j)^T \bar{\boldsymbol{\xi}}_{ij} \\ &= - \sum_{i=1}^n \frac{2\mathcal{T}_i}{m_i} \mathbf{z}_i^T \mathbf{R}(\mathbf{Q}_i)^T \mathbf{S}(\bar{\mathbf{q}}_i) \tilde{\mathbf{q}}_i - \sum_{i=1}^n k_i^v \mathbf{z}_i^T \mathbf{z}_i \\ &\quad - \sum_{i=1}^n \sum_{j=1}^n k_{ij} \mathbf{z}_i^T (\boldsymbol{\xi}_j - \boldsymbol{\xi}_j(t - \tau_{ij})), \end{aligned} \quad (\text{A.128})$$

where we have used: $(\boldsymbol{\xi}_{ij} - \bar{\boldsymbol{\xi}}_{ij} = (\boldsymbol{\xi}_j - \boldsymbol{\xi}_j(t - \tau_{ij}))$ and a similar relation to (A.99), *i.e.*,

$$\frac{1}{2} \sum_{i=1}^n \sum_{j=1}^n k_{ij} (\mathbf{z}_i - \mathbf{z}_j)^T \bar{\boldsymbol{\xi}}_{ij} = \sum_{i=1}^n \sum_{j=1}^n k_{ij} \mathbf{z}_i^T \bar{\boldsymbol{\xi}}_{ij}, \quad (\text{A.129})$$

which can be verified using $k_{ij} = k_{ji}$ and $\boldsymbol{\delta}_{ij} = -\boldsymbol{\delta}_{ji}$. From the error signals definition (6.5), we know that $\frac{d\boldsymbol{\xi}_j(s)}{ds} = \mathbf{z}_j(s)$, and therefore the following relation holds:

$$(\boldsymbol{\xi}_j - \boldsymbol{\xi}_j(t - \tau_{ij})) = \int_{t-\tau_{ij}}^t \mathbf{z}_j ds. \quad (\text{A.130})$$

Also, using young's inequality, we can verify that

$$2\mathbf{z}_i^T \int_{t-\tau_{ij}}^t \mathbf{z}_j ds \leq \epsilon_{ij} \mathbf{z}_i^T \mathbf{z}_i + \frac{1}{\epsilon_{ij}} \left(\int_{t-\tau_{ij}}^t \mathbf{z}_j ds \right)^T \left(\int_{t-\tau_{ij}}^t \mathbf{z}_j ds \right), \quad (\text{A.131})$$

for some strictly positive ϵ_{ij} . Without loss of generality, we consider $\epsilon_{ij} = \epsilon_{ji} = \epsilon > 0$. Furthermore, Jensen's inequality (Seuret *et al.*, 2009) leads to

$$\left(\int_{t-\tau_{ij}}^t \mathbf{z}_j ds \right)^T \left(\int_{t-\tau_{ij}}^t \mathbf{z}_j ds \right) \leq \tau_{ij} \int_{t-\tau_{ij}}^t \mathbf{z}_j^T \mathbf{z}_j ds. \quad (\text{A.132})$$

Exploiting the above relations, an upper bound of \dot{V}_{t_1} can be obtained as

$$\begin{aligned} \dot{V}_{t_1} \leq & - \sum_{i=1}^n \frac{2\mathcal{T}_i}{m_i} \mathbf{z}_i^T \mathbf{R}(\mathbf{Q}_i)^T \mathbf{S}(\bar{\mathbf{q}}_i) \tilde{\mathbf{q}}_i - \sum_{i=1}^n k_i^v \mathbf{z}_i^T \mathbf{z}_i \\ & + \frac{1}{2} \sum_{i=1}^n \sum_{j=1}^n k_{ij} \left(\epsilon \mathbf{z}_i^T \mathbf{z}_i + \frac{\tau_{ij}}{\epsilon} \int_{t-\tau_{ij}}^t \mathbf{z}_j^T \mathbf{z}_j ds \right). \end{aligned} \quad (\text{A.133})$$

On the other hand, the time-derivative of V_{k_1} in (A.127) can be obtained as

$$\dot{V}_{k_1} = \sum_{i=1}^n \sum_{j=1}^n \frac{k_{ij} \tau}{2\epsilon} \left(\tau \mathbf{z}_j^T \mathbf{z}_j - \int_{t-\tau}^t \mathbf{z}_j^T \mathbf{z}_j ds \right). \quad (\text{A.134})$$

The time-derivative of V_{a_1} in view of (A.123) and (6.12) yields

$$\begin{aligned}\dot{V}_{a_1} &= \sum_{i=1}^n \left(-k_i^\Omega \Omega_i^T \Omega_i + k_i^q \tilde{\mathbf{q}}_i^T \beta_i \right) \\ &= \sum_{i=1}^n \left(-k_i^\Omega \Omega_i^T \Omega_i - k_i^q k_i^\beta \tilde{\mathbf{q}}_i^T \tilde{\mathbf{q}}_i + \frac{2\mathcal{T}_i}{m_i} \tilde{\mathbf{q}}_i^T \mathbf{S}(\bar{\mathbf{q}}_i)^T \mathbf{R}(\mathbf{Q}_i) \mathbf{z}_i \right).\end{aligned}\quad (\text{A.135})$$

Therefore, the time-derivative of V evaluated along the closed loop dynamics can be upper bounded, using (A.133)-(A.135), as

$$\dot{V} \leq \sum_{i=1}^n \left(-k_i^z \mathbf{z}_i^T \mathbf{z}_i - k_i^\Omega \Omega_i^T \Omega_i - k_i^q k_i^\beta \tilde{\mathbf{q}}_i^T \tilde{\mathbf{q}}_i \right), \quad (\text{A.136})$$

with k_i^z given in (6.14), where we have used the properties of the undirected graph, *i.e.*, $k_{ij} = k_{ji}$, and the relation

$$\tau_{ij} \int_{t-\tau_{ij}}^t \mathbf{z}_j^T \mathbf{z}_j ds \leq \tau \int_{t-\tau}^t \mathbf{z}_j^T \mathbf{z}_j ds. \quad (\text{A.137})$$

As a result, the time-derivative \dot{V} is negative semi-definite if condition (6.14) is satisfied. Hence, we can conclude that \mathbf{z}_i , $\tilde{\mathbf{q}}_i$ and Ω_i are bounded for $i \in \mathcal{N}$ and $(\boldsymbol{\xi}_i - \boldsymbol{\xi}_j)$ is bounded for all $(i, j) \in \mathcal{E}$. Since the communication graph is assumed connected, this last result is valid for all $i, j \in \mathcal{N}$. Now, using the relation

$$(\boldsymbol{\xi}_i - \boldsymbol{\xi}_j(t - \tau_{ij})) = (\boldsymbol{\xi}_i - \boldsymbol{\xi}_j) + \int_{t-\tau_{ij}}^t \mathbf{z}_i ds, \quad (\text{A.138})$$

we can conclude that $(\boldsymbol{\xi}_i - \boldsymbol{\xi}_j(t - \tau_{ij}))$ is bounded for $(i, j) \in \mathcal{E}$ and consequently $\dot{\mathbf{z}}_i$ is bounded for $i \in \mathcal{N}$.

From equation (6.12), we know that β_i is bounded since $\tilde{\mathbf{q}}_i$ and \mathbf{z}_i are bounded, and consequently $\tilde{\omega}_i$ is bounded. Therefore, we conclude that $\tilde{\mathbf{q}}_i$ is bounded from (2.14). In addition, we can conclude from (A.123) that $\dot{\Omega}_i$ is bounded. As a result, \ddot{V} is bounded and by invoking Barbălat lemma we conclude that $\mathbf{z}_i \rightarrow 0$, $\Omega_i \rightarrow 0$ and $\tilde{\mathbf{q}}_i \rightarrow 0$, and therefore, $\beta_i \rightarrow 0$ and $\tilde{\omega}_i \rightarrow 0$ for $i \in \mathcal{N}$.

Exploiting the above results, we can verify that $\boldsymbol{\xi}_{ij}$ is uniformly continuous, for $(i, j) \in \mathcal{E}$, since τ_{ij} and δ_{ij} are constant and we have shown that \mathbf{z}_i is bounded for $i \in \mathcal{N}$. Invoking the extended Barbălat Lemma (Lemma 2.3), we can conclude from (A.122)

that $\dot{\mathbf{z}}_i \rightarrow 0$ for $i \in \mathcal{N}$ and therefore, we know from (A.122) that

$$\sum_{j=1}^n k_{ij}(\boldsymbol{\xi}_i - \boldsymbol{\xi}_j(t - \tau_{ij}) - \boldsymbol{\delta}_{ij}) \rightarrow 0, \quad \text{for } i \in \mathcal{N}. \quad (\text{A.139})$$

Since $\mathbf{z}_i \rightarrow 0$, we can show that $\int_{t-\tau_{ij}}^t \mathbf{z}_i ds \rightarrow 0$. Therefore, equation (A.139), in view of (A.138), is equivalent to

$$\sum_{j=1}^n k_{ij}(\boldsymbol{\xi}_i - \boldsymbol{\xi}_j - \boldsymbol{\delta}_{ij}) \rightarrow 0, \quad \text{for } i \in \mathcal{N}, \quad (\text{A.140})$$

which is equivalent to (A.102) in the proof of Theorem 5.1. Consequently, using similar steps as in the proof of Theorem 5.1, we conclude that $(\boldsymbol{\xi}_i - \boldsymbol{\xi}_j) \rightarrow \boldsymbol{\delta}_{ij}$, for all $i, j \in \mathcal{N}$, since the communication graph is connected.

To this point, the dynamics of the variable $\boldsymbol{\theta}_i$ in (6.3) can be rewritten as in (2.35), with $\boldsymbol{\varepsilon}_i = -\mathbf{u}_i = \left(k_i^v \mathbf{z}_i + \sum_{j=1}^n k_{ij}(\boldsymbol{\xi}_i - \boldsymbol{\xi}_j(t - \tau_{ij}) - \boldsymbol{\delta}_{ij}) \right)$. We can verify from the above results that $\boldsymbol{\varepsilon}_i$ is bounded and converges asymptotically to zero. Therefore, using the result of Lemma 2.6, we conclude that $\boldsymbol{\theta}_i$ and $\dot{\boldsymbol{\theta}}_i$ are bounded and $\boldsymbol{\theta}_i \rightarrow 0$, $\dot{\boldsymbol{\theta}}_i \rightarrow 0$, for $i \in \mathcal{N}$. Finally, we conclude from (6.5) that \mathbf{v}_i and $(\mathbf{p}_i - \mathbf{p}_j)$ are bounded and $\mathbf{v}_i \rightarrow 0$ and $(\mathbf{p}_i - \mathbf{p}_j) \rightarrow \boldsymbol{\delta}_{ij}$ for all $i, j \in \mathcal{N}$.

A.5.2 Proof of Theorem 6.2

Similar to the proof of Theorem 6.1, if the control gains satisfy condition (6.13), we can always extract the magnitude of the thrust and the desired attitude from (4.6) and (4.7) respectively. Also, the attitude error dynamics are given in (A.123) and the translational error dynamics are obtained from (6.2)-(6.3) and (6.23)-(6.26) as

$$\dot{\mathbf{z}}_i = -k_i^v \mathbf{z}_i - \sum_{j=1}^n k_{ij} \boldsymbol{\xi}_{ij}, \quad (\text{A.141})$$

with $\boldsymbol{\xi}_{ij} = (\boldsymbol{\xi}_i - \boldsymbol{\xi}_j(t - \tau_{ij}) - \boldsymbol{\delta}_{ij})$. Consider the following Lyapunov-Krasovskii candidate

$$V = V_{t_1} + V_{a_1} + V_{k_2}, \quad (\text{A.142})$$

where V_{t_1} and V_{a_1} are given respectively in (A.125) and (A.126) and

$$V_{k_2} = \frac{1}{2} \sum_{i=1}^n \sum_{j=1}^n \frac{k_{ij}}{\epsilon} \bar{\tau} \left(\int_{-\bar{\tau}}^0 \int_{t+s}^t \mathbf{z}_j(\varrho)^T \mathbf{z}_j(\varrho) d\varrho ds \right), \quad (\text{A.143})$$

where $\tau_{ij}(t) \leq \bar{\tau}$ for all $t > 0$, and $i, j \in \mathcal{N}$, and $\epsilon > 0$. Note that V_{k_2} is equivalent to V_{k_1} in (A.127) when $\bar{\tau} = \tau$. Therefore, the time-derivative of V_{k_2} can be obtained similar to (A.134) with τ replaced by $\bar{\tau}$.

Following similar steps as in the proof of Theorem 6.1, the time-derivative of V_{t_1} in view of (A.141) can be upper bounded as

$$\dot{V}_{t_1} \leq - \sum_{i=1}^n k_i^v \mathbf{z}_i^T \mathbf{z}_i + \frac{1}{2} \sum_{i=1}^n \sum_{j=1}^n k_{ij} \left(\epsilon \mathbf{z}_i^T \mathbf{z}_i + \frac{\tau_{ij}}{\epsilon} \int_{t-\tau_{ij}}^t \mathbf{z}_j^T \mathbf{z}_j ds \right). \quad (\text{A.144})$$

In addition, the time-derivative of V_{a_1} is obtained from the first equality in (A.135) and (6.28) as

$$\dot{V}_{a_1} = \sum_{i=1}^n \left(-k_i^\Omega \Omega_i^T \Omega_i - k_i^q k_i^\beta \tilde{\mathbf{q}}_i^T \tilde{\mathbf{q}}_i \right). \quad (\text{A.145})$$

Then, using the relation

$$\tau_{ij}(t) \int_{t-\tau_{ij}(t)}^t \mathbf{z}_j^T \mathbf{z}_j ds \leq \bar{\tau} \int_{t-\bar{\tau}}^t \mathbf{z}_j^T \mathbf{z}_j ds, \quad (\text{A.146})$$

the time-derivative of V evaluated along (A.141) and (A.123) can be upper bounded in view of (A.144), (A.134) and (A.145) as

$$\dot{V} \leq \sum_{i=1}^n \left(-\bar{k}_i^z \mathbf{z}_i^T \mathbf{z}_i - k_i^\Omega \Omega_i^T \Omega_i - k_i^q k_i^\beta \tilde{\mathbf{q}}_i^T \tilde{\mathbf{q}}_i \right), \quad (\text{A.147})$$

where \bar{k}_i^z is given in (6.29). Then, following the same arguments as in the proof of Theorem 6.1, we can show that \mathbf{z}_i , $\tilde{\mathbf{q}}_i$ and $\tilde{\omega}_i$ and $(\boldsymbol{\xi}_i - \boldsymbol{\xi}_j)$ are bounded for all $i, j \in \mathcal{N}$ and $\tilde{\omega}_i \rightarrow 0$, $\tilde{\mathbf{q}}_i \rightarrow 0$ and $\mathbf{z}_i \rightarrow 0$ for $i \in \mathcal{N}$.

With these results, we conclude that $\boldsymbol{\xi}_{ij}$ is uniformly continuous since $\dot{\boldsymbol{\xi}}_{ij}$ is bounded. This can be verified using the fact that \mathbf{z}_i and τ_{ij} are bounded. Invoking Lemma 2.3, we conclude from (A.141) that $\dot{\mathbf{z}}_i \rightarrow 0$ for $i \in \mathcal{N}$. Therefore, using similar steps as in the proof of Theorem 6.1, we can show that $(\boldsymbol{\xi}_i - \boldsymbol{\xi}_j) \rightarrow \boldsymbol{\delta}_{ij}$ for all $i, j \in \mathcal{N}$.

To this point, the dynamics of the variable $\boldsymbol{\alpha}_i$ in (6.24) can be rewritten as

$$\ddot{\boldsymbol{\alpha}}_i = -L_i^p \boldsymbol{\alpha}_i - L_i^d \dot{\boldsymbol{\alpha}}_i - \phi_i - \frac{2\mathcal{T}_i}{m_i} \mathbf{R}(\mathbf{Q}_i)^T \mathbf{S}(\bar{\mathbf{q}}_i) \tilde{\mathbf{q}}_i, \quad (\text{A.148})$$

for $i \in \mathcal{N}$, which represents the dynamics of a double integrator with a bounded and asymptotically vanishing perturbation $\left(-\phi_i - \frac{2\mathcal{T}_i}{m_i} \mathbf{R}(\mathbf{Q}_i)^T \mathbf{S}(\bar{\mathbf{q}}_i) \tilde{\mathbf{q}}_i \right)$. Hence, follow-

ing similar arguments as in the proof of Theorem 5.3, we can verify that $\dot{\boldsymbol{\alpha}}_i$ and $\boldsymbol{\alpha}_i$ are bounded and $\boldsymbol{\alpha}_i \rightarrow \dot{\boldsymbol{\alpha}}_i \rightarrow 0$. As a result, the dynamics of $\boldsymbol{\theta}_i$ will reduce to (2.35) with $\boldsymbol{\varepsilon}_i = \left(L_i^p \boldsymbol{\alpha}_i + L_i^d \dot{\boldsymbol{\alpha}}_i \right)$, which satisfies the condition of Lemma 2.6. Therefore, we conclude that $\boldsymbol{\theta}_i \rightarrow \dot{\boldsymbol{\theta}}_i \rightarrow 0$, for $i \in \mathcal{N}$, which leads to the results of the theorem.

A.5.3 Proof of Theorem 6.3

Similar to the proof of Theorem 6.1, from condition (6.13), we can use the extraction algorithm in Lemma 4.1 to extract the necessary thrust and the desired attitude. For analysis purposes, we define the new vector

$$\mathbf{r}_i = \mathbf{z}_i + \lambda \sum_{k=1}^n k_{ij} \boldsymbol{\xi}_{ij}, \quad (\text{A.149})$$

with $\boldsymbol{\xi}_{ij} = (\boldsymbol{\xi}_i - \boldsymbol{\xi}_j(t - \tau_{ij}) - \boldsymbol{\delta}_{ij})$. The time-derivative of this error vector can be obtained from (5.1) and (6.25) using (6.3), (6.24) and (6.33), as

$$\begin{aligned} \dot{\mathbf{r}}_i &= \dot{\mathbf{v}}_i - \ddot{\boldsymbol{\theta}}_i - \ddot{\boldsymbol{\alpha}}_i + \lambda \sum_{j=1}^n k_{ij} \mathbf{z}_{ij} \\ &= \boldsymbol{\phi}_i + \lambda \sum_{j=1}^n k_{ij} \mathbf{z}_{ij} \\ &= -k_i^v \mathbf{r}_i - \lambda \sum_{j=1}^n k_{ij} \mathbf{z}_{ij}, \end{aligned} \quad (\text{A.150})$$

where $\mathbf{z}_{ij} = (\mathbf{z}_i - \mathbf{z}_j(t - \tau_{ij}))$. Also, the attitude error dynamics are given similar to the proof of Theorem 6.1 as in (A.123). Consider the following Lyapunov-Krasovskii functional candidate

$$\begin{aligned} V &= \frac{1}{2} \sum_{i=1}^n \mathbf{r}_i^T \mathbf{r}_i + \frac{1}{2} \sum_{i=1}^n \lambda \sum_{j=1}^n k_{ij} \int_{t-\tau_{ij}}^t \mathbf{z}_j^T \mathbf{z}_j ds \\ &\quad + \frac{1}{2} \sum_{i=1}^n \lambda^2 \left(\sum_{j=1}^n k_{ij} \boldsymbol{\xi}_{ij} \right)^T \left(\sum_{j=1}^n k_{ij} \boldsymbol{\xi}_{ij} \right) + V_{a1}, \end{aligned} \quad (\text{A.151})$$

where V_{a_1} is given in (A.126). The time-derivative of V is given as

$$\begin{aligned} \dot{V} &= \sum_{i=1}^n \mathbf{r}_i^T \left(-k_i^v \mathbf{r}_i - \lambda \sum_{k=1}^n k_{ik} \mathbf{z}_{ik} \right) \\ &\quad + \frac{1}{2} \sum_{i=1}^n \sum_{j=1}^n k_{ij} \left(\mathbf{z}_j^T \mathbf{z}_j - \mathbf{z}_j(t - \tau_{ij})^T \mathbf{z}_j(t - \tau_{ij}) \right) \\ &\quad + \sum_{i=1}^n \lambda^2 \left(\sum_{j=1}^n k_{ij} \mathbf{z}_{ij} \right)^T \left(\sum_{j=1}^n k_{ij} \boldsymbol{\xi}_{ij} \right) + \dot{V}_{a_1}. \end{aligned} \quad (\text{A.152})$$

Then, using the expression of \mathbf{r}_i in (A.149) with (A.145) and the relation $\mathbf{z}_{ij} = (\mathbf{z}_i - \mathbf{z}_j(t - \tau_{ij}))$ yields

$$\begin{aligned} \dot{V} &= - \sum_{i=1}^n \left(k_i^v \mathbf{r}_i^T \mathbf{r}_i + k_i^\Omega \boldsymbol{\Omega}_i^T \boldsymbol{\Omega}_i + k_i^q k_i^\beta \tilde{\mathbf{q}}_i^T \tilde{\mathbf{q}}_i \right) \\ &\quad - \sum_{i=1}^n \sum_{j=1}^n \lambda k_{ij} \mathbf{z}_i^T (\mathbf{z}_i - \mathbf{z}_j(t - \tau_{ij})) \\ &\quad + \frac{1}{2} \sum_{i=1}^n \sum_{j=1}^n \lambda k_{ij} \left(\mathbf{z}_j^T \mathbf{z}_j - \mathbf{z}_j(t - \tau_{ij})^T \mathbf{z}_j(t - \tau_{ij}) \right). \end{aligned} \quad (\text{A.153})$$

Finally, since the communication flow is undirected and $k_{ij} = k_{ji}$, we obtain

$$\dot{V} = - \sum_{i=1}^n \left(k_i^v \mathbf{r}_i^T \mathbf{r}_i + k_i^\Omega \boldsymbol{\Omega}_i^T \boldsymbol{\Omega}_i + k_i^q k_i^\beta \tilde{\mathbf{q}}_i^T \tilde{\mathbf{q}}_i + \frac{1}{2} \sum_{j=1}^n \lambda k_{ij} \mathbf{z}_{ij}^T \mathbf{z}_{ij} \right), \quad (\text{A.154})$$

which is negative semi-definite. Then, we conclude that \mathbf{r}_i , $\boldsymbol{\Omega}_i$, $\tilde{\mathbf{q}}_i$ and $\left(\sum_{j=1}^n k_{ij} \boldsymbol{\xi}_{ij} \right)$ are bounded and consequently, we know that \mathbf{z}_i is bounded. Hence, from (A.150) and the above results, we conclude that $\dot{\mathbf{r}}_i$ is bounded which in turn leads us to conclude that $\dot{\mathbf{z}}_i$ is bounded from (A.150) and the fact that \mathbf{z}_i is bounded. On the other hand, using similar arguments as in the proof of Theorem 6.1, we can verify that $\dot{\boldsymbol{\Omega}}_i$ and $\dot{\tilde{\mathbf{q}}}_i$ are bounded, for $i \in \mathcal{N}$. As a result, we have \dot{V} is bounded, and by Barbălat Lemma, we conclude that $\mathbf{r}_i \rightarrow 0$, $(\mathbf{z}_i - \mathbf{z}_j(t - \tau_{ij})) \rightarrow 0$, $\boldsymbol{\Omega}_i \rightarrow 0$ and $\tilde{\mathbf{q}}_i \rightarrow 0$, and therefore, $\boldsymbol{\beta}_i \rightarrow 0$ and $\tilde{\boldsymbol{\omega}}_i \rightarrow 0$ for $i \in \mathcal{N}$.

Exploiting the above results and invoking Lemma 2.3, we can conclude from (A.150) that $\dot{\mathbf{r}}_i \rightarrow 0$, for $i \in \mathcal{N}$, and therefore we know from the definition of \mathbf{r}_i in (A.149) that $\dot{\mathbf{z}}_i \rightarrow 0$, for $i \in \mathcal{N}$. Consequently, using a similar relation to (A.138) in the proof of Theorem 6.1, we can show that $(\mathbf{z}_i - \mathbf{z}_j(t - \tau_{ij})) \rightarrow 0$ is equivalent to $(\mathbf{z}_i - \mathbf{z}_j) \rightarrow 0$.

As a result, using the fact that \mathbf{z}_i is bounded and $\dot{\mathbf{z}}_i \rightarrow 0$, we conclude that $\mathbf{z}_i \rightarrow \mathbf{z}_c$, where \mathbf{z}_c is a constant vector, for all $i \in \mathcal{N}$, and we can write $\int_{t-\tau_{ij}}^t \mathbf{z}_i ds = \mathbf{z}_c \tau_{ij}$. Now, taking the sum of the variables \mathbf{r}_i in (A.149) over $i \in \mathcal{N}$ at the limit gives

$$\begin{aligned} \sum_{i=1}^n \mathbf{r}_i &= \sum_{i=1}^n \left(\mathbf{z}_i + \lambda \sum_{k=1}^n k_{ij} (\bar{\boldsymbol{\xi}}_{ij} + \int_{t-\tau_{ij}}^t \mathbf{z}_j ds) \right) \\ &\rightarrow n \mathbf{z}_c \left(n + \lambda \sum_{i=1}^n \sum_{j=1}^n k_{ij} \tau_{ij} \right), \end{aligned} \quad (\text{A.155})$$

where $\bar{\boldsymbol{\xi}}_{ij} = (\boldsymbol{\xi}_i - \boldsymbol{\xi}_j - \boldsymbol{\delta}_{ij})$, and we have used the relations $k_{ij} = k_{ji}$ and $\boldsymbol{\delta}_{ij} = -\boldsymbol{\delta}_{ji}$ to conclude that $\sum_{i=1}^n \sum_{j=1}^n k_{ij} \bar{\boldsymbol{\xi}}_{ij} = 0$. Therefore, we conclude that $\mathbf{z}_c = 0$, since $\mathbf{r}_i \rightarrow 0$, and consequently we know that $(\boldsymbol{\xi}_i - \boldsymbol{\xi}_j(t - \tau_{ij})) \rightarrow (\boldsymbol{\xi}_i - \boldsymbol{\xi}_j)$. As a result, and from the definition of \mathbf{r}_i in (A.149), we can see that $\sum_{j=1}^n k_{ij} \bar{\boldsymbol{\xi}}_{ij} \rightarrow 0$, and using the same procedure as in the proof of Theorem 6.1, we conclude that $(\boldsymbol{\xi}_i - \boldsymbol{\xi}_j) \rightarrow \boldsymbol{\delta}_{ij}$, for all $i, j \in \mathcal{N}$.

Exploiting the above results, we can see that $\boldsymbol{\phi}_i$ in (6.33) is bounded and converges asymptotically to zero. Using the same arguments as in the proof of Theorem 6.2 with the result of Lemma 2.6, we can verify that $\boldsymbol{\alpha}_i$, $\dot{\boldsymbol{\alpha}}_i$, $\boldsymbol{\theta}_i$ and $\dot{\boldsymbol{\theta}}_i$ are bounded and $\boldsymbol{\alpha}_i \rightarrow 0$, $\dot{\boldsymbol{\alpha}}_i \rightarrow 0$, $\boldsymbol{\theta}_i \rightarrow 0$ and $\dot{\boldsymbol{\theta}}_i \rightarrow 0$, for $i \in \mathcal{N}$, which leads to the results of the theorem.

A.5.4 Proof of Lemma 6.1

Consider the Lyapunov-krashovskii functional candidate

$$\begin{aligned} W &= \frac{1}{2} \sum_{i=1}^n \dot{\boldsymbol{\alpha}}_i^T \dot{\boldsymbol{\alpha}}_i + \frac{1}{4} \sum_{i=1}^n \sum_{j=1}^n k_{ij} \bar{\boldsymbol{\alpha}}_{ij}^T \bar{\boldsymbol{\alpha}}_{ij} \\ &\quad + \sum_{i=1}^n \sum_{j=1}^n \frac{k_{ij}}{2\epsilon} \tau \int_{-\tau}^0 \int_{t+s}^t \dot{\boldsymbol{\alpha}}_j^T(\varrho) \dot{\boldsymbol{\alpha}}_j(\varrho) d\varrho ds, \end{aligned} \quad (\text{A.156})$$

where $\boldsymbol{\alpha}_{ij} = (\boldsymbol{\alpha}_i - \boldsymbol{\alpha}_j(t - \tau_{ij}) - \boldsymbol{\delta}_{ij})$ and $\bar{\boldsymbol{\alpha}}_{ij} = (\boldsymbol{\alpha}_i - \boldsymbol{\alpha}_j - \boldsymbol{\delta}_{ij})$ and $\epsilon > 0$. Following similar steps as in the proof of Theorem 6.1, the time-derivative of W evaluated along (6.42) can be upper bounded as

$$\dot{W} \leq - \sum_{i=1}^n \left(k_i^z \|\dot{\boldsymbol{\alpha}}_i\| - \bar{\epsilon}_i^b \right) \|\dot{\boldsymbol{\alpha}}_i\|, \quad (\text{A.157})$$

with k_i^z given in (6.14). It is clear that $\dot{W} < 0$ outside the set

$$\bar{\mathcal{S}} = \left\{ \dot{\boldsymbol{\alpha}}_i \mid \|\dot{\boldsymbol{\alpha}}_i\| \leq \frac{\bar{\boldsymbol{\varepsilon}}_i^b}{k_i^z} \right\}, \quad (\text{A.158})$$

and consequently $\dot{\boldsymbol{\alpha}}_i$, for $i \in \mathcal{N}$, and $(\boldsymbol{\alpha}_i - \boldsymbol{\alpha}_j)$, for all $(i, j) \in \mathcal{E}$, are bounded outside $\bar{\mathcal{S}}$. Since every vehicle can communicate with at least one other vehicle in the team, this last result is valid for all $i, j \in \mathcal{N}$.

It is also clear that $\dot{\boldsymbol{\alpha}}_i$ will ultimately reach the set $\bar{\mathcal{S}}$ and will be driven to zero as $\bar{\boldsymbol{\varepsilon}}_i \rightarrow 0$. Invoking Lemma 2.3, we can conclude that $\ddot{\boldsymbol{\alpha}}_i \rightarrow 0$, and (6.42) reduces to

$$\sum_{j=1}^n k_{ij} (\boldsymbol{\alpha}_i - \boldsymbol{\alpha}_j(t - \tau_{ij}) - \boldsymbol{\delta}_{ij}) = 0, \quad (\text{A.159})$$

for $i \in \mathcal{N}$. Following similar steps as in the proof of Theorem 6.1, we can conclude that $(\boldsymbol{\alpha}_i - \boldsymbol{\alpha}_j) \rightarrow \boldsymbol{\delta}_{ij}$ for all $i, j \in \mathcal{N}$.

A.5.5 Proof of Theorem 6.4

Similar to the proof of Theorem 6.1, the intermediary input (6.38) can be used to extract the necessary thrust input and desired attitude if condition (6.13) is satisfied. The translational error dynamics can be obtained from (6.45) in view of, (5.1), (6.39)-(6.40) and (6.43), as

$$\begin{aligned} \dot{\mathbf{z}}_i &= \dot{\mathbf{v}}_i - \ddot{\boldsymbol{\theta}}_i - \ddot{\boldsymbol{\alpha}}_i \\ &= -L_i^p \boldsymbol{\xi}_i - L_i^d (\boldsymbol{\xi}_i - \boldsymbol{\psi}_i). \end{aligned} \quad (\text{A.160})$$

Also, the attitude error dynamics are given similar to the proof of Theorem 6.1 in (A.123). Consider the following Lyapunov function candidate

$$V = V_{t_2} + V_{a_1}, \quad (\text{A.161})$$

where V_{a_1} is given in (A.126) and

$$V_{t_2} = \frac{1}{2} \sum_{i=1}^n \left(\mathbf{z}_i^T \mathbf{z}_i + L_i^p \boldsymbol{\xi}_i^T \boldsymbol{\xi}_i + L_i^d (\boldsymbol{\xi}_i - \boldsymbol{\psi}_i)^T (\boldsymbol{\xi}_i - \boldsymbol{\psi}_i) \right). \quad (\text{A.162})$$

The time-derivative of V evaluated along (A.160) and (A.123) with (6.44) and (6.28) is obtained as

$$\begin{aligned}\dot{V} &= \sum_{i=1}^n \left(-L_i^d \dot{\boldsymbol{\psi}}_i^T (\boldsymbol{\xi}_i - \boldsymbol{\psi}_i) - k_i^\Omega \boldsymbol{\Omega}_i^T \boldsymbol{\Omega}_i + k_i^q \tilde{\mathbf{q}}_i^T \boldsymbol{\beta}_i \right) \\ &= \sum_{i=1}^n \left(-L_i^d L_i^\psi (\boldsymbol{\xi}_i - \boldsymbol{\psi}_i)^T (\boldsymbol{\xi}_i - \boldsymbol{\psi}_i) - k_i^\Omega \boldsymbol{\Omega}_i^T \boldsymbol{\Omega}_i - k_i^q k_i^\beta \tilde{\mathbf{q}}_i^T \tilde{\mathbf{q}}_i \right).\end{aligned}\quad (\text{A.163})$$

The time-derivative of V is then negative semi-definite, and we conclude that \mathbf{z}_i , $\boldsymbol{\xi}_i$, $\boldsymbol{\psi}_i$, $\tilde{\mathbf{q}}_i$ and $\boldsymbol{\Omega}_i$ are bounded for $i \in \mathcal{N}$. In addition, we can see from (A.123) that $\boldsymbol{\Omega}_i$ is bounded. Also, since $\tilde{\mathbf{q}}_i$ is bounded, we know that $\boldsymbol{\beta}_i$ is bounded and consequently $\tilde{\boldsymbol{\omega}}_i$ is bounded. Hence, we conclude that $\tilde{\mathbf{q}}_i$ is bounded. In addition, we can see from (6.44) that $\dot{\boldsymbol{\psi}}_i$ is bounded. As a result, we have \ddot{V} is bounded, and invoking Barbălat Lemma, we conclude that $(\boldsymbol{\xi}_i - \boldsymbol{\psi}_i) \rightarrow 0$, $\tilde{\mathbf{q}}_i \rightarrow 0$ and $\boldsymbol{\Omega}_i \rightarrow 0$, for $i \in \mathcal{N}$. As a result, we can conclude that $\tilde{\boldsymbol{\omega}}_i \rightarrow 0$.

Furthermore, we can easily verify that $(\ddot{\boldsymbol{\xi}}_i - \ddot{\boldsymbol{\psi}}_i)$ is bounded from (6.44) and (A.160). Therefore, by virtue of Barbălat Lemma and since $(\boldsymbol{\xi}_i - \boldsymbol{\psi}_i) \rightarrow 0$, we conclude that $\mathbf{z}_i \rightarrow \dot{\boldsymbol{\psi}}_i$, and consequently we know that $\mathbf{z}_i \rightarrow 0$ for $i \in \mathcal{N}$. Also, we can verify from the time-derivative of (A.160) that $\ddot{\mathbf{z}}_i$ is bounded, and we conclude that $\dot{\mathbf{z}}_i \rightarrow 0$, and as a result we have $\boldsymbol{\xi}_i \rightarrow 0$ for $i \in \mathcal{N}$.

The dynamics of the virtual system (6.40) with the input (6.41) can be rewritten as

$$\ddot{\boldsymbol{\alpha}}_i = -k_i^v \dot{\boldsymbol{\alpha}}_i - \sum_{j=1}^n k_{ij} (\boldsymbol{\alpha}_i - \boldsymbol{\alpha}_j(t - \tau_{ij}) - \boldsymbol{\delta}_{ij}) + \bar{\boldsymbol{\varepsilon}}_i, \quad (\text{A.164})$$

with $\bar{\boldsymbol{\varepsilon}}_i = \left(-\boldsymbol{\phi}_i - \frac{2\mathcal{T}_i}{m_i} \mathbf{R}(\mathbf{Q}_i)^T \mathbf{S}(\tilde{\mathbf{q}}_i) \tilde{\mathbf{q}}_i \right)$. We can verify from the above results that the latter term is bounded and converges asymptotically to zero. Therefore, we conclude from the result of Lemma 6.1 that if the control gains satisfy condition (6.14), the signals $\dot{\boldsymbol{\alpha}}_i$ and $(\boldsymbol{\alpha}_i - \boldsymbol{\alpha}_j)$ are bounded and $\dot{\boldsymbol{\alpha}}_i \rightarrow 0$ and $(\boldsymbol{\alpha}_i - \boldsymbol{\alpha}_j) \rightarrow \boldsymbol{\delta}_{ij}$, for all $i, j \in \mathcal{N}$. As a result, we have the term $\boldsymbol{\varepsilon}_i = -\mathbf{u}_i$ is bounded and converges asymptotically to zero. Therefore, we conclude from (6.39) with (6.38) and the results of Lemma 2.6 that $\boldsymbol{\theta}_i$ and $\dot{\boldsymbol{\theta}}_i$ are bounded and $\boldsymbol{\theta}_i \rightarrow 0$ and $\dot{\boldsymbol{\theta}}_i \rightarrow 0$. Finally, from the error signals definition (6.45) and the above results, we conclude that \mathbf{v}_i and $(\mathbf{p}_i - \mathbf{p}_j)$ are bounded and $\mathbf{v}_i \rightarrow 0$ and $(\mathbf{p}_i - \mathbf{p}_j) \rightarrow \boldsymbol{\delta}_{ij}$ for all $i, j \in \mathcal{N}$. This ends the proof.

Curriculum Vitae

Name:	Abdelkader Abdessameud
Post-secondary Education and Degrees:	<p>1997-1999 M.Sc (Magister) Electrical Engineering (Robotique, Automatique et Informatique Industrielle) The Military Polytechnic School EMP ex-ENITA, Algiers, Algeria</p> <p>1990-1995 Engineer degree Electrical Engineering The National Institute of Electricity and Electronics INELEC, Boumerdes, Algeria</p>
Related Work Experience	<p>Teaching Assistant The University of Western Ontario 2007-2010</p> <p>Research Assistant University M'hamed Bouguara Boumerdes, Algeria 2004-2006</p> <p>Lecturer University M'hamed Bouguara Boumerdes, Algeria 2001-2006</p>

Journal Publications:

- [1] Abdessameud, A. and Tayebi, A. (2010). Formation control of VTOL unmanned aerial vehicles with communication delays. *Automatica*, provisionally accepted.
- [2] Abdessameud, A. and Tayebi, A. (2010). On consensus algorithms for double-integrator dynamics without velocity measurements and with input constraints. *Systems and Control Letters*, 59, 812-821.

- [3] Abdessameud, A. and Tayebi, A. (2010). Global trajectory tracking control of VTOL-UAVs without linear velocity measurements. *Automatica*, 46(6), 1053-1059.
- [4] Abdessameud, A. and Tayebi, A. (2009). Attitude synchronization of a group of spacecraft without velocity measurements. *IEEE Transactions on Automatic Control*, 54(11), 2642-2648.
- [5] Abdessameud, A. and Khelfi, M. F. (2006). A variable structure observer for the control of robot manipulators. *International Journal of Applied Mathematics and Computer Science*, 16(2), 189-196.

Conference Publications (Since 2007):

- [1] Abdessameud, A. and Tayebi, A. (2010). Formation stabilization of VTOL UAVs subject to communication delays. In *Proceedings of the 49th Conference on Decision and Control* (to appear).
- [2] Abdessameud, A. and Tayebi, A. (2010). Velocity-free consensus algorithms for double-integrator dynamics with input saturations constraints. In *Proceedings of the 49th Conference on Decision and Control* (to appear).
- [3] Abdessameud, A. and Tayebi, A. (2010). Formation control of VTOL UAVs without linear-velocity measurements. In *Proceedings of the American Control Conference*, 2107-2112.
- [4] Abdessameud, A. and Tayebi, A. (2009). On the coordinated attitude alignment of a group of spacecraft without velocity measurements. In *Proceedings of the 48th IEEE Conference on Decision and Control*, 1476-1481.
- [5] Abdessameud, A. and Tayebi, A. (2009). Formation control of VTOL UAVs. In *Proceedings of the 48th Conference on Decision and Control*, 3454-3459.
- [6] Abdessameud, A. and Tayebi, A. (2008). Attitude synchronization of a spacecraft formation without velocity measurement. In *Proceedings of the 47th IEEE Conference on Decision and Control*, 3719-3724.
- [7] Abdessameud, A. and Tayebi, A. (2008). Decentralized attitude alignment control of spacecraft within a formation without angular velocity measurements. In *Proceedings of the 17th IFAC World Congress*, 1766-1771.
- [8] Khelfi, M. F. and Abdessameud, A. (2007). Robust H-infinity trajectory tracking controller for a 6 D.O.F PUMA 560 robot manipulator. In *Proceedings of the IEEE International Electric Machines and Drives Conference*, 88-94.